

Development of a consistent approach for design and assessment of structural concrete members using stress fields and strut-and-tie models

THÈSE N° 7911 (2017)

PRÉSENTÉE LE 25 AOÛT 2017

À LA FACULTÉ DE L'ENVIRONNEMENT NATUREL, ARCHITECTURAL ET CONSTRUIT
LABORATOIRE DE CONSTRUCTION EN BÉTON
PROGRAMME DOCTORAL EN GÉNIE CIVIL ET ENVIRONNEMENT

ÉCOLE POLYTECHNIQUE FÉDÉRALE DE LAUSANNE

POUR L'OBTENTION DU GRADE DE DOCTEUR ÈS SCIENCES

PAR

Filip NIKETIĆ

acceptée sur proposition du jury:

Prof. D. Lignos, président du jury
Prof. A. Muttoni, Dr M. Fernández Ruiz, directeurs de thèse
Prof. L. C. Hoang, rapporteur
Prof. D. Zastavni, rapporteur
Prof. K. Beyer, rapporteuse



ÉCOLE POLYTECHNIQUE
FÉDÉRALE DE LAUSANNE

Suisse
2017

Foreword

Since the early developments of structural concrete, designers have searched for consistent and comprehensive methods for its design. One approach developed in this frame was the stress field method, grounded on the theory of plasticity and allowing designers for an enhanced freedom to arrange the reinforcement and deciding upon the main load-carrying actions. Currently, other than tools suitable for design of new structures, the assessment of the strength of existing structures is becoming a significant task to be performed by engineers. Such assessment allows checking on the level of safety of existing structures and if they are suitable for new or upgraded actions without the need of retrofitting them.

Within this frame, the thesis of Filip Niketić investigates on the application of stress fields both for cases related to design and to assessment. The work presents first the conceptual differences between design and assessment and possible approaches for both cases. Also, the possibility of developing suitable stress fields in an automated manner valid both for design and assessment purposes is discussed. This latter is approached by developing elastic-plastic stress fields, which are justified to yield exact solutions according to limit analysis as, at failure, they yield a licit stress field compatible with a licit failure mechanism. The research of Filip Niketić on elastic-plastic stress fields is completed with a systematic comparison to test results, showing excellent agreement, as well as a discussion on the safety format issues.

In addition, the thesis presents a detailed investigation on the strength of compression fields developing in concrete accounting for the influence of transverse strains and its interaction with the web reinforcement. This discussion, usually referred to as the strength reduction factors or efficiency factors of concrete, is one of the basic inputs to calculate the strength of stress fields. In the thesis, a new approach to the issue is presented, based on a mechanical model describing the various potential failure modes. The results of this approach are observed to be consistent to test observations and to explain the results of currently used formulas with an empirical ground.

Lausanne, July 2017

Prof. Dr Aurelio Muttoni

Dr Miguel Fernández Ruiz

*To my dear parents,
Snežana and Živorad*

Grateful son

A handwritten signature in blue ink, appearing to be 'Darius', written in a cursive style.

*“Let the future tell the truth and evaluate each one according to his work and accomplishments.
The present is theirs; the future, for which I have really worked, is mine.”*

Nikola Tesla, April 1927

Acknowledgements

I would like to express the deepest gratitude to my thesis supervisor Prof. Aurelio Muttoni, and co-supervisor Dr. Miguel Fernández Ruiz at the Structural Concrete Laboratory (IBETON) at Swiss Federal Institute of Technology in Lausanne (EPFL) for giving me the opportunity to become an active member of their research team, and providing me with the necessary support to carry out my work. Under your supervision I have grown both as a person and as an engineer, and for that I am forever grateful.

I would also like to thank Dr. Eckart Hars for his generous help and encouragement. Working with you has truly been an honour and a blessing. Thank you for each second of your time.

I would like to acknowledge the members of my thesis jury, namely Prof. Linh Cao Hoang from the Department of Civil Engineering at Technical University of Denmark (DTU), Prof. Denis Zastavni from the Faculty of Architecture, Architectural Engineering and Urban Planning at Catholic University of Louvain (UCL), Prof. Katrin Beyer, head of the Earthquake Engineering and Structural Dynamics Laboratory at EPFL and Prof. Dimitrios Lignos (president of the jury), head of the Resilient Steel Structures Laboratory at EPFL for their engagement and useful comments that improved the quality of my thesis.

My work was funded by the Federal Roads Office (FEDRO) to whom I would like to give many thanks.

The support of Dr. Peter Tanner and Dr. Miguel Prieto from the Eduardo Torroja Institute of Construction Sciences in Spain is fully acknowledged.

Special thanks goes to Dr. Olivier Burdet for helping me create the webpage with my database and providing me with the technical support for writing this thesis.

I would like to acknowledge Garbiela Jovičić for proofreading my thesis and correcting my English in a very short period of time.

Ann, Fabio, Dr. Burdet, Raffaele, Michael, Francesco, Max, Bastian, Marie-Rose and Dražen are thanked for proofreading my abstract and translating it to French, Italian and German.

I would like to thank João for many interesting discussions we had during the last two years of my work, and for driving me to school almost each morning for the last two years!

Our secretary, Yvonne Bühl-Brauch, is thanked for the administrative and personal support she generously provided during my stay at IBETON.

Acknowledgements

Over the period of my PhD studies, I sheared my office with ten amazing people: Stefano, Francesco (Donarini), Rinaldo, Hugo, Joël, Quentin, Simone, Carlos, Francesco (Moccia), Luca and Francesco (Moccia again!). I would like to thank each and every one of you for making my days at EPFL fun and my studies enjoyable. I am looking forward to joining you on the “Wall of Fame”.

Special thanks goes to the officemate who managed to put up with me the longest: Francesco Moccia. We spent a lot of great moment together, and I am lucky to have you as a friend.

I would like to thank Fabio and his family (Riccardo, Claire and Sandro) for accepting me from the very beginning, and making me feel at home in Switzerland. I am glad to have met you, and I am looking forward to our future moments.

I am more than happy to know Marie-Rose, Qianhui, Angelica, Raluca, Sarah, Pia, Maléna, Francisco, Frédéric, Dan, Jürgen, Darko, Michael, Patrick, Raffaele, Ioannis, Francesco (Cavagnis), Ovidiu, (big) João, Shenghan, Alessandro, Hadi and many more interesting, talented and fun people from EPFL. I will cherish the time we spent together for as long as I live.

I would also like to thank my old friends Zoki, Ilija, Miloš, Luka, Vasja, Mile, Nemanja, Dražen, Šeki, Paja, Buda, Knele, Isi and Urke for supporting me regardless of the physical distance and the little time we spent together over the past four years.

To my family: Mira, Vasa, Vlada, Miša, Bane, Bojka, Buca, Stevan and Naca I say thank you for giving me your love and attention, for nourishing and forming me as a person. I love you all.

I am lucky to have a cousin who loves and supports me with all her hart. Ana you showed me what it means to have a sister. I am glad that life brought us closer together.

Mici always had a special place in my heart, and the words cannot quantify the amount of love and support she gave me from the very beginning. For this, I thank her greatly.

I could not ask for more loving and generous parents than Sneža and Žika. To you I owe my life, my soul my everything. You have carried me swiftly through the darkest moments of my life and have always made me feel safe and loved. Thank you for teaching me how to be confident, persistent and strong.

Filip Niketić, July 2017

Abstract

Designing new concrete members and assessing the strength of existing elements subjected to in-plane stress state conditions is often conducted by means of Stress Fields (SF) and Strut-and-Tie Models (STM). These methods are usually accounting for identical load-carrying mechanisms for design and assessment, even if the goals for these two tasks are not the same. When designing new elements, the aim is to obtain solutions that are in equilibrium with external actions, with simple reinforcement layouts while ensuring satisfactory behaviour at serviceability limit state. When assessing the ultimate strength of existing elements, the goal is to avoid an unnecessary strengthening and limit the amount of retrofitting. The required complexity of assessment models depends on the strength requirements, and need to be gradually refined if the results from current models prove to be insufficient. This refinement process ultimately leads to increasingly more exact solutions that eventually correspond to the largest possible strength according to the limit analysis.

This thesis presents various strategies which can be employed to develop SF and STM suitable for the design and assessment of structural concrete members. The idea of a gradual model refinement (both for design and assessment) is introduced through practical examples, while potential challenges related to each solution are indicated and discussed.

Moreover, the accuracy and the generality of exact solutions obtained using Elastic-Plastic Stress Fields (EPSF) are investigated. To do this, ultimate loads estimated with EPSF are compared to test results found in the literature. To facilitate further studies by other researchers, they are available online. The analysis of structural members with insufficient anchorage and indirectly supported concrete elements with EPSF are presented and discussed.

Furthermore, this thesis focuses on a sensitivity analysis of the EPSF, to investigate the stability of the results as a function the size, shape and orientation of the finite elements. The influence of the number of iteration steps on the accuracy of EPSF models is evaluated, and clear recommendations are provided.

Stress fields based on exact solutions of the theory of plasticity simulate the physical behaviour of structural concrete members more accurately than current code provisions. On this basis, a procedure for tailoring partial safety factors for steel and concrete is presented and discussed. Reduced PSF could potentially be used when assessing the strength of existing reinforced and prestressed concrete elements, which would (could?) lead to significant cost reductions in the field of structural maintenance.

To better understand the mechanical origins of concrete compression softening (important for an accurate application of stress fields), a mechanical model for estimating the

effective concrete compressive strength is developed and discussed. Concrete cover spalling, concrete crushing and crack sliding are taken into account. Special attention is given to the dowel action of the reinforcement and its effects on the surrounding concrete matrix. The model is validated using experimental results found in literature. Finally, the pertinence of existing semi-empirical approaches for determining the effective concrete compressive strength is evaluated and discussed.

Key-words: strut-and-tie models, stress fields, design, assessment, insufficient anchorage length, partial safety factors, concrete compressive strength constitutive law, mechanical model, efficiency factor

Résumé

Le dimensionnement d'éléments en béton armé et l'évaluation de la résistance de structures existantes soumises à un état de contrainte plan sont souvent effectués au moyen de Champs de Contraintes (CC) et de Modèles de Bielles-et-Tirants (MBT). Ces méthodes complémentaires sont typiquement utilisées en prenant en compte des mécanismes de transfert de charge similaires, même si les objectifs principaux du dimensionnement et de l'évaluation soient fondamentalement différents. Dans le cadre du dimensionnement de nouveaux éléments, le but est d'obtenir des solutions qui sont en équilibre avec les actions extérieures, ce qui permet d'obtenir des schémas d'armature simples, tout en garantissant un comportement satisfaisant à l'état limite de service. Dans le cadre de l'évaluation de la résistance d'un ouvrage existant, le but est d'éviter tout renforcement inutile. La complexité requise pour les modèles d'évaluation dépend donc des exigences de résistance de la structure et doit être progressivement raffinée si les résultats s'avèrent insuffisants. Cette procédure itérative conduit finalement à la solution exacte selon la théorie de la plasticité, qui est associée à la résistance la plus grande.

Cette thèse présente plusieurs stratégies qui peuvent être employées pour développer des CC et MBT appropriés tant pour le dimensionnement que pour l'évaluation d'éléments structuraux en béton armé. Un raffinement graduel de ces modèles est proposé au travers d'exemples pratiques et les enjeux associés à chacune de ces solutions sont discutés.

Des investigations supplémentaires permettent d'appréhender la précision et l'applicabilité des solutions exactes obtenues par la méthode des Champs de Contraintes Élastiques-Plastiques (CCEP). Ceci a été réalisé au travers de comparaisons entre les valeurs de charges ultimes estimées par cette méthode et celles provenant de la littérature spécifique. Pour faciliter l'approfondissement de cette étude par d'autres chercheurs, les résultats sont disponibles en ligne. L'analyse par CCEP traite des éléments structuraux avec ancrage insuffisants, des éléments à supports indirects ainsi que des éléments précontraints.

Cette thèse présente également une analyse de la stabilité de la solution CCEP en fonction de la taille, de la forme et de l'orientation des éléments finis utilisés. L'influence du nombre d'itérations sur la précision des modèles CCEP est évaluée et des recommandations particulières sont données.

Les champs de contraintes basés sur les solutions exactes de la théorie de la plasticité simulent le comportement structural d'éléments en béton armé de manière plus précise que les normes actuelles. Cela pourrait permettre d'adapter les facteurs partiels de sécurité pour l'acier et le béton. Une réduction de ces derniers peut être envisagée dans le cadre de l'évaluation

d'ouvrages existants en béton armé ou précontraint, ce qui peut conduire à une réduction significative des coûts associés à la réparation dans le domaine des structures et ouvrages d'art.

Pour mieux comprendre l'origine des mécanismes liés au comportement adoucissant du béton en compression (primordial pour une application optimale des champs de contraintes), un modèle mécanique a été développé pour estimer la résistance effective du béton à la compression. L'éclatement du béton d'enrobage, l'écrasement du béton et le glissement dans les fissures sont pris en compte. Une attention particulière est donnée à l'effet goujon de l'armature et ses effets sur la matrice de béton avoisinante. Le modèle est validé par des résultats expérimentaux provenant de la littérature spécifique. Finalement, la pertinence des approches semi-empiriques actuelles est évaluée vis-à-vis de la réduction de la résistance à la compression provoquée par la présence de déformations transversales.

Mots-clés: modèles bielles-et-tirants, champs de contraintes, ancrage insuffisant, dimensionnement, assainissement, éléments avec appuis indirects, facteurs de sécurité partiels, résistance à la compression, lois constitutives, modèle mécanique, facteurs d'efficacité

Zusammenfassung

Häufig werden Spannungsfelder und Fachwerkmodelle für die Bemessung und Prüfung von neuen bzw. bestehenden Stahlbetonbauteilen verwendet. Üblicherweise berücksichtigen diese Methoden bei der Bemessung neuer und dem Tragwiderstandsnachweis bestehender Bauwerke dieselben Widerstandsmechanismen, obwohl die verfolgten Ziele unterschiedlich sind. Bei der Bemessung von neuen Elementen möchte man eine sich mit den äusseren Belastungen im Gleichgewicht befindende Lösung ermitteln, welche zu einer einfachen Bewehrung führt und ein gutes Verhalten am Grenzzustand der Gebrauchstauglichkeit vorweist. Beim Tragsicherheitsnachweis bestehender Bauwerke möchte man hingegen nicht erforderliche Verstärkungsmassnahmen vermeiden und die Instandsetzungsarbeiten so gering wie möglich halten. Hierfür müssen, abhängig von der erforderlichen Widerstandsfähigkeit, unterschiedlich komplexe Modelle verwendet werden: sollten die Ergebnisse von einem Modell keine ausreichenden Lastreserven vorweisen, dann muss dieses Modell schrittweise verfeinert werden. Der Verfeinerungsprozess führt zu fortschreitend genaueren Ergebnissen, welche letztlich dem Widerstandswert gemäss der Grenzwertanalyse entsprechen.

Diese Arbeit beschreibt verschiedene Strategien, die für die Erstellung von Spannungsfelder und Fachwerkmodellen für den Entwurf und die Bewertung der Tragfähigkeit von Stahlbetonbauteilen verwendet werden können. Das Prinzip der schrittweisen Verfeinerung wird anhand praktischer Beispiele erläutert. Für jede Strategie werden möglicherweise auftretende Schwierigkeiten und Probleme beschrieben und diskutiert.

Die Anwendbarkeit von Elastisch-Plastischen Spannungsfeldern (EPSF) sowie die Genauigkeit der hiermit gefundenen Lösungen werden untersucht. Die ermittelten Grenzlaster werden mit Versuchsergebnissen aus der Literatur verglichen. Um zukünftige Studien zu erleichtern sind alle durchgeführten Simulationen online verfügbar. Die Analyse von Stahlbetonträgern mit unzureichender Bewehrungsverankerung wurde ebenfalls durchgeführt und diskutiert.

Die vorliegende Arbeit beinhaltet desweiteren eine Sensibilitätsstudie der EPSF, welche die Auswirkung von Grösse, Form und Orientierung der finiten Elemente auf die Ergebnisse untersucht. Auch der Einfluss der Anzahl der Iterationsschritte wird diskutiert, sodass klare Empfehlungen formuliert werden können.

Spannungsfelder, welche auf den exakten Lösungen der Plastizitätstheorie basieren, simulieren das physische Verhalten von Stahlbetonbauteilen genauer als derzeitige Normvorgaben. Darauf aufbauend wird ein Verfahren zur Ermittlung der Teilsicherheitskoeffiziente für Beton und Bewehrungsstahl präsentiert und diskutiert. Tiefere Teilsicherheitskoeffiziente

könnten für die Auswertung von bestehenden Stahlbeton- und Spannbetonbauteile verwendet werden, was zu bedeutend niedrigeren Kosten für die Instandsetzung und Instandhaltung von Bauwerken führen kann.

Um die mechanische Ursache der Druckfestigkeitsabnahme im Nachbruchbereich besser zu verstehen, wurde ein mechanisches Modell für die Schätzung der wirksamen Betondruckfestigkeit entwickelt. Dieses ist für die Anwendung der Spannungsfelder ausschlaggebend. Das Abplatzen der Betondeckung, der Betondruckbruch, sowie das Gleiten von Rissen werden hierbei berücksichtigt. Besondere Aufmerksamkeit wird der Dübelwirkung der Bewehrung geschenkt, sowie dessen Einfluss auf die umliegende Betonmatrix. Das Modell wird anhand von Versuchsergebnissen aus der Literatur validiert. Schliesslich wird die Validität existierender semi-empirischer Ansätze zur Ermittlung der wirksamen Betondruckfestigkeit gewertet und diskutiert.

Stichwörter: Fachwerkmodelle, Spannungsfelder, Entwurf, mechanisches Modell, unzureichende Bewehrungsverankerung, Bewertung, Teilsicherheitsbeiwerte, Effizienzfaktor, Betondruckfestigkeit, konstitutives Stoffgesetz

Riassunto

La progettazione di nuove strutture e la stima della resistenza ultima per strutture esistenti soggette ad uno stato di sforzi membranali sono spesso condotte mediante modellazioni che utilizzano campi di tensione o sistemi puntone-tirante. Questi metodi sono spesso utilizzati sia per il dimensionamento che per la verifica ipotizzando legami costitutivi e meccanismi di trasmissione sostanzialmente simili malgrado gli scopi possano essere differenti. Nel caso del dimensionamento di nuove strutture, l'obiettivo del calcolo è l'ottenimento di soluzioni che siano in equilibrio con le forze esterne, con disposizioni semplici delle armature e assicurando allo stesso tempo un comportamento soddisfacente allo Stato Limite di Esercizio. Nel caso della verifica della resistenza ultima di strutture esistenti, lo scopo è, invece, evitare rinforzi strutturali non necessari.

La complessità richiesta nei modelli di verifica dipende dai requisiti di resistenza, e necessita di un raffinamento graduale se i risultati ottenuti coi modelli attuali forniscono risultati insufficienti. Questo processo di raffinamento porta a soluzioni sempre più esatte che corrispondono, infine, alla massima resistenza ammissibile calcolata attraverso l'analisi limite.

Questa tesi presenta varie strategie che possono essere adottate in caso di modellizzazioni di campi di tensione e modelli puntone-tirante nel caso di dimensionamento e verifica di strutture in calcestruzzo armato. L'idea di un graduale raffinamento del modello (sia per il dimensionamento che per la verifica) verrà introdotta mediante esempi pratici. Allo stesso tempo, potenziali raffinamenti legati ad ogni soluzione saranno elencati e discussi.

Saranno inoltre investigate l'accuratezza e la generalità di soluzioni esatte ottenute con Campi di Tensione Elasto-Plastici (CTEP). A tal fine, i carichi di rottura ottenuti mediante tali campi saranno confrontati con risultati sperimentali presi dalla letteratura. Al fine di facilitare futuri studi, tali risultati sono stati inseriti in un database disponibile online. Saranno presentati e discussi, inoltre, analisi mediante CTEP di elementi strutturali con ancoraggi insufficienti o indirettamente appoggiati.

Questa tesi si focalizza, anche, su analisi di sensitività dei campi di tensione elasto – plastici, al fine di investigare la stabilità dei risultati in funzione della taglia, forma e dell'orientamento degli elementi finiti. Infine, sarà analizzata l'influenza del numero di incrementi di carico e chiare raccomandazioni saranno fornite a riguardo.

Campi di tensione basati su soluzioni esatte della teoria della plasticità simulano il comportamento fisico di elementi strutturali in calcestruzzo in maniera più accurata che gli attuali codici. Per tale motivo, una procedura di calibrazione dei fattori parziali di sicurezza per il calcestruzzo e l'acciaio sarà presentata e discussa. I fattori di sicurezza parziali ridotti possono

essere utilizzati nel caso di verifica della resistenza di strutture esistenti o in elementi strutturali precompressi. Tali riduzioni potrebbero portare, a significativi abbassamenti dei costi nel campo della manutenzione strutturale.

Al fine di comprendere al meglio gli aspetti costitutivi legati al comportamento di softening del calcestruzzo in compressione (importante per l'applicazione dei campi tensionali), un modello meccanico per la stima della resistenza effettiva a compressione del calcestruzzo sarà sviluppato e trattato in dettaglio. Lo “spalling” del copriferro, lo schiacciamento del calcestruzzo per elevati sforzi di compressione e lo scorrimento della fessura saranno presi in considerazione.

Un'attenzione speciale sarà data al contributo dell'effetto spinotto prodotto dalle armature e ai suoi effetti sulla matrice di calcestruzzo circostante. Il modello sarà validato mediante risultati sperimentali presenti in letteratura. Infine, sarà valutata la pertinenza degli approcci semi-empirici esistenti per tenere conto della riduzione della resistenza a compressione per softening, in presenza di deformazioni trasversali.

Parole-chiave: modelli puntone-tirante, campi tensionali, dimensionamento, verifica, lunghezza di ancoraggio insufficiente, fattori parziali di sicurezza, legge costitutiva della resistenza a compressione, modello meccanico, fattore di efficienza

Сиже

Пројектовање нових и процена носивости постојећих елемената у равном стању напона, често се врши коришћењем модела Притиснутих и Затегнутих Штапова (ПЗШ), односно развојем Поља Напона (ПН) читавог носача. Иако коначни циљ самог процеса пројектовања и процене стања није идентичан, обе методе (ПЗШ и ПН) се често употребљавају на исти начин током обављања ових принципијелно другачијих задатака. Када говоримо о пројектовању нових конструкција, задовољавајуће решење произилази из модела који је у равнотежи са нанетим оптерећењем и уједно даје једноставне планове арматуре који гарантују задовољавајуће понашање елемената у граничном стању употребљивости. Током процене носивости, модели имају за циљ да избегну непотребна ојачавања постојећих објеката или смање обим неопходних интервенција. Комплексност ових модела зависи од захтеваног нивоа носивости. Почевши од једноставних решења, комплексност модела треба постепено повећавати све док се гарантована отпорност не нађе изнад захтеване. Ово усложњавање је могуће све до достизања егзактног решења, које по принципима теорије пластичности даје максималну теоретску носивост једног елемента.

У оквиру ове тезе представљени су различити процеси развоја ПН као и модела ПЗШ оптималних за пројектовање нових или процену отпорности постојећих елемената. Идеја постепеног усложњавања модела је показана кроз практичне примере. Уједно, потенцијални проблеми који могу настати као последица неправилног моделирања су назначени и објашњени.

Применљивост и прецизност егзактних решења која су добијена применом методе Еласто-Пластичних Поља Напона (ЕППН) је истражена кроз поређење процењених и експериментално измерених вредности лома носећих елемената. Како би се обезбедила апсолутна транспарентност представљеног истраживања и уједно олакшао будући рад у овом домену, сви модели су доступни онлајн. Посебна пажња посвећена је елементима са неадекватно анкерисаном арматуром и индиректним ослонцима.

У циљу анализе стабилности решења добијених применом ЕППН (која су заснована на Методи Коначних Елемената - МКЕ), одређени носачи су моделирани помоћу КЕ различите величине, облика и оријентације. Утицај броја итерација на прецизност коначног решења је испитана и препоруке за практичну примену ЕППН су јасно назначене.

Чињеница да еласто-пластична поља напона приказују расподелу унутрашњих сила далеко прецизније од препорука актуелних правилника за бетонске конструкције,

омогућава редукују Парцијалних Коефицијента Сигурности (ПКС) бетона и челика. Посебна метода која дозвољава прерачунавање ПКС узимајући у обзир тачност ЕППН је представљена и дискутована. У случају процене стања постојећих конструкција, редукација ПКС би водила ка потенцијално значајним уштедама.

Ради бољег разумевања процеса омекшавања бетона под оптерећењем (веома битном параметру од којег зависи прецизност поља напона) посебна пажња посвећена је развоју механичког модела за процену његове ефективне чврстоће, који директно узима у обзир три различита механизма лома (дробљење, клизање и одвајање заштитног слоја бетона). Поред тога, кривљење арматуре услед отварања пукотина које су управне на правац шипки је узет у обзир. Механички модел је искоришћен како би се измоделирали армирано бетонски панели који су оптерећени на смицање, и добијени резултати су упоређени са експериментално измереним вредностима. Поред тога постојећи полу-емпиријски модели за омекшавања бетона су упоређени са резултатима механичког приступа ради даље валидације.

Кључне речи: модел притиснутих и затегнутих штапова, поље напона, пројектовање, процена, недовољна дужина анкерисања арматуре, парцијални коефицијенти сигурности, ефективна чврстоћа бетона на притисак, механички модел

Table of content

Foreword.....	i
Acknowledgements.....	vii
Abstract.....	ix
Résumé.....	xi
Zusammenfassung.....	xiii
Riassunto.....	xv
Сиже.....	xviii
Notation.....	xxiii
Upper Latin characters.....	xxiii
Lower Latin characters.....	xxiii
Upper Greek characters.....	xxiv
Lower Greek characters.....	xxiv
Subscript.....	xxv
Upper Latin characters.....	xxv
Lower Latin characters.....	xxv
Greek characters.....	xxvi
Numbers.....	xxvi
Acronyms.....	xxvi
Chapter 1: Introduction.....	1
1.1 Aims of the research.....	3
1.2 Structure of the thesis.....	4
1.3 Scientific contributions of the thesis.....	5
Chapter 2: Strut-and-tie models and stress fields as tools for design and assessment of structural concrete members.....	7
2.1 Introduction.....	7
2.2 State of the art on strut-and-tie models and stress fields.....	13
2.3 Suitable approaches for designing new structural elements with stress fields.....	26
2.3.1 Design models inspired by the existing cases.....	26

2.3.2 Design models based on deviated thrust lines.....	28
2.3.3 Design models inspired by elastic uncracked stress fields.....	31
2.3.4 Design models inspired by cracked stress fields.....	32
2.4 Suitable approaches for assessing the ultimate strength of structural concrete elements with stress fields.....	34
2.4.1 Assessing the ultimate strength using a rigid-plastic stress field approach.....	34
2.4.2 Assessing the ultimate strength using elastic-plastic stress field approach.....	40
2.5 Collected database and validation of the elastic-plastic stress fields.....	42
Chapter 3: Advanced modelling of structural concrete members with EPSF.....	47
3.1 Sensitivity analysis of EPSF method with respect to its finite element implementation.....	47
3.1.1 Investigating the influence of finite element size on EPSF analysis.....	48
3.1.1.1 Structural concrete members subjected to pure compression.....	49
3.1.1.2 Structural concrete members subjected to pure tension.....	50
3.1.1.3 Structural concrete members subjected to pure shear.....	51
3.1.1.4 Structural concrete beam under four-point-bending.....	52
3.1.2 Investigating the influence of finite element shape on EPSF analysis.....	55
3.1.3 Investigating the influence of finite element orientation on EPSF analysis.....	57
3.1.4 Convergence and required number of iterations for an EPSF analysis.....	59
3.2 Modelling elements with insufficient anchorage length using EPSF.....	61
3.3 Analysis of indirectly supported structural concrete members using EPSF.....	66
3.4 Tailoring partial safety factors suitable for EPSF method.....	72
Chapter 4: Effectiveness factor for concrete compressive strength accounting for the presence of cracks and interaction with the reinforcement.....	81
4.1 Introduction and state of the art.....	81
4.1.1 Concrete compressive strength brittleness factor – η_{fc}	83
4.1.2 Concrete softening caused by imposed transversal strains – η_{ϵ}	86
4.1.3 Concrete softening caused by the presence of post-tensioning ducts.....	94
4.1.4 Critique of the multiplicative approach for estimating effective concrete compressive strength.....	99
4.2 Mechanical model for compression softening of reinforced concrete panels.....	102
4.2.1 Stages of mechanical behaviour.....	102
4.2.1.1 First stage: Linear elastic response.....	102
4.2.1.2 Second stage: Cracked behaviour.....	104
4.2.1.3 Third Stage: Behaviour after yielding.....	104
4.2.2 Plastic strength of rebars subjected to doweling and elongation.....	105

4.2.3 Concrete strength accounting for the presence of initial cracks and rebars.....	111
4.2.3.1 Strength of the damaged struts.....	113
4.2.3.2 Strength of the undamaged struts.....	117
4.2.4 Parameters governing the compressive strength of concrete.....	118
4.3 Numerical solving procedure for the proposed compression softening model.....	120
4.3.1 Cracking of the panel.....	120
4.3.2 Onset of yielding or early concrete crushing.....	120
4.3.3 Failure of the panel.....	123
4.4 Experimental validation and comparison to available methods.....	124
Chapter 5: Conclusions and future research.....	131
5.1 Conclusions.....	131
5.1.1 Regarding the application of STM and SF as tools for design and assessment	131
5.1.2 Regarding the advanced modeling of structural concrete with EPSF method....	133
5.1.3 Regarding the effectiveness factor for concrete compressive strength.....	134
5.2 Future research.....	135
References.....	137
Appendix	
Curriculum vitae	

Notation

Following notation is used in this thesis:

Upper Latin characters

A	: area
D	: aggregate diameter
E	: young's modulus of elasticity
F	: applied force
M	: bending moment
N	: normal (axial) force
P	: pole of rotation
Q	: applied load
R	: reaction force; resistance
S	: strut
T	: tie
V	: shear force

Lower Latin characters

a	: general dimension of a structure
b	: thickness
c	: concrete cover
d	: differentially small section
f	: material strength
h	: size of a panel in z -direction
l	: size of a panel in x -direction ; length
m	: normalized moment
n	: normalized normal force; number of layers; number of initial cracks in one half

	of an analysed panel
n'	: number of damaged struts in a critical section of analysed panel
q	: applied distributed load; relative amount
s	: spacing between two consecutive cracks; spacing between two neighbouring rebars
u	: displacement in horizontal direction
v	: displacement in vertical direction
w	: crack width

Upper Greek characters

Δ	: one half of the total rebar elongation between the two plastic hinges
\emptyset	: rebar diameter
Φ	: normal distribution function
Ψ	: rotation

Lower Greek characters

α	: rebar tilting angle due to the doweling
β	: reliability index
γ	: shear strain; partial safety factor
δ	: slip of a plastic hinge
δ'	: ratio between the external rebar diameter and the sum of the double effective concrete cover thickness and the external rebar diameter
ε	: strains
η	: effectiveness factor
θ	: direction of the principal compressive strains (stresses)
λ	: integration factor
ν	: applied stress on the panel; effectiveness factor
ξ	: normalized slip of the plastic hinges in the doweling
ρ	: reinforcement ratio
σ	: stress
τ	: shear/bond stress
φ	: friction angle
ω	: local stress field disturbance ratio

Subscript

Upper Latin characters

<i>D</i>	: duct
<i>DS</i>	: damaged struts
<i>EPSF</i>	: according to elastic-plastic stress field
<i>MODEL</i>	: according to proposed model
<i>U</i>	: ultimate
<i>UDS</i>	: undamaged struts
<i>V</i>	: shear force

Lower Latin characters

<i>a</i>	: width of the local disturbance zone
<i>anch</i>	: anchorage
<i>b</i>	: bond
<i>c</i>	: concrete
<i>cc</i>	: confined/confining concrete
<i>ce</i>	: effective concrete
<i>cr</i>	: crack
<i>cte</i>	: effective tensile concrete strength
<i>ctm</i>	: mean tensile concrete strength
<i>conf,1</i>	: direction perpendicular to the direction of confining concrete stress
<i>conf,2</i>	: direction parallel to the direction of confining concrete stress
<i>d</i>	: design values
<i>dow</i>	: doweling
<i>eff</i>	: effective
<i>ext</i>	: external
<i>fc</i>	: accounting for the brittle behavior of the concrete
<i>k</i>	: characteristic values
<i>m</i>	: mean
<i>max</i>	: maximal
<i>min</i>	: minimal
<i>model</i>	: model
<i>nom</i>	: nominal values

Notation

p	: inside a plastic hinge
r	: reduced
s	: steel; accounting for the presence of steel
$s,1$: at the location of a crack
$s,2$: at the mid-point between the two cracks
t	: tensile; time
$test$: tested
ult	: refers to stain (stress) state at ultimate limit state
x	: in x -direction; height of the compressed zone
xz	: in xz -plane
w	: web
y	: yielding
z	: in z -direction

Greek characters

ε	: accounting for induced transverse strains
τ	: accounts for the presence of the initial cracks in concrete

Numbers

0	: reference value; refers to concrete compressive strength
1	: direction of the principal tensile strains (stresses)
3	: direction of the principal compressive strains (stresses)

Acronyms

ACI	: American Concrete Institute
CoV	: Coefficient of Variation
EC	: Euro Code
EPSF	: Elastic-Plastic Stress Field
CCEP	: Champs de Contraintes Élastiques-Plastiques
CTEP	: Campi di Tensione Elasto-Plastici
ЕППН	: Еласто-Пластична Поља Напона
FE	: Finite Element
GSP	: Global Safety Format
LoA	: Level of Approximation

<i>MC</i>	: Model Code
<i>MCFT</i>	: Modified Compression Field Theory
<i>PSF</i>	: Partial Safety Format
<i>RC</i>	: Reinforced Concrete
<i>RPSF</i>	: Rigid-Plastic Stress Field
<i>SF</i>	: Stress Field
<i>SLS</i>	: Serviceability Limit State
<i>std</i>	: Standard deviation
<i>STM</i>	: Strut-and-Tie Model
<i>ULS</i>	: Ultimate Limit State

Chapter 1: Introduction

Application of reinforced and prestressed concrete in civil engineering has been steadily increasing over the past century, ever since Hennebique [101] patented a manufacturing process for ribbed reinforced concrete slabs, and used it in practice by the late nineteenth century. Purely intuitive structural concrete analysis gradually evolved into mechanically based models by the end of the fifties, when the development of exact solutions according to the theory of plasticity took place. The increased demands for the residential, infrastructural and industrial facilities caused by the global urbanization popularized the application of concrete as reliable and accessible building material.

The end of the twentieth century marked the end of the designed life span for many concrete structures, which now required assessment to reinsure safety of further usage. Retrofitting the existing objects became a frequent engineering task, since the available construction space was decreasing and the idea of sustainable building gained on importance. At the same time, the general knowledge on mechanical behaviour of reinforced and prestressed concrete members increased and the current codes of practice have been updated. Compared to their previous versions, more conservative criteria for acceptable structural behaviour have sometimes been imposed, which resulted in structural strengthening. However, the fact that the design models usually govern conservative results compared to reality (some load-carrying mechanisms are neglected), means that the strengthening can often be avoided by increasing the accuracy of the applied methods.

Limit analysis provides a consistent frame suitable for the design and the assessment of structural concrete members. Lower-bound theorem can be used to develop models that give safe estimates of element's strength, and as such they can be used for the structural design. On the other hand, upper-bound theorem governs unsafe results by definition. Nevertheless, in combination with the lower-bound theorem it can be used to obtain the exact solution which, according to the theory of plasticity, gives the highest possible strength of an analysed element and is therefore suitable for structural assessment.

This thesis focuses on the differences between the models that can be used when designing new structural concrete members subjected to plane stress state and assessing the strength of existing ones. It aims to show that the difference in principal goals (design or assessment) dictates the form and accuracy of the final solution. Various procedures for designing and assessing the strength of structural concrete members are presented and discussed, using a deep beam with an opening as an example (originally introduced by Schlaich et al. [107]).

Special attention is given to the Elastic-Plastic Stress Field (EPSF) approach, which automatically accounts for all potential load-carrying mechanisms at ultimate limit state, thus giving an exact solution according to the limit analysis. Results obtained using the EPSF are compared to experimentally-measured values found in the literature in order to prove its accuracy and generality. Based on this, a database containing 315 reinforced and prestressed concrete members is created and placed online.

Robustness of the EPSF method has been evaluated by conducting a detailed sensitivity analysis. Influence of finite element size, shape and orientation on the convergence of EPSF are estimated and discussed.

Additional focus is placed on the development of EPSF suitable for investigating members with insufficient anchorage length and elements with indirect supports (which is particularly useful when analysing bridge diaphragms). In order to profit from increased accuracy of the EPSF models, a procedure for tailoring partial safety format is presented and discussed.

If the strength of an element is governed by the concrete, accuracy of the exact solution depends on the pertinence of the approach used to estimate the effective concrete compressive strength. This has been observed in the late seventies, and since then various semi-empirical softening equations have been proposed by different authors (Vecchio and Collins [120], Hsu [47], Pang [94], Kaufmann [52, 53], Muttoni [82, 89], Hars [41], etc.). However, none of the existing models take directly into account the influence of the different failure modes (crushing of the struts, spalling of the concrete cover and sliding of the struts along the weakest planes). In order to overcome this, a mechanically based procedure for estimating the effective concrete compressive strength has been developed and presented. The model showed satisfactory results when compared to experimentally measured values. Finally, the results of the presented mechanical approach were used to justify the accuracy and the consistency of the existing semi-empirical approaches.

1.1 Aims of the research

The research presented in this thesis aims to:

- Show and compare various design procedures for reinforced and prestressed concrete members with discontinuity regions;
- Show and compare various procedures for estimating the maximal load-bearing capacity of reinforced and prestressed concrete members with discontinuity regions;
- Underline the main differences between the procedures suitable for design and assessment of structural concrete members;
- Assemble a database of tested structural concrete members found in literature, estimate their ultimate strength using models based on the exact solution of the theory of plasticity (employing the EPSF method);
- Conduct a detailed sensitivity analysis of the EPSF method, with respect to its finite element implementation;
- Propose a procedure for taking into account the insufficient reinforcement anchorage in EPSF models;
- Propose a procedure for EPSF analysis of indirectly supported structural concrete members;
- Propose a procedure for tailoring the partial safety factors for EPSF method, taking into account its increased accuracy;
- Investigate the influence of concrete crushing, concrete cover spalling and sliding on effective concrete compressive strength;
- Investigate the interaction between the concrete compressive strength and the formation of cracks appearing at different load-stages;
- Investigate the interaction between the concrete compressive strength and doweled rebars in structural panels failing in shear;
- Develop a mechanically based model for estimating the effective concrete compressive strength and validate it using the results from experimental campaigns found in literature.

1.2 Structure of the thesis

The thesis is organized in the following manner:

- Chapter 2 consists of results which were published in the 112th volume of ACI Structural Journal (issue number 5) in September - October of 2015, titled “Design versus Assessment of Concrete Structures Using Stress Fields and Strut-and-Tie Models”, written by Aurelio Muttoni, Miguel Fernández Ruiz, and Filip Niketić. The chapter gives a brief introduction and state-of-the-art on structural analysis using strut-and-tie models and stress-fields. It also presents various strategies for design and assessment of structural concrete members based on limit analysis. Finally, it compares the results of the highest level of accuracy (exact solutions obtained with the EPSF method) to an online database;
- Chapter 3 consists of results which were published in October 2016 as a part of the FEDRO (Federal Roads Office) report number 680, titled “Assessment of Existing Structures Based on Elastic-Plastic Stress Fields and Modelling of Critical Details and Investigation of the In-Plane Shear Transverse Bending Interaction”, written by Aurelio Muttoni, Miguel Fernández Ruiz, Filip Niketić and Marie-Rose Backes. The report was a part of the research project AGB 2009/009, requested by the AGB bridge research group. It presents the details of the finite elements sensitivity analysis performed on the EPSF method. It also shows the modelling procedures for elements with insufficient reinforcement anchorage length, as well as indirectly supported structural concrete members. Finally, it presents a procedure for tailoring partial safety factors for steel and concrete that could be used with the EPSF method;
- Chapter 4 consists of results which were accepted for publishing on the 7th of July 2017 by the Magazine of Concrete Research under the article number MACR-D-17-00077R1. The work was titled: “Response of RC panel accounting for crack development and its interaction with rebars”, and was written by Eckart Hars, Filip Niketić and Miguel Fernández Ruiz. The chapter gives an introduction and state-of-the-art on various factors for estimating the effective concrete compressive strength. It presents a mechanically based model for the reduction of concrete compressive strength. The model takes into account the effects of rebar doweling. Finally, it compares the obtained results to the semi-empirical softening equation of Vecchio and Collins [120], and validates the consistency of the proposed procedure using a database of tested reinforced concrete panels found in literature.
- Chapter 5 gives conclusions based on the work presented in this thesis and proposes recommendations for future research.

1.3 Scientific contributions of the thesis

The scientific contributions of this thesis are:

- Clarifying the difference between the development procedure of strut-and-tie models and stress fields used for design and ultimate strength assessment of structural concrete members;
- Assembling an open-source database containing 315 reinforced and prestressed concrete members from 30 different experimental campaigns and the corresponding EPSF models;
- Performing a detailed sensitivity analysis of the EPSF method and giving clear recommendations on how the models should be conceived;
- Presenting and validating a strategy for taking into account the insufficient anchorage length of the reinforcement in EPSF models;
- Presenting and validating a strategy for modelling crossed reinforced and prestressed concrete members with EPSF method;
- Presenting a strategy for tailoring partial safety factors which can be applied on EPSF models;
- Presenting and validating a mechanically based model for estimating the concrete compressive strength effectiveness factor, which takes into account different failure mechanisms occurring in the concrete;
- Presenting a procedure for taking into account dowelling for the reinforcement and incorporating it into the concrete compressive strength effectiveness factor;
- Validating the accuracy of semi-empirical approach of Vecchio and Collins [120] by comparing it to mechanically based approach developed in this thesis.

Chapter 2: Strut-and-tie models and stress fields as tools for design and assessment of structural concrete members

The work presented in the following chapter is based on a technical paper titled “Design versus Assessment of Concrete Structures Using Stress Fields and Strut-and-Tie Models”, written by Aurelio Muttoni, Miguel Fernández Ruiz, and Filip Niketić. The article was published in ACI Structural Journal, volume 112, number 5 as a part of the September - October 2015 issue of the paper.

The contributions of Filip Niketić to creation of this publication involved:

1. Developing the examples of stress fields and strut-and-tie models suitable for designing a deep beam with an opening;
2. Developing the examples of stress fields and strut-and-tie models suitable for assessing the ultimate strength of a deep beam with an opening;
3. Validating the generality and accuracy of the EPSF method by assembling a database containing 150 structural elements (the database was later extended to a total of 315 structural elements presented in this thesis);
4. Making a web page which contains the basic geometrical and mechanical properties of analysed elements, as well as the corresponding EPSF models which can be downloaded and recalculated in ICONC

2.1 Introduction

Structural analysis of concrete elements in modern civil engineering is widely done using Stress Fields (SF) and Strut-and-Tie Models (STM). These approaches have been incorporated in most codes of practice in the last decades. Given a fact that up to recently the demand for assessing the ultimate strength of existing structural concrete members was relatively low, means that most of the code recommendations were mainly directed towards the design. However, this trend is gradually changing as retrofitting of the existing structures becomes more and more common due to:

1. Limited space for conceiving new structures in heavily populated areas;

2. Application of more rigorous criteria for the acceptable behaviour of structural elements by the valid codes of practice.

Consequently, some of the codes (such as MC 2010 [34] for example) have incorporated the concepts related to life cycle design, or are providing recommendation for the structural evaluation and rehabilitation (which is the case with ACI 364 [2], ACI 437 [3] and SIA 269 [109]).

Today stress fields and strut-and-tie models are often used in the same manner when designing new and assessing the strength of existing structures. Developing a suitable model for these two conceptually different tasks should not necessarily be performed following the same approach. The aim of the models used for designing is to derive simple solutions which are in equilibrium with the external load, and are able to provide safe solutions at the Ultimate Limit State (ULS). Out of multiple options, the ones showing acceptable behaviour at Serviceability Limit State (SLS) should be selected. On the other hand, the aim of SF and STM used for assessment of the existing structures is to avoid or minimize any element strengthening. In this case it is usually not necessary to model structural behaviour at SLS, since the structure itself has already been in usage and its current condition can be validated through thorough in-situ inspection. Given the fact that the aim of the models used for design and assessment is clearly different, indicates that the process of their development as well as their final form should not always be the same. It is therefore necessary to clearly distinguish between these two modelling techniques, and provide the engineers with the recommendations for their development.

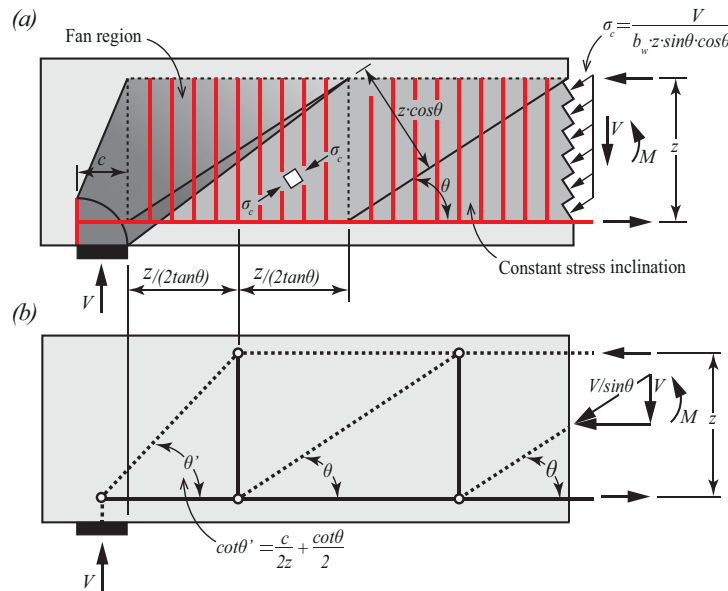


Figure 2.1: (a) Stress field of a simple beam; (b) corresponding strut-and-tie model

Stress field and strut-and-tie methods share many analogies. They are complimentary tools which should be used in parallel whether designing new or assessing the strength of existing structures. Stress field method [34] allows determining a licit stress state of a member

subjected to external actions (as presented in *Fig.2.1a*). Combining the internal forces with the geometrical properties of the cross-section, allows one to determine the direction (θ) and the intensity (σ_c) of the principal compressive stresses in the concrete. Combining them with the number, position, and diameter of the rebars on the other hand determines the stress state inside the reinforcement. Strut-and-tie model corresponding to a specific stress field, represents nothing else but its resultant (refer to *Fig.2.1b*). It is easier to find an equilibrium between the applied actions and the internal forces in this manner, and to determine which regions of the analysed element are subjected to tension or compression. The inclination of the struts and ties and the intensity of the forces inside them can be determined through integration of the stress field over areas indicated in *Fig.2.1*. This becomes more obvious when comparing the inclination of the strut which is closest to the support to the inclination of the other struts in the beam. As it can be seen θ' is not parallel to θ , since it corresponds to the resultant of the fan region, and not the compressive field with constant inclination.

When searching for an optimal solution for design and assessment, the final goal is formally the same: reduce the cost while ensuring a satisfactory structural behaviour. With this in mind, the appropriate SF and STM for structural design leads towards the solutions that minimize the amount of necessary material (both steel and concrete), and are easy to develop and build (requiring little time and labour force). The two goals do not necessary have the same direction, and sometimes more material is required for achieving simpler reinforcement layouts. This means that the optimal solution for design will always depend on the current market. The optimization process of the models used for strength assessment on the other hand is more straightforward, since the cost are always reduced by minimizing or possibly avoiding any structural strengthening. However, this does not mean that the model which accounts for all potential load-carrying mechanisms of an element is the appropriate solution. It is rather the simplest one which proves that the structure has sufficient resistance with respect to the required design loads. Only in case a model does not provide sufficient structural safety, it should be changed to account for the additional load-carrying mechanisms. According to the limit analysis, this process can be repeated until exact solution has been obtained. Only if the exact solution shows insufficient resistance compared to the design loads, the structure should be strengthened accordingly.

This concept of gradual model refinement is known as the Levels-of-Approximation (LoA) approach and was introduced in MC 2010 [34] by Muttoni et Fernández-Ruiz [85,86]. As presented in *Fig.2.2a* the lower LoA models take less time to develop but are more conservative compared to the actual element resistance. As the LoA increases, so does the models computational time and accuracy.

Fig.2.2b gives an example of the correct application of the LoA approach, by calculating the shear resistance of a rectangular cross section according to section 7.3.3.3 of MC 2010 [34]. Assuming that this is an existing element whose required resistance (V_{req}) is indicated in the graph using a dashed line (see *Fig.2.2b*), the modelling process should start using the simplest solution – the 1st LoA where the minimal SF inclination is limited to 30° and the concrete compressive strength effectiveness factor is 0.55. As presented in *Fig.2.2b*, the obtained resistance does not satisfy the imposed requirements, which means that the 2nd

LoA model should be applied. According to MC 2010 [34], this implies more accurate estimation of the minimal SF inclination angle as well as a re-evaluation of the concrete compressive strength effectiveness factor. As presented in Fig.2.2b, the necessary requirements have now been met, which means that there is no need to develop models of the 3rd and the 4th LoA.

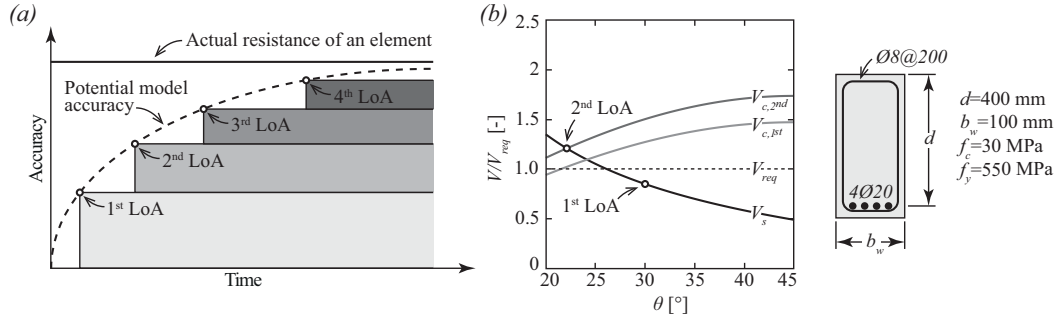


Figure 2.2: Levels-of-Approximation (LoA) approach: (a) accuracy of a model in function of the time necessary for its development; (b) shear strength of a given cross-section estimated with two LoA according to MC 2010 [34]

Stress field and strut-and-tie methods are in agreement with limit analysis and provide a consistent frame for the design and assessment of structural concrete. Since both methods respect the yield condition at all points and are in equilibrium with applied loads, SF and STM can be treated as lower-bound solutions. Drucker [27], described the application of the lower-bound theorem to structural concrete in the following manner: “If an equilibrium distribution of stress can be found in the concrete and the steel which is nowhere tensile in the concrete and is everywhere at or below yield, the structure will not collapse or will just be at the point of collapse”. It can therefore be seen that if a model respects the lower-bound theorem of the limit analysis, the estimated strength of the corresponding element will be conservative, and the members will have sufficient ductility. In other words, SF and STM based on the lower bound theorem are suitable tools for the design of structural concrete.

A few examples of the lower-bound solutions are presented in Fig.2.3 b to d, where stress fields (given in a form of moment diagrams) are developed for a double clamped beam subjected to uniformly distributed load. Each of the models is in equilibrium with the applied loads (refer to M -diagrams presented in red) and the ultimate strength of concrete and steel is never exceeded along the beam (M_R -diagrams always surpass the M -diagrams), which makes them licit lower-bound solutions. SF which show a positive behaviour at SLS while assuring sufficient safety at ULS should be selected when designing a structural concrete member (as described by Muttoni et al. [89]). Given a fact that placing reinforcement only in the upper part of the beam’s cross-section (see Fig.2.3b) or only in its lower part (see Fig.2.3c) leads to unacceptably wide cracks in the middle of the beam or close to the supports, means that the solution presented in Fig.2.3d is the most acceptable one (shows the best performance at SLS). Whether it is an optimal solution or not depends on the amount of applied material, simplicity of the final reinforcement layout, and the amount of robustness required from the newly designed structure. Given a fact that in Fig.2.3d M_R -diagram never touches the M -

diagram, indicates that there is some margin for the reduction of applied materials. Whether this reduction is necessary to make or not is a question that should be answered by the responsible designer.

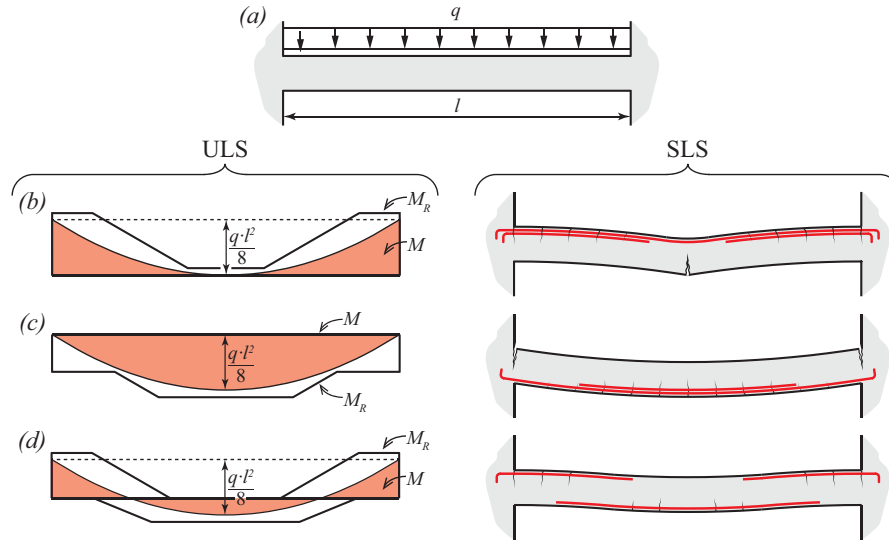


Figure 2.3: Lower-bound solutions (suitable for design): (a) Geometry and loading properties of a double clamped beam; (b) to (d) moment diagrams and corresponding deformed shapes resulting from reinforcement being placed: (b) on the top of the beam; (c) at the bottom of the beam; (d) both on the top and at the bottom of the beam

Limit analysis has also an upper bound theorem which can be used to calculate the strength of the existing structural concrete elements. According to Drucker [27]: “The structure will collapse if there is any compatible pattern of plastic deformation for which the rate of work of the external loads exceeds the rate of internal dissipation”. Once more, there are multiple solutions which can satisfy the upper-bound theorem and they are non-conservative by definition. Referring to the double clamped beam from Fig.2.4a, two mechanisms (amongst infinite number of solutions) presented in Fig.2.4d and c can be assumed to determine an upper bound of its strength. Both are kinematically admissible and correspond to SF which is in equilibrium with the applied loads (refer to M_1 and M_2 -diagrams). However, estimated resistances of the same element using these two different mechanisms are not equal. The solution presented in Fig.2.4b governs higher ultimate loads compared to the one from Fig.2.4c. In addition to this SF from Fig.2.4b violates the yield condition in the middle of the beam. Therefore, such mechanism cannot be accepted as a licit solution and is therefore disregarded. On the other hand, the mechanism of Fig.2.4c fully respects the yield condition along the beam yet allows the development of the assumed kinematics. In addition to this it is in equilibrium with applied loads, which means that it respects both lower and upper-bound theorems of the limit analysis. Such solution is called the exact solution. According to the limit analysis, it is considered to be the best potential SF which can develop in an existing structure, since it provides the largest strength of all potential safe (lower bound) solutions. When assessing the strength of an existing element, exact solutions present the most refined (highest LoA) models, which minimize the cost of

structural strengthening either by avoiding it or making the minimal necessary interventions in the critical regions.

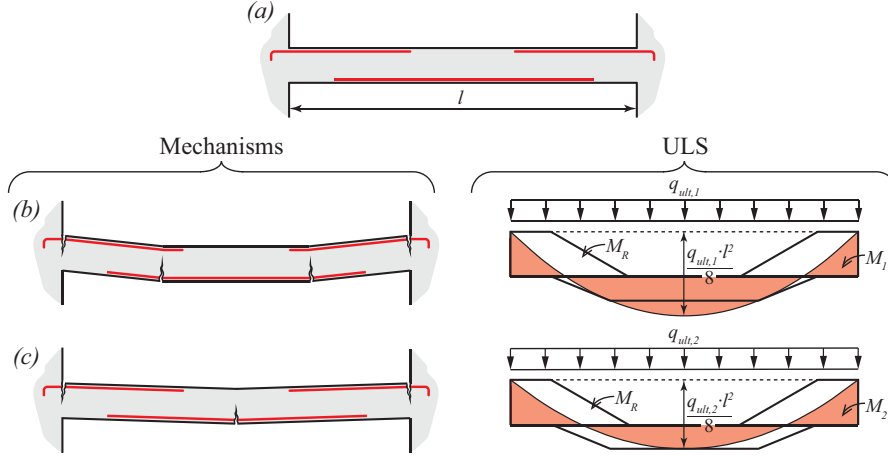


Figure 2.4: Lower-bound solutions (suitable for the ultimate strength assessment) (a) Geometry properties and the reinforcement layout of a double clamped beam (b) and (c) assumed mechanisms and corresponding moment diagrams resulting from a: (b) four-hinge mechanism; (c) three-hinge mechanism

It can be concluded that the lower-bound solutions are suitable for design of structural concrete members, but can also be used as tools for safe assessment of the strength of existing structures. The upper-bound models on the other hand, generally lead towards unsafe solutions, but they can be optimized in order to find an exact solution. Such solution can be used as a powerful tool when estimating the strength of existing structural concrete element, in which case it requires the analysis of the highest LoA. Exact solution can also be used for designing, in case it is required to determine the minimal amount of building materials necessary to support the applied loads. However, such level of accuracy is not necessarily positive in designing, since it leaves little space to compensating for the unexpected actions during the construction and over the lifetime of a structure.

This chapter will focus on presenting various strategies which can be used for developing suitable stress fields and strut-and-tie models for design and assessment of structural concrete members, through practical examples and references. The concepts are explained from a general point of view even though structural design and strength assessment are performed on elements subjected to in-plane loading. The accuracy of limit analysis is finally compared to available test data showing the consistency of the approach and its generality.

2.2 State of the art on strut-and-tie models and stress fields

Initial design of structural concrete elements was purely intuitive. First patents and guidelines which came out by the late nineteenth century, were based on simple mechanisms and engineering experience. One of such systems (presented in *Fig.2.5*) was introduced by Hennebique [101]. Recommendations on how to place the longitudinal reinforcement according to different boundary conditions were given (refer to *Fig.2.5a*), along with proper rebar anchorage details. In addition to this, guidelines for shaping and placing the transverse reinforcement (which was also used to keep the longitudinal reinforcement in place) were included (refer to *Fig.2.5b* and *c*).

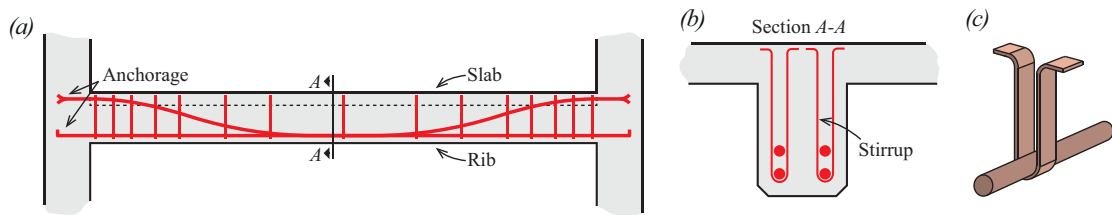


Figure 2.5: Reinforcement layout patented by Hennebique: (a) shape of the longitudinal rebars and disposition of the transverse reinforcement; (b) correct placing the reinforcement in the cross-section of the rib; (c) detail of the stirrup (adopted from [101])

Inspired by the patent of Hennebique, Ritter [101] introduced a simple approach for designing structural concrete beams, presented in *Fig.2.6*.

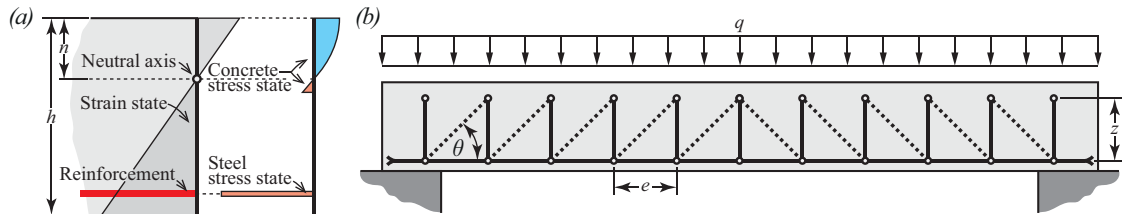


Figure 2.6: Design approach proposed by Ritter: (a) stress and strain state of an analysed cross-section; (b) truss-model (adopted from [101])

Determining the necessary area of the longitudinal steel and concrete, was based on sectional analysis presented in *Fig.2.6a*. After obtaining the position of the neutral axis, a linear strain distribution across the section is assumed. This determines the strain state of every fibre, and consequently its stress state. According to Ritter, concrete can take compression stresses (following a nonlinear distribution) as well as the tensile stresses (following a linear distribution). However, since the tensile strength of concrete is quite small (approximately 1/10 of its compressive strength), it was proposed that the entire tensile force acting across a section should be supported by the reinforcement.

In addition to this, Ritter introduced a truss model which should be used to calculate the position and the amount of the stirrups in a beam (refer to *Fig.2.6b*). The model was based on an observation that a reinforced concrete beam subjected to external loads develops cracks which form at approximately 45° . This means that a truss-like mechanism is formed inside

such an element, allowing the compressive forces that pass between the cracks to be taken by the concrete, before being suspended by the vertical stirrups (which cross the cracks), until finally reaching the supports. This implies that the principal direction of concrete struts is parallel to the direction of the cracks ($\theta=45^\circ$), and that the vertical reinforcement should be sufficient to take the applied shear force. According to the presented truss model, recommended stirrup spacing (e in Fig.2.6c) is equal to the beam's lever arm (z). Finally, based on the equilibrium conditions, Ritter concluded that the optimal stirrup inclination is 45° (perpendicular to the compressed struts). However, since vertical reinforcement can be disposed on a construction site with greater accuracy, 90° inclinations should be used in practice.

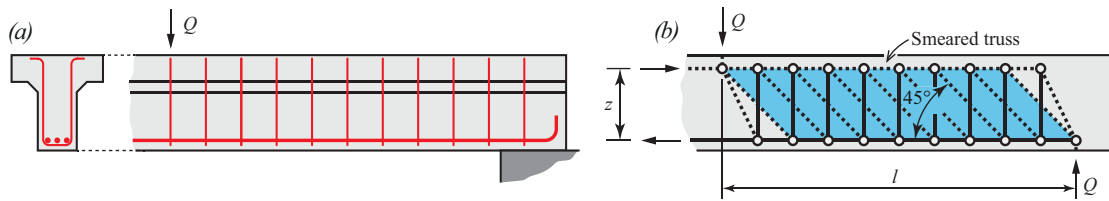


Figure 2.7: (a) RC beam with vertical stirrups tested by Mörsch; (b) smeared truss model

Truss model of Ritter was later investigated and improved by Mörsch [80], who conducted a large experimental campaign containing reinforced concrete beams with vertical stirrups (refer to Fig. 2.7a), reinforced concrete beams with inclined rebars (refer to Fig. 2.8a and c), and reinforced concrete beams with no transverse reinforcement (refer to Fig.2.9a).

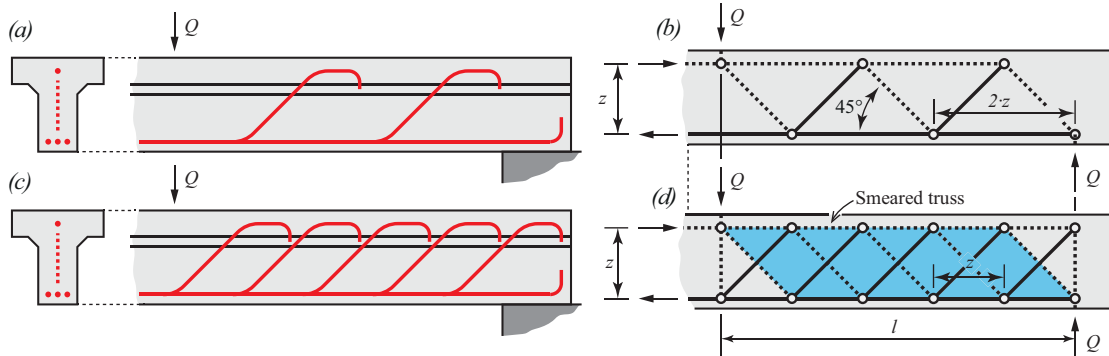


Figure 2.8: (a) RC beam with inclined rebars tested by Mörsch; (b) truss model of a beam with inclined rebars; (c) RC beam with closely spaced inclined rebars tested by Mörsch; (d) smeared truss model for beams with inclined rebars

The spacing of the transverse bars in the investigated elements was reduced compared to recommendations given by Ritter [101]. Consequently, the compression field of the beam was able to spread over the entire web of the element, leading to more efficient usage of the concrete (as presented in Fig. 2.7b). The same conclusion was obtained after conducting a similar experimental campaign involving beams with inclined rebars (notice the difference between the two trusses in Fig. 2.8b and Fig. 2.8d).

Investigation of elements with no transverse reinforcement led to a conclusion that a significant shear force can be transferred by a beam even though none of the truss load-

carrying mechanisms presented in *Fig. 2.7* and *Fig. 2.8* can be formed. Mörsch explained this by introducing a direct strut action (refer to *Fig. 2.9b*), where shear force is carried through the web by means of a single element in compression. Aside from the material properties of steel and concrete, strength of such elements mainly depends on their slenderness (ratio between l and z in *Fig. 2.9b*, later investigated by Kani [50], followed by many others [84]).

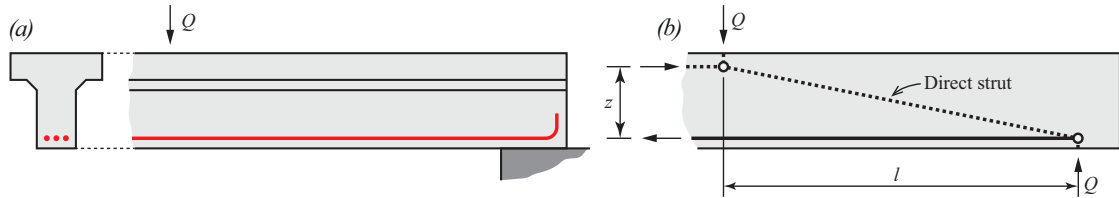


Figure 2.9: (a) RC beam without transverse reinforcement tested by Mörsch; (b) direct strut action

Mörsch also combined the direct strut action with the smeared truss model, obtaining a more realistic picture of the load-carrying mechanisms in a structural concrete beam (refer to *Fig. 2.10a*). All this finally gave birth to a new truss model (presented in *Fig. 2.10b*). As it can be seen, it implied a variable inclination of the struts as well as smaller inclination of the compression field ($\theta < 45^\circ$). Nevertheless, the truss of Mörsch was not used in practice at the time, since he himself recommended that the inclination of the concrete struts should be equal to 45° for the design purposes.

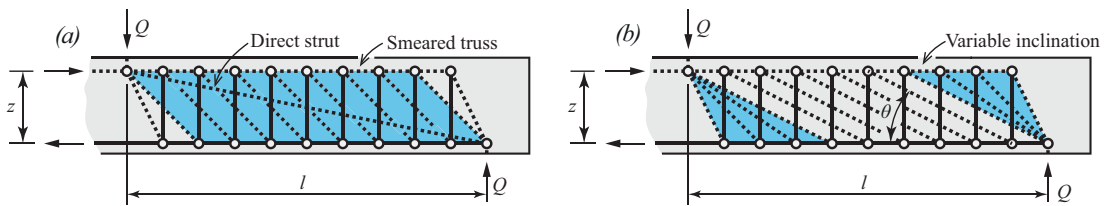


Figure 2.10: Truss models of Mörsch with: (a) smeared struts and direct strut action; (b) variable strut inclination

The practical application of variable stress fields with compressive strut direction lower than 45° was not used until the sixties when Kupfer [64] reintroduced this idea in order to reduce the material costs of newly designed reinforced concrete structures. He showed that the reduction of the stress field inclination increases the number of stirrups which are actively participating in carrying shear force, thus allowing to reduce the total area of transverse reinforcement. He also distinguished the fan region (presented in *Fig. 2.1a*) from the region having a constant stress field inclination in a reinforced concrete beam.

Truss models were later developed so that they could be used for analysing various structural concrete elements (such as deep beams, members with openings or dapped-ends, pile caps, bridge diaphragms etc.). Deriving a consistent approach for analysis of such elements was initially led by Leonhardt and Walther [69] who conducted an experimental campaign on reinforced concrete deep beams and intersecting elements. It was shown that there is no need for a load-carrying model to be an actual truss (statically determinate or indeterminate system). Instead funicular models which are in equilibrium with the applied actions are also suitable for analysis of structural concrete elements (refer to *Fig. 2.11c*). This

discovery lead towards to the development of modern strut-and-tie models which are still used today. The work of Leonhardt was later continued and generalized by Schlaich et al. [107], who focused on defining methods which can be used for defining the suitable geometry of STM. His approach was based on elastic uncracked stress field of a member (presented in *Fig.2.11b*), which can be used to determine the location of the strut and the ties (the resultant of compressive stresses corresponds to location of struts, and the resultant of tensile stresses defines the geometry of the ties, as shown in *Fig.2.11c*).

Such approach was very convenient at that time since elastic uncracked internal forces could be calculated using the photoelasticity or linear finite element method. Schlaich et al. [107] also proposed a simplification when analysing a structure with STM. Instead of developing a STM for an entire member, it is sufficient to analyse just the regions where Bernoulli-Naviers hypothesis is not respected. The rest of the member can be easily calculated using the beam theory. Hence, an element would be divided into Beam regions (B-regions) and Discontinuity regions (D-regions), as presented *Fig.2.11a*, and a STM would only be required to verify the detail close to the supports.

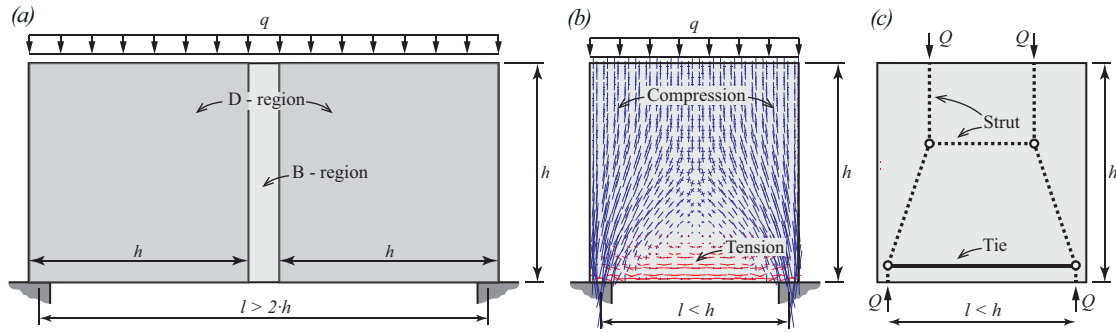


Figure 2.11: Strut-and-tie models proposed by Schlaich et al.: (a) B-regions and D-regions of a deep beam (adopted from Schlaich et al. [107]); (b) elastic uncracked stress field of a deep beam; (c) corresponding strut-and-tie model of a deep beam

The stress fields originated from a completely different basis compared to STM. It involved the direct application on the theory of plasticity based on a crude assumption that the materials do not deform until they have reached the point of yielding (refer to adopted constitutive laws in *Fig.2.12a* and *b*).

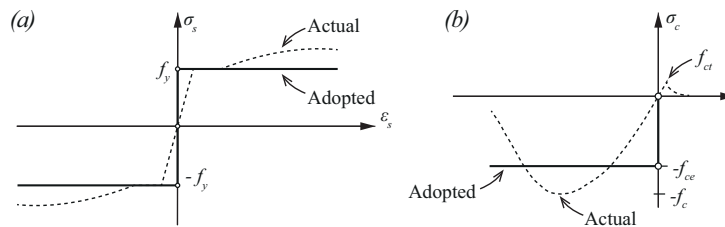


Figure 2.12: Rigid-plastic constitutive laws: (a) actual and adopted stress-strain diagram for steel; (b) actual and adopted stress-strain diagram for concrete

This assumption is acceptable in case a constitutive law shows significant deformation capacity of the material once it reached its elastic limit, such is the case with steel (refer to

actual stress-strain diagram from *Fig.2.12a*). The actual stress-strain diagram of concrete on the other hand, does not show a similar behaviour (see *Fig.2.12b*). In order to insure sufficient ductility of concrete, the actual compressive strength (f_c) has to be reduced down to effective compressive strength (f_{ce}) while the tensile strength of concrete has to be neglected (as can be seen in *Fig.2.12b*). The reduction of the concrete strength was first introduced in Denmark 1969 [91], where it was argued that the lower bound solution of theory of plasticity can give unconservative results in case unreduced concrete compressive strength is used. In 1979 Exner [30] gave the first theoretical bases for estimating the concrete compressive strength effectiveness factor. Based on the test results involving RC beams with no transverse reinforcement he introduced the following empirical expression:

$$\nu = \frac{3.2}{\sqrt{f_c}} \quad (2.1)$$

The effective concrete compressive strength would then be calculated as:

$$f_{ce} = \nu \cdot f_c \quad (2.2)$$

where f_c represents the concrete compressive strength obtained from the standard cylinder test.

The effective concrete compressive strength was later investigated by many authors (Muttoni [82, 89], Vecchio and Collins [120], Hsu [47], Pang [94], Kaufmann [52, 53], Hars [41], etc.), as it will be presented in Chapter 4 of this thesis. However, in the beginning of the 20th century when the theory of plasticity was first applied on structural concrete the ductile behaviour of elements was ensured by imposing steel yielding as the principal failure mode.

Even though the origins of the theory of plasticity can first be found in the works of Ingerlsev [48] and Johansen [49], Gvozdev [40] was the first to consistently formulate the concepts of the yield surface, upper- and lower-bound solutions as well as the flow rule (the initial publication of Gvozdev was made in 1936 and was translated in English in 1960).

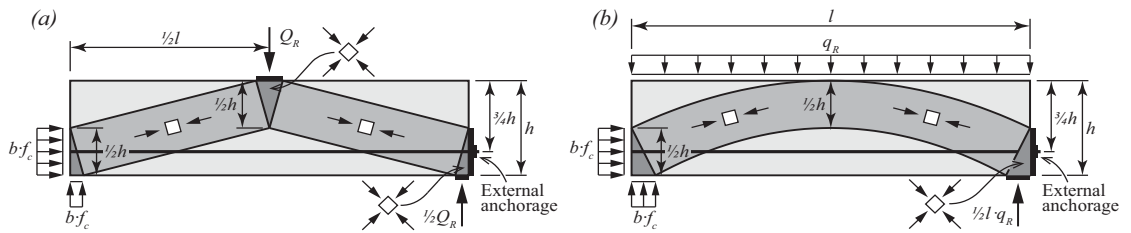


Figure 2.13: Lower-bound stress field of a simple beam: (a) subjected to point load; (b) subjected to distributed load (adopted from Drucker [27])

The theory of plasticity was later used by Drucker [27] to develop a stress field for a simply supported beam subjected to a point load (refer to *Fig.2.13a*) and distributed loading (refer to *Fig.2.13b*). Both models are in equilibrium with external action and are not surpassing the strength of applied materials (steel and concrete), meaning that they are licit lower-bound solutions. As indicated in *Fig.2.13*, light grey zones of the SF are subjected to

uniaxial compression equal to concrete compressive strength (f_c). This maximises the lever-arm of a beam, and reduces the total amount of reinforcement. Due to the fact that the tensile strength of concrete is neglected (as presented in Fig.2.12b), these zones have a constant width. Dark grey regions are subjected to equal stresses in all directions (quasi-hydrostatic stress state equal to f_{ce}), while the rest of the beam is stress free.

In addition to the lower-bound solution presented in Fig.2.13, Drucker also focused on the upper-bound solutions using a simple beam subjected to a point load (refer to Fig.2.14). Two potential mechanisms were assumed. One having completely rigid reinforcement and failing due to the concrete crushing in the mid-span and next to the external anchorage plates (as presented in Fig.2.14a), and the other assuming yielding of the reinforcement along with the concrete crushing in the mid-section of the element (as indicated in Fig.2.14c).

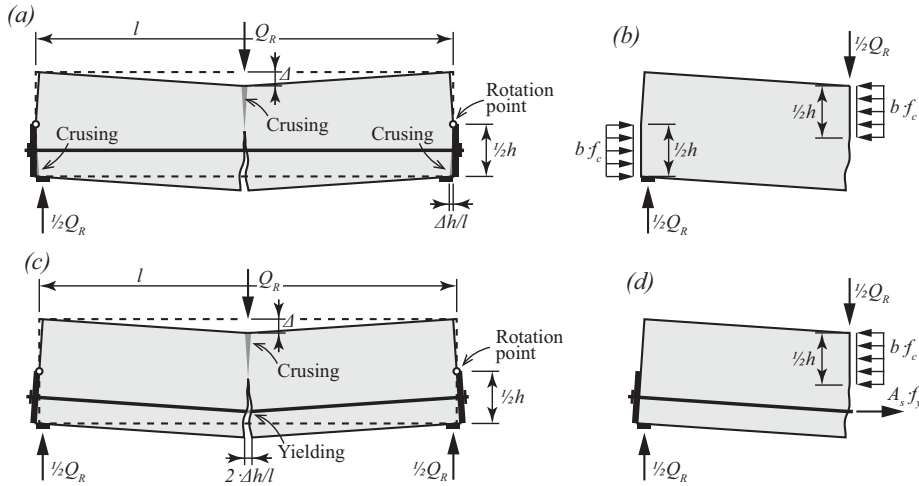


Figure 2.14: Upper-bound solution: (a) “mechanism 1” – assuming concrete crushing in the middle of the beam and concrete crushing close to the supports; (b) free-body corresponding to the “mechanism 1”; (c) “mechanism 2” – assuming concrete crushing and steel yielding in the middle of the beam; (d) free-body corresponding to the “mechanism 2” (adopted from Drucker [27])

Free-bodies corresponding to the mechanisms in Fig.2.14a and c are given on their right (Fig.2.14b and d). After expressing all the necessary displacements of the two mechanism as a function of Δ (see Fig.2.14b and d), the expression for internal and external work can be written. Drucker then showed that both mechanisms governed the same ultimate load (Q_R) which is identical to the one in equilibrium with the lower-bound stress field from Fig.2.14a, thus obtaining the exact solution according to the theory of plasticity. Even though ultimate loads derived from Drucker's exact solution were sometimes unconservative compared to experimentally obtained values (due to the fact that the concrete strength effectiveness factor was not applied, as indicated in Fig.2.12b), he established a clear theoretical bases which is still used today.

The stress fields were later developed particularly in Denmark and Switzerland. An alternative approach for obtaining the exact solution using stress fields was proposed by

Nielsen and Hoang [92]. A free body of a deep beam indicated in *Fig.2.15a* was divided into triangles having a constant stress state (regions 1 to 3 in *Fig.2.15b*).

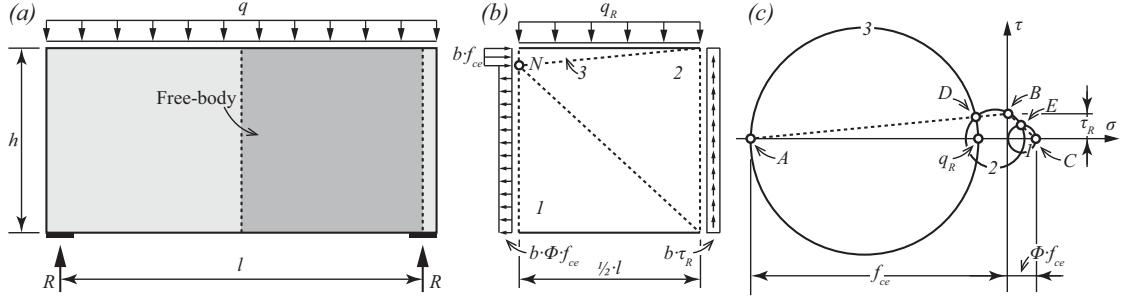


Figure 2.15: Stress field of a simply supported deep beam: (a) geometry and loading properties; (b) stress field and border stresses inside the analysed free-body; (c) stress state of each region represented with a Mohr's circle (adopted from Nielsen et Hoang [92])

As it can be seen, the analysed disk (deep beam in this case) is assumed to have plastic tensile strength, which can be determined using the degree of reinforcement (noted as Φ in *Fig.2.15b* and *c*). In order to maximize the lever arm, point N in *Fig.2.15b* should be placed high enough so that the border stress acting on the vertical surface of the area 3 is equal to f_{ce} . Once the location of this point is determined, the geometry of all three triangles is known. This can then be used to obtain the stress state of all the regions using the Mohr's circle (presented in *Fig.2.15c*). Point C represents the pole of circle 1 and point A the pole of circle 3. Lines $A-B$ and $B-C$, which are parallel to the lines separating zones 2-3 and 1-2, are used to determine the shear and normal stress acting along the borders between the zones (points D and E in *Fig.2.15c*). Once all the points are determined Mohr's circles can be drawn, and the ultimate load q_R is obtained.

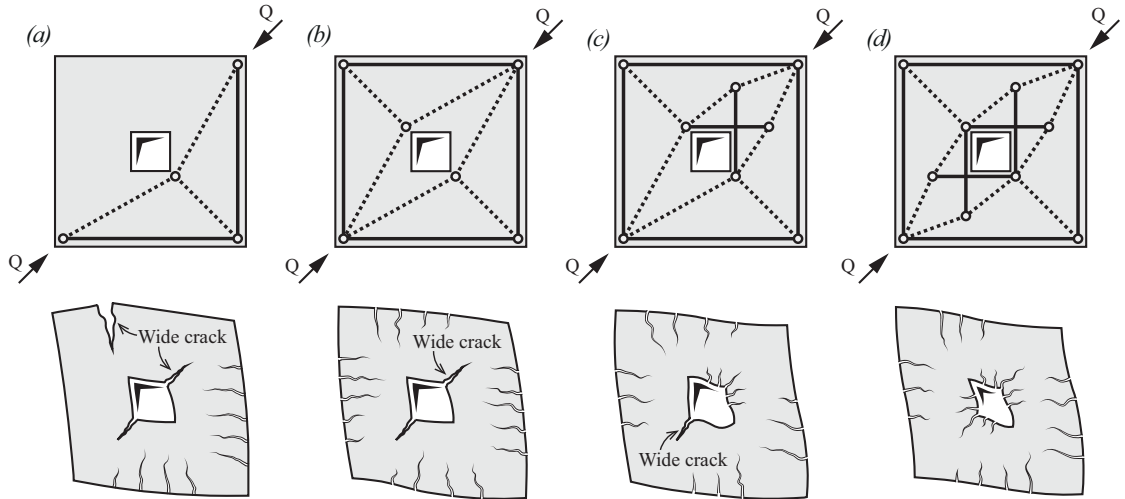


Figure 2.16: Developing a suitable stress field for a panel with an opening: (a) to (d) potential strut-and-tie models at ULS and corresponding behaviour at SLS (adopted from Muttoni [89])

Some of the most significant works in the field of stress fields and strut-and-tie models can be found in Thürlimann et al. [116], Müller [81], Marti [73] and Muttoni et al. [89] who

gave clear recommendations for the design of reinforced and prestressed concrete elements using SF method and STM, most of which can be found in codes of practice. A general procedure for the development of SF for nonstandard structural concrete members (such as elements with opening, dapped-ends or complex loading) was introduced by Muttoni et al. [89] (see Fig.2.16).

The procedure takes into account the behaviour of a member at ULS (refer to the top row in Fig.2.16) and in a qualitative manner at SLS (refer to bottom row in Fig.2.16). When talking about the ULS, all the models indicated in Fig.2.16a to d seem suitable (due to the fact that they are in equilibrium with the external loads). However, when looking at SLS it becomes clear that only the last STM shows appropriate behaviour, since some of the cracks indicated in Fig.2.16a to c are unacceptably wide. It is important to indicate that the procedure proposed by Muttoni et al. is iterative. In this sense Fig.2.16 does not show four independent models that can be used to design the same structural concrete element, but rather an evolution (refinement) of a single solution. The stress transfer mechanism should always be kept as simple as possible, and the model should be modified until the structural behaviour at ULS and SLS becomes acceptable.

In order to overcome the fact that modelling of elements with D-regions using SF and STM is time consuming and requires good engineering intuition and experience, various procedures for their automatic development have been proposed. Inspired by the approach of Dorn et al. [26] who worked on the automatic optimization of steel trusses, Kumar [62] introduced a procedure which could generate STM starting from an initial truss using the energy deformation criterion. Similar procedures then followed using different optimization criteria. Xie and Steven [125] used an algorithm which favored elements in tension based on the amount of force they carried. Biondini et al. [12] used the material volume criterion whereas Ali and White [4] focused on determining the amount of virtual work of each potential tie in the model, favouring those having minimal work as well as the ties which were placed in horizontal and vertical direction.

Starting from the work of Ali and White [4] Kostić [59] developed a procedure which transforms a STM (presented in Fig.2.17a) into a SF (see Fig.2.17b) using an algorithm that optimized the geometry of the nodal regions by imposing a pseudo-hydrostatic state of stress.

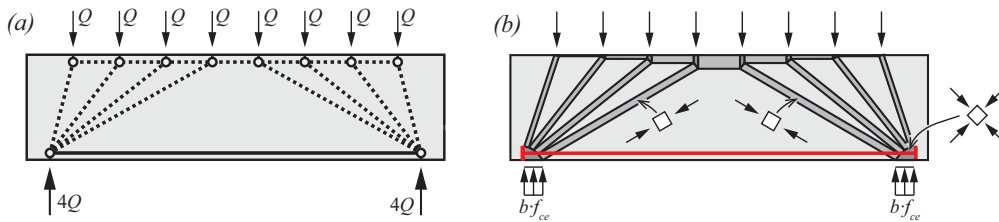


Figure 2.17: (a) Generated strut-and-tie model; (b) corresponding stress field with pseudo hydrostatic nodes (adopted from Kostić [59])

The process of automatic stress field generation was taken one step further by Fernández Ruiz and Muttoni [32] who developed the Elastic-Plastic Stress Field method (EPSF) and implemented it in a finite element program (JCONC – which has been integrated

as an applet into an educational web site <http://i-concrete.epfl.ch/>). According to this approach stress fields are obtained iteratively for each load step by assessing the stresses in concrete and reinforcement based on constitutive laws (elastic-plastic material behaviour) and imposed deformations.

Reinforcing steel is assumed to behave as an elastic-plastic material in tension and compression with the possibility to account for the strain hardening as presented in *Fig.2.18a*. It is important to mention that a small amount of strain hardening $E_h=0.33$ is automatically introduced in every model, in order to assure the numerical stability of the results. Its response is governed by the yield strength of the material (f_y), its elastic modulus (E_s) and its hardening modulus (E_h). Both can be estimated based on the actual stress-strain diagram, as indicated in *Fig.2.18a*. The strain hardening part can also be neglected in case the EPSF are used for design of structural concrete elements. However, when the ultimate strength of the existing members needs to be assessed, introduction of strain hardening modulus can significantly increase the ultimate resistance, especially when hot rolled reinforcement has been applied (since the difference between the yield and the ultimate strength of the material can be noticeable).

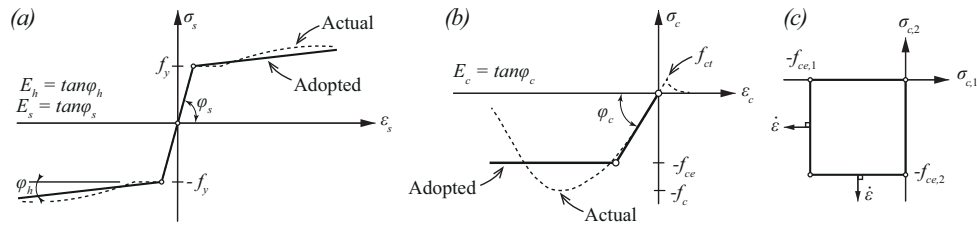


Figure 2.18: Elastic-plastic constitutive laws: (a) actual and adopted stress-strain diagram for steel; (b) actual and adopted stress-strain diagram for concrete; (c) concrete failure surface

The concrete constitutive law is presented in *Fig.2.18b*. Its behaviour under compression is assumed to be elastic-perfectly plastic, whereas its tensile strength is completely neglected. Concrete modulus of elasticity (E_c) is adopted as secant modulus of the material, and the effective concrete strength (f_{ce}) is calculated in the following manner:

$$f_{ce} = f_c \cdot \eta_{fc} \cdot \eta_\epsilon \quad (2.3)$$

where f_c represents the uniaxial concrete compressive strength measured in cylinders;

η_{fc} represents the concrete compressive strength reduction factor, which accounts for its brittle behaviour and can be calculated according to Muttoni [82,89] in the following manner:

$$\eta_{fc} = \sqrt[3]{\frac{f_{co}}{f_c}} \leq 1 \quad (2.4)$$

where f_{co} is equal to 30 MPa in case of normal strength concrete [34].

η_ϵ represents the concrete compressive strength reduction factor which takes into account the presence of transverse strains in the concrete struts, which can be evaluated on the basis of the compression-softening law proposed by Vecchio and Collins [122]:

$$\eta_\varepsilon = \frac{1}{0.8 + 170 \cdot \varepsilon_1} \leq 1 \quad (2.5)$$

where ε_1 represents the transverse strains in concrete struts.

One of the most significant advantages of the EPSF compared to RPSF, is related to the estimation of the effective concrete compressive strength (refer to Eq.2.3). Unlike the compression-softening law proposed by Vecchio and Collins (η_ε), rigid-plastic stress field approach uses fixed reduction values (v), depending on the angle between the struts and ties (see Fig.2.19). The coefficients were proposed by Muttoni et al. [89] and later adopted by MC2010 [34] and SIA262:2013 [108]. As it can be seen, compressive strength of a plain concrete which is not subjected to any imposed strains (Fig.2.19a) assumes a v value equal to 1.0, in which case the effective compressive strength is equal to the plastic concrete strength ($f_{ce} = f_c \cdot \eta_{fc}$). On the other hand, imposing the transverse strains means reducing the concrete compressive strength by the factor 0.75-0.80 in case the strains are perpendicular to concrete struts or 0.55-0.60 in case they are inclined (angle between the stress field and the reinforcement is smaller than 65 [34]).

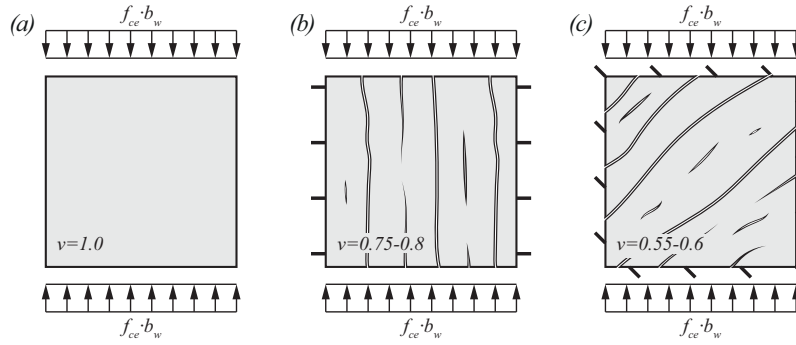


Figure 2.19: Reduction factors for concrete compressive strength in RPSF: (a) no imposed transverse strains; (b) imposed perpendicular strains; (c) imposed inclined strains

In-plane concrete strength can be represented using a Mohr-Coulomb yield surface with a tension cut-off (refer to Fig.2.18c). The effect which transverse strains have on material strength can be understood as shrinkage in the yield surface with respect to the positive transverse strain increase. It should be noted that effective concrete strength (f_{ce}) cannot be increased due to application of negative transverse strains (concrete confinement is neglected).

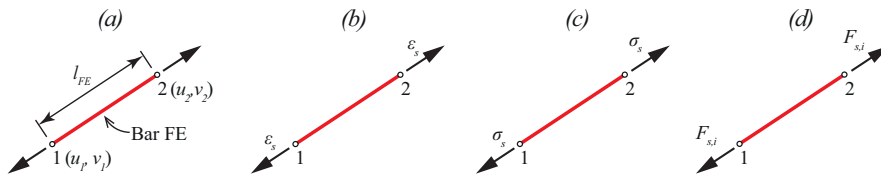


Figure 2.20: Bar finite element: (a) geometry properties and imposed nodal displacements; (b) strain state; (c) stress state; (d) nodal forces

Finally, bond between the reinforcement and surrounding concrete is assumed to be perfect, meaning that these two materials have equal strains in the direction of reinforcement ($\varepsilon_s = \varepsilon_c$) resulting in zero slip.

Implementation of the previous constitutive laws into a nonlinear finite element method analysis [32] can be performed by means of two different types of element: link elements and constant strain triangles.

Reinforcement bars and prestressing tendons are modelled using link (1D) finite elements with uniaxial behaviour (neglecting the dowel effect) as presented in Fig.2.20. Based on a given displacement and the length of a FE (refer to Fig.2.20a), strain state of the structural steel member can be obtained directly (see Fig.2.20b). This value is then used as an input parameter to determine the stress state (refer to Fig.2.20c) based on the constitutive law presented in Fig.2.18a. The stresses can then be used to determine the nodal ($F_{s,i}$) by means of simple integration over the cross-section surface of the analysed element (refer to Fig.2.20d).

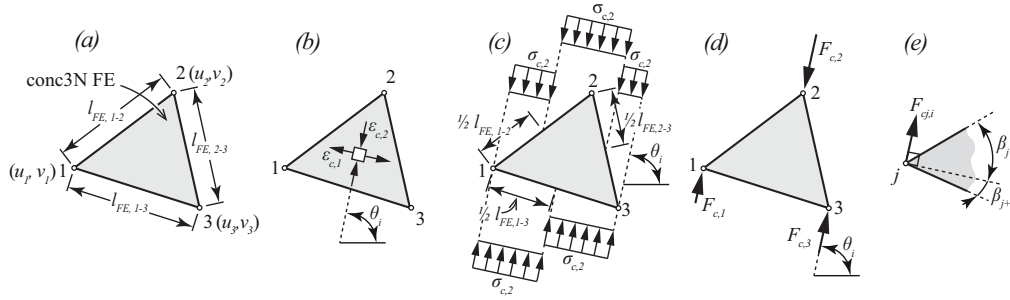


Figure 2.21: Concrete finite element: (a) geometry properties and imposed nodal displacements; (b) strain state; (c) stress state; (d) nodal forces; (e) definition of the characteristic angle β in the node j

Concrete is modelled using constant strain triangles. Once again, a displacement field is imposed on a concrete FE (refer to Fig.2.21a) which is then used to obtain a strain state (ε_x , ε_y and γ_{xy}). Using the Mohr's transformations the principle strains (ε_1 and ε_2) as well as their principle direction θ_i are obtained (refer to Fig.2.21b).

Assuming that the principal stresses are parallel to the principal strains, concrete stresses can be directly calculated (refer to Fig.2.21c) using the constitutive law defined in Fig.2.18b. Finally as presented in Fig.2.21d and e, nodal forces can be derived as following:

$$F_{cj,i} = \sigma_i \cdot \left(\frac{l_j}{2} \cdot \cos(\beta_j) - \frac{l_{j+1}}{2} \cdot \cos(\beta_{j+1}) \right) \quad i = \{1,2\} \& j = \{1,2,3\} \quad (2.6)$$

where $F_{cj,i}$ represents the nodal force in j -node and i -principle stress direction determined from a concrete FE;

$\sigma_{c,i}$ represents the concrete stress in i -principle direction;

l_j represents the length of j -side of the FE triangular;

β_j represents the characteristic angle in j -node presented in Fig.2.21e.

The iterative process for obtaining an EPSF for a given load, geometry and reinforcement layout starts with a linear elastic FEM calculation, in which both materials (concrete and steel) have infinite strength in tension and compression. This is done in order to obtain an initial displacement field, which is then imposed back to the model. This time however, the materials (concrete and steel) are assuming with an elastic-plastic behaviour (as presented *Fig.2.18*). Strains, stresses and nodal forces coming from the bar and concrete FE are obtained (as described above), after which equilibrium of each node is checked. This usually results in having some residual (un-equilibrated) forces. The intensity and the direction of these forces are then used to correct the initial displacement field, by moving the nodes at a certain rate using the Newton-Raphson algorithm. This defines a second displacement field, which is then reused in the same manner. The entire process is repeated for a predefined number of steps until a convergence is reached (a point in which residual forces become insignificant).

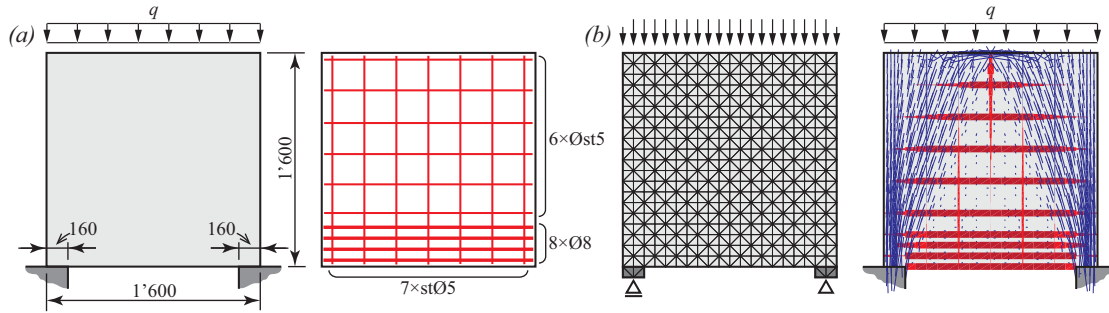


Figure 2.22: Elastic-plastic stress field method: (a) geometry properties and reinforcement layout of a RC wall tested by Leonhardt [59]; (b) corresponding FE mesh and EPSF

As described above, the method verifies the equilibrium of the system and the yield condition everywhere (lower bound theorem is respected). It also respects compatibility conditions and eventually becomes a failure mechanism (the upper bound theorem is respected). According to the theory of plasticity, this means that the final solution is the exact solution. One major advantage of the EPSF is the fact that the failure kinematics of an analysed member is clearly visible, and can be used to develop an upper bound solution according the RPSF to verify the results. An example of an EPSF is given in *Fig.2.22*. Geometry properties and the reinforcement layout of a deep beam tested by Leonhardt [69] are presented in *Fig.2.22a*. The corresponding EPSF at its ULS is given in *Fig.2.22b*. Blue lines indicate the principal concrete compressive stress direction and intensity (with their inclination and length) and the thickness of the red lines indicated the stress level in the reinforcement (dark red represents yielding).

An alternative approach to EPSF was introduced by Kuchma and Tjhin [61]. Their Computer Aided Strut-and-Tie design tool (CAST) has been used to generate the STM of elements with D-region and estimate the minimal necessary space to pass the concrete struts and place the critical nodes.

Hoogenboom [46] introduced an iterative procedure that uses linear and nonlinear stringer-panel models to optimize both geometry and reinforcement layout of a structural

concrete element, based on the maximal acceptable crack width at SLS and required design load at ULS.

Another computer aided design tool was developed by Lourenço and Almeida [71] as a part of their Adaptive Stress Field Approach, which offers a different SF for different load level. As a part of their research they conducted an advanced analysis of RC deep beams (tested by Leonhardt [69]) during which they focused on elements ductility, deformations and crack width. The method proved to be very useful when analysing structural concrete members at SLS.

Considering the practical application of stress fields and strut-and-tie models, it can be concluded that each method has its advantages. Using them in a combined manner is perhaps the most suitable approach, as both are expressing the same physical behaviour in a different manner. Stress fields can be used to determine the minimal necessary width of the struts in order to satisfy the compatibility condition, or estimate the stress state in a specific region of the structure in order to compare it to concrete strength. In addition to this they allow understanding and identifying the location where smeared reinforcement is to be arranged. The development of stress fields is thus particularly useful for detailing (required space for the struts, reinforcement bents, stresses in the nodal regions) and to account for variable angle of the compression fields (fan or constant-angle compression fields). Nevertheless, a complete development of the stress field for a structural concrete element may be too time-consuming. This becomes even more evident during the design, when an iterative procedure involving a gradual model refinement is applied. In order to overcome this, stress fields can be combined with strut-and-tie models, which in fact represent nothing else but a simplification accounting only for the resultants (forces) of the stress fields. However, a single STM can be interpreted in different manners leading to different reinforcement layout (refer to [42]). This is why a local stress field analysis of the critical concrete regions based on the final reinforcement layout needs to be conducted in order to assure a satisfactory behaviour of the structural members.

2.3 Suitable approaches for designing new structural elements with stress fields

Design of new elements should be performed in order to obtain safe structures at ULS with satisfactory behaviour at SLS while keeping the reinforcement layout as simple as possible (thus accommodating a precise and fast execution at the construction site). There are various strategies which can be used for this purpose, four of which will be presented and compared in the following section.

The methods can be used separately or be combined, depending on the given case. The selection of the most suitable approach should be decided by the designer based on his/her experience, the complexity of the problem and the required level of accuracy of the analysis.

2.3.1 Design models inspired by the existing cases

Design of new structural elements is often performed based on their loading and geometrical analogies to some well-known solutions found in literature. This will be presented using a practical example given in *Fig.2.23a*, where a deep beam with an opening (first used by Schlaich et al. [107]), is loaded with 2'000 kN concentrated force.

In a very simplistic manner, this element can be considered as a dapped-end beam (neglecting the presence of vertical and horizontal member around the opening), which allows the application of a STM as indicated in *Fig.2.23b*. Consequently, the tension and compression forces can be estimated (refer to *Tab.2.1*), which governs the amount of necessary reinforcement. In case further refinement of the model is required, the load-carrying mechanism can be improved by taking into account the contribution of the column and the coupling beam around the opening (see *Fig.2.23b*). This results in strut-and-tie model presented in *Fig.2.23c*, which once again allows a simple design of the main reinforcement (refer to *Tab.2.1*).

Comparing the STM models from *Fig.2.23b* and *c* one can see that the amount of the main reinforcement (the ties around the opening and the tie on the bottom of the deep beam) is quite similar. However, the second model does provide some reduction in the amount of the reinforcement in the upper point of the wall while in the bottom point, reinforcement has to be provided to respect SLS requirements. As already indicated, whether this difference is sufficient enough to invest the additional time for its development or not depends on the responsible designer. The resulting reinforcement layout (using the mixed STM from *Fig.2.23c*) is given in *Fig.2.23d*. The assumed design yield strength of the reinforcement is equal to 435 MPa.

Table 2.1: Forces corresponding to the strut-and-tie models from *Fig.2.23b* and *c*

Struts "S"	Force [kN]	Struts "S"	Force [kN]	Struts "S"	Force [kN]	Ties "T"	Force [kN]	Ties "T"	Force [kN]
<i>S1</i>	-946	<i>S7</i>	-638	<i>S13</i>	-591	<i>T1</i>	691	<i>T7</i>	311
<i>S2</i>	-632	<i>S8</i>	-844	<i>S14</i>	-837	<i>T2</i>	620	<i>T8</i>	461
<i>S3</i>	-911	<i>S9</i>	-576	<i>S15</i>	-606	<i>T3</i>	593	<i>T9</i>	83
<i>S4</i>	-597	<i>S10</i>	-322	<i>S16</i>	-1460	<i>T4</i>	99	<i>T10</i>	433
<i>S5</i>	-1460	<i>S11</i>	-207	-	-	<i>T5</i>	289	<i>T11</i>	509
<i>S6</i>	-665	<i>S12</i>	-248			<i>T6</i>	691	-	-

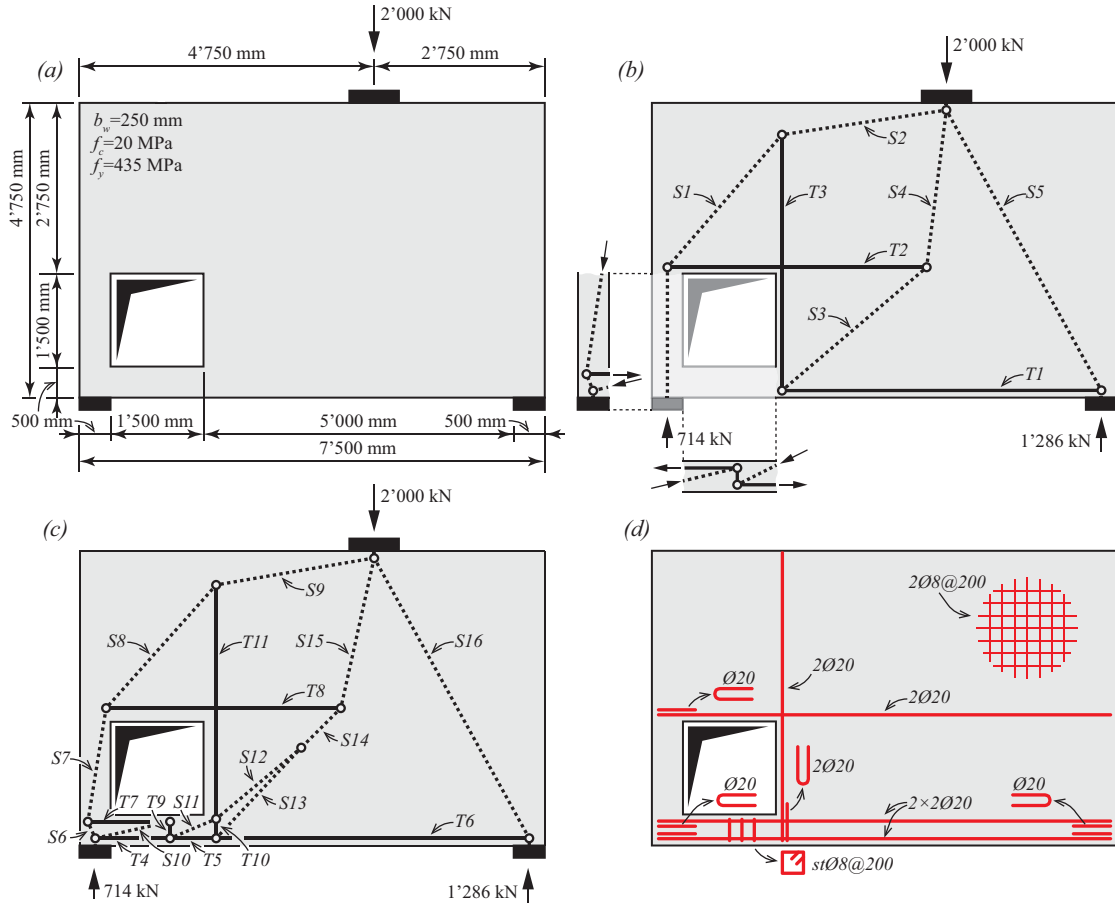


Figure 2.23: Developing a design model based on analogies with the existing solutions: (a) geometry and load properties of the analysed element; (b) strut-and-tie model of a dapped-end detail combined with the contribution of the column and beam around the opening; (c) merged model; (d) reinforcement layout

Some of the nodes ($S6-S10-T4$, $S6-S7-T7$, $S7-S8-T8$, $S13-T5-T6-T10$ and $S16-R-T6$) are placed in the proximity of the elements surface, meaning that the anchorage of the reinforcement needs to be sufficient enough to assure the required force transfer [13]. In order to do that, the U-shaped re-bars having the same diameter as the once from the main reinforcement (dimeter $\varnothing 20$ in this case) are placed in the nodal regions (see Fig.2.23d). The reinforcement is usually completed with a minimum smeared reinforcement in order to control the cracking and to allow spreading of the concentrated loads (refer to the ground mesh of Fig.2.23d). Applying the minimal reinforcement increases the load-bearing capacity of the element. Even though this reinforcement can be taken into account in the STM (making it more accurate), having some reserve in the ultimate strength is considered as positive when designing new elements. Over its expected lifetime, a structure might change its purpose (which imposes different load conditions), or experience unexpected events that could jeopardise its integrity. Both situations would benefit from unaccounted load-carrying mechanisms. When developing STM suitable for design, it is important to keep in mind that from a practical point of view exact solutions do not necessarily give the most satisfying

results since they leave very little space for human errors that can occur during the construction phase and can be time consuming to develop and validate.

2.3.2 Design models based on deviated thrust lines

Another manner to design the element from *Fig.2.23a* consists of drawing the “ideal” STM which would carry the forces to the supports in the most direct manner, regardless of the actual geometry of the member. Such model is presented in *Fig.2.24b*.

This clearly indicates parts of STM that are violating the boundary condition of the element (strut *S1* in this case, since it is passing through the opening). After extracting the free-body (as indicated in *Fig.2.24a*), and making sure that it is in equilibrium, suitable reinforcement should be placed in order to deviated the struts while making sure that they remain within the available concrete.

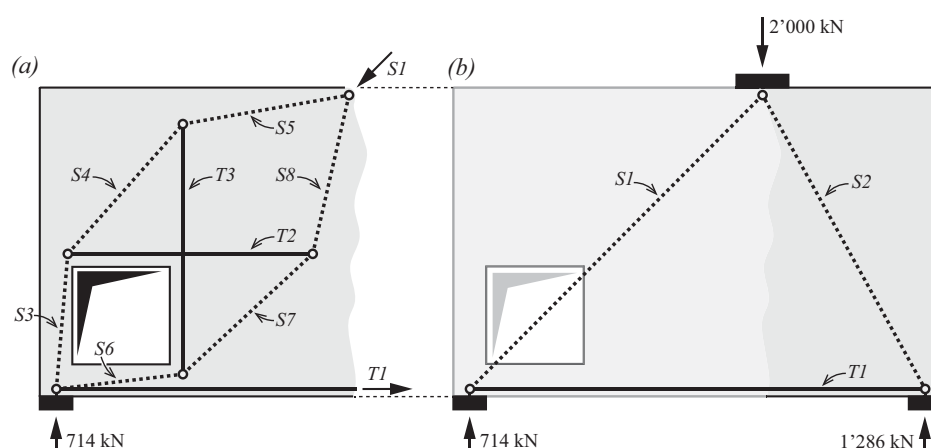


Figure 2.24: Developing a design model for a deep beam with an opening using the deviated thrust lines: (a) STM spreading the strut around an opening; (b) funicular STM

The internal forces corresponding to the STM from *Fig.2.24* are given in *Tab.2.2* and can be used to determine the reinforcement layout, similar to the one presented in *Fig.2.23d*.

Table 2.2: Forces corresponding to the strut-and-tie models from *Fig.2.24*

Struts “S”	Force [kN]	Struts “S”	Force [kN]	Ties “T”	Force [kN]
<i>S1</i>	-944	<i>S5</i>	-575	<i>T1</i>	691
<i>S2</i>	-1460	<i>S6</i>	-644	<i>T2</i>	510
<i>S3</i>	-634	<i>S7</i>	-871	<i>T3</i>	510
<i>S4</i>	-845	<i>S8</i>	-606	-	-

Deviating thrust line method has been acknowledged as a general tool for developing stress fields, especially for the cases where direct analogy with a known solution is not so evident. However, not every funicular shape which is in equilibrium with external loads is automatically acceptable. The development process is iterative, and in order to obtain a model with acceptable behaviour at ULS and SLS, four following cases should absolutely be avoided:

1. Having zones without reinforcement where tensile stresses are expected;
2. Having unacceptably low angles between the struts and the ties;
3. Having STM with TTT nodes (see Fig. Fig.2.26d);
4. Having uncontrolled cracking related to anchorage issues.

The first problem is presented in Fig.2.25b. It shows a model where the primary tension tie located above the opening (disregarding the lower part of the structure). The proposed solution is statically admissible (the internal forces are in equilibrium). However, in order to activate the assumed STM, large flexural cracks may develop in an unsuitable manner within the unreinforced region (refer to *Crack 1* in Fig.2.25b). Even in case the reinforcement for crack control is placed below the tie, *Crack 1* might still be unacceptably wide. In order to avoid such cases, Muttoni et al. [89] proposed their iterative approach described in Fig.2.16. For the case presented in Fig.2.25a, this means qualitative analysis of the crack pattern (given in Fig.2.25b) and adapting the reinforcement layout until more suitable structural response is achieved. In other words, another tie needs to be added below the opening (as presented in Fig.2.23d or Fig.2.24).

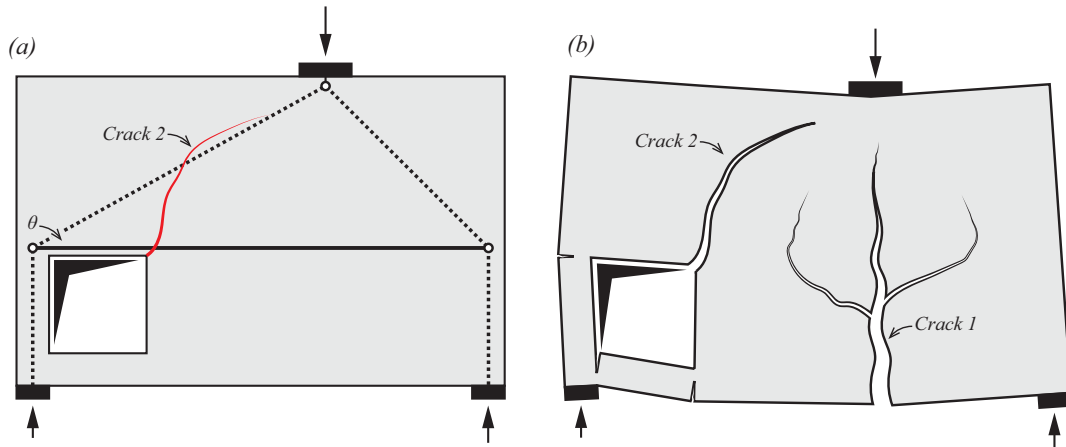


Figure 2.25: Potential problems of a STM neglecting the presence of lower part of the wall:
(a) statically admissible solution; (b) corresponding deformed shape

The second issue regards the limit of the angle between the struts and the ties in STM, and is presented in Fig.2.25 (refer to *Crack 2*). When no compatibility conditions are accounted (assuming for instance a rigid-plastic material behaviour) and if no transverse reinforcement is available, the angle between the struts and the ties should usually be considered larger or equal than 45° (refer to Muttoni et al. [89]). In case the transverse reinforcement is present in a model, the angle between the struts and the ties can be reduced. However, the angle between struts and ties (named θ in Fig.2.25a) should not be lower than 20° - 25° . This limit is grounded by Grob [39] on the fact that otherwise the strain state of the member (tension in the reinforcement and compression in the concrete) can otherwise become incompatible, requiring large tensile strains as well as crack widths to develop (refer to *Crack 2* in Fig.2.25a and b). This potentially reduces the effective concrete compressive

strength (ν reduction factor to be exact, refer to *Fig.2.19*) below the conventional thresholds (0.55-0.6 in this case), resulting in an un-conservative estimation of elements load capacity.

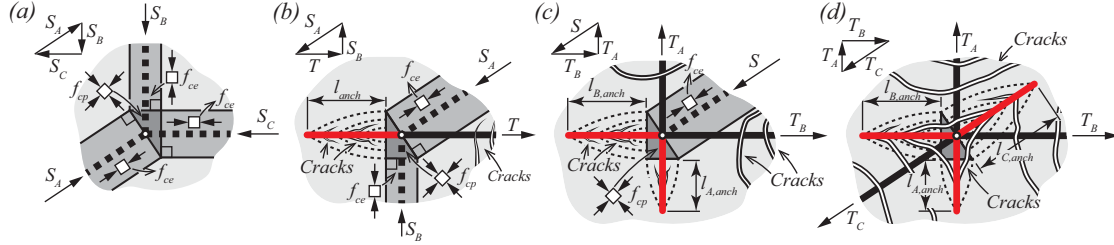


Figure 2.26: Nodal regions of RPSF: (a) Compression-Compression-Compression (CCC); (b) Compression-Compression-Tension (CCT); (c) Compression-Tension-Tension (CTT); (d) Tension-Tension-Tension (TTT)

Application of RPSF implies using four different types of nodes presented in *Fig.2.26*: CCC, CCT, CTT and TTT (where C refers to compression and T to tension). CCC nodes (see *Fig.2.26a*) can be used in design without any restrictions. As shown by Tepfers [115], each tie induces cracking of the surrounding concrete matrix, caused by steel-to-concrete stress transfer mechanisms. This occurs along tie's anchorage length (refer to red ties in *Fig.2.26b* to *d*), as well as it's body (refer to black ties in *Fig.2.26b* to *d*), which consequently reduces the effective concrete compressive strength (see *Fig.2.19b* and *c*). Providing that each tie has sufficient anchorage length, and that the minimum angles between the struts and the ties are respected (as previously discussed), CCT and CTT nodes can be used. On the contrary, TTT (Tension-Tension-Tension) nodes (presented in *Fig.2.26d*) should absolutely be avoided. This is justified by the fact that large crack widths can potentially develop inside the nodal region, leading to very low values of the strength reduction factor ν . Each time a TTT node is present in a load-carrying model, the topology has to be modified in order to avoid such kind of node. Prestressing of at least one of the ties could also be an acceptable solution.

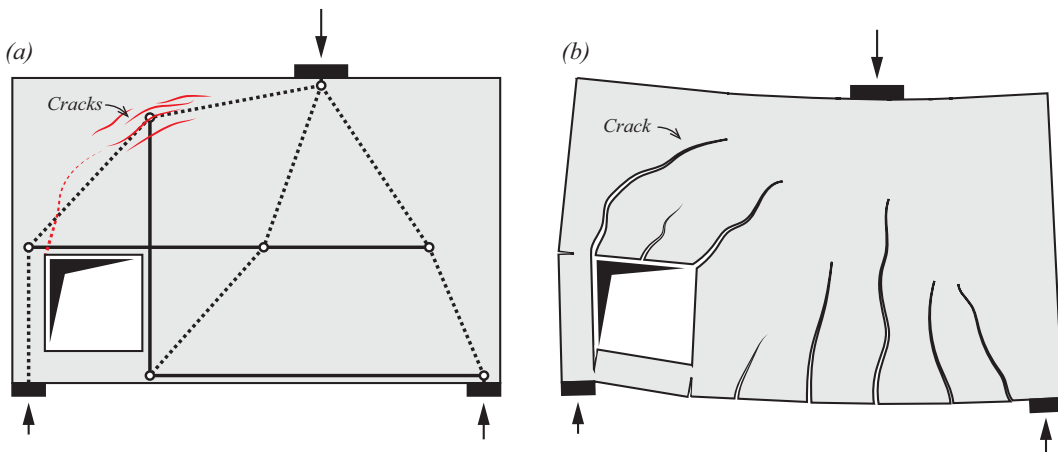


Figure 2.27: Potential problems of a STM resulting in a reinforcement layout without any crack control reinforcement: (a) statically admissible solution; (b) corresponding deformed shape

As discussed by Schlaich et al. [107] or Muttoni et al. [89], the strut-and-tie model has to consider that compression in concrete tends to occupy all available space following the St-Venant's principle. This is particularly significant with respect to the introduction of concentrated loads [14], and should be also considered for the anchorage of tension ties. For instance, *Fig.2.27* presents a load-carrying model where the vertical tension tie is anchored within the element but not at its edge.

As experimentally shown by Maxwell [77], this may lead to development of wide cracks on top of the anchorage region, since the strut tends to occupy all available concrete (unreinforced anchorage region of the vertical tie, indicated in *Fig.2.27a*). These cracks ultimately join with the crack that originates from the top left corner of the opening (see *Fig.2.27b*) forming a kinematically admissible mechanism.

2.3.3 Design models inspired by elastic uncracked stress fields

A classical approach to development of strut-and-tie models was early investigated by Leonhardt [69] and later refined by Schlaich [107]. The approach considers the elastic uncracked stress field analysis of a member (refer to *Fig.2.28a*) and arranges the reinforcement following the location, the direction, and the intensity of the tensile stresses (as presented in refer to *Fig.2.28b*).

This method generally gives a conservative solution with respect to its ULS as well as a satisfactory behaviour at SLS due to the fact that the deformation of the tensile zones is controlled by the reinforcement.

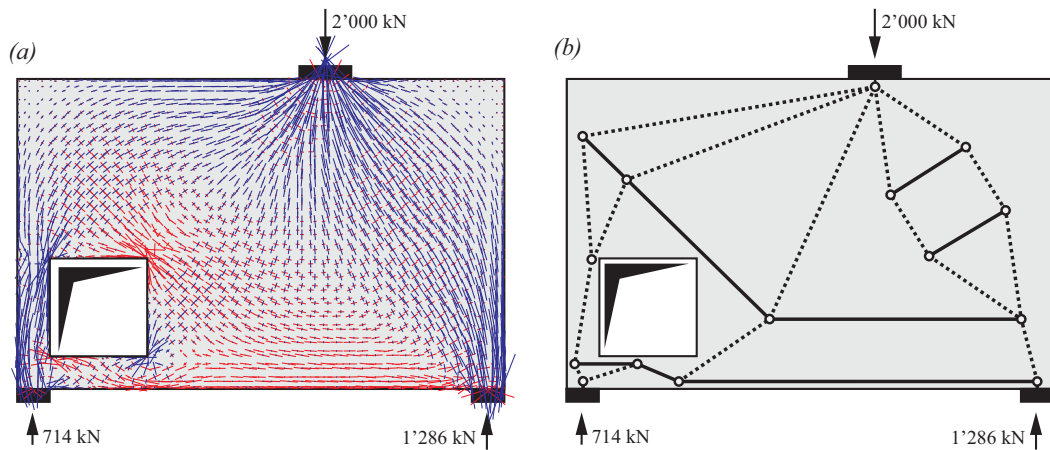


Figure 2.28: Element design inspired by an elastic uncracked behaviour: (a) elastic uncracked stress field of a deep beam with an opening; (b) corresponding STM

Nevertheless, this approach does have a few weak points:

1. The location and arrangement of the reinforcement is not decided by the designer. Following the distribution of elastic stresses inside an uncracked member leads to application of inclined bars which may be difficult to put in place and inspect at the construction site (see *Fig.2.28b*). Nonetheless such reinforcement layout assures a positive behaviour.

2. The method leads potentially to TTT nodes (for instance for corner frames with opening moments), which need to be avoided in design.
3. Finally, the amount of required reinforcement is not necessarily the minimum required for equilibrium reasons. This is for instance the case when imposed strains are considered as actions (imposed strains can be dissipated provided that the member has sufficient ductility). Also, this results from the location of the tension ties, which are generally more efficient when placed at the outermost fiber of the member respecting concrete cover to maximize the lever arms (as presented in *Fig.2.29c*), rather than at the resultant of the uncracked stress field (see *Fig.2.29a* and *b*). In a similar manner, placing the concrete strut in the resultant of compressive stresses leads to reduction of the lever arm, and thus increases the required amount of reinforcement for the design.

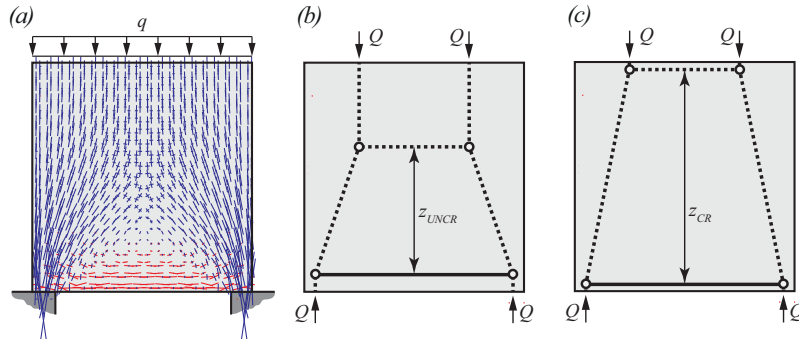


Figure 2.29: (a) Uncracked elastic SF of a deep beam subjected to uniformly distributed load; (b) STM resulting from the uncracked elastic SF; (c) STM resulting from a plastic SF

2.3.4 Design models inspired by cracked stress fields

More suitable stress fields that can be used to develop consistent load-carrying models accounting for the cracked behaviour of concrete using advanced constitutive material models. Fernández Ruiz and Muttoni [32] proposed a simple elastic-plastic stress field approach, accounting for the cracked behaviour of concrete. This can be seen as a simplification of a more general constitutive model that leads to suitable results when sufficient transverse reinforcement is available to avoid crack localization. *Fig.2.30a* shows an EPSF of previously investigated deep beam with an opening (see *Fig.2.23a*). The EPSF clearly indicates the location of the compression field (its intensity is presented using blue lines with different length) and intensity of tensile forces carried by the reinforcement (dark red indicates yielding of the steel).

As shown in [32], cracked SF can be used to develop strut-and-tie models (or rigid-plastic stress fields) the same way elastic uncracked SF were used by Schlaich et al. [107]. However, the results of the EPSF can also be directly applied for the design and optimization of the reinforcement given a fact that they already represent a licit stress field. An approach to optimize the reinforcement layout and amount has been also presented by Fernández Ruiz and Muttoni [32]. Starting from a preliminary analysis where a minimum reinforcement required for the crack control ($A_{si,min}$) is arranged according to the designers preferences (for example

the orthogonal mesh from Fig.2.30a), the stress state of the reinforcement can be calculated for each bar FE (σ_{si}). In the next step, the area of the reinforcement (A_{si}) can then be updated so that the steel stress does not violate the yield strength of the material:

$$A_{si,j} = A_{si,j-1} \frac{\sigma_{si}}{f_{yi}} \geq A_{si,min} \quad (2.7)$$

where f_{yi} represents the yield strength of the reinforcement;

i represents the bar FE number;

j represents the iteration number ($j = 2$ is the first iteration, while $j = 1$ is the initial step corresponding to $A_{si,min}$).

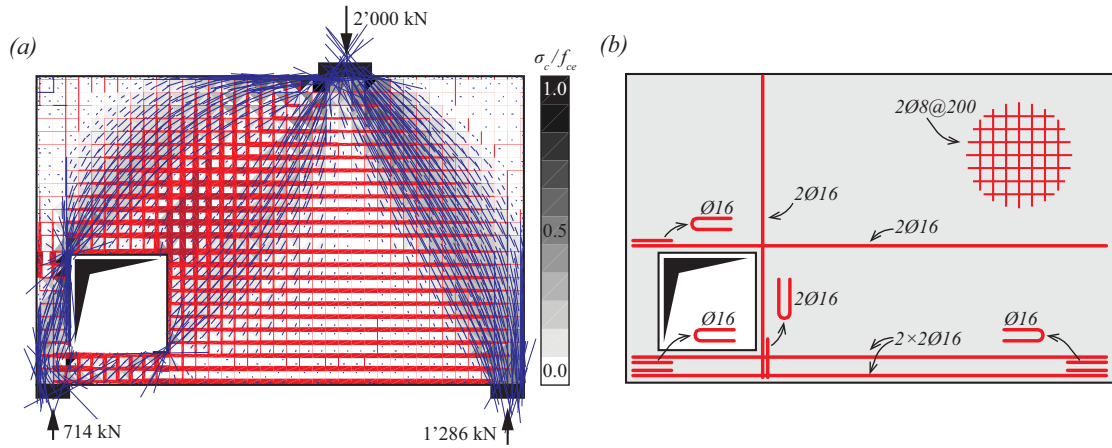


Figure 2.30: Design of a deep beam with an opening using the EPSF method: (a) EPSF of fully cracked element; (b) resulting reinforcement layout

With the updated reinforcement area, the EPSF analyses can be repeated until the solution converges to a final reinforcement layout, such as the one presented in Fig.2.30b (assuming design yield strength of the reinforcement equal to 435 MPa). The final rebar diameter is slightly increased to round it to available commercial value (Ø8 and Ø16 in this cases), which introduces some reserve of the ultimate strength. The required number of iterations to attain the final solution is quite low, and the method is robust for its practical application (investigated by Kostić [59]).

Unlike previous approaches, where minimum crack control reinforcement ($A_{s,min}$) was added in the end of the calculations to assure a positive behaviour of the model at SLS and ULS, the EPSF considers it from the beginning. In this manner, its contribution to resist the applied design loads is taken into account, which leads to potential savings of the reinforcement amount. Finally, taking advantage of the compatibility conditions of the EPSF, the final reinforcement layout can be also analysed at serviceability limit state, both for deflections and cracking.

2.4 Suitable approaches for assessing the ultimate strength of structural concrete elements with stress fields

In case an existing structure is subjected to increased loads, requires retrofitting or is deteriorated after several decades of usage, its structural assessment is usually performed. In addition to this, estimation of a load-carrying capacity is also required when new code provisions become more severe compared to the existing ones, making the structural assessment more and more common in modern engineering practice.

Nonetheless structural retrofitting is an expensive and complicated procedure that involves a number of constraints during its physical execution. Therefore, estimating the load-carrying capacity of existing structures is directed towards avoiding or minimizing the necessary interventions. As already stated in the beginning of this chapter, the modelling process can be performed following a Levels-of-Approximation approach [85], starting with simple load-carrying models and refining them whenever the obtained structural resistance proves to be insufficient.

During the process of structural design, even when using rational approaches that were previously presented, some elements are not considered within the load-carrying model. This usually refers to the minimal reinforcement for crack control. Nevertheless, this additional reinforcement should be considered as part of the load-carrying mechanism for an assessment, since it increases the strength of the member in potentially non-negligible manner (especially when analysing RC walls with significant quantity of crack control reinforcement). In addition to this, design based on lower-bound solutions according to limit analysis (such as stress fields or strut-and-tie models) implies that more efficient load-carrying mechanisms may develop within the member for the available geometry and reinforcement (which was graphically presented in *Fig. 2.4h*).

In case conventional analyses do not allow ensuring sufficient strength with respect to the design actions, refined estimates of the strength are required. In this case, it means selecting a lower-bound solution that gives the highest possible resistance according to the limit analysis, in other words exact solution (refer to *Fig. 2.4h*). Different techniques can be used to obtain it, and in the following section two approaches will be examined:

1. The one based on rigid-plastic stress field approach;
2. The one based on elastic-plastic stress field approach.

As for design, strength assessment will be presented using a practical example. Therefore, a deep beam with an opening from *Fig. 2.23a* will be analysed assuming the reinforcement layout presented in *Fig. 2.23d*.

2.4.1 Assessing the ultimate strength using a rigid-plastic stress field approach

The use of rigid-plastic stress fields combined with mechanisms for the search of an exact solution has been discussed by Muttoni et al. [89]. This can be performed by selecting a licit collapse mechanism (upper-bound solution) whose free bodies are separated with discrete

cracks and concrete hinges as presented in *Fig.2.31a*. According to the upper-bound theorem of the theory of plasticity, all rebars crossing the cracks have already reached their yield strength, which means that the intensity of the forces in the ties at ultimate limit state can be directly calculated (refer to *Fig.2.32* and *Tab.2.3*). The contact zones between the free bodies are considered as compression zones, which accommodate the development of the struts or the nodal regions. There are two methods to calculate the load-carrying capacity of a given mechanism:

1. Using the work equation, where the work of external loads (sum of scalar product of external forces and related displacements) has to be equal to the internal plastic dissipation (sum of all reinforcement yielding forces and concrete forces multiplied by their elongation or shortenings);
2. Finding the equilibrium of every free-body.

With respect to the second method, solving the equilibrium equations of every free body can be performed by:

1. Following an iterative procedure based on optimizing the thrust -lines inside the free-bodies;
2. Determining the contact forces between the free-bodies and then solving a system of equations relating all the implied variables.

In order to qualitatively define the crack length and the location of the compressed zones of the assumed failure mechanism, detailed analysis of its kinematic behaviour is conducted and presented in *Fig.2.31c*.

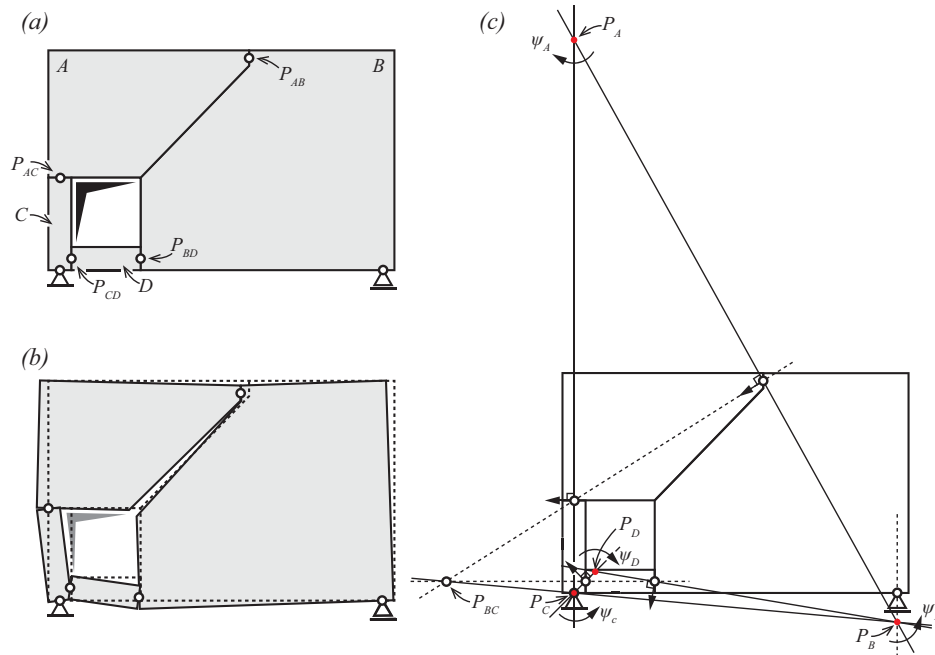


Figure 2.31: Kinematical analysis of an assumed failure mechanism: (a) rigid plates A to D; (b) corresponding deformed shape; (c) plan of rotation poles

The deep beam is separated in four rigid-plates (marked as A , B , C and D in *Fig.2.31a*), whose intermediate poles of rotation (P_{AB} , P_{BD} , P_{CD} and P_{AC}) are indicated using white circles. Red circles in *Fig.2.31c* present the rotation poles of each rigid plate which were determined using the Arnold-Kennedy's Theorem. According to it, three intermediate rotation poles of the rigid plates have to lie on a straight line, and have to be between the poles of the corresponding plates. Once the rotations Ψ_A , Ψ_B , Ψ_C and Ψ_D are known, the crack opening can be qualitatively defined (as presented in *Fig.2.31b*). The internal forces associated to reinforcing bars can then be calculated directly (refer to *Fig.2.32* and the *ties* of the free-bodies A , B , C and D in *Tab.2.3*). However, since the exact depth of the compression zones between the free-bodies is not known, nor is the precise location and the direction of the compression forces (see the struts S_{AB} , S_{AC} , S_{CD} and S_{BD} in *Fig.2.32*), the system has to be solved through iterations.

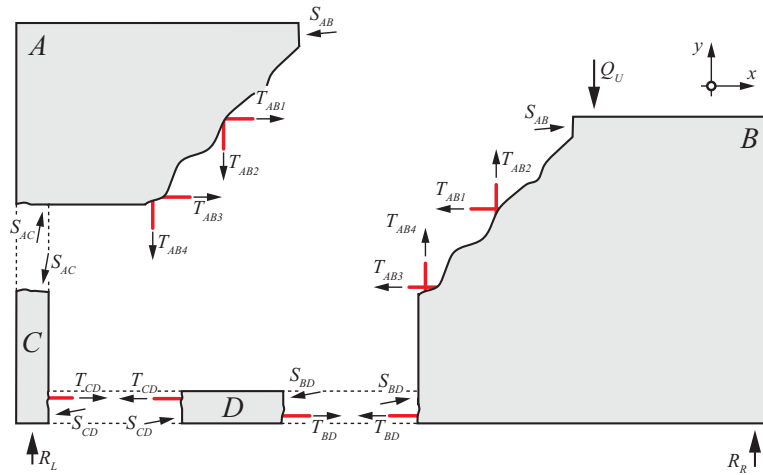


Figure 2.32: Free-body equilibrium of parts A to D

Looking back at the *free-body A*, presented in *Fig.2.33a*, the intensity of the internal forces S_{AB} and S_{AC} as well as the location of points A and B can be calculated on the basis of the concrete compressive strength (refer to *Fig.2.33b*).

Using the kinematic considerations from *Fig.2.31c*, it can be concluded that at the ULS, strut S_{AB} has to touch the upper surface of the deep beam and that the strut S_{AC} has to touch the top left corner of the deep beam opening (as is presented in *Fig.2.33a*).

As a first approximation in this case, it can be assumed that the force S_{AC} is vertical, which allows determining the moment equilibrium for the point A , whose location is also known since the intensity of S_{AB} can be obtained from an equilibrium of forces in the horizontal direction. This allows calculating the shear strength of the free body A, which can also be determined by using the force diagram shown in *Fig.2.33b* (the represented diagram relates to the final result where S_{AC} has a horizontal component). The same approach can be followed for the other free bodies. In the case of free body D , the steel forces T_{BD} and T_{CD} are known (reinforcement at yielding). It can be assumed (as a first approximation) the axial force of the coupling beam is negligible (which is consistent with the previous assumption that S_{AC}

is vertical). Thus, the horizontal component of concrete forces S_{BD} and S_{CD} can be calculated (equal to T_{CD} and T_{BD}) and vertical component is assumed equal to 0. The next step could be the investigation of body C which allows calculating the force at the left support (R_L) and the horizontal component S_{AC} . The latter is however not compatible with previous assumptions so that a second iteration step is needed. To do so, the horizontal component of the force S_{AC} increases the shear strength of the free body A as the shear span is reduced (as presented in Fig.2.33a). However, it also reduces the shear strength of the free body D as a tensile normal force acts now on the coupling beam. The iterative process is finished when the calculated horizontal component of S_{AC} from equilibrium of the free-body C equals the assumed value for investigating body A . Once the iterations are completed, equilibrium can be checked investigating the equilibrium of body B , and therefore the load-carrying capacity of the member (Q_U) is obtained (refer to Tab.2.3 to see the intensity of analysed struts and ties after the 1st and final iteration). This check can also be done by developing the force diagrams (refer to Fig.2.33b) which is also called the Cremona diagram.

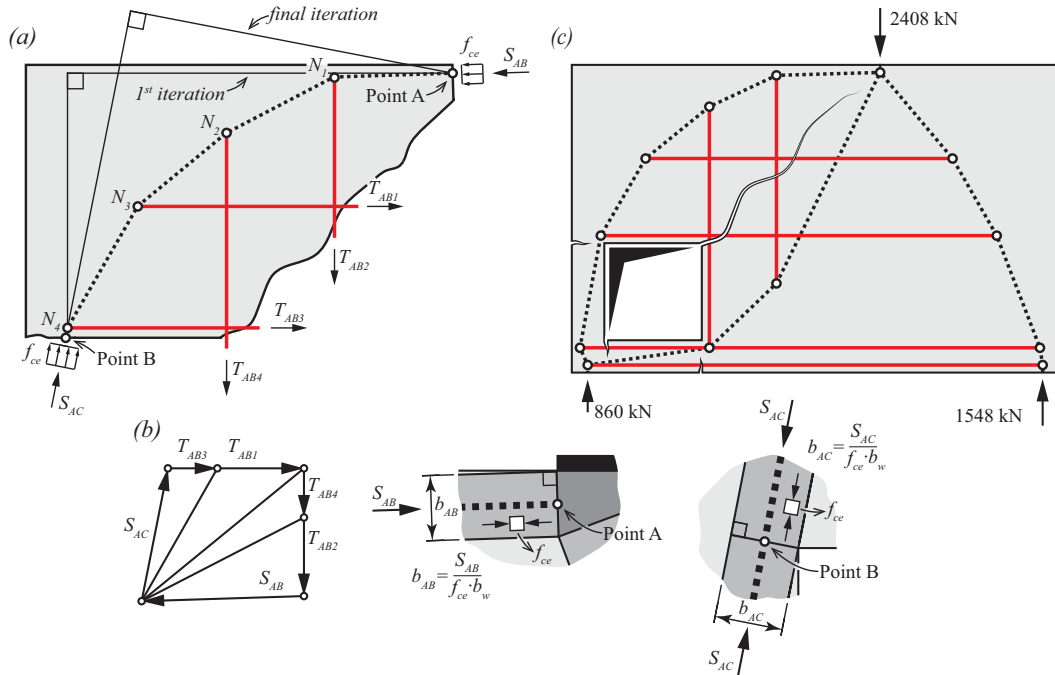


Figure 2.33: Verifying equilibrium and boundary conditions of an assumed mechanism: (a) analysis of the A free-body using RPSF approach; (b) cremona diagram of the thrust lines inside the free-body and RPSF details of points A and B; (c) resulting STM

Alternatively, the contact forces between the free-bodies can be determined directly, without the need of performing any iterations. This holds true as the 12 unknown force components (two components of each of the four contact forces S_{ij} plus the load-carrying capacity Q_U and the three reactions of the statically determinate system, refer to Fig.2.32) can be calculated using the 12 equilibrium conditions (3 for each of the four free bodies). In addition to this, the location of the points A and B can be calculated on the basis of the width of the struts (b_{AB} and b_{AC} in Fig.2.33b) in the following manner:

$$b_{ij} = \frac{S_{ij}}{b_w \cdot f_{ce}} \quad (2.8)$$

where b_w represents the width of the wall;

S_{ij} represents the compressive force in a strut between the free-bodies i and j ;

f_{ce} represents the effective concrete compressive strength (as defined in Eq.2.3 using ν reduction factor presented in Fig.2.19 instead of η_e).

Table 2.3: Forces corresponding to the strut-and-tie models from Fig.2.32 and 2.33

Free body	Struts "S"	Force 1 st iteration [kN]	Force final iteration [kN]	Ties "T"	Force 1 st iteration [kN]	Force final iteration [kN]
"A"	$S_{AB,x}$	-754	-897	T_{AB1}	481	481
	$S_{AB,y}$	71	-28	T_{AB2}	-437	-437
	$S_{AC,x}$	0	143	T_{AB3}	273	273
	$S_{AC,y}$	639	738	T_{AB4}	-273	-273
"B"	$S_{AB,x}$	754	897	T_{AB1}	-481	-481
	$S_{AB,y}$	-71	28	T_{AB2}	437	437
	$S_{BD,x}$	590	447	T_{AB3}	-273	-273
	$S_{BD,y}$	0	122	T_{AB4}	273	273
	R_R	1150	1548	T_{BC}	-590	-590
	Q_U	-1789	-2408	-	-	-
"C"	$S_{AC,x}$	0	-143	T_{CD}	590	590
	$S_{AC,y}$	-639	-738	-	-	-
	$S_{CD,x}$	-590	-447			
	$S_{CD,y}$	-275	-122			
	R_L	639	860			
"D"	$S_{CD,x}$	590	447	T_{CD}	-590	-590
	$S_{CD,y}$	275	122	T_{BD}	590	590
	$S_{BD,x}$	-590	-447	-	-	-
	$S_{BD,y}$	-275	-122			

The load carrying capacity Q_U of the selected mechanism (presented in Fig.2.31a), calculated by any of the previous procedures, is still not proved to be corresponding to that of the exact solution according to limit analysis, as other potential mechanisms (such as the one shown in Fig.2.34b) can develop. As this procedure is based upon the upper-bound theorem of limit analysis, the exact load carrying capacity ($Q_{U,exact}$) could be lower than the calculated value Q_U . An interesting approach to verify if the selected mechanism corresponds to the exact solution can be performed by combining both theorems of limit analysis. As stated by Drucker [27]: "agreement of upper and lower bounds proves that the load carrying capacity is exactly halved". This procedure can be seen as an optimization where the criterion is related to the load-carrying capacity.

In our example, this can be done by developing a stress fields (STM) inside the investigated element in order to verify if the boundary conditions, as well as the strengths of steel and concrete elements will be respected. This is shown in Fig.2.33a and c. The location of the node N_4 can be determined by using the direction of the forces S_{AC} and T_{AB3} . After solving the nodal equilibrium, a similar procedure can be used to obtain the location of the

node N_3 . The strut deviates at every intersection with the reinforcement, until it reaches the internal force S_{AB} on the opposite side of the free-body A . Provided that the compression fields remain within concrete (as is the case in Fig.2.33c), a licit solution will have been obtained.

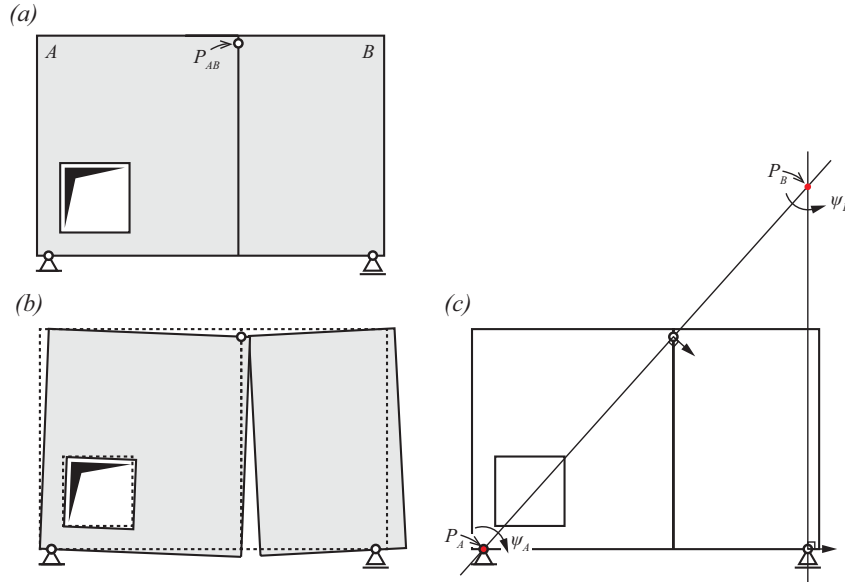


Figure 2.34: Kinematical analysis of an assumed failure mechanism: (a) rigid plates A and B; (b) corresponding deformed shape; (c) plan of rotation poles

On the contrary, when the calculated stress field leads to compression forces developing where no concrete is available (as it is presented in Fig.2.35b), the selected mechanism is not corresponding to the exact solution and the ultimate strength is overestimated ($Q_U = 3'201$ kN).

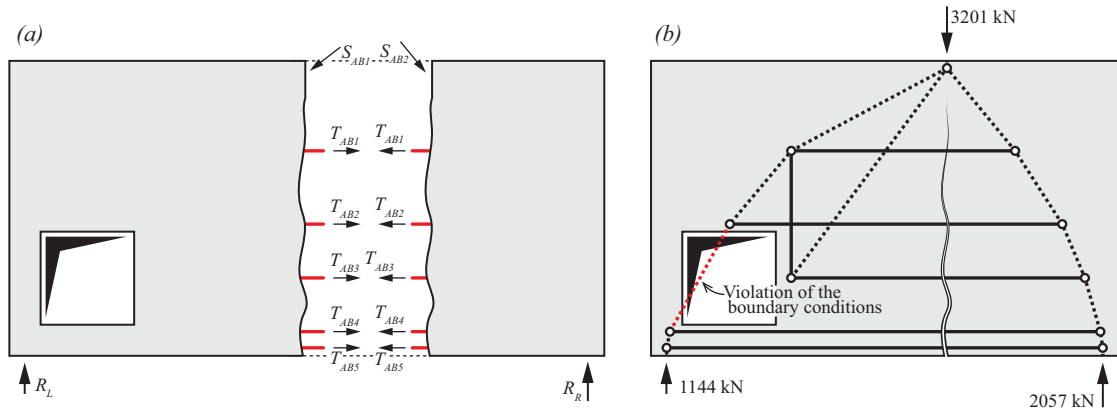


Figure 2.35: (a) Free-body equilibrium of parts A and B; (b) corresponding STM

In this cases, other mechanisms have to be investigated. The kinematics of the corresponding mechanism is presented in Fig.2.34, which shows the discontinuity lines (in Fig.2.34a), deformed shape of the deep beam in Fig.2.34b and plan of the rotation poles for the rigid plates A and B in Fig.2.34c. As it was the case with the mechanism analyzed in

detail from *Fig.2.31a*, the ultimate force corresponding to the kinematics from *Fig.2.34a*, can be determined through iterations or by solving a system of equations (having 8 unknown in this case). The intensity of the contact forces presented in *Fig.2.35a* can be found in *Tab.2.4*.

The obtained result (from *Fig.2.33c*) for the reinforcement layout of *Fig.2.23d*, leads to a failure load of 2'408 kN. This result is above the original design load of 2'000 kN and shows a strength reserve of 20%. This is due to the fact that:

1. The selected strut-and-tie model for design of the main reinforcement is a lower bound;
2. Necessary reinforcement was rounded (increased) to the next available commercial rebar diameter;
3. The minimum reinforcement amount was not considered to contribute to the beam's strength (contrary to the EPSF approach for design shown in *Fig.2.30b*).

Table 2.4: Forces corresponding to the strut-and-tie models from *Fig.2.35* and *2.34*

Free body	Struts "S"	Force [kN]	Ties "T"	Force [kN]
"A"	$S_{AB1,x}$	-1700	T_{AB1}	435
	$S_{AB1,y}$	-1144	T_{AB2}	370
	R_L	1144	T_{AB3}	305
	-	-	T_{AB4}	295
			T_{AB5}	295
"B"	$S_{AB2,x}$	1700	T_{AB1}	-435
	$S_{AB2,y}$	-2057	T_{AB2}	-370
	R_R	2057	T_{AB3}	-305
	-	-	T_{AB4}	-295
			T_{AB5}	-295

2.4.2 Assessing the ultimate strength using elastic-plastic stress field approach

Despite the generality of the approach explained in the previous section, obtaining a solution following a rigid-plastic approach might be time-consuming. It requires iterations to solve as well as the analysis of more than a single failure mechanism. In addition to this, sometimes it is not so evident how a potential failure mechanism might develop due to complex geometry of the element and its loading conditions. In case of over-reinforced structures, where elements can potentially fail due to the crushing of the concrete, the analysis of an upper-bound solution becomes even more challenging.

A suitable alternatively overcoming this shortcoming is the development of elastic-plastic stress fields, that can be used to obtain exact solutions according to limit analysis in an automated and time-efficient manner. This type of stress field considers an elastic behaviour for concrete and steel (following their elastic stiffness) until the plastic plateau is reached. No tensile stresses are also considered for concrete. This type of stress field, since it accounts for the conditions of a lower-bound solution (equilibrium and yield conditions) but also for the compatibility of displacements (stress field calculated on the basis of a displacement field), allows obtaining exact solutions in an automated manner. In addition to this, the effective

concrete compressive strength (refer to *Eq.2.3*) is estimated in a much more consistent manner, using the Vecchio and Collins softening equation [120], unlike the ν reduction factors proposed for the rigid-plastic stress field approach (see *Fig.2.19*).

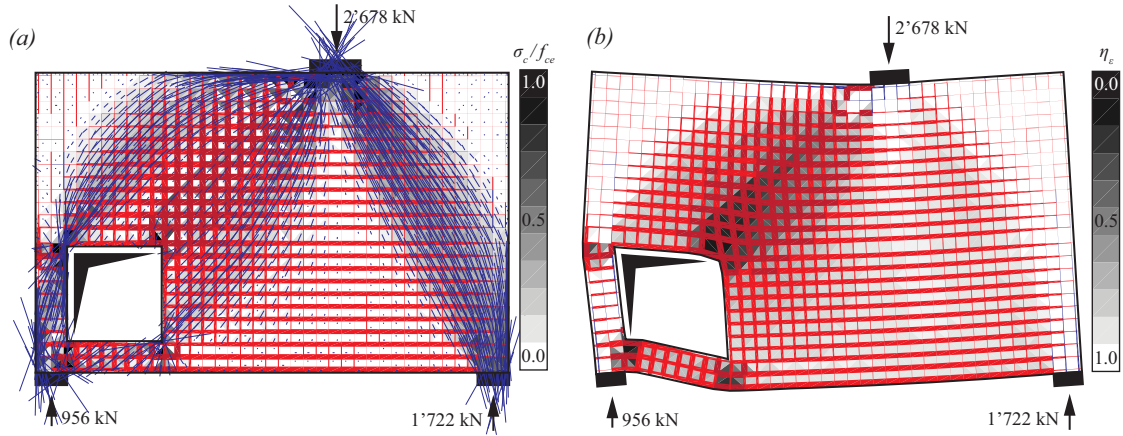


Figure 2.36: Exact solution obtained using the EPSF approach: (a) stress fields; (b) corresponding kinematics

This is for instance shown in *Fig.2.36* where the elastic-plastic stress field (*Fig.2.36a*) and its corresponding displacement field (*Fig.2.36b*) are presented for the investigated member using the reinforcement layout of *Fig.2.23d*. The blue lines indicate the intensity and the direction of the concrete stresses whereas the thickness of the red lines represents the label of stress in the reinforcement, with dark red lines indicating yielding. The dark surfaces in *Fig.2.36b* show the concrete compressive strength reduction according to Vecchio and Collins [120], marking more significant reduction (which translates into increased transverse strains of the concrete and therefore more damage) with darker shades of grey.

The failure load according to the EPSF method is 2'678 kN. The difference with respect to the mechanism calculated using the rigid-plastic approach can mostly be explained by the vertical reinforcement of the column at the left-hand side of the opening (which was neglected for the rigid-plastic analysis) and by the role of the compression reinforcement (also neglected for the rigid-plastic analysis shown previously). It can also be noted that the computed failure mechanism (from *Fig.2.36b*) nicely agrees with the selected mechanism at failure for the rigid-plastic analysis.

2.5 Collected database and validation of the elastic-plastic stress fields

In order to investigate the accuracy of the EPSF method and explore the limits of its applicability for analysis of structural concrete elements, a database containing 315 reinforced and prestressed concrete elements (such are beams, corner frames, dapped-ends, diaphragms and walls with and without openings) was assembled and placed online at <http://i-concrete.epfl.ch/epsf/epsf.html>.

The database contains finite element models of all 315 members, which are available for download, and can be used to further explore the structural behaviour of the members by focusing on deformations, failures mechanism, inclination of the compression field in the elements, etc. The investigations have shown that the kinematics of the EPSF models were always in agreement with the test results, and so was the ultimate strength. The average ratio of the actual failure load to predicted one is equal to 1.04 with a fairly low value of the coefficient of variation ($CoV = 0.10$ considering all the tests), as it can be seen in *Fig.2.37*. *Tab.2.5* gives a summary of the online database.

Table 2.5: Summary of the Online Database

N°	Ref.	Type :	N°of el.	Cross-section	Loading
1	Vecchio et Shim, 2004 [122]	RC	9	Rec. CS	3PB
2	Yoon, Cooc et Mitchell, 1996 [126]	RC	9	Rec. CS	3PB
3	Sagaseta et Vollum, 2011 [104]	RC	7	Rec. CS	3PB/CLCB
4	Mansur et al., 1991 [72]	RC	8	Rec. CS	CLCB
5	Hong et all., 2002 [45]	RC	7	Rec. CS	4PB
6	Sørensen., 1974 [110]	RC	10	T CS	4PB
7	Leonhardt et Walter, 1963 [68]	RC	16	T CS	4PB
8	Kaufmann et Marti, 1996 [54]	RC	4	TT CS	PB
9	Nagrodzka-Godycka et Piotrkowski, 2012 [90]	RC	12	Dapped-end	4PB
10	Mata Falcón, 2015 [76]	RC	50	Dapped-end	3PB
11	Chan, 1979 [19]	RC	8	Dapped-end	3PB
12	Khan, 1981 [55]	RC	9	Dapped-end	3PB
13	Cook, 1987 [23]	RC	3	Dapped-end	3PB
14	Zhu et all., 2003 [128]	RC	6	Dapped-end	3PB
15	Herzinger, 2007 [43]	RC	18	Dapped-end	4PB
16	Campana et Muttoni, 2011 [17]	RC	13	Corner el.	PB
17	Placas, 1969 [96]	RC	23	Rec. CS + T CS	3PB
18	Bach et al., 1980 [8]	RC	12	T CS	4PB
19	Leonhardt et Walter, 1966 [69]	RC	2	Rec. CS	SBCL
19	Leonhardt et Walter, 1966 [69]	RC	2	Cross-beam	3PB
20	Leonhardt et all., 1968 [70]	RC	5	Cross-beam	4PB
21	Baumann, Rüschi, 1970 [9]	RC	7	Cross-beam	4PB
22	Saqan et Frosch, 2009 [105]	PC	9	Rec. CS	3PB
23	Kaufman et Ramirez, 1988 [51]	PC	6	TT CS	4PB

24	Kuchma, D. et al., 2008 [60]	PC	19	TT CS	SBCL
25	Rupf et Muttoni, 2012 [103]	PC	13	TT CS	CLCB
26	Fernández Ruiz et Muttoni, 2008 [31]	PC	6	TT CS	4PB
27	Moore, 2014 [79]	PC	11	TT CS	3PB
28	De Wilder K. et al., 2015 [25]	PC	6	TT CS	4PB
29	Leonhardt et al., 1973 [66]	PC	3	Cross-beam	3PB
30	Büeler et Thoma, 2010 [15]	PC	2	Cross-beam	3PB
RC: Reinforced concrete		PC: Prestressed concrete			
Rec. CS: Rectangular cross section		Dapped-end: Dapped end beam			
T CS: T cross section		Cross-beam : Crossed beams elements			
TT CS: Double T cross section					
3PB: Three-point bending		PB: Pure bending			
4PB: Four-point bending		SBCL: Simple beam continuous load			
CLCB: Concentrated load on a continuous beams					

The results from *Fig.2.37* are presented in function of four physical parameters (concrete compressive strength, average prestress, longitudinal and transversal reinforcement ration).

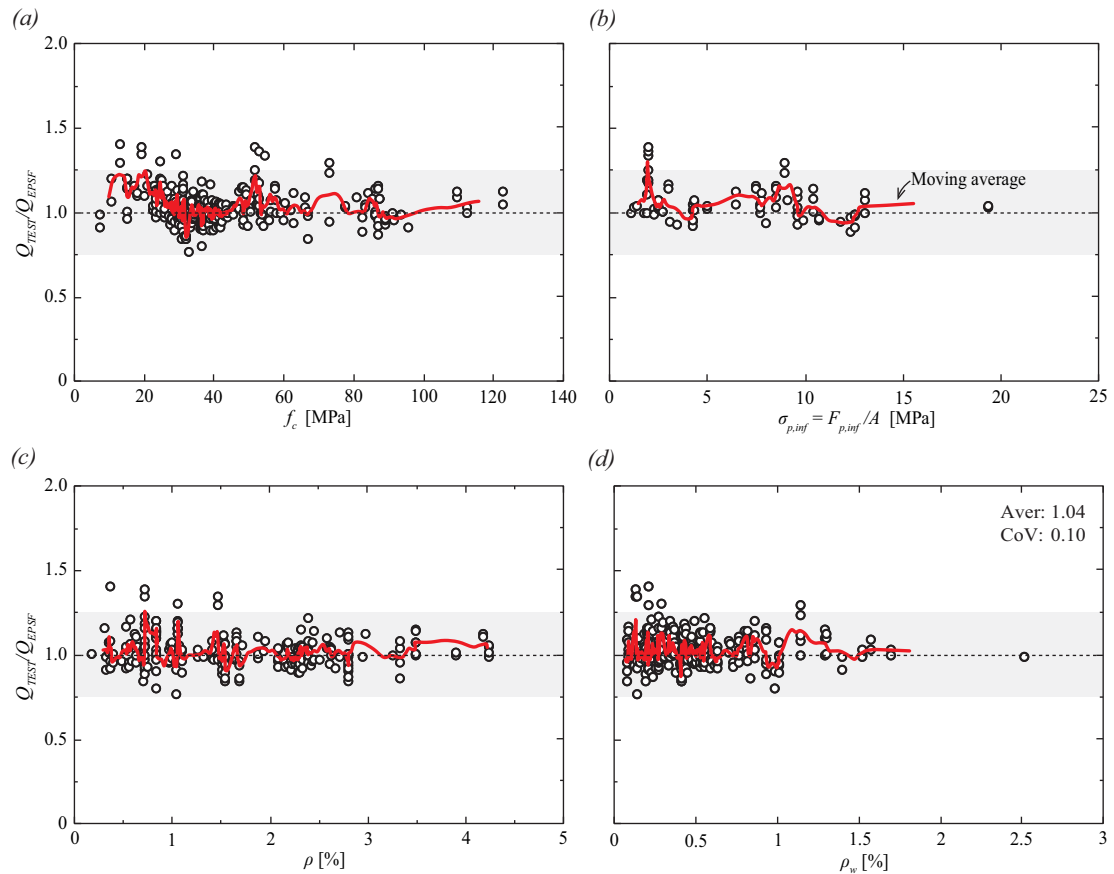


Figure 2.37: Ratio of measured and estimated strength of the elements from the online database using the EPSF method in function of: (a) concrete compressive strength; (b) initial prestress; (c) longitudinal reinforcement ratio; (d) transversal reinforcement ratio

Each of the graphs contains a red line, which was obtained by computing an average value of the five nearest points in each graph (averaging values on both axis). This “moving average”, as it was named, facilitates observing any trends in the results. As it can be seen no trends have been noted in the results despite the wide range of physical parameters, investigated by numerous researchers from different institutes (which makes the results even more satisfying due to the fact that certain level of scatter caused by human error or various types of measurement equipment is already present).

Tab.2.6 gives the results of EPSF analysis of each experimental campaign (average and coefficient of variation). Once again it can be seen that the EPSF prediction of the ultimate resistance is sufficiently accurate for all investigated cases. Elements which failed in compression due to the spalling of the concrete cover (refer to dapped-end beams in the online database), required application of link finite elements that introduce the fracture energy of concrete back into the system (refer to Mata Falcón 2015 [76] for further details).

Table 2.6: Synthesis of the EPSF results

Nº	Ref.	$Q_{\text{test}}/Q_{\text{EPSF}}$	CoV
1	Vecchio et Shim, 2004 [122]	1.03	0.05
2	Yoon, Cooc et Mitchell, 1996 [126]	0.95	0.07
3	Sagaseta et Vollum, 2011 [104]	1.03	0.09
4	Mansur et al., 1991 [72]	0.99	0.06
5	Hong et all., 2002 [45]	1.06	0.05
6	Sørensen., 1974 [110]	1.16	0.06
7	Leonhardt et Walter, 1963 [68]	1.11	0.06
8	Kaufmann et Marti, 1996 [54]	1.03	0.03
9	Nagrodzka-Godycka et Piotrkowski, 2012 [90]	0.98	0.07
10	Mata Falcón, 2015 [76]	0.99	0.07
11	Chan, 1979 [19]	1.02	0.05
12	Khan, 1981 [55]	1.03	0.07
13	Cook, 1987 [23]	0.99	0.04
14	Zhu et all., 2003 [128]	1.06	0.07
15	Herzinger, 2007 [43]	0.99	0.06
16	Campana et Muttoni, 2011 [17]	0.97	0.06
17	Placas, 1969 [96]	1.04	0.14
18	Bach et al., 1980 [8]	1.14	0.12
19	Leonhardt et Walter, 1966 [69]	1.02	0.04
19	Leonhardt et Walter, 1966 [69]	1.02	0.04
20	Leonhardt et all., 1968 [70]	1.01	0.04
21	Baumann, Rüsch, 1970 [9]	1.06	0.06
22	Saqan et Frosch, 2009 [105]	1.23	0.10
23	Kaufman et Ramirez, 1988 [51]	1.07	0.07
24	Kuchma, D. et al., 2008 [60]	1.09	0.07

25	Rupf et Muttoni, 2012 [103]	1.06	0.05
26	Fernández Ruiz et Muttoni, 2008 [31]	0.98	0.05
27	Moore, 2014 [79]	1.00	0.07
28	De Wilder K. et al., 2015 [25]	0.98	0.04
29	Leonhardt et al., 1973 [66]	1.05	0.03
30	Büeler et Thoma, 2010 [15]	1.01	0.01
Total:		1.04	0.10

However, it can be seen that the EPSF method gives conservative results for a few elements ($Q_{test}/Q_{EPSF} > 1.25$). These were the members, which had no transverse reinforcement (Saqa and Frosh [105]), or had very low concrete compressive strength (less than 15 MPa). Limit analysis is not applicable in the first case, since members experienced crack concentration (refer to Campana [16]), and the concrete quality of element in the second case was not well documented.

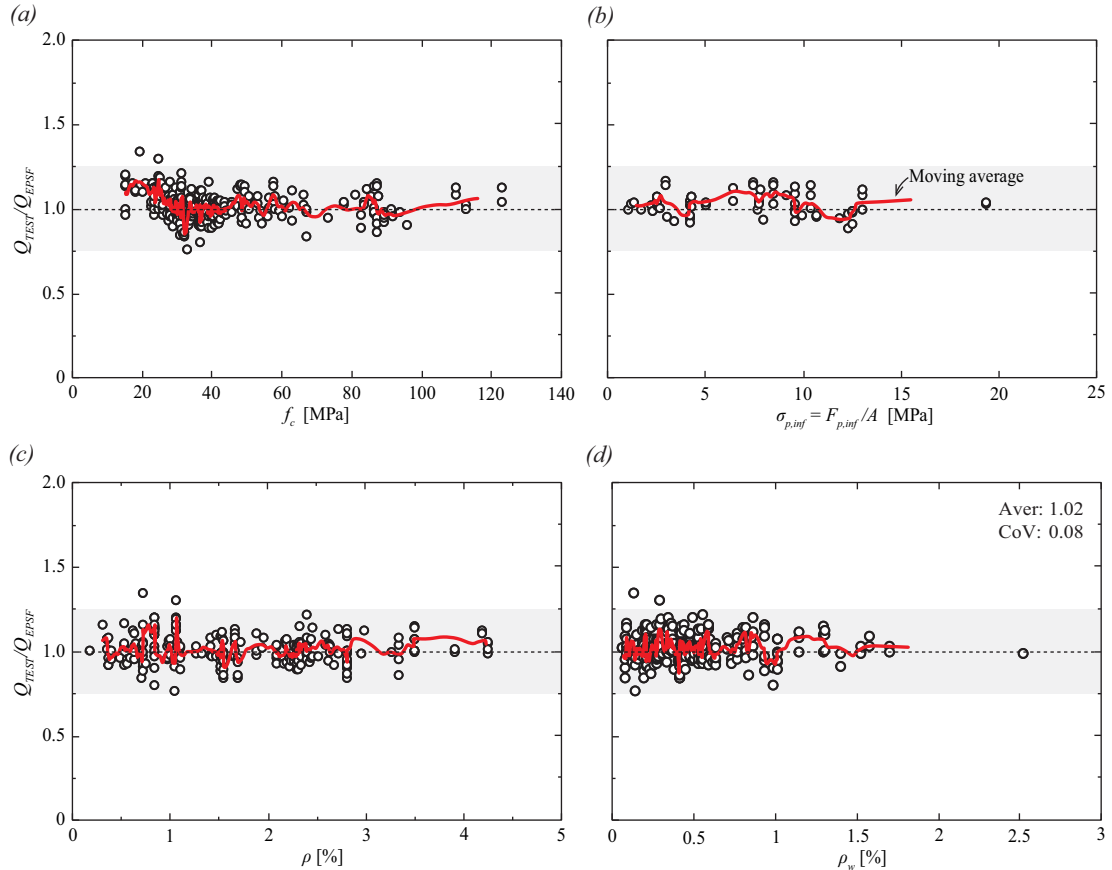


Figure 2.38: Selected EPSF results from the Database presented in function of: (a) concrete compressive strength; (b) initial prestress; (c) longitudinal reinforcement ratio; (d) transversal reinforcement ratio

After taking such elements out from Fig.2.37, the results become even better (average Q_{test}/Q_{EPSF} is equal to 1.02 with 0.08 CoV, as presented in Fig.2.38). The two remaining models with slightly conservative results are beams with significant doweling action

(Sørensen [110] and Placas [96]). Once again, no trends in the results have been observed, thus confirming the generality and accuracy of the approach.

It is important to emphasise that the current database is the results of the collective work of multiple PhD students who applied the EPSF during their research at IBETON (Structural Concrete Laboratory, at École Polytechnique Fédérale de Lausanne in Switzerland): Kostić [59], Campana [16], Rupf [103], Mata-Falcon [76], Argirova [6, 7], Moccia [79] and myself (all the models have been revised by the author). The main reason for assembling a database containing work of multiple authors is to assure the generality of the approach before introducing it into every-day engineering practice. In this manner additional user related uncertainties can be taken into account, which would not be the case if the entire modelling has been done by a single author. The mesh size, shape and refinement, number of iterations, introduction of concentrated loads in ICONC (FE implementation of EPSF available for free download at <http://i-concrete.epfl.ch> in the “applets” menu) was slightly varied by each user, which had some influence on the final result (more on this will be presented in following chapter of the thesis). In the future, as more EPSF models are provided the Database is expected to grow, potentially opening new areas of research.

Chapter 3: Advanced modelling of structural concrete members with EPSF

This chapter is based on the FEDRO (Federal Roads Office) report number 680, titled “Assessment of Existing Structures Based on Elastic-Plastic Stress Fields and Modelling of Critical Details and Investigation of the In-Plane Shear Transverse Bending Interaction”, written by Prof. Aurelio Muttoni, Dr. Miguel Fernández Ruiz, Filip Niketić and Marie-Rose Backes. This was part of the research project AGB 2009/009, requested by the AGB bridge research group. The report was published by the OFROU in October 2016.

Contributions of Filip Niketić involved:

1. Conducting a sensitivity analysis of the EPSF method with respect to FE size, shape, orientation and number of iterations until the convergence;
2. Developing and validating a procedure for modelling rebars with insufficient anchorage length using the EPSF method;
3. Developing and validating a procedure for modelling indirectly loaded and/or supported structural concrete members using the EPSF method;
4. Tailoring partial safety factors which can be used with the EPSF method following the works of P. Tanner et al. [112, 113, 114].

3.1 Sensitivity analysis of EPSF method with respect to its finite element implementation

Considering the fact that EPSF are developed using finite element analysis, it is important to investigate the sensitivity of the method with respect to mesh properties. In other words, it is necessary to show how size, shape and finite element orientation affect the form of ultimate stress fields and if this has any influence on the estimated strength of a member. Consequently, it is important to determine what are the limits in which satisfactory accuracy is ensured, and how much error is introduced in case optimal meshes cannot be applied.

When developing an EPSF, the number of iterations steps until the convergence needs to be predefined, which could also play an important role in the accuracy of the results. This is why special attention is given to this parametric study, with a goal to determine the smallest number of iterations required to obtain satisfactory results.

3.1.1 Investigating the influence of finite element size on EPSF analysis

The total number of applied FE can significantly increase the computation time of an elastic-plastic stress field, meaning that it is beneficial to use as little FE as possible for each simulation. One of the most effective strategies involves targeted mesh refinement (FE size is reduced in the critical regions of a structure). Even though this approach is effective, sometimes the location of the critical regions is not obvious, and the prediction of the licit failure mechanism is challenging. In such cases FE meshes are best kept uniform, so that the ultimate stress field can be derived with equal precision in each segment of the structure.

However, the size of applied FE can have an influence on the final results in nonlinear calculations. Therefore, clear recommendations on how to choose a suitable mesh needs to be provided. In addition to this it is important to investigate potential problems which might occur when some of the given recommendations cannot be respected due to various reasons (geometrical or load constraints for example). The effect which finite element size has on the development of EPSF at the ULS was investigated using two groups of numerical models:

1. Members with uniform stress state (presented in *Fig.3.1a*)
2. Members with non-uniform stress state (presented in *Fig.3.1b*)

Elements subjected to uniform stress state consisted of three groups of reinforced concrete panels subjected to pure compression, pure tension and pure shear (as can be seen in *Fig.3.1a*).

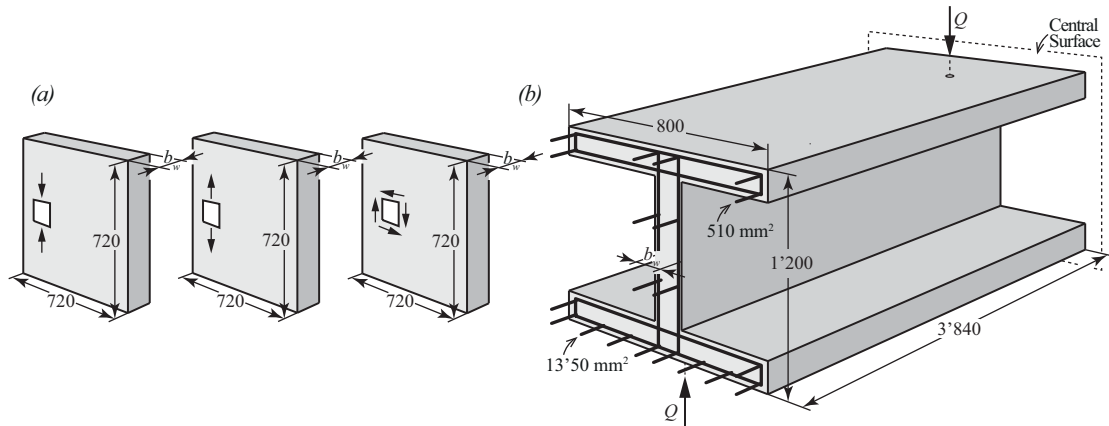


Figure 3.1: Geometry properties of structural concrete members used to investigate the sensitivity analysis of EPSF method: (a) RC Panels subjected to uniform compression, tension and shear; (b) RC beam subjected to 4-point bending

This allows to investigate the behaviour and stability of EPSF models used to simulate the basic stress states which can occur in structural concrete elements separately. The sensitivity analysis also involved a reinforced concrete beam subjected to four-point bending (refer to *Fig.3.1b*), which was used to perform the same sensitivity analysis of a non-uniform stress state. The idea behind it was to investigate a realistic model which combines all three stress states in a structure with potential redistributions amongst the elements.

Four types of meshes (M_1 to M_4 , presented in Fig.3.2) were applied when modelling each of the structural concrete elements presented in Fig.3.1. Meshes were kept uniform (all FE had identical shape and orientation), while the area of applied FE triangles was varied (surface of the FE triangle from mesh M_4 is four times the size of that from mesh M_1). This allowed a direct comparison of the results and avoided the influence of any undesired mesh parameters (such as presence of skewed FE and local mesh refinement).

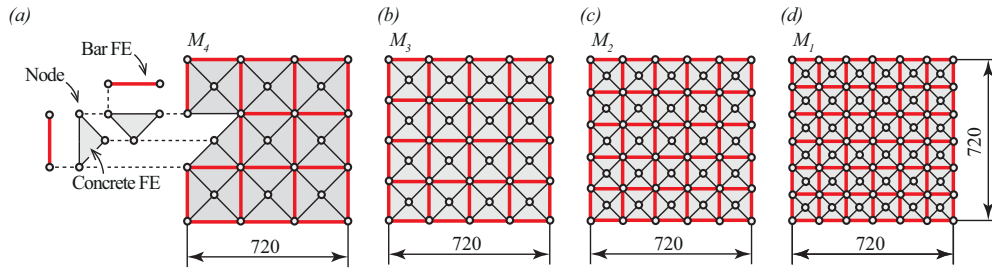


Figure 3.2: Investigation of different finite element mesh size: (a) geometry properties of mesh M_4 – disposition of the concrete FE, bar FE and corresponding nodes; (b) geometry properties of mesh M_3 ; (c) geometry properties of mesh M_2 ; (d) geometry properties of mesh M_1

As it is presented in Fig.3.2a, each mesh consists of blocks of four concrete FE triangles which are surrounded with four bar FE. Given the fact that the concrete cannot carry any tensile stresses (one of the main assumptions of the EPSF method) means that it is important to avoid models where concrete FE are not connected to at least a single bar FE. In extreme cases where the spacing of the rebars is such that the corresponding mesh would be unacceptably crude (too big FE), one could refine it. However, in such cases it is important to pay attention to the concrete compressive strength reduction factor (η_c) that can be unrealistically low, which would lead to conservative estimates of failure loads. This can be explained by the fact that assumed deformations of concrete FE are exaggerated (due to the fact that nothing can resist the tension forces). In such cases, it is better to smear the reinforcement (place smaller fictitious bars closer to each other) so that the deformation of concrete FE would be more realistic. It is important to emphasise that the actual rebar spacing was always sufficient to assure satisfactory behaviour of EPSF models within the scope of presented investigation, and the reinforcement was never smeared.

When modelling structural concrete panels (refer to Fig.3.1a), each concrete FE in the model shared nodes with bar FE in both directions (as it is presented in Fig.3.2), which is an exaggeration (a more realistic case will be used when analysing the I cross-section beam presented in Fig.3.1b). However, such disposition was selected in order to avoid any anisotropy in the RC panels.

3.1.1.1 Structural concrete members subjected to pure compression

Sensitivity of EPSF models simulating the behaviour of structural elements subjected to pure compression was investigated on a RC panel presented in Fig.3.3c (with reinforcement ratio equal to 0.1% in both directions). Plastic concrete compressive strength was 38 MPa, and

steel yielding strength was 550 MPa. The element was subjected to a uniformly distributed load over the two facing edges, as presented in Fig.3.3b and c.

The element was modelled using four meshes presented in Fig.3.2 (M_1 to M_4), and the corresponding ultimate loads Q_{M1} to Q_{M4} were compared (all models are available for download at <http://i-concrete.epfl.ch/epsf/epsf.html>).

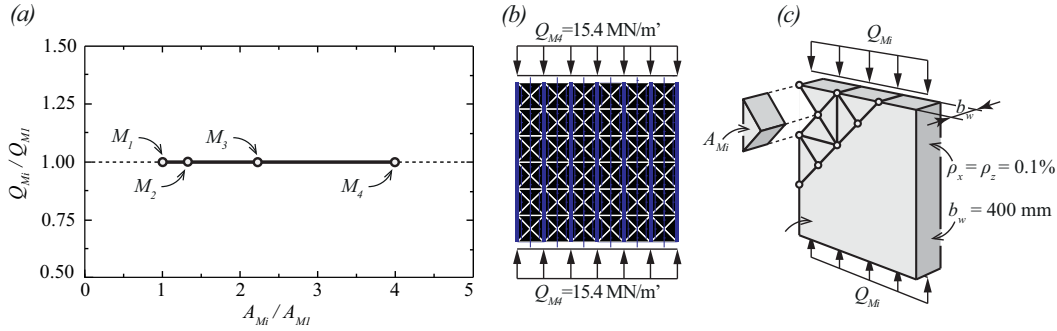


Figure 3.3: Sensitivity of EPSF results obtained after analysing structural concrete elements subjected to pure compression: (a) ultimate strength estimated using four meshes with different FE size; (b) ultimate stress field of a model using M_4 mesh; (c) geometry properties and load conditions of analysed member

The results are presented in Fig.3.3a. As it can be observed there is no mesh dependency, and all models failed at exactly the same load level. The horizontal axis shows the normalized area of applied FE (area of applied FE triangles was divided with the area of the FE applied in M_1 -mesh), and vertical axis shows the normalized failure loads (Q_{ult} of each simulation was divided with the Q_{ult} obtained after applying the M_1 -mesh). The stress field of the panel at ULS is presented in Fig.3.3b, black FE triangles indicate concrete crushing, whereas the blue lines mark the direction of the principal compressive stresses.

3.1.1.2 Structural concrete members subjected to pure tension

The sensitivity analysis of EPSF method was further investigated on elements subjected to pure tension. For this purpose, an element presented in Fig.3.4c was used.

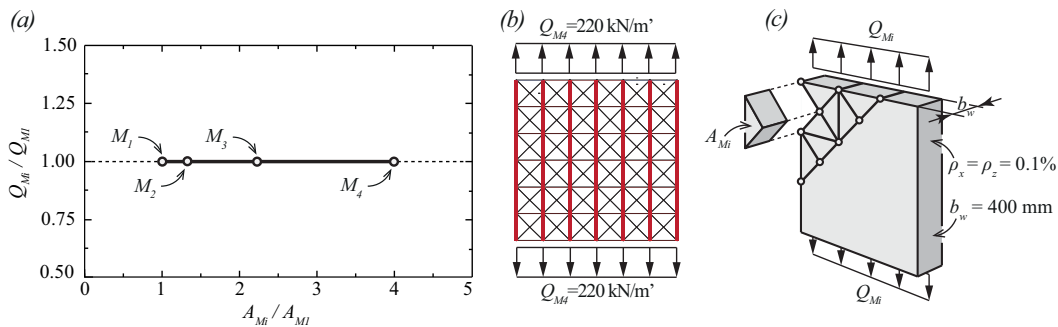


Figure 3.4: Sensitivity of EPSF results obtained after analysing structural concrete elements subjected to pure tension: (a) ultimate strength estimated using four meshes with different FE size; (b) ultimate stress field of a model using M_4 mesh; (c) geometry properties and load conditions of analysed member

The material and geometry properties of a panel subjected to pure tension are the same as the one subjected to pure compression ($f_{cp}=38\text{MPa}$ and $f_y=550\text{MPa}$). After applying the meshes given in Fig.3.2 (M_1 to M_4) no difference in the governing ultimate load was observed (as it can be seen in Fig.3.4a). Once more the two axis show normalized values of the FE area and failure load and the models can be downloaded at <http://i-concrete.epfl.ch/epsf/epsf.html>.

Ultimate stress field of the panel using the M_4 -mesh is presented in Fig.3.4b. Dark red colour of the reinforcement indicates yielding of the steel, and white concrete triangles suggest that they are not subjected to any stresses.

3.1.1.3 Structural concrete members subjected to pure shear

The method proved to be quite stable in case of elements subjected to uniform shear stress state as well. This was investigated using a panel *PV4* (refer to Fig.3.5c), tested by Vecchio and Collins [120].

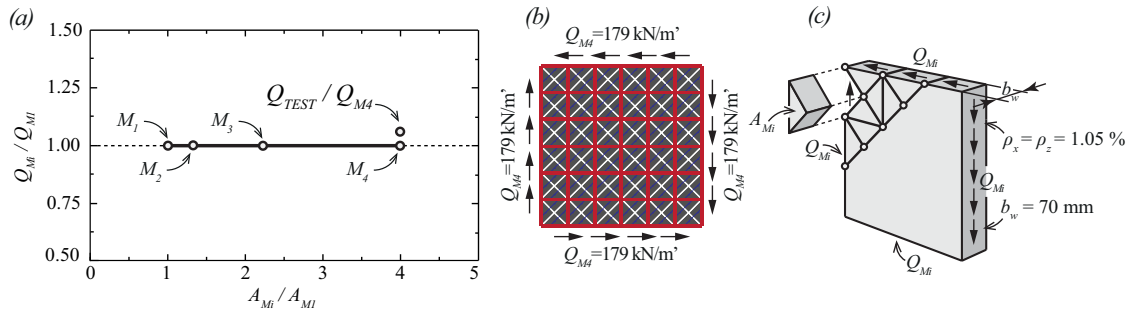


Figure 3.5: Sensitivity of EPSF results obtained after analysing structural concrete elements subjected to pure shear: (a) ultimate strength estimated using four meshes with different FE size; (b) ultimate stress field of a model using M_4 mesh; (c) geometry properties and load conditions of analysed member

Once again four different meshes, presented in Fig.3.2 (M_1 to M_4) were applied. No difference in the ultimate shear stress was observed between the models, and all of them failed when 2.56 MPa shear force was applied (compared to the measured 2.86 MPa). Element's geometry properties and the results of the EPSF analysis are presented in Fig.3.5a. Concrete compressive strength was 26.6MPa, and structural steel yielded at 242 MPa. Same as before, horizontal and vertical axis are normalized and the applied models can be found at <http://i-concrete.epfl.ch/epsf/epsf.html>.

The ultimate stress field of the panel using the M_4 mesh is presented in Fig.3.5b. Dark red colour of the reinforcement indicates yielding of the steel, whereas the dark grey triangles indicate the solicitation of the concrete. In this case concrete compressive strength was uniformly reduced over the entire surface of the panel ($\eta_c=0.278$) and the solicitation of the concrete was equal to 69% ($\sigma_{c3}/f_{ce}=0.69$).

Previous example showed that the FE size does not have any influence on EPSF result in case of symmetrically reinforced structural concrete panels subjected to pure shear ($\rho_x = \rho_z$). In order to push the limits of the sensitivity analysis even further, the same panel was

investigated assuming different reinforcement ratio in horizontal and vertical direction ($\rho_x = 0.5 \times \rho_z$). The final results are given in Fig. 3.6.

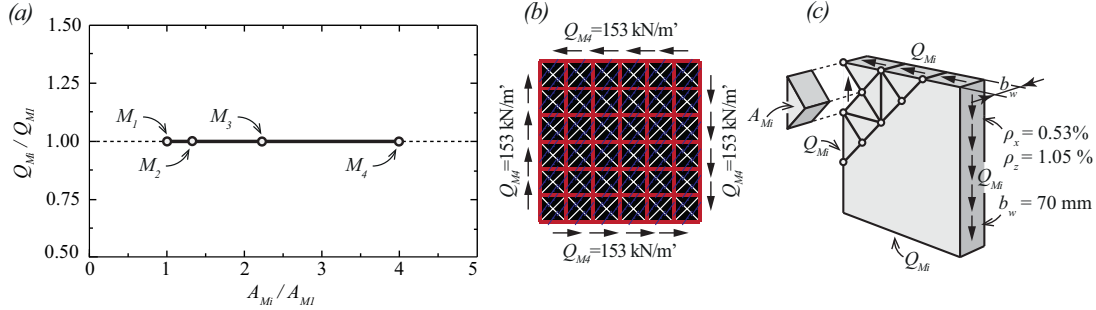


Figure 3.6: Sensitivity of EPSF results obtained after analysing structural concrete elements subjected to pure shear: (a) ultimate strength estimated using four meshes with different FE size; (b) ultimate stress field of a model using M4 mesh; (c) geometry properties and load conditions of analysed member

Ultimate strength of an unsymmetrically reinforced concrete panel estimated with the EPSF method did not depend on the applied FE size (all four model failed at exactly the same load, as presented in Fig. 3.6a and b). Reinforcement yield in both directions and concrete compressive strength was uniformly reduced to approximately 15% of its initial value ($\eta_\epsilon = 0.145$). The solicitation of compressive struts was at 100% ($\sigma_{c3}/f_{ce} = 1.00$), which is very important to underline. Therefore, it can be concluded that the EPSF method governs identical ultimate loads of members subjected to uniform shear stresses regardless of applied FE size.

3.1.1.4 Structural concrete beam under four-point-bending

In order to investigate the sensitivity of EPSF models that can experience stress redistributions (as is usually the case in real structures), meshes presented in Fig. 3.2 were used to model a web of a reinforced concrete beam with I cross-section subjected to four-point bending.

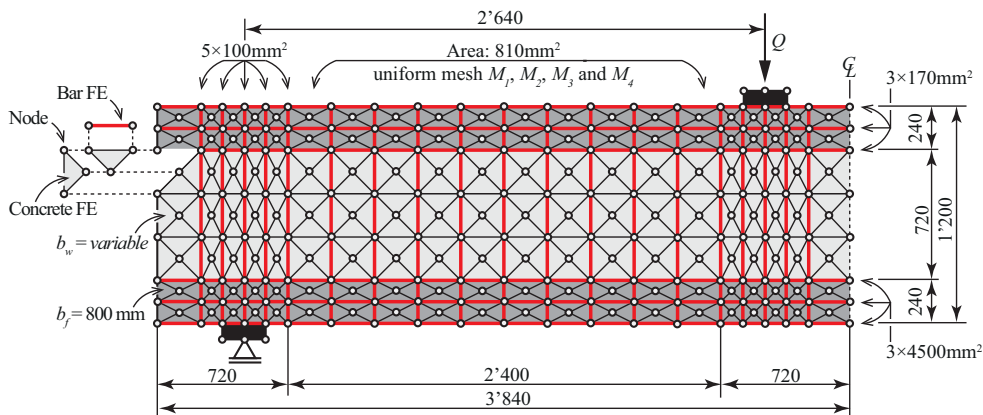


Figure 3.7: Geometry properties of an I-cross section beam used to investigate the influence of finite element size on EPSF results – disposition of concrete FE, bar FE and corresponding nodes

Geometry and mesh properties of analysed beam (modelled using M_4 mesh) can be seen in Fig.3.7. The beam was designed to experience shear failure of its central (web) region. Web provided a space with uniform geometrical properties, which allowed direct application of meshes M_1 to M_4 . Total amount of transverse steel in the web (810 mm^2) was kept constant for all investigated models. Vertical reinforcement was smeared between concrete finite elements as presented in Fig.3.7 (4 concrete FE triangles were placed between 2 bar FE). It is important to emphasize that in this case (contrary to previous investigations of elements subjected to pure compression, tension and shear), applied meshes could not be entirely uniform, due to the presence of flanges where slightly elongated finite elements were applied. However, this influence became negligible by forcing the beam to fail inside the web.

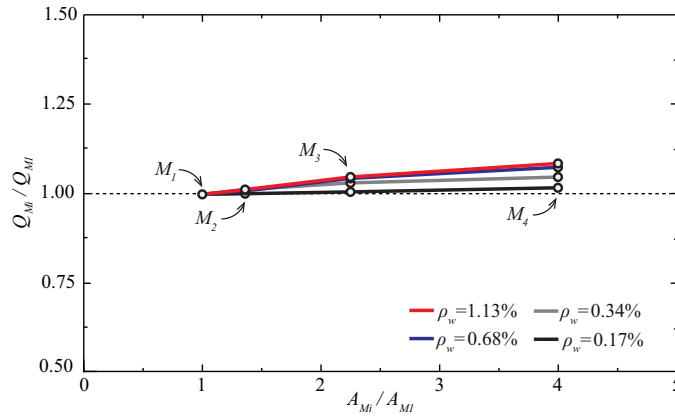


Figure 3.8: Sensitivity of EPSF results obtained after analysing structural concrete elements subjected to non-uniform stress state with ultimate strength estimated using four meshes with different FE size on four beams with different transverse reinforcement ratio

In order to cover a wide range of shear failure modes (starting from yielding of the stirrups, to crushing of the concrete) four beams having four different web thicknesses were analysed:

1. $b_w = 200 \text{ mm}$ corresponding to $\rho_w = 0.17\%$
2. $b_w = 100 \text{ mm}$ corresponding to $\rho_w = 0.34\%$
3. $b_w = 50 \text{ mm}$ corresponding to $\rho_w = 0.68\%$
4. $b_w = 30 \text{ mm}$ corresponding to $\rho_w = 1.13\%$

where ρ_w presents the transverse shear reinforcement ratio.

Plastic concrete compressive strength was equal to 38 MPa and steel yield strength was equal to 550 MPa.

As it can be seen in Fig.3.8, EPSF models showed some mesh dependency. Application of smaller FE governed lower failure loads for all four transverse reinforcement ratios. However, it can be observed that the difference between the ultimate loads obtained using meshes M_1 and M_4 was almost 9% in case RC beam had $\rho_w = 1.13\%$, whereas this difference dropped down to around 5% and 1% when relative amount of transverse reinforcement was

equal to $\rho_w = 0.34\%$ and $\rho_w = 0.17\%$. This means that the stability of the results depends on the type of failure. Structural members which experienced concrete crushing without yielding of the transverse reinforcement (refer to $\rho_w = 1.13\%$) are more sensitive to FE size compared to elements that failed in concrete crushing along with yielding of the steel (refer to $\rho_w = 0.17\%$).

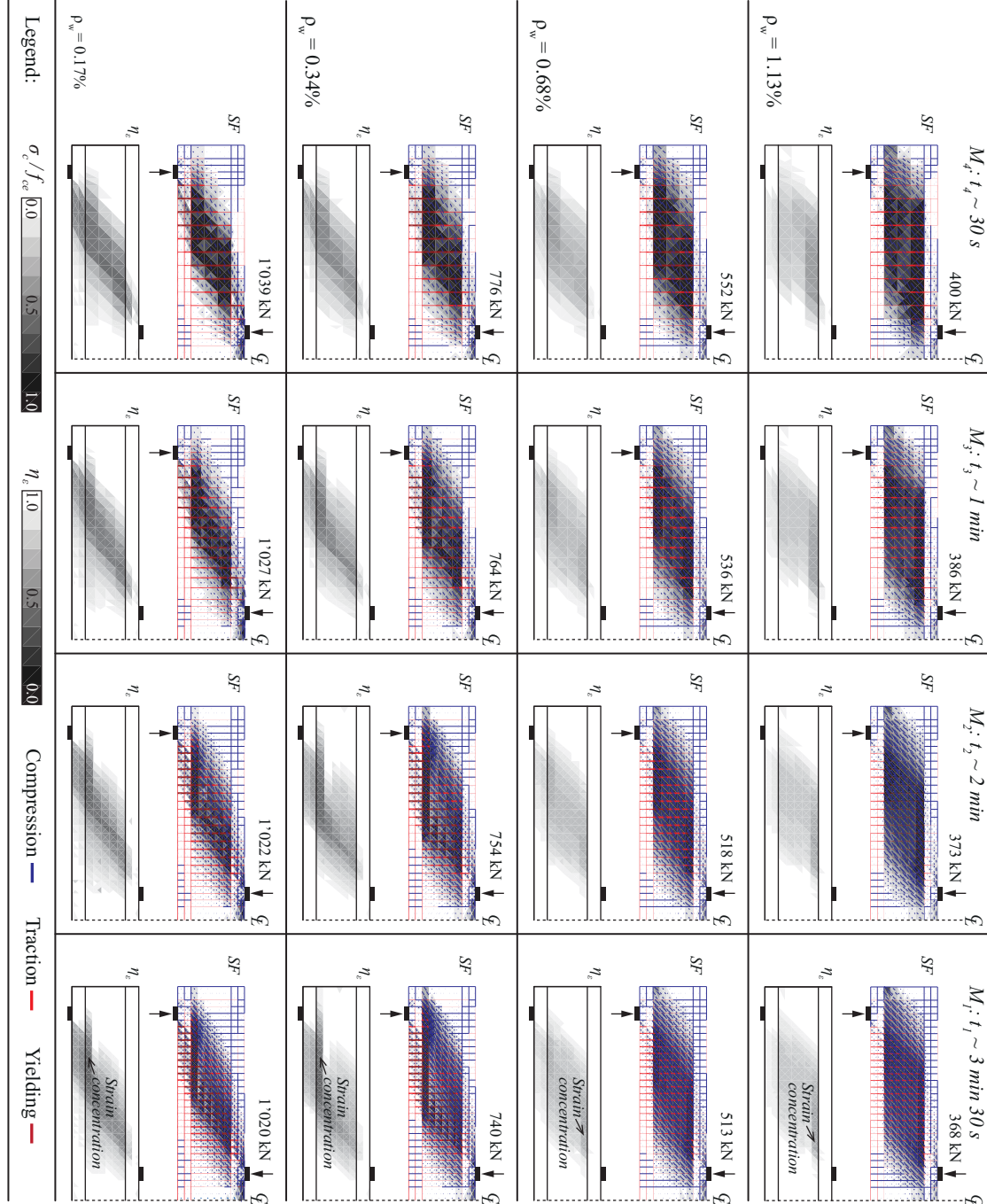


Figure 3.9: Stress fields and concrete compressive strength reduction factor for I-cross section beams having four different transverse reinforcement ratios analysed with four finite elements mesh sizes

The reason for this can be observed in *Fig.3.9*, which shows the stress field (SF), the concrete compressive strength efficiency factor (η_ϵ) as well as the calculation time for all sixteen analysed beams (four different web thicknesses modelled using four meshes M_1 to M_4 , available to download at <http://i-concrete.epfl.ch/epsf/epsf.html>). All models failed locally due to crushing of the concrete close to one of the flanges (top flange in case of models with higher transverse reinforcement ratio, and bottom flange in case of the beams with lower transverse reinforcement ratio). As the FE area decreased, so did the size of the damaged zone. Since models did not have any longitudinal reinforcement in the web, there was nothing to evenly spread the deformations (especially in case of $\rho_w = 1.13\%$). Therefore, the concrete compressive strength was significantly reduced in a single FE row – in other words, strain concentration was observed. Since the reinforced concrete beam was only numerically analysed (it was not a part of an experimental campaign) it is not sure whether or not the strain localization close to the flange would actually appear in real life of not.

The reason why the beams with lower transverse reinforcement ratio ($\rho_w = 0.34\%$ and $\rho_w = 0.17\%$) were less affected by this phenomenon lays in the fact that the strains were much better averaged over the web once the stirrups yielded. Since concrete compressive strength reduction factor (η_ϵ) is directly depended on the principal tensile strains, the ultimate strength of the reinforced concrete beams with higher transverse reinforcement ratio was much more affected by the reduction of FE size.

Considering the fact that the area of applied FE in M_1 models is four times smaller than the one in M_4 proves that the results are reasonably stable even in case of non-uniform stress fields. Higher drop in ultimate load was observed on a series of beams which had significantly high amount of transverse reinforcement (more than 1%), which is usually not the case in engineering practice. When this ratio dropped down to 0.4% or less, the results were much more stable.

It can be concluded that the EPSF method gives stable results for various sizes of applied FE. A general recommendation when selecting an optimal FE size is to use the stirrup spacing as main grid for meshing, and place two concrete FE triangles in between (as presented in *Fig.3.7*). Using this criterion along with the recommendations concerning the FE shape and FE orientation (that will be presented in following sections) ensured satisfactory behaviour of EPSF models. Online database was generally modelled in this manner, and final results proved to be quite accurate when compared to experimentally measured values (average Q_{TEST}/Q_{EPSF} equal to 1.04 with coefficient of variation equal to 0.10).

3.1.2 Investigating the influence of finite element shape on EPSF analysis

The shape of applied finite elements is another parameter which affects EPSF analysis. In order to investigate its significance and provide practical recommendations for meshing, a reinforced concrete beam with 100 mm thick web (corresponding to $\rho_w = 0.34\%$), presented in *Fig.3.7* was investigated using 5 additional meshes:

1. M_{DR} that served as a benchmark;
2. M_{D1} to M_{D4} whose geometry properties are given in *Fig.3.10*.

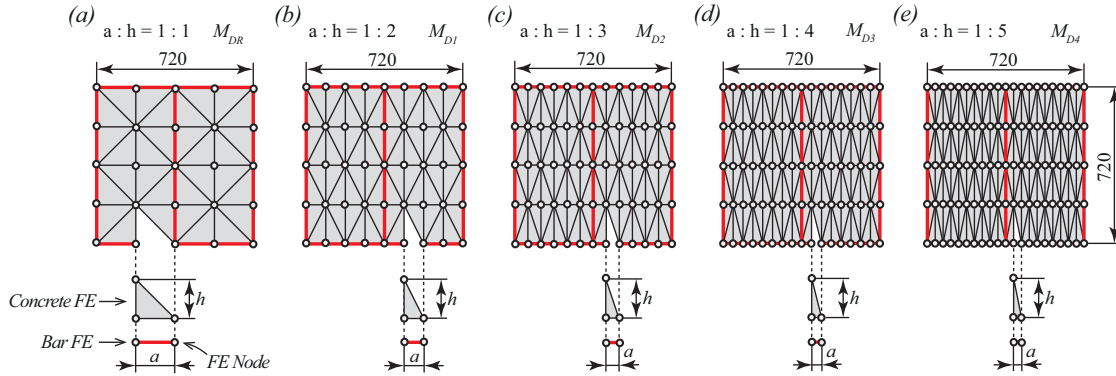


Figure 3.10: Investigation of the finite element distortion on EPSF results: (a) geometry properties of the reference mesh M_{DR} – disposition of concrete FE, bar FE and corresponding nodes; (b) geometry properties of mesh M_{D1} ; (c) geometry properties of mesh M_{D2} ; (d) geometry properties of mesh M_{D3} ; (e) geometry properties of mesh M_{D4}

Finite element distortion was defined as ratio between the height of a constant strain triangle and length of its corresponding side ($a:h$ ratio presented in Fig.3.10). As it can be seen this ratio varied from 1:1 to 1:5.

Meshes M_{DR} to M_{D4} (presented in Fig.3.10) were used to form beam webs of all five FE models. The results of EPSF analyses are given in Fig.3.11, which shows that the ultimate load was quite stable regardless of applied mesh. Maximal difference between the reference model (M_{DR}) and the most distorted one (M_{D4}) was approximately 2%, proving that the presence of FE distortion has little influence on the final results.

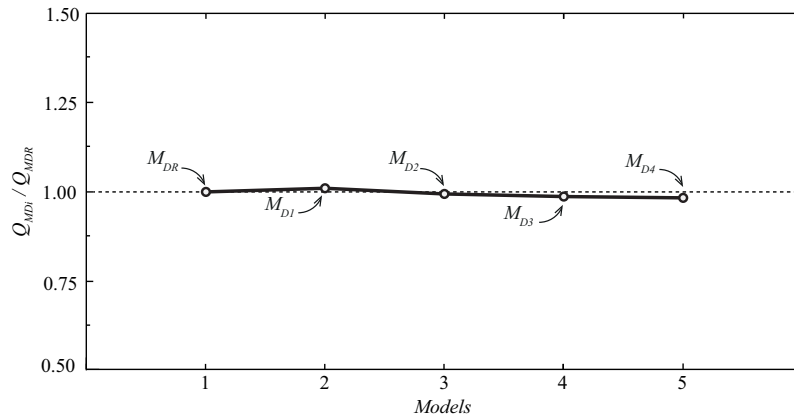


Figure 3.11: Sensitivity of EPSF results obtained after analysing I cross-section beam using five meshes with different FE shape

Based on the general recommendations for FE analysis found in literature [35], maximal triangle height-to-side ratio used in practice should not be greater than 1:3. A fact that the difference in results is not too big even if this ratio is larger than the recommended values is definitely reassuring, but should be avoided as much as possible. Meshes containing zones with distorted finite elements due to the complex geometry of the element for example can be locally accepted. All 5 models can be downloaded from <http://i-concrete.epfl.ch/epsf/epsf.html>.

3.1.3 Investigating the influence of finite element orientation on EPSF analysis

Orientation of finite element triangles forming a mesh has an effect on the final results. The fact that the hypotenuses of the constant strain triangles are parallel throughout a model affects the shape of the ultimate EPSF as well as the value of ultimate strength.

In order to investigate this phenomenon, the reinforced concrete beam presented in Fig.3.7 (with web thickness of $b_w = 100\text{mm}$, corresponding to $\rho_w = 0.34\%$) was modelled once more, using a regular mesh, formed out of FE triangles with 1:1 height-to-side ratio. Triangles were first orientated in a way which allowed their hypotenuses to descend from top left to bottom right corner (refer to Fig.3.12a), and then vice versa (refer to Fig.3.12d). Zig-zag FE orientation was also analysed (refer to Fig.3.12c) and finally, a mesh with random FE triangle orientation was applied (refer to Fig.3.12b). Fig.3.12 shows all 4 meshes, along with corresponding stress fields at ULS and concrete compressive strength effectiveness factors (η_e).

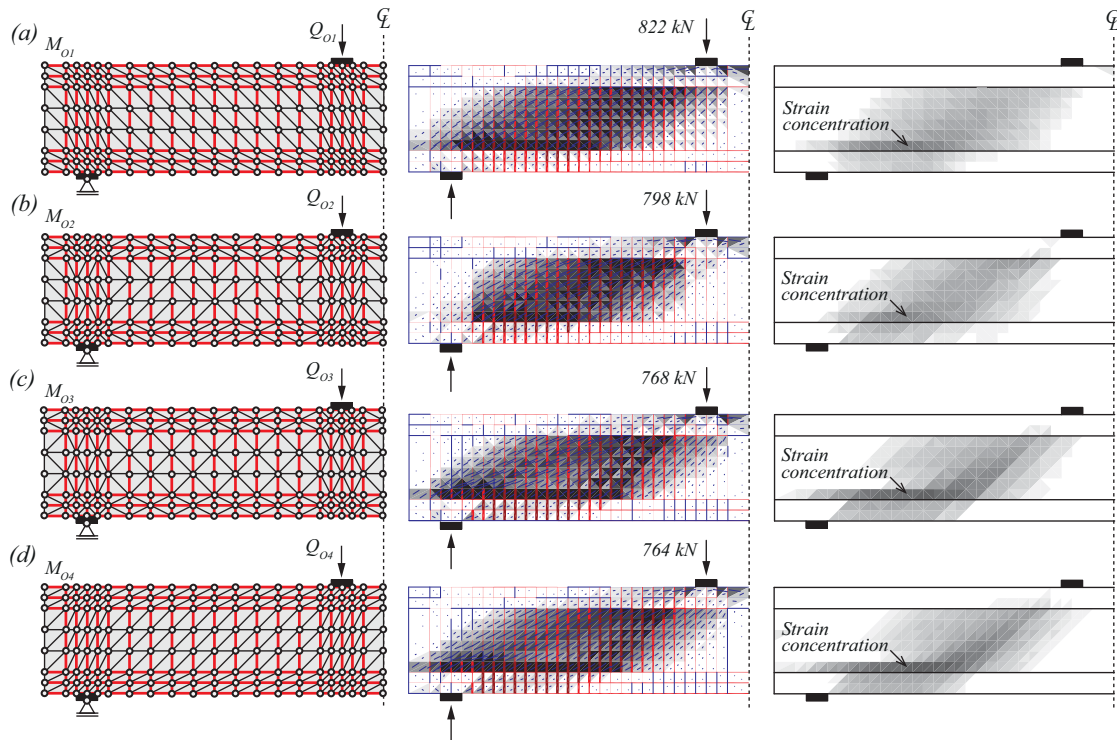


Figure 3.12: Investigation of the finite element orientation on EPSF results - geometry properties, corresponding stress field and concrete compressive strength reduction factor - η_e of: (a) mesh M_{O1} ; (b) M_{O2} ; (c) M_{O3} ; (d) M_{O4}

As it can be seen, the difference between the ultimate loads is not negligible and can be as high as 8% ($Q_{ult}=822\text{ kN}$ in case of M_{O1} compared to $Q_{ult}=764\text{ kN}$ in case of M_{O4}). In addition to this, difference in shape between the four stress fields can be also observed. If an angle between the hypotenuses of the concrete FE triangles and the direction of the principle compressive stresses is small, compressive stress field tends to be more concentrated governing a lower ultimate load (refer to M_{O4}).

On the other hand, if the finite element hypotenuses are almost perpendicular to the principle compressive stresses, the stress field tends to spread over a wider web area, governing a higher ultimate load (refer to M_{O1}).

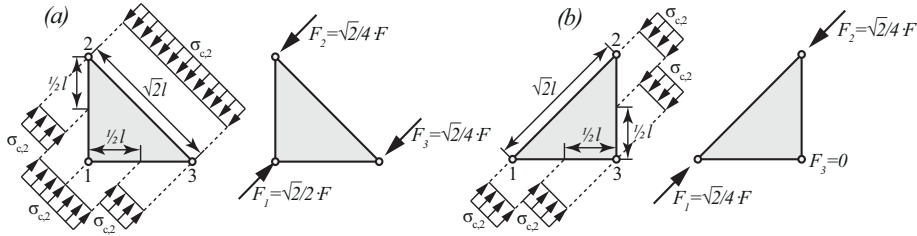


Figure 3.13: Derivation of the nodal forces from concrete stresses for: (a) FE with descending hypotenuses; (b) FE with ascending hypotenuses

The explanation behind this behaviour lies in the process of nodal force derivation, which depends on the angle between the principle stress direction and each side of the constant strain triangles (refer to Fig.3.13). Assuming that the direction of the principal concrete compressive stress is equal to 45° , nodal forces have been derived for two cases FE with descending hypotenuses from top-left to bottom-right and vice-versa. It can be clearly seen that application of the first mesh (presented in Fig.3.13a) activates all three nodes, contrary to the second mesh, which activates only two (as shown in Fig.3.13b). In case of a uniform stress state in which principal compressive stress direction does not change over a certain region of FE (for example in panels presented in Fig.3.5), the two meshes will govern identical resistances. However, when the direction changes, application of the first over the second FE results in larger ultimate strength, due to the fact that a single concrete FE generates 3 instead of 2 nodal forces and distributes them more evenly across the mesh (as it was observed in Fig.3.12).

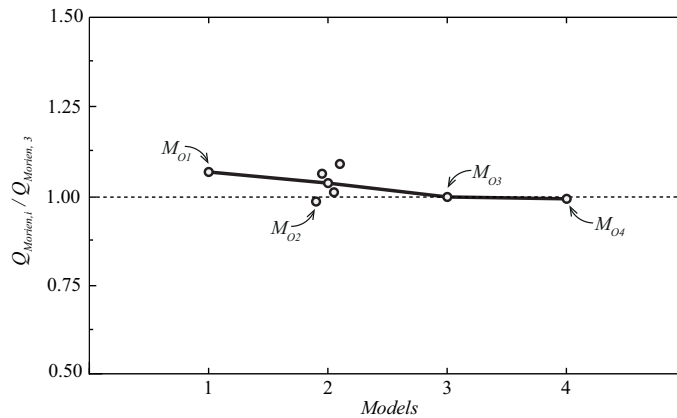


Figure 3.14: Sensitivity of EPSF results obtained after analysing I cross-section beam using four meshes with different FE orientation

In order to overcome this, suitable FE mesh should not have any preferential hypotenuses inclination. Instead, zig-zag FE (refer to M_{O3} in Fig.3.12) or random FE inclination (refer to M_{O2} in Fig.3.12) are preferred. However, it is important to mention that in case of random FE inclination it is necessary to perform more than one simulation in order to obtain acceptable results.

Fig.3.14 summarises failure loads obtained with meshes presented in *Fig.3.12*. Ultimate resistances are normalized using the value acquired with a zig-zag FE disposition (corresponding to $Q_{ult}=768$ kN governed by M_{03} mesh from *Fig.3.12*). It can be concluded that the application of meshes which favour certain FE orientation should be avoided as much as possible. Meshes with zig-zag inclination of hypotenuses or the ones with horizontal and vertical FE hypotenuses (presented in *Fig.3.2*) should be selected instead. In case a random FE orientation is applied, average value of at least 5 different simulations should be taken as representative (unfortunately this can be time consuming depending on the size of analysed models). All 8 FE models that were investigated in this chapter can be found at <http://i-concrete.epfl.ch/epsf/epsf.html>.

3.1.4 Convergence and required number of iterations for an EPSF analysis

EPSF are developed based on assumed displacement fields, which are validated through iterations. This process can lead to the convergence of the model (thus obtaining exact solutions according to the theory of plasticity) or its divergence (failure of the element). Convergence process is expressed through an error which is displayed at the end of each iteration, and represents the ratio between the vector sum of residual (un-equilibrated) nodal forces and the vector sum of applied loads.

During a calculation process, this error initially increases (refer to the two peaks in *Fig.3.15*), and then gradually decreases ultimately reaching a stable asymptotic value. If this is the case, the analysed model converged (refer to red line in *Fig.3.15*). Otherwise the model diverged indicating that the applied loads are too high (presented with black line in *Fig.3.15*). It can be seen that the difference in the final error between the two simulations presented in *Fig.3.15* is quite significant, making it quite clear if a simulation in question converged or not.

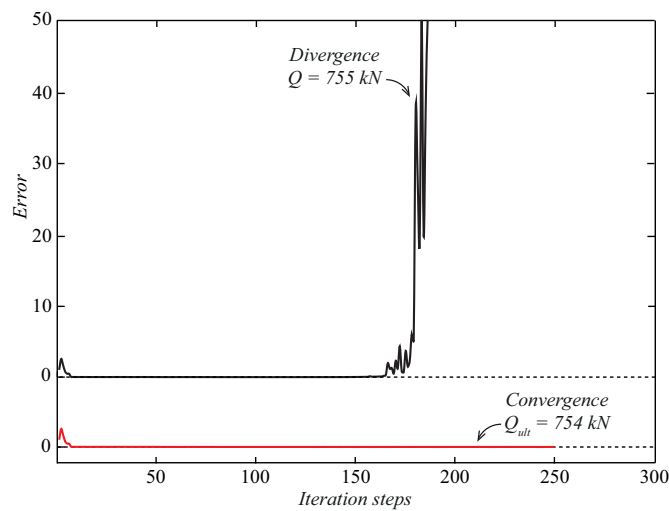


Figure 3.15: Convergence and divergence of an EPSF simulation

Element in question was the reinforced concrete beam from *Fig.3.7* (web thickness $b_w = 100$ mm, corresponding to $\rho_w = 0.34\%$) applying the M_2 mesh (refer to *Fig.3.9*). The model converged under 754 kN load but diverged under 755 kN (as presented in *Fig.3.15*), thus

indicating that its ultimate strength is equal to 754 kN. Aside from looking at the error and visual validation of the obtained stress field, two more checks should be performed in order to validate if the EPSF is exact or not. The sum of the reaction forces should correspond to the applied loads, and the deformation of the analysed element should be the biggest at ULS. As the applied load approaches its maximal value, sometimes even if the simulation converged (error is acceptably small), element deformation is smaller for higher loads, which is physically impossible. In this case the biggest load that governs the largest deformations at the same time should be selected as governing.

Graph presented in *Fig.3.15* rises a bit of concern, since there are no indications that any of the two models will diverge until the 150th iteration. This could lead to a conclusion that if the predefined number of iterations was 150, instead of 250 steps, both simulations would converge and therefore overestimate the element strength. This is why a sensitivity analysis of this parameter (number of necessary iteration steps) was investigated.

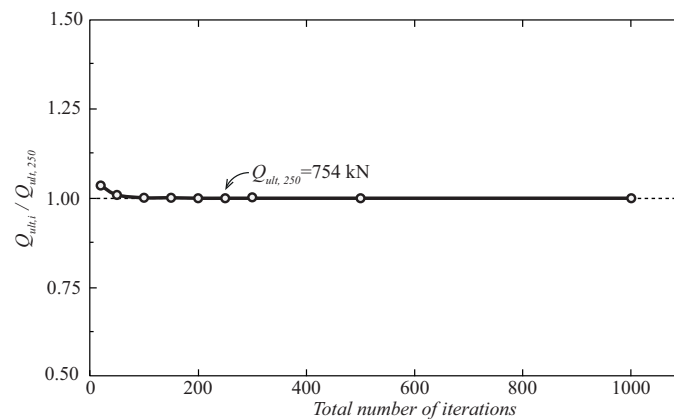


Figure 3.16: Estimated ultimate strength of an I cross-section reinforced concrete beam using EPSF analysis with different number of iterations

The ultimate strength of the same reinforced concrete beam from *Fig.3.15* was estimated using different number of iterations. The obtained results are presented in *Fig.3.16*. It can be seen that the difference between estimated ultimate loads obtained with 250 and 1000 iterations is negligible (in this case there is no difference at all). Moreover, the value of maximal load became quite stable after performing simulations with 100 iteration steps. Even though, the given example indicates that 100 iteration steps are sufficient for achieving sufficient accuracy, after modelling 315 structural concrete elements from the online database, general recommendation for the minimal number of required iterations is 250 steps.

3.2 Modelling elements with insufficient anchorage length using EPSF

Elastic-plastic stress field method assumes perfect bond behaviour, meaning that there is no displacement between the nodes of concrete and bar FE. Consequently, yielding of the reinforcement is possible regardless of the provided anchorage length, and a rebar can be fully activated already within the first FE of the model.

Previous assumption differs from reality, where complex stress-transfer mechanism between the two materials exists. In case re-bars are not properly anchored, effects of bond need to be indirectly introduced in EPSF, otherwise the obtained solutions might be unconservative.

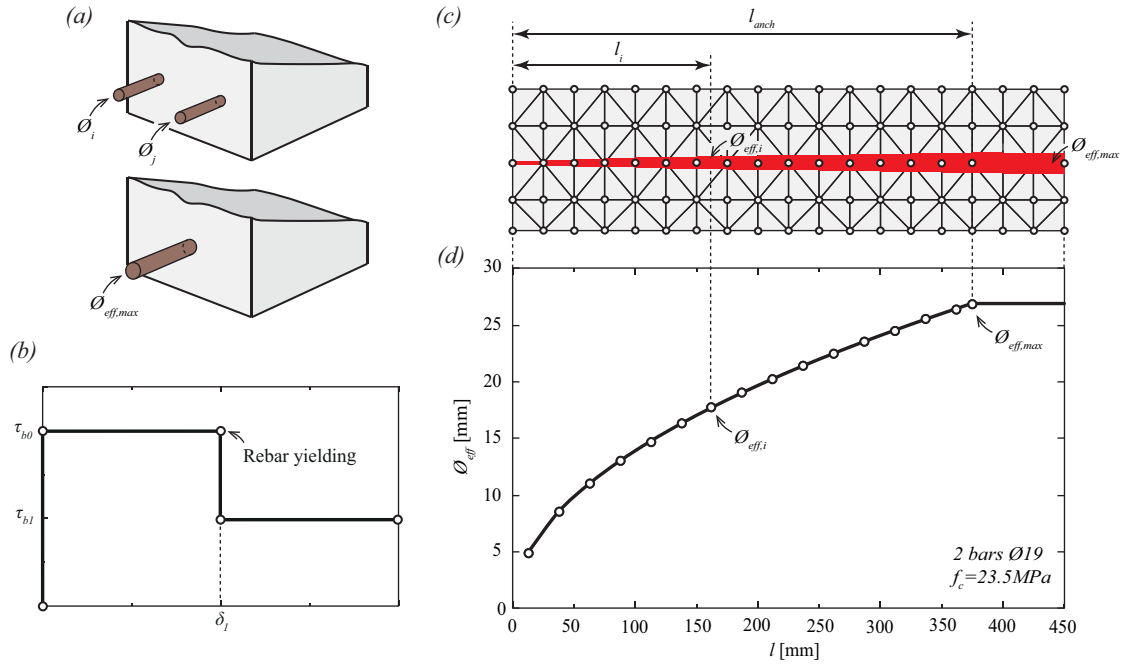


Figure 3.17: Modelling rebars with insufficient reinforcement anchorage using EPSF approach: (a) actual and effective rebars introduced to EPSF model; (b) concrete-to-steel bond stress; (c) varying bar FE area over rebar's anchorage length; (d) effective bar diameter representing two Ø19 rebars imbedded in 23.5 MPa concrete accounting for their actual anchorage length

Fig.3.17 shows the modelling process of two rebars Ø19 with insufficient anchorage length (yield strength of the steel is equal to 390 MPa), imbedded in 23.5 MPa concrete. Actual disposition of the bars is presented on the top of Fig.3.17a. However, the two rebars cannot be modelled separately according to EPSF method, and instead need to be replaced with a single (effective) bar (refer to the bottom Fig.3.17a), whose diameter is calculated in the following manner:

$$\phi_{eff,max} = \sqrt{\sum \left(\phi_i^2 \cdot \frac{f_{y,i}}{f_{y,eff}} \right)} \quad (3.1)$$

where ϕ_i represents the diameter of the rebars which are placed at the same cross-section depth

$f_{y,i}$ represents the yield strength of corresponding rebar;

$f_{y,eff}$ represents the yield strength of effective rebar.

Concrete-to-steel bond law can be assumed as rigid-plastic, according to the Tension Chord Model (TCM), introduced by Marti et al. [74]. The TCM adopts a simplified bond stress-slip relationship (refer to Fig.3.17b) that assumes a constant transition of bond stress between reinforcement and concrete equal to:

$$\tau_{b0} = 2 \cdot f_{ctm}, \text{ up to yielding point of ordinary ribbed bars, and} \quad (3.2)$$

$$\tau_{b1} = f_{ctm}, \text{ once the bars have reached yielding.} \quad (3.3)$$

Mean tensile strength of concrete is represented with f_{ctm} in previous equations (Eq.3.2 and Eq.3.3), and according to MC2010 [34] it can be estimated in the following manner:

$$f_{ctm} = \begin{cases} 0.3 \cdot (f_c)^{2/3}, & \text{for } f_c \leq 50 \text{ MPa} \\ 2.12 \cdot \ln(1 + 0.1 \cdot f_c), & \text{for } f_c > 50 \text{ MPa} \end{cases} \quad (3.4)$$

where f_c represents the uniaxial concrete compressive strength measured in cylinder.

The anchorage length necessary to fully yield a rebar can therefore be estimated assuming bond stress equal to τ_{b0} (refer to Eq.3.2) in the following manner:

$$l_{anch} = \frac{\emptyset \cdot f_y}{4 \cdot \tau_{b0}} \quad (3.5)$$

where \emptyset represents the actual re-bar diameter;

f_y represents the yielding strength of the reinforcing steel.

It is important to emphasise that in case the actual anchorage length of the rebar is equal or larger than the one calculated in Eq.3.5, reinforcement can be modelled using the equivalent re-bar diameter throughout its entire length, thus keeping the model as simple as possible. Otherwise, the applied diameter needs to be reduced over the calculated anchorage length (refer to Eq.3.5), as presented in Fig.3.17c. In this manner, the amount of tensile force that can be taken by a single bar FE is physically limited, which is an indirect way of accounting for the bond stress.

Since the geometry of the rebar is discretized using bar FE, the reduction of the effective diameter is done in steps. Each FE assumes the average diameter of the bar over its length using the following equation:

$$\emptyset_{eff,i} = \emptyset_{eff,max} \cdot \sqrt{\frac{l_i}{l_{anch}}} \quad (3.6)$$

where $\emptyset_{eff,i}$ represents the diameter of a rebar in i^{th} FE;

$\emptyset_{eff,max}$ represents the effective re-bar diameter (refer to Eq.3.1);

l_{anch} presents the minimal necessary anchorage length (refer to Eq.3.5);

3.2 Modelling elements with insufficient anchorage length

l_i presents the distance between the beginning of the bar and the mid-point of the i^{th} FE (refer to Fig.3.17c).

The reduction of the effective rebar diameter over an anchorage length of two Ø19 rebars (yield strength of the steel equal to 390 MPa), imbedded in concrete that has a compressive strength of 23.5 MPa is presented in Fig.3.17d. In order to limit the maximum force that can be taken by the rebars the effective diameter was varied from 4.9 mm to 26.9 mm, over the anchorage length of 375 mm. Each point in the graph represents the effective diameter of a rebar corresponding to a FE from Fig.3.17c.

Table 3.1: Geometry and material properties of RC beams tested by Hong et al. [45]

N°	Spec.	a/d	s_w [mm]	l_{anch} [mm]	N°	Spec.	a/d	s_w [mm]	l_{anch} [mm]
1	SS-1	0.75	250	78	5	LBS-1	1.00	250	0
2	SS-2	1.00	250	78	6	LBS-2	1.00	250	156
3	SS-3	1.25	250	78	7	VSR-1	1.00	200	78
4	SS-4	1.5	250	78	8	VSR-2	1.00	150	78
$d = 520$ mm; $f_c = 23.5$ MPa; $f_y = 392$ MPa									

The presented modelling strategy was used to investigate a series of reinforced concrete beams subjected to four-point bending tested by Hong et al. [45]. The elements were designed to fail in shear due to an insufficient anchorage length. Their geometrical and material properties are given in Tab.3.1, and the results of the EPSF analysis are presented in Tab.3.2. All the FE models can be downloaded from <http://i-concrete.epfl.ch/epsf/epsf.html>.

Table 3.2: Results of EPSF analysis of RC beams tested by Hong et al. [45]

N°	Spec.	Q_{test} [kN]	Q_{EPSF} [kN]	Q_{test} / Q_{EPSF}	N°	Spec.	Q_{test} [kN]	Q_{EPSF} [kN]	Q_{test} / Q_{EPSF}	Aver.	CoV
1	SS-1	2×331	2×305	1.09	5	LBS-1	2×199	2×185	1.08	1.06	0.05
2	SS-2	2×305	2×269	1.13	6	LBS-2	2×290	2×288	1.01		
3	SS-3	2×280	2×252	1.11	7	VSR-1	2×297	2×282	1.05		
4	SS-4	2×240	2×247	0.97	8	VSR-2	2×329	2×304	1.08		

As it can be seen, the presented procedure gives satisfactory results when compared to measured values (average $Q_{test}/Q_{EPSF} = 1.06$), with very small dispersion (coefficient of variation – CoV equal to 5%). Detailed results of the EPSF analysis are presented in Fig.3.18 and Fig.3.19. Each figure shows a stress field of a specimen (corresponding to its ULS), the reduction of concrete compressive strength (η_c) along with its deformed shape, and a sketch of the crack patterns observed by Hong et al. [45] at failure. Fig.3.18 summarises the EPSF results corresponding to the beam LBS-1, which had longitudinal reinforcement without any anchorage length (refer to Tab.3.1 for more details). Looking at the ultimate stress field (see Fig.3.18a) it can be seen that the strength of the model is governed by local failure of the concrete above the support plate (induced by the reduction of concrete compressive strength - η_c) along with the local yielding of the rebars (refer to dark red sections of the longitudinal bars in Fig.3.18b). Even though the concrete was locally crushed in this case, it is actually the reinforcement which is limiting the amount of compression which can be deviated by the between the loading plate and the supports. Looking at the ultimate crack pattern

(presented in *Fig.3.18c*), it can be observed that a shear crack which originated from the support plate caused the failure of the system. Such failure was characterized as anchorage failure by Hong et al [45]. When comparing the results from *Fig.3.18c* to disposition of concrete compressive strength reduction factors from *Fig.3.18b*, a clear analogy can be observed. The EPSF results correspond quite well to the behaviour observed in experimental campaign. Both EPSF model and the tested beam experienced the same anchorage failure.

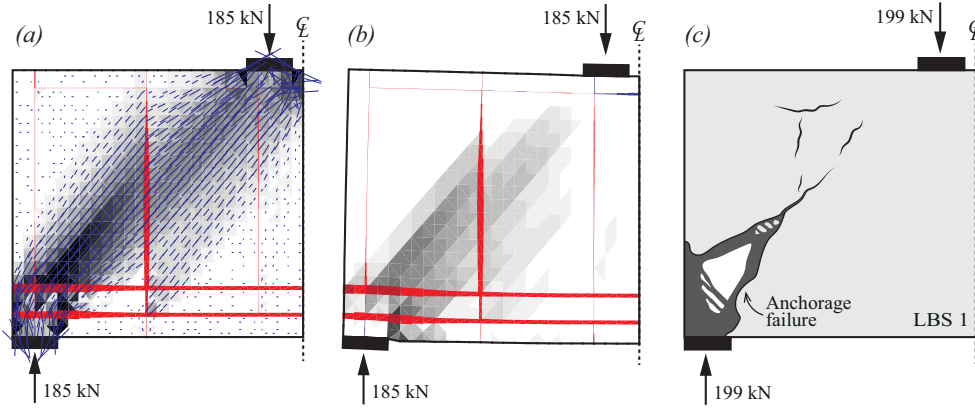


Figure 3.18: Results of EPSF analysis of a beam LBS 1 investigated by Hong [45]: (a) stress field at ULS; (b) deformed shape of the beam with concrete compressive strength reduction factor - $\eta\epsilon$; (c) observed crack pattern and measured strength of the element

Similar conclusion can be drawn after analysing *Fig.3.19* that gives detail of the EPSF simulation of beam *VSR-1* (refer to *Tab.3.1* for more details). Crack pattern at ULS (refer to *Fig.3.19c*) correspond quite well to the disposition of the concrete compressive strength reduction factor (refer to *Fig.3.19b*). The EPSF failed due to concrete crushing induced by the local yielding of the rebar close to the support. Such behaviour corresponds well to observed anchorage problems indicated by Hong et al. [45].

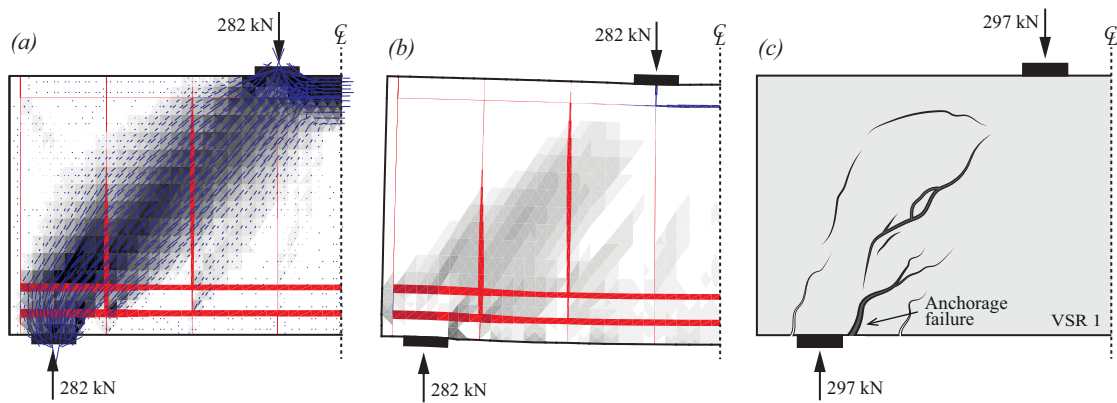


Figure 3.19: Results of EPSF analysis on a beam VSR 1 investigated by Hong [45]: (a) stress field at ULS; (b) deformed shape of the beam with concrete compressive strength reduction factor - $\eta\epsilon$; (c) observed crack pattern and measured strength of the element

An alternative approach to what was described in this chapter involves reduction of the yield strength of the steel over the anchorage length of a rebar. An argument for doing so would

be to maintain the axial stiffness of the element. However, this could result in underestimating the deformations of the analysed member (due to the fact that the slip is neglected and the reinforcement maintained its stiffness). On the other hand, the amount of tensile force which can be taken by each rebar would be the same compared to what was obtained after reducing the effective rebar diameter. Another approach would be to actually model the bond stress transfer mechanism (presented in *Fig.3.17b*) by introducing additional spring FE. This would significantly increase the computational time of the elastic-plastic stress fields, and would still represent an approximation of the reality. At the same time, the amount of tensile force which can be taken by a single rebar at ULS would be identical to what is obtained by reducing the effective bar diameter. In order to keep the EPSF models as simple as possible without decreasing their accuracy at ULS, a general recommendation for taking into account the insufficient anchorage length of the rebars is to simply reduce their effective diameter.

It can be concluded that the presented modelling procedure gives satisfactory results when compared to test results. Ultimate resistance and failure modes are accurately predicted with EPSF, and a clear view inside the stress distribution of analysed elements is given. Finally, it should be noted that the presented approach governs slightly conservative solutions by definition, since the bond properties are enhanced by confining concrete stresses, which was here not taken into account.

3.3 Analysis of indirectly supported structural concrete members using EPSF

Elastic-plastic stress field method proved to be a powerful tool when analysing individual structural concrete members (simple beams, deep beams, dapped ends, wall with openings etc. which can be modelled as plane members - 2D members). It was able to accurately predict structural resistance along with the governing failure mode and give a clear view of the distribution of internal forces at ULS of tested specimens (as can be seen at <http://i-concrete.epfl.ch/epsf/epsf.html>). However, in reality individual elements are often connected into statically indeterminate systems, which are able to facilitate additional internal stress redistribution. Even though such systems can be analysed element-per-element by developing each stress field separately and imposing boundary and loading conditions in between, actual structural behaviour might be overlooked due to such crude assumptions. This becomes especially important when assessing the ultimate resistance of existing structures, when all potential load-carrying mechanisms should be accounted for (so that any unnecessary structural strengthening can be avoided). In order to investigate this complex phenomena, the EPSF method has been used to analyse behaviour of crossed structural concrete members (reinforced and prestressed concrete beams that have been indirectly loaded and/or supported) found in literature.

Crossed members as load carrying mechanisms in civil engineering are most commonly used in bridge diaphragms, where they allow bearings to be placed outside of bridge-web planes (as presented in *Fig.3.20*). Bridge diaphragms of box-girder bridges also allow development of uniform torsion conditions in order to resist asymmetrical cross-section loading in more efficient manner.

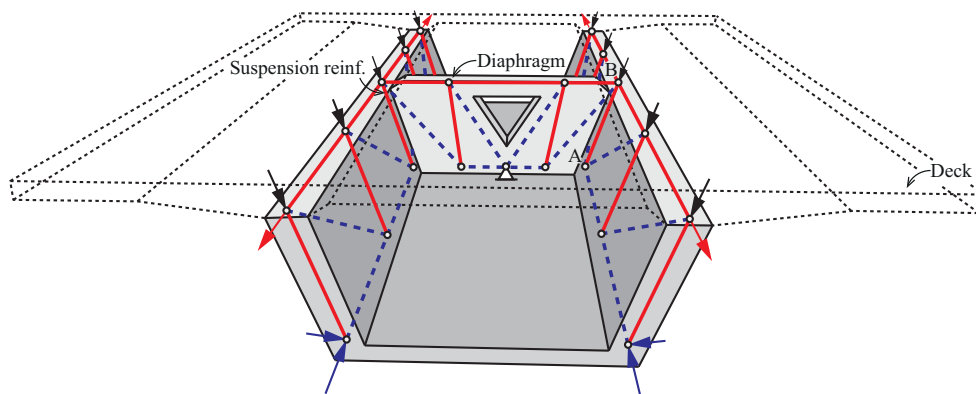


Figure 3.20: Bridge diaphragm – principle function and strut-and-tie model

Looking back at *Fig.3.20*, it can be seen how the internal forces are deviated from the longitudinal webs, through suspension reinforcement to bridge diaphragms in order to reach the support. In the perspective of EPSF method, this means that two simultaneous simulations are required in order to analyse the stress states of members in different planes in order to correctly distribute shear force transfer from one element to another. Analysing elements separately and assuming that the entire shear force is suspended from point *A* (see *Fig.3.20*) can be too conservative, while assuming that it is entirely applied in point *B* (*Fig.3.20*) might be unsafe.

3.3 Analysis of indirectly supported structural concrete members

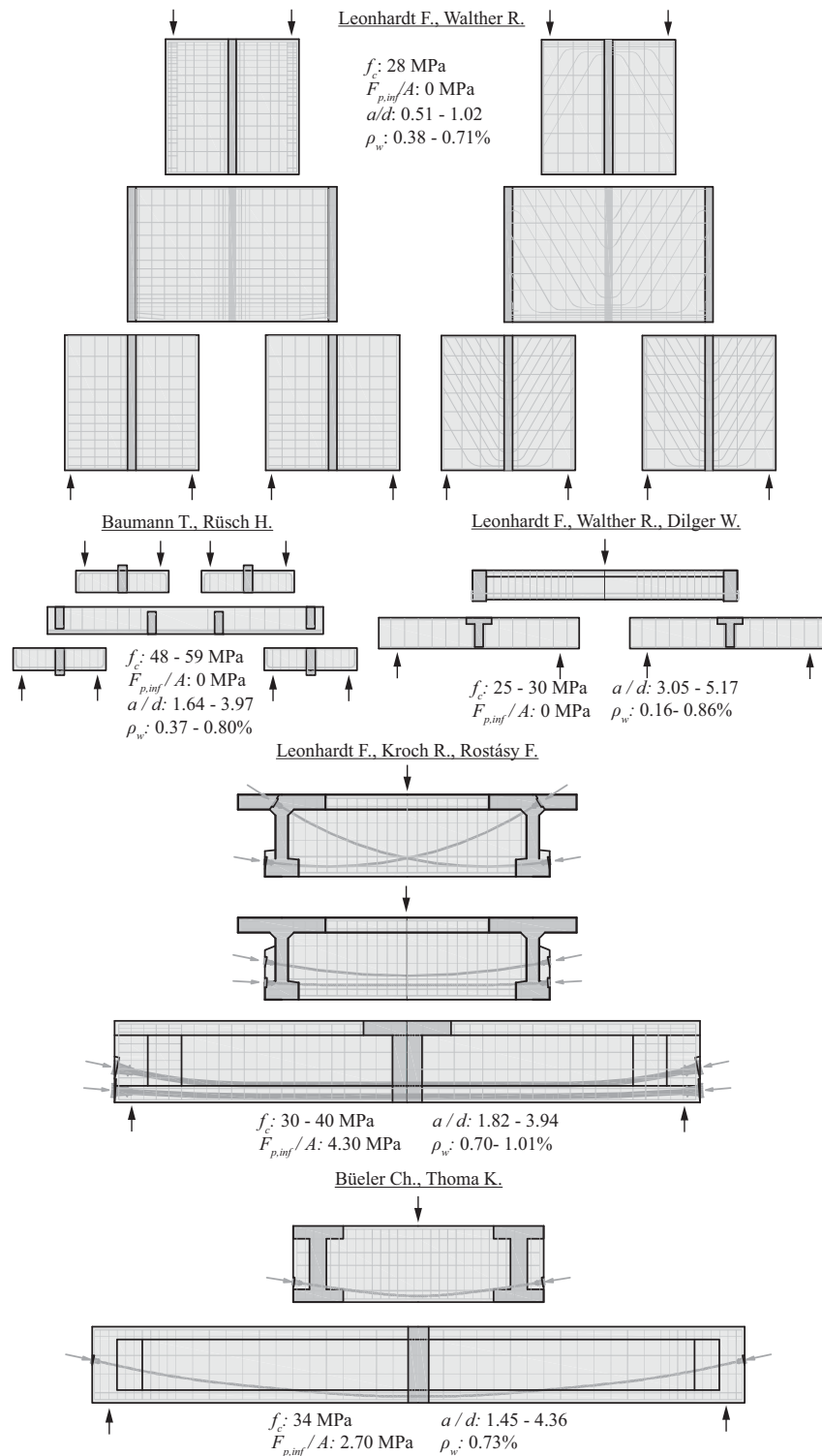


Figure 3.21: Mechanical and geometrical properties of crossed structural concrete members investigated with EPSF method

Placing the suspension reinforcement exactly in the crossing zone of the longitudinal and transversal elements can be physically impossible (due to limited space or construction site

constraints). In such cases suspension reinforcement is distributed over a wider zone which brings up a question whether such arrangement can still effectively transfer the shear force, and if this can affect the failure mechanism of the system. However, the most important question that will be addressed in this chapter is: can the EPSF method be used to correctly predict the ultimate capacity and failure mechanisms of such systems and with what accuracy?

For the purpose of this research a database containing 19 results from 5 different experimental campaigns was compiled:

1. Leonhardt F. and Walther R. (1966) - 2 tests [69]
2. Leonhardt F., Walther R. and Dilger W. (1968) - 5 tests [70]
3. Baumann T. and Rüschi H. (1970) - 7 tests [9]
4. Leonhardt F., Koch R. and Rostasy F. (1973) - 3 tests [66]
5. Büeler Ch. and Thoma K. (2010) - 2 tests [15]

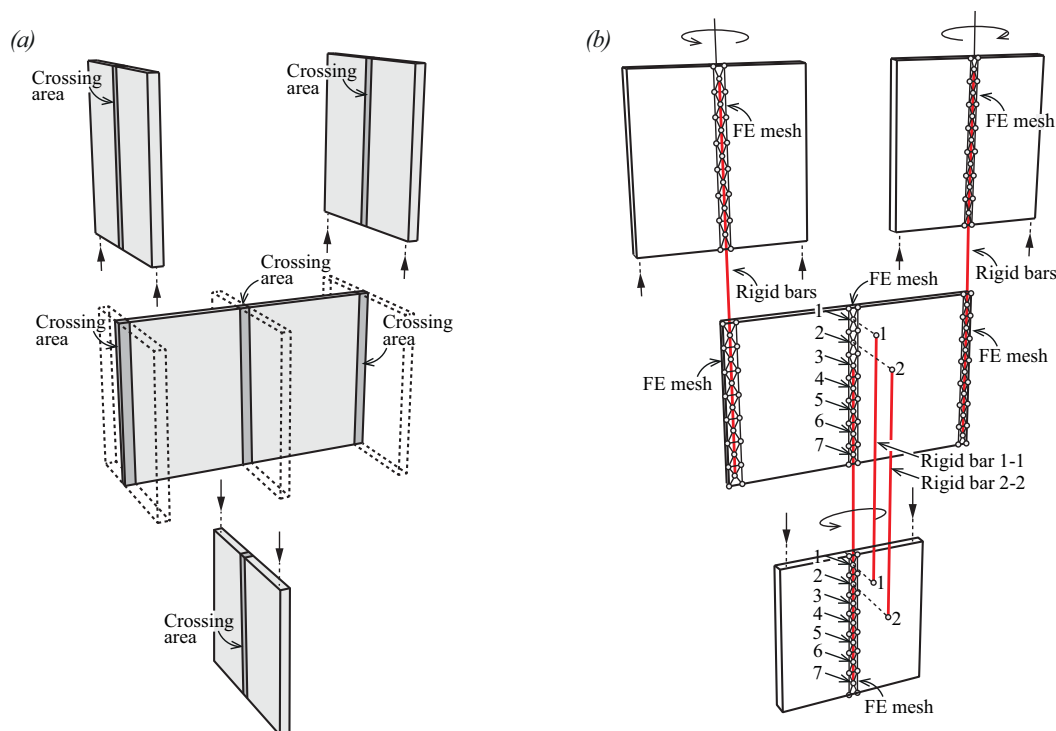


Figure 3.22: Modelling technique for crossed-members using EPSF method: (a) decomposition of the analysed specimen; (b) connecting crossed-members with rigid bar FE

The first three experimental campaigns contain only reinforced concrete specimens, whereas the last two applied prestressed concrete beams. All five experimental campaigns were conducted in order to better understand the mechanism of beam to beam shear transfer action, and as such are adequate to simulate behaviour of bridge diaphragms (reinforcement details and main parameter are given in Fig.3.21).

The modelling technique that was applied in order to analyse crossed members by means of EPSF method is presented in *Fig.3.22*.

In this figure, a crossed system consists of 4 elements: 3 transverse walls connected by a longitudinal wall (as can be seen in the middle of *Fig.3.22a*). The 2 exterior transverse elements act as supports while the load is applied indirectly through the central transverse wall. In order to analyse the entire system using EPSF method all specimens need to be placed in a single plane (as presented in *Fig.3.22b*). In a given example this means that the transverse members need to be rotated for 90° (refer to *Fig.3.22b*) and placed above the longitudinal element in case they serve as supporting members, or below it in case they are used to introduce the loads. Finally, finite elements in the crossing zone need to be linked node-by-node using rigid bars in order to impose equal nodal displacement between the members (refer to *Fig.3.22b*). In order to keep *Fig.3.22b* more comprehensible, FE mesh was not shown for the entire specimen, but only for its crossing zones. *Node 1* placed both in longitudinal and transversal walls are connected using the *Rigid bar FE 1-1*. The same is valid for the *Node 2*, and so on until *Node 7*. It was observed that the best results are obtained in case the linking is done in a single line where the symmetry axes of the two elements cross each other. Following the general meshing recommendations given in section “3.1 Sensitivity analysis” of this thesis, it is important to form such a mesh that allows each concrete FE triangle to have at least one connection with a bar FE (which is able to take tensile forces and control the nodal displacement). This is especially important for FE in crossing areas (see *Fig.3.22b*). All this implies that the meshes of the crossing regions need to have equal number of FE over their height (as presented in refer to *Fig.3.22b*) in order to equally distribute the points that are used to impose equal deformations of the specimens.

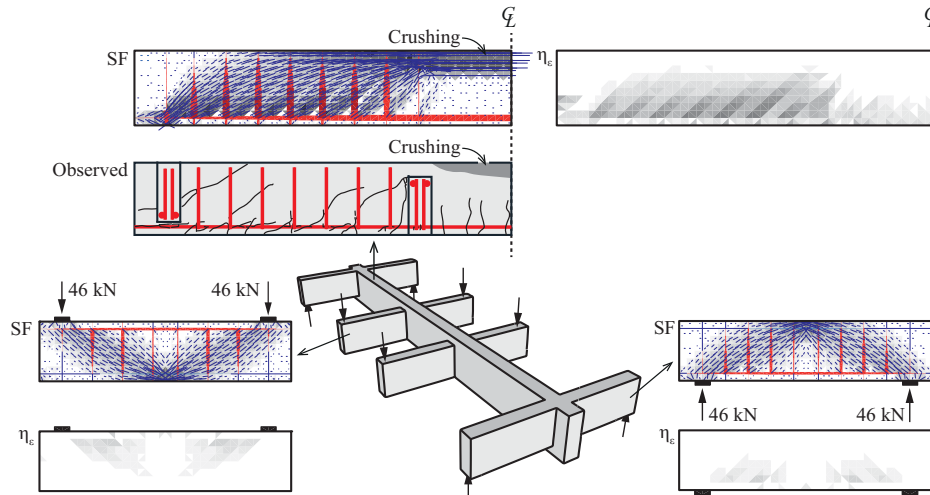


Figure 3.23: Results of EPSF analyses performed on a 65/2A specimen tested by Baumann and Rüsç – governing flexural failure of the member

EPSF obtained after applying the described modelling procedure is presented in *Fig.3.23*. The element in question is 65/2A, which was a part of the experimental campaign conducted by Baumann and Rüsç [9]. General outline as well as the loading and supporting

conditions of the specimen can be seen in the centre of the *Fig.3.23*. The stress field of the longitudinal beam at ULS, as well as the corresponding concrete compressive strength reduction factor (η_ϵ) along with the crack pattern observed during the experimental campaign are presented above the 3D sketch of the specimen. The behaviour of the transverse elements (both stress field and distribution of the η_ϵ factor) are shown on the sides.

It can be seen that the behaviour of the specimen observed during the test corresponds well to the stress field resulting from the EPSF analysis. Distribution of the concrete compressive strength reduction factor (η_ϵ) is well correlated with the observed crack pattern at ULS. The specimen failed due to crushing of the concrete in the upper zone close to the symmetry line (as indicated in *Fig.3.23*), which was also the case in experimental campaign.

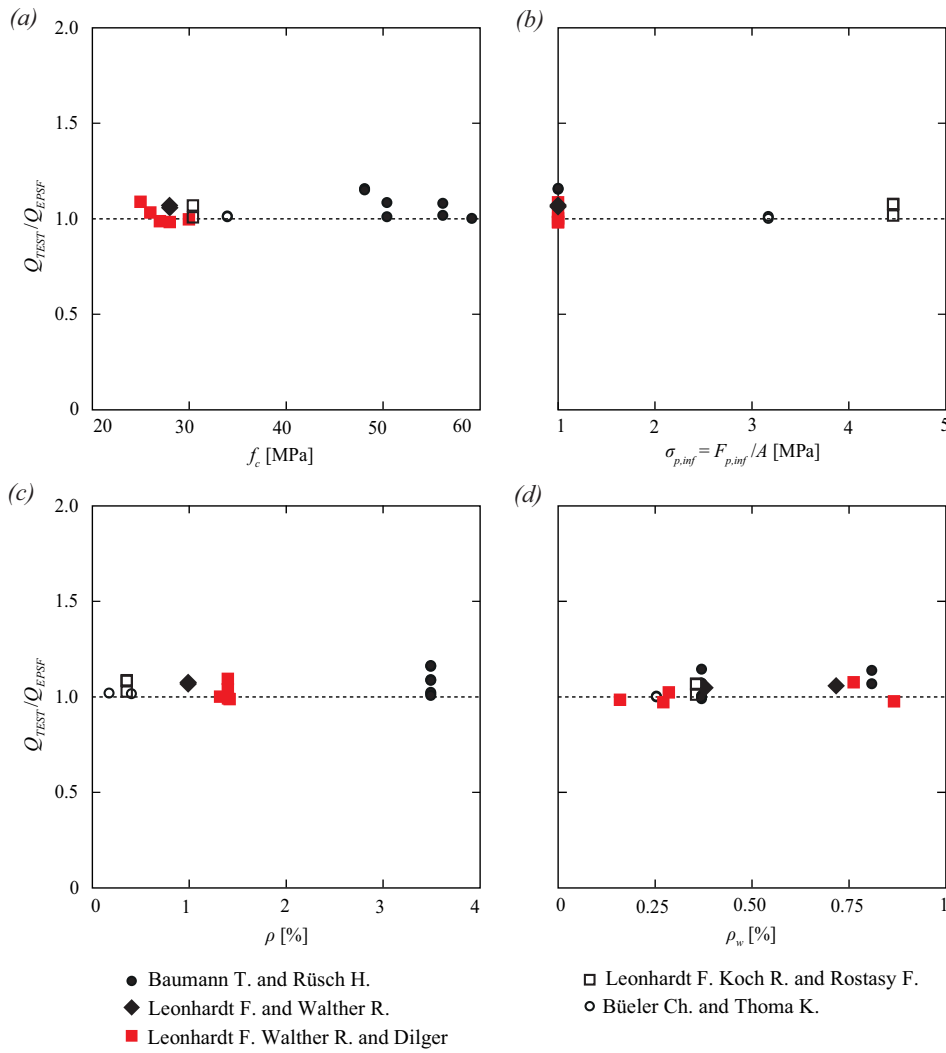


Figure 3.24: Ratio of measured and estimated strength of indirectly supported structural concrete members using EPSF method in function of: (a) concrete compressive strength; (b) initial prestress; (c) longitudinal reinforcement ratio; (d) transverse reinforcement ratio

3.3 Analysis of indirectly supported structural concrete members

EPSF accurately predicted the ultimate strength of all analysed crossed structural specimens, and each time correctly indicated the failure mode (the models can be downloaded from <http://i-concrete.epfl.ch/epsf/epsf.html>). In some cases, the failures occurred in one of the crossed-beams (as was the case presented in *Fig.3.23* for example), while the others failed close to the connecting regions (as was the case with specimen *IWT2* tested by Leonhardt and Walther [69]).

Satisfactory results have been obtained after applying the described modelling technique on all 19 specimens found in literature (see *Tab.3.3*). As it can be seen, each of the five analysed series gave satisfactory results with respect to the ultimate strength prediction as well as the governing failure mode (which is very important when it comes to assessing the ultimate strength of existing structural members).

On average EPSF method yielded 4% lower values of specimen's ultimate strength when compared to what was measured during the tests (average $Q_{test}/Q_{EPSF}=1.04$). In addition to this the results showed very little scatter ($CoV=0.05$) and no trends presented as a function of 4 basic mechanical parameters (concrete strength, prestress level, longitudinal and transverse reinforcement ratio, as can be seen in *Fig.3.24*).

Table 3.3: The results of the EPSF for crossed structural concrete members

N°	$Spec.$	$\frac{Q_{test}}{[kN]}$	$\frac{Q_{EPSF}}{[kN]}$	$\frac{Q_{test}}{Q_{EPSF}}$	$Aver.$	CoV	N°	$Spec.$	$\frac{Q_{test}}{[kN]}$	$\frac{Q_{EPSF}}{[kN]}$	$\frac{Q_{test}}{Q_{EPSF}}$	$Aver.$	CoV
Leonhardt et Walter [69]							Baumann, Rüschi [9]						
1	IWT1	1152	1130	1.02	1.04	-	1	64/1	102	102	1.00	1.06	0.06
2	IWT2	1177	1114	1.06			2	65/1A	140	130	1.08		
Leonhardt et all. [70]							3	65/1B	104	104	1.00		
1	ETI1	273	276	0.99	1.01	0.04	4	65/2A	93	92	1.01		
2	ETI2	257	250	1.03			5	65/2B	103	96	1.07		
3	ETI3	240	222	1.08			6	65/3A	92	80	1.15		
4	ETI4	245	250	0.98			7	65/3B	112	98	1.14		
5	ETI5	240	246	0.98			Leonhardt et all. [66]						
Büeler et Thoma [15]							1	ILT1	1810	1690	1.07	1.05	0.03
1	LT1	635	630	1.01	1.01	-	2	ILT2	1565	1540	1.02		
2	LT2	863	860	1.00			3	IILT1	1667	1552	1.07		

Based on the presented results the EPSF method has proved to be efficient and accurate tool for simulating behaviour of crossed-beam members capable of predicting the correct ultimate load and failure kinematics both on local and global level.

3.4 Tailoring partial safety factors suitable for EPSF method

The level of risk associated with the design and assessment of reinforced and prestressed concrete elements varies depending on the amount of available information regarding their usage and specifications. Analysis of new elements involves more uncertainty concerning material properties, load level, load history, geometry and reinforcement layout compared to existing structures. In addition to this, models used for design often employ more conservative assumptions compared to approaches that are used for assessment of existing elements. In order to ensure the same probability of failure for each member over its expected lifetime (regardless of the fact that it is being designed or assessed) certain type of safety format is applied for each simulation. Due to increased accuracy of models used for assessment, it seems natural that corresponding safety factors should be decreased compared to the ones which are applied for structural design.

This chapter investigates different strategies that could be used to ensure sufficient structural safety of EPSF models (global and partial safety format), and recommends which one is best suited for stress field analysis. In addition to this, it discusses pertinence of partial safety format being applied with global nonlinear structural analysis. Finally, it gives tailored values of partial safety factors that can be used when estimating ultimate strength of existing structural concrete members with EPSF, based on work of Tanner et al. [112, 113, 114].

When dealing with global nonlinear finite element analysis in practice, there is always a question of what is the correct implementation of structural safety. There are two main approaches:

1. Partial Safety Format (PSF)
2. Global Safety Format (GSF)

PSF implies reducing the material characteristic resistance values (f_{ck} for concrete and f_{sk} for steel that correspond to 5% fractile on a normal resistance distribution) in order to obtain the design values (f_{cd} and f_{sd}), which are then used to determine the design resistance of analysed members. In other words:

$$f_{cd} = \frac{f_{ck}}{\gamma_c} \quad (3.7)$$

$$f_{sd} = \frac{f_{sk}}{\gamma_s} \quad (3.8)$$

$$R_d = f(f_{cd}; f_{sd}; a_{nom}) \quad (3.9)$$

where γ_c represents the partial safety factor for concrete equal to 1.50 [29,34];

γ_s represents the partial safety factor for steel equal to 1.15 [29,34];

R_d represents the design resistance of an element;

a_{nom} represents the nominal geometry values.

On the other hand, GSF uses mean values of material properties and nominal values of geometry properties in order to determine the mean elements resistance, after which a single (global) safety factor is applied in order to determine design resistance in the following manner:

$$R_m = f(f_{cm}; f_{sm}; a_{nom}) \quad (3.10)$$

$$R_d = \frac{R_m}{\gamma_d} \quad (3.11)$$

where R_m represents the mean resistance of an element;

R_d represents the design resistance of an element;

γ_d represents the global safety factor.

Since the PSF uses different factors to reduce the strength of steel and concrete, this means that in case of global nonlinear FE analyses, internal stress redistribution that occurs between a structural element is not necessarily the most probable one. Instead it favours a brittle failure mode, which is the main reason why some modern codes of practice (for example EC2 [29]) recommend that only GSF should be applied when conducting a global nonlinear FE analysis. This recommendation is debatable (which is clearly indicated in the EC2[29] itself), since it is not in agreement with the general design format of the code (partial safety format). Nevertheless, GSF gives more accurate estimates of the absolute magnitude of deformations which is important when taking into account the second order effects in the nonlinear calculations. In addition to this EC2 [29] does suggest that PSF is suitable for hand-calculations of STM, which presents a global nonlinear calculation method, and as such takes into account the internal stress redistributions between steel and concrete. This raises a question of why PSF should not be used with nonlinear FE models, since the fact that a calculation is done by hand or by means of nonlinear FE does not change the physical nature of the approach. Finally, EC2 [29] concludes that a non-linear analysis with PSF is acceptable but conservative since the potential benefits of using a refined calculation method are lost.

According to subsection 7.11.3 of MC2010 [34] PSF can be applied for global non-linear analyses giving a safe estimate of the design resistance. This approach is consistent since it employs the same safety strategy for hand and finite element based calculation methods (in other words RPSF and EPSF). Thus, the classical partial safety factors ($\gamma_c=1.5$ and $\gamma_s=1.15$) should be applied when designing new structures with EPSF method. When it comes to assessment of the existing structures it is pertinent to keep the same safety format but one can argue that such approach gives slightly conservative results. This is why MC2010 [34] also allows application of the probabilistic design methods when conducting the nonlinear FE simulations. Aside from performing a full Monte-Carlo simulation to determine the design resistance, MC2010 [34] introduces an approach that estimates the coefficient of variation of the ultimate resistance and allows one to calculate the global safety factor for each particular case (depending on the sensitivity of the element's resistance towards the variation in material strength). In addition to this, fixed values of the global safety factor are also provided as a further simplification.

In order to take advantage of enhanced accuracy of nonlinear FEM analysis while keeping the PSF when assessing the strength of structural concrete members, a method for tailoring partial safety factors was developed by Tanner et al. [112, 113, 114]. So far this methodology showed that it is in agreement with code recommendations, but is sensitive to scatter of concrete compressive strength (systematic assessment of actual material properties on site is required for this approach). Therefore, the reduction of the partial safety factors should be taken with caution. Based on this work, custom partial safety factors which are meant to be used with EPSF when assessing the strength of existing structural concrete members were calculated.

When talking about structural uncertainties, there are two major groups that influence the final value of partial safety format for steel and concrete:

1. Uncertainties related to material properties (γ_C for concrete and γ_S for steel);
2. Uncertainties related to model and geometrical dimensions ($\gamma_{Rd,c}$ and $\gamma_{Rd,s}$).

The two factors are multiplied in order to obtain the final value of partial safety coefficient for concrete and steel in the following manner:

$$\gamma_c = \gamma_C \cdot \gamma_{Rd,c} \text{ for the concrete partial safety factor} \quad (3.12)$$

$$\gamma_s = \gamma_S \cdot \gamma_{Rd,s} \text{ for the steel partial safety factor} \quad (3.13)$$

In the previous equations (Eq. 3.12 and 3.13), partial safety factor taking into account material uncertainty can be estimated as following [58]:

$$\gamma_C = \frac{f_{ck}}{f_{cm} \cdot e^{-\alpha \cdot \beta \cdot (COV)_{fc}}} \geq 1.00 \text{ for the concrete} \quad (3.14)$$

$$\gamma_S = \frac{f_{sk}}{f_{sm} \cdot e^{-\alpha \cdot \beta \cdot (COV)_{fs}}} \geq 1.00 \text{ for the steel} \quad (3.15)$$

where f_{ck} and f_{cm} respectively represent the characteristic and the mean value of concrete compressive strength (assuming a log-normal distribution of the variable);

$(COV)_{fc}$ represents the coefficient of variation of concrete compressive strength;

α represents the sensitivity factor;

β is the reliability index.

The notation for the steel safety factors is the same except the index letter “S” indicating steel instead of “C” indicating concrete.

The reliability index depends on the acceptable probability of failure (p_f) and the corresponding reference period (n) in years. For a standard design case acceptable probability of failure is equal to 10^{-6} [34] and the design reference period is equal to 50 years [34]. The reliability index can be calculated in the following manner [95]:

$$\beta_1 = \Phi^{-1}(1 - p_f) \quad (3.16)$$

$$\beta = \Phi^{-1}(\Phi(\beta_1)^n) \quad (3.17)$$

where Φ is the normal distribution function;

β_1 represents the reliability index for one year reference period;

n represents the design reference period (in years).

After introducing the recommended values to *Eq.3.16* the reliability index for one year is equal to 4.75. Based on *Eq.3.17* the same index for 50-year reference period is equal to 3.89. MC2010 [34] recommends a value of 3.80 for the reliability index (50-year reference period), which was assumed for the purpose of this research.

The sensitivity factor is separating dominating uncertainties from non-dominating uncertainties. The final value of a partial safety factor (refer to *Eq.3.12* and *Eq.3.13*) is obtained assuming that one of the two sub-factors is dominating (due to the material uncertainties or modelling uncertainties) and the other one is not. Out of the two combinations the one governing the maximum value of the total partial safety factor is selected. According to MC2010 [34] in case the variable uncertainty is of key importance (dominant variable) it should be assumed a sensitivity factor equal to $\alpha=0.80$; otherwise $\alpha=0.24$.

As it was already indicated, the most significant parameter (the one having the strongest impact on the final value of the partial safety factor) is the coefficient of variation of the materials. For steel, this scatter is not very high and a value of 0.055 is assumed as fixed (according of MC2010 [34]). The *CoV* was back-calculated assuming lognormal distributions of the variable with $f_{sk}=500$ MPa and $f_{sm}=550$ MPa. Variation of the concrete compressive strength on the other hand is something which is much less uniform. In addition to this, quality control systems have changed a lot over the past century, so it is very difficult to give general recommendations. This is why it is very important to conduct a thorough statistical analysis of concrete compressive strength for each particular structure which is being assessed. However, in order to have an idea of the scatter of concrete compressive strength, a literature review has been conducted based on information for concrete cast in the 1960 [44, 28, 97] and presented in *Fig.3.25*, which compares the results from three different authors (Himsworth [44], Erntroy [28] and Rüsç [97]) to modern code recommendations (MC2010 [34]).

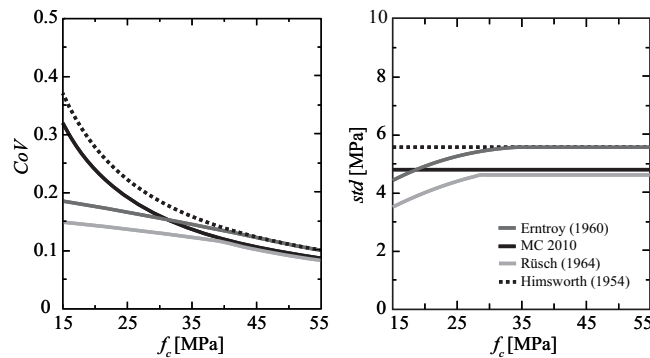


Figure 3.25: Coefficient of variation and standard deviation of concrete compressive strength according to various authors

Geometry and model uncertainties governing the value of partial safety coefficient can be expressed in the following manner [58]:

$$\gamma_{Rd,c} = \frac{(Q_{TEST}/Q_{MODEL})_k}{(Q_{TEST}/Q_{MODEL})_m \cdot e^{-\alpha \cdot \beta \cdot \sqrt{(COV_{MODEL})^2 + (COV_{geometry,c})^2}}} \geq 1.00 \quad (3.18)$$

$$\gamma_{Rd,s} = \frac{(Q_{TEST}/Q_{MODEL})_k}{(Q_{TEST}/Q_{MODEL})_m \cdot e^{-\alpha \cdot \beta \cdot \sqrt{(COV_{MODEL})^2 + (COV_{geometry,s})^2}}} \geq 1.00 \quad (3.19)$$

where $(Q_{TEST}/Q_{MODEL})_m$ represents the average ratio between the actual (tested) and estimated resistance for a specific calculation method;

COV_{MODEL} represents the corresponding coefficient of variation;

$(Q_{TEST}/Q_{MODEL})_k$ represents the characteristic value of the model uncertainty (corresponding to 5% fractile on a log-normal distribution);

$COV_{geometry,c}$ represents the coefficient of variation of the geometry properties which are relevant for the resistance strength of concrete (external cross section dimensions and effective depth);

$COV_{geometry,s}$ represents the coefficient of variation of the geometry properties which are relevant for the resistance strength of steel (effective depth and reinforcement diameter).

The first three parameters $(Q_{TEST}/Q_{MODEL})_m$, COV_{MODEL} and $(Q_{TEST}/Q_{MODEL})_k$ can be estimated using the elements from the online database (<http://i-concrete.epfl.ch/epsf/epsf.html>). In addition to this the analysed members can be divided into two groups:

1. Members failing in flexure
2. Members failing in shear

For each of these groups the average Q_{TEST}/Q_{MODEL} ratio and COV_{MODEL} can be estimated using the EPSF method. Reinforced concrete elements from the same database have been assessed using the recommendations from MC2010 [34] in order to compare the final values of partial safety coefficient. It is expected that the PSF for EPSF will be lower (due to the higher accuracy of the method) compared to code recommendations, and that the PSF for code recommendations should be equal to $\gamma_c=1.5$ and $\gamma_s=1.15$. *Tab.3.4* shows the results of EPSF analysis and code recommendations of the database.

Table 3.4: Ultimate strength of structural concrete elements from the online database estimated using EPSF method and MC2010 code provisions

Model	EPSF		MC2010		
	Flexural	Shear	Flexural	Shear- Lo1	Shear- Lo2
Q_{TEST}/Q_{MODEL}	1.075	1.048	1.059	1.439	1.223
COV_{MODEL}	0.060	0.083	0.080	0.212	0.168

It is important to emphasise that the following test campaigns were selected from the database for the purpose of this research, in order to account only for the specimens that had clear flexural and shear failures (Vecchio and Shim [122], Yoon et al. [126], Sagaseta and

Vollum [104]; Sørensen [110], Leonhardt and Walter [68], Kaufmann and Marti [54]; Kaufman and Ramirez [51], Kuchma et al. [60] without specimen G10, Rupf and Muttoni [103] without specimen SR31B, Moore [79] and Fernández Ruiz and Muttoni [31]). Specimens which experienced some local failures during the experiments were therefore discarded. Selected EPSF results are presented in Fig. 3.26.

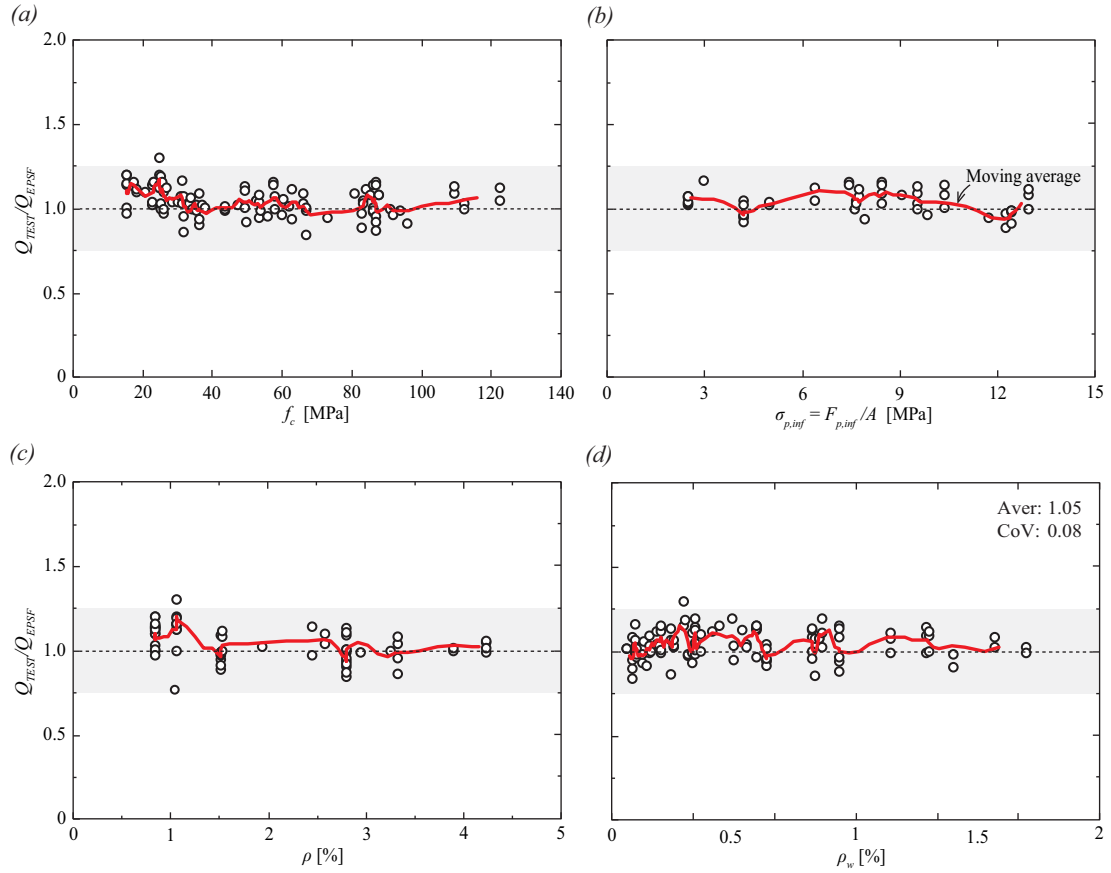


Figure 3.26: Selected member from the online database used to estimate the tailored partial safety coefficients for EPSF analysis - predicted and estimated strength in function of: (a) concrete compressive strength; (b) initial prestress; (c) longitudinal reinforcement ratio; (d) transverse reinforcement ratio

When it comes to variation of geometry properties applied CoV are given in Tab.3.5 (taken from Tanner et al. [112, 113, 114]). All variables assume normal distribution.

Table 3.5: Main parameters estimating geometrical uncertainties in structural concrete

Variable	R_k/R_m^*	CoV
External cross-section	1.000	0.030
Effective depth	1.000	0.040
Reinforcement diameter	1.000	0.020
*Bias value – ratio between characteristic and mean value of a variable		

Final values of PSF for concrete are presented in *Fig.3.27* to *Fig.3.28* (where MC2010 [34] equations were used to assess the ultimate strength of the elements for the database) and *Fig.3.29* to *Fig.3.30* (where the same was done using the EPSF method).

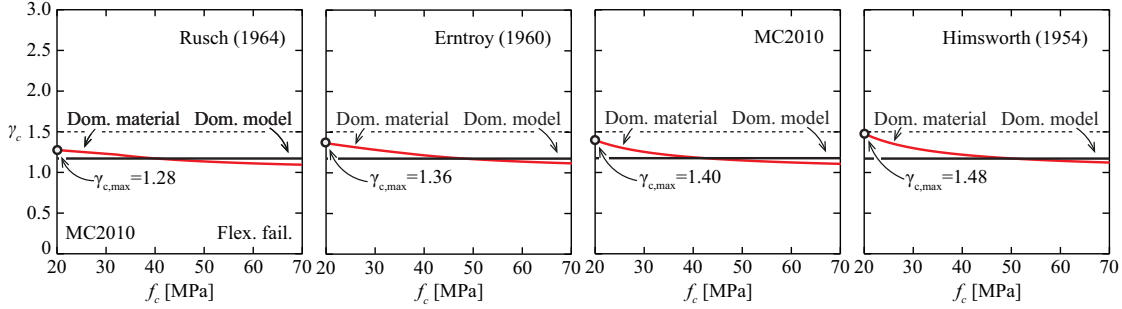


Figure 3.27: Tailored partial safety factors for concrete (flexural failure estimated with MC2010)

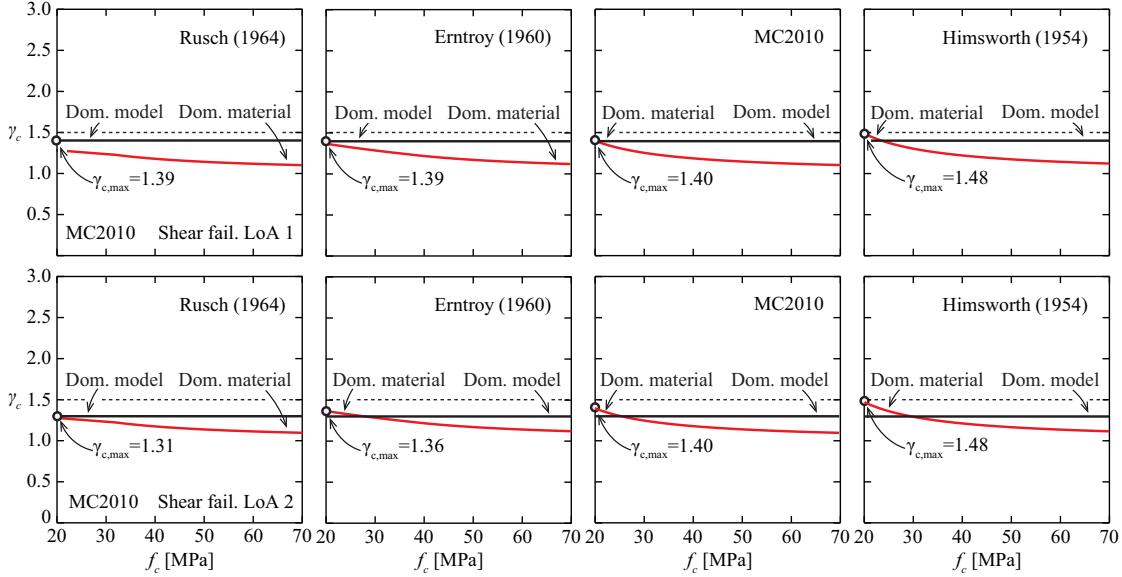


Figure 3.28: Tailored partial safety factors for concrete (shear failure estimated with MC2010)

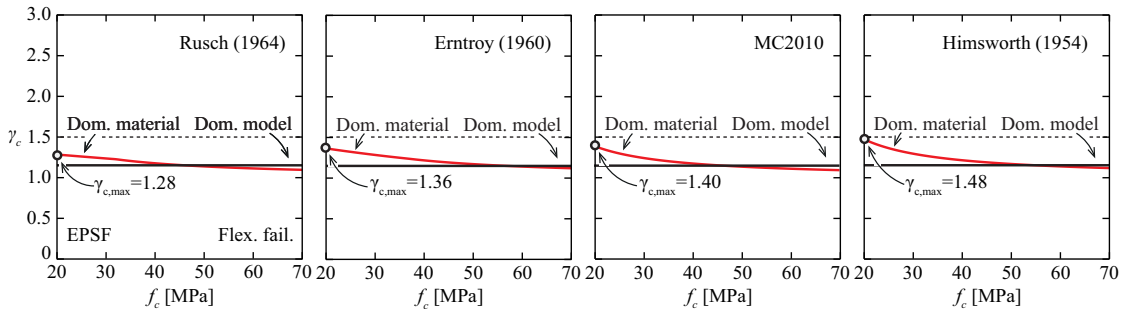


Figure 3.29: Tailored partial safety factors for concrete (flexural failure estimated with EPSF)

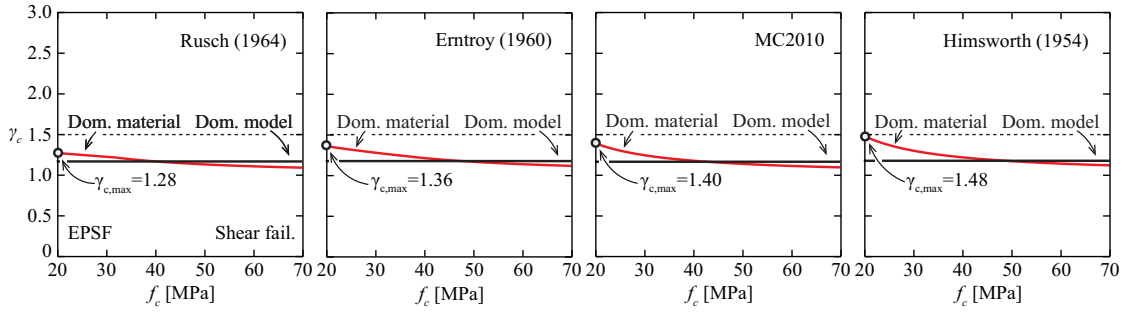


Figure 3.30: Tailored partial safety factors for concrete (shear failure estimated with EPSF)

Shear resistance of the elements has been estimated using both first and second Level of Approximation (LoA) from MC2010 [34]. In each of the graphs, the red line gives the value of the partial safety factor for concrete assuming that the material uncertainties are dominant. On the other hand, the black line gives the same values assuming that model and geometry uncertainties are dominant. The PSF are given in a function of concrete compressive strength. Each of the four graphs in Fig.3.27 to Fig.3.30 assumes different scatter of concrete compressive strength (indicated each time in the upper right corner of the graph).

In case the structural analysis is based on equations presented in MC2010 [34] highest partial safety factor for the concrete is equal to 1.48 (which is close to 1.50 indicated by the codes) for elements failing in flexure and shear. This value is governing each time for the low strength concrete (around 20 MPa) if the dispersion of the concrete compressive strength is assumed according to Himsforth [44]. In case of elements failing in flexure, it can be observed that the PSF for concrete can be reduced as the concrete compressive strength increases, due to the low CoV of concrete compressive strength and high accuracy of the applied model. Elements failing in shear, on the other hand, do not experience the same significant reduction of partial safety factors. This is due to the fact that the applied model is much less accurate compared to the one for flexure (refer to Tab.3.4). In addition to this, it can be observed that the first level of approximation for shear according to MC2010 [34] governs higher partial safety factor for concrete ($\gamma_c=1.39$) compared to the second level of approximation $\gamma_c=1.31$ for higher concrete compressive strength, which is to be expected. In order to keep a uniform value of the PSF for concrete, the maximal obtained should be selected (referring to 1.48 in this case), which indicates that the tailoring procedure is in agreement with the code regulations.

For the EPSF method partial safety factors are similar for both failure modes (refer to Fig.3.29 and Fig.3.30), due to high model accuracy for both types of failure (refer to Tab.3.4). Similarly to elements failing in flexure estimated with MC2010 [34], the material uncertainties are dominant in case of lower strength concrete (around 20 MPa), and govern the maximal value of PSF ($\gamma_c=1.48$). It can be observed that this value is highly dependent on CoV of concrete compressive strength (in case concrete compressive strength scatter is assumed according to Rüsçh [97] for example the maximal PSF for concrete is $\gamma_c=1.28$). This is why it is crucial to accurately estimate the level of concrete compressive strength dispersion. PSF tailored for EPSF method can be reduced as the concrete compressive strength increases (refer to Fig.3.29 and Fig.3.30). According to the proposed procedure, it can be as low as 1.17 in case of 70 MPa

concrete, at which point it becomes almost equal to PSF for steel, indicating that the partial safety factor practically becomes a global safety factor.

The final value of partial safety factor for concrete that should be used with EPSF method is not explicitly given in this chapter. Similarly, to LoA approach, one should first apply $\gamma_c = 1.5$. In case this simulation does not give satisfying accuracy, the value of PSF for concrete could potentially be reduced according to the proposed procedure. Thorough statistical analysis needs to be conducted in order to verify the scatter of concrete compressive strength for a given element. In addition to this, the value of sensitivity coefficients needs to be revised in order to make sure that the 0.24 and 0.8 are pertinent values for that particular case.

The partial safety factor for steel has also been calculated, but since the dispersion of the yield strength is much smaller, the results are not presented in the form of a graph. *Tab. 3.6* summarizes the obtained results.

Table 3.6: Tailored partial safety factors for steel

<i>Failure mode</i>	<i>Flexural Failure</i>	<i>Shear Failure</i>
<i>MC2010</i>	1.171	-
<i>EPSF</i>	1.146	1.162

It can be observed that the PSF for steel are much more uniform and are not that different from 1.15 indicated by the codes. The reason why the PSF for steel was not calculated in case of elements failing in shear for the MC2010 [34] is due to the fact that in reality, failure of the tested specimens was always governed by the simultaneous failure of concrete and reinforcement. Even though the codes have predicted a few simulations failures of elements in shear, the available number of such elements was not sufficient for a pertinent statistical analysis.

Chapter 4: Effectiveness factor for concrete compressive strength accounting for the presence of cracks and interaction with the reinforcement

Technical paper titled “Response of RC panel accounting for crack development and its interaction with rebars”, written by Dr. Eckart Hars, Filip Niketić and Dr. Miguel Fernández Ruiz was based on this chapter. The article was accepted for publishing by the Magazine of Concrete Research on the 7th of July 2017 under an article number MACR-D-17-00077R1.

Contributions of Filip Niketić to creation of this publication involved:

1. Developing expression for estimating the plastic strength of rebars subjected to doweling;
2. Deriving the expression for estimating plastic strength of damaged and undamaged concrete struts;
3. Quantifying damaged and undamaged concrete struts in a panel;
4. Developing and implementing a solving procedure for estimating the shear strength of the RC panels using the proposed model;
5. Assembling a database with 77 structural panels and validating the proposed procedure;
6. Producing figures for the article;
7. Writing the manuscript of the article.

4.1 Introduction and state of the art

Limit analysis (through application of stress fields and strut-and-tie models) provides a consistent framework for design and assessment of structural concrete members. It can be applied to a wide range of cases, involving elements with various geometry, and material properties subjected to in-plane as well as out-of-plane loading [92]. However, the application of the theory of plasticity on structural concrete elements was challenged, due to the brittleness of concrete. Unlike the stress-strain diagram of steel, which shows ductile behaviour in tension and compression after reaching its yielding point (see f_y in *Fig.4.1b*), the strength of concrete decreases once its ultimate resistance (f_c) has been achieved (see *Fig.4.1a*). Such behaviour

compromises the development of the plastic zones in concrete and therefore the application of limit analyses, especially for cases where the ultimate resistance of structural elements is governed by crushing of the compressed zones. In order to overcome this, early elements were designed in a way that avoid reaching the concrete compressive strength at ULS. In other words, ultimate load-bearing capacity of members was governed by yielding of the reinforcement.

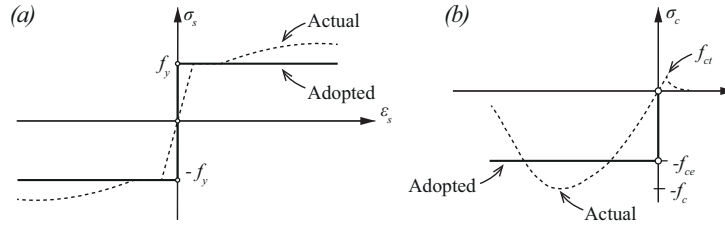


Figure 4.1: Actual and adopted stress-strain diagram for: (a) steel; (b) concrete according to full plastic approach

When Drucker [27] used the theory of plasticity to obtain the exact solution of a simple beam subjected to a point load in 1961, the direct application of the limit analysis on structural concrete members was theoretically proven. Experimental campaign of Leonhardt and Walther, conducted in 1962 [67], showed that reinforced concrete beams which failed in flexure did experience plasticisation of the compressed zones. All this lead to further development of stress fields and strut-and-tie models as general tools for design and assessment of structural concrete elements.

In 1979 Exner [30] proved that the application of the theory of plasticity in combination with unreduced concrete compressive strength (f_c in Fig.4.1a) can lead to unconservative solutions. He argued that the concrete compressive strength needs to be reduced as a consequence of material softening. In other words, an effective concrete compressive strength f_{ce} should be applied instead of f_c (see Fig.4.1a). Using the experimental results of RC beams with no transversal reinforcement, he defined an empirical expression for concrete compressive strength effectiveness factor:

$$\nu = \frac{3.2}{\sqrt{f_c}} \quad (4.1)$$

According to Exner [30], the effective concrete compressive strength can be estimated in the following manner:

$$f_{ce} = \nu \cdot f_c \quad (4.2)$$

Current codes of practice (such as MC2010 [34], EC2 [29] or ACI 318 [1]) include reduction of concrete compressive strength measured on a cylinder when estimating structural capacity of load-bearing members. According to MC2010 [34], the effective concrete compressive strength is obtained in the following manner:

$$f_{ce} = \eta_{fc} \cdot k_e \cdot \alpha_{cc} \cdot f_c \quad (4.3)$$

where η_{fc} represents the concrete compressive strength brittleness factor;

k_ϵ represents the concrete compressive strength softening due to imposed transversal strains;
 α_{cc} takes into account the effects of loading rate and loading level on concrete compressive strength.

According to MC2010 [34], the effects of the post-tensioning ducts on effective concrete compressive strength are taking into account indirectly, by reducing the thickness of the analysed web in the following manner:

$$b_{w,nom} = b_w - k_D \cdot \sum \phi_D \quad (4.4)$$

where $b_{w,nom}$ represents the nominal web thickness;

b_w represents the initial web thickness;

ϕ_D represents the diameter of the post-tensioning ducts.

This chapter analyses all concrete compressive strength reduction factors from *Eq. 4.3* except the last one (α_{cc}). The most significant models in this field are presented and discussed. A critique of the MC2010 [34] multiplicative approach (refer to *Eq. 4.3*) is introduced, and finally, a mechanically based model for assessing the concrete compressive strength effectiveness factor that takes into account different failure mechanisms of structural elements (concrete crushing, spalling and sliding) is presented and discussed. Its consistency is validated by means of extensive comparison to available test data found in literature.

4.1.1 Concrete compressive strength brittleness factor - η_{fc}

Response of a standard concrete cylinder subjected to uniaxial compression, consist of an ascending branch that reaches up to its ultimate strength, followed by a descending softening branch. Constitutive law of concrete has been investigated by many authors in numerous experimental campaigns, resulting in simplified empirical expressions such as the one proposed by Fernández et al. [33]:

$$\sigma_c = \frac{1}{1 + (\epsilon_c / \epsilon_0)^\alpha} \cdot E_c \cdot \epsilon_c \quad (4.5)$$

$$\epsilon_0 = \frac{\alpha \cdot f_c}{E_c \cdot (\alpha - 1)^{(1-1/\alpha)}} \quad (4.6)$$

$$\alpha = 0.5 + f_c / 20 + f_c^2 / 1'500 \quad (4.7)$$

where σ_c represents the concrete compression stress;

ϵ_c represents concrete compressive strain;

E_c represents Young's modulus of elasticity for concrete;

f_c represents the concrete compressive strength.

Dashed lines in *Fig. 4.2a* represent the actual behaviour of concrete subjected to uniaxial compression (described in *Eq. 4.5*). As it can be seen, brittleness of concrete increases in

function of the uniaxial compressive strength. Descending branch of a 100 MPa concrete for example is much steeper (hence, more brittle) compared to the one corresponding to a 40 MPa concrete, while the stress-strain diagram of 20 MPa concrete leaves an impression of an almost ductile material behaviour.

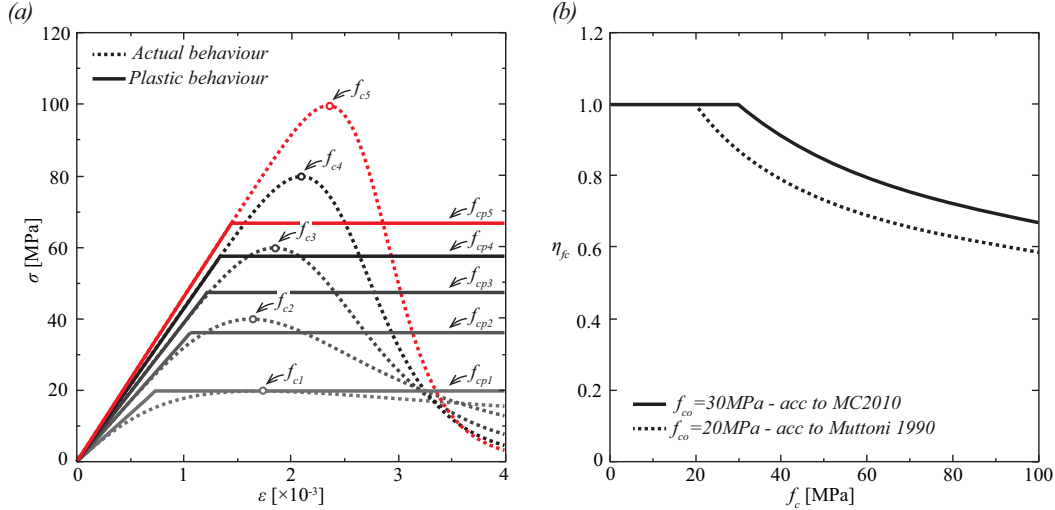


Figure 4.2: Concrete brittleness factor: (a) actual and plastic constitutive law of concrete; (b) the brittleness factor according to Muttoni [82]

If the limit analysis is to be applied on structural concrete, actual stress distribution at ULS should correspond to the one assumed by the theory of plasticity (constant stress blocks). Fig.4.3 illustrates this problem, using an element subjected to pure bending. Assuming that the maximal compressive strains are approximately equal to 3.5‰, and that the sections remain perfectly plane at ULS (refer to Fig.4.3a), allows one to estimate the concrete stress distributions at the critical cross-section. Applying the concrete constitutive law presented in Eq.4.5 results in stress distribution presented in Fig.4.3b, which does not correspond to constant stress block assumed by the theory of plasticity. In order to overcome this, a concrete compressive strength brittleness factor (η_{fc}), which smears the actual stress distribution down to a block with constant stress intensity needs to be applied (refer to $f_c \cdot \eta_{fc}$ in Fig.4.3c).

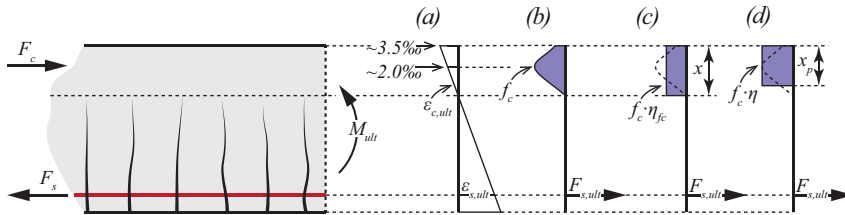


Figure 4.3: Analysis of a critical section subjected to pure bending at ULS: (a) strain distribution; (b) stress distribution assuming actual concrete constitutive law; (c) stress distribution assuming plastic concrete constitutive law with brittleness factor; (d) stress distribution assuming plastic concrete constitutive law without the brittleness factor

Applying the strength reduction factor while smearing the stresses over the entire compression zone (marked as x in Fig.4.3c) is only one approach for dealing with brittleness of concrete. An alternative method is presented in Fig.4.3d, where the intensity of the stresses

block is equal to $f_c \cdot \eta$ while the height of the compression zone is reduced down to x_p . According to MC2010 [34]:

$$x_p = 0.8 \cdot x \quad \text{for } f_c \leq 50 \text{ MPa} \quad (4.8)$$

$$x_p = 0.8 - (f_c - 50)/400 \quad \text{for } 50 < f_c \leq 90 \text{ MPa} \quad (4.9)$$

$$\eta = 1.0 \quad \text{for } f_c \leq 50 \text{ MPa} \quad (4.10)$$

$$\eta = 1.0 - (f_c - 50)/200 \quad \text{for } 50 < f_c \leq 90 \text{ MPa} \quad (4.11)$$

Even though the second approach can be applied for bending, in other cases (such as shear for example), the reduction of the area upon which compressive stresses are acting is not so evident. Hence, the application of a brittleness factor provides more consistent solutions for various stress states. It now becomes evident why the resistance of structural concrete elements can be overestimated in case the intensity of stress block remains equal to f_c while the height of the compressed zone (x) stays the same (as argued by Exner [30]).

In order to compensate for the brittle behaviour of concrete Muttoni [82] proposed a following expression:

$$\eta_{fc} = \sqrt[3]{\left(\frac{f_{c0}}{f_c}\right)} \leq 1.0 \quad (4.12)$$

where f_{c0} represents the concrete compressive strength up to which the actual constitutive law for concrete exhibits a ductile behaviour.

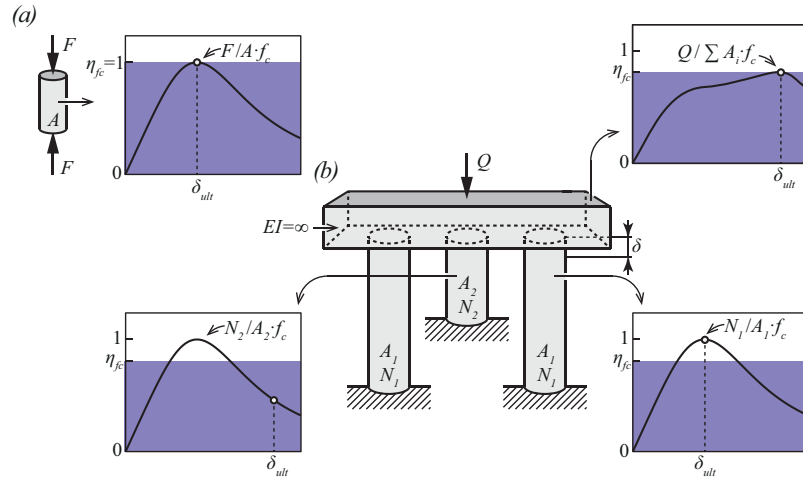


Figure 4.4: Redistribution mechanisms: (c) response of a standard concrete cylinder; (b) response of a system consisting of three cylinders and an infinitely rigid beam (adopted from Muttoni *et al.* [89])

Fig.4.2b shows the concrete compressive strength brittleness factor according to Muttoni [82]. The initial limit which separates ductile from brittle behaviour of concrete cylinders was set equal to $f_{c0}=20$ MPa (refer to the dashed line in Fig.4.2b), but was later

modified to 30 MPa (refer to the full line in *Fig.4.2b*). Applying the brittleness factor on actual stress-strain diagrams for concrete, results in the elastic-perfectly plastic constitutive laws for cylinders, presented in *Fig.4.2a* with full lines. The reduction of concrete compressive strength becomes more significant as the ultimate resistance increases (refer to *Fig.4.2a* and *b*), and the actual behaviour becomes more brittle.

Brittleness factors should also be applied when estimating ultimate resistance of structural concrete members subjected to constant compressive strains; not just when there is a distribution of strains over the compressed zone (such is the case with bending, presented in *Fig.4.3* for example). The reason for this is schematically presented in *Fig.4.4*, which compares the behaviour of a standard cylinder (see *Fig.4.4a*) to a system of three columns connected with an infinitely stiff beam (see *Fig.4.4b*). Obtaining the failure load of a cylinder does not require the application of a brittleness reduction factor, since the maximal material stress is reached at the same point across the entire cross-section, and the element does not need to facilitate any additional redistribution (in other words $\eta_c=1$ as presented in *Fig.4.4a*). On the other hand, applying the same displacement (δ) over three short columns made out of identical concrete, results in different strain states in each one of them. The shortest (interior) column is already plasticized by the time the system fails (see the bottom left graph in *Fig.4.4b*). On the other hand, the longer (exterior) columns have just reached the peak of the stress-strain diagram (refer to bottom right graph in *Fig.4.4b*). Consequently, summing the individual resistances of the three members while using the actual concrete compressive strength (f_c), results in overestimation of the system's strength. In order to compensate for this, a concrete compressive strength brittleness factor (η_c) should be applied to all three columns (as indicated in *Fig.4.4b*). The same effect can be observed within a single structural concrete element which has reinforcement in compression. Strain-wise, the yielding point of the two materials (concrete and steel) does not coincide, thus leading to softening of concrete prior to reaching the yielding of the reinforcement (similarly to what is described in *Fig.4.4b*).

It can be concluded that the stress redistribution in structural concrete elements should be anticipated in case of isostatic as well as hyperstatic systems. Therefore, the concrete compressive strength brittleness factors (η_c) should always be applied in order to facilitate safe usage of the limit analysis.

4.1.2 Concrete softening caused by imposed transversal strains - η_e

Being a quasi-brittle material which cracks at relatively low loads, concrete relies on reinforcement in order to obtain the necessary strength and ductility when subjected to various actions. As the reinforcement starts to deform, it induces strains by means of concrete-to-steel bond, causing the formation of smeared cracks (as presented in *Fig.4.5a*). This reduces the compressive strength of concrete and limits the ultimate resistance of analysed elements. In addition to this, the physical presence of the rebars in the concrete matrix introduces discontinuities which deviate the compressive stress path. Depending on the geometry properties of analysed members, this might lead to structural failures.

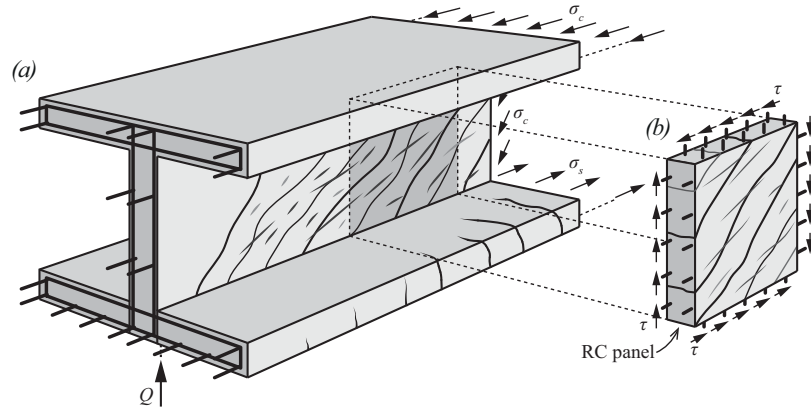


Figure 4.5: Physical behaviour of concrete: (a) in a reinforced concrete beam; (b) in a panel

Many experimental programmes have been conducted in the past in order to better understand this complex problem ([5], [10], [47], [56], [57], [75], [94], [106], [118], [119], [121], [124], [127]), and their results are today incorporated in modern codes of practice (MC2010 [34], EC2 [29], ACI 318 [1]), as well as nonlinear numerical methods [35]. Most of the studies have been performed on reinforced concrete panels (such as the one presented in *Fig. 4.5b*), since the specimens can be tested until failure while being subjected to uniform stress states (pure shear, shear combined with tension or compression, pure compression, compression combined with tension etc.). However, some of the experimental campaigns focusing on the investigation of effective concrete compressive strength were performed on reinforced concrete beams failing in shear (Muttoni [82] and Zwicky [129] for example). Such elements were subjected to a non-uniform stress state, meaning that a part of shear was taken by the compressed flange, as well as the direct strut action and doweling of the longitudinal reinforcement. Consequently, estimating the effective concrete compressive strength becomes much more challenging, which is why the application of reinforced concrete panels was preferred. However, it is important to emphasise that experimental investigation of beams gives crucial information on the realistic behaviour of structural elements, and as such, it is very important from a practical point of view.

Fig. 4.6 shows the influence of transversal strains on concrete compressive strength. The black line represents the stress-(transversal) strain diagram of a standard cylinder test, showing a clear softening of the material once the compressive strength (f_c) has been reached. Given a fact that similar curves can be obtained for a structural concrete panel (refer to the red curve in *Fig. 4.6*) Muttoni [82] proposed that the softening branch of the stress-strain diagram can be used as a failure criterion for the element, allowing one to determine the effective concrete compressive strength (f_{ce}). The average transversal strain (ϵ_l) of a panel can be obtained based on the crack opening in the direction of the reinforcement (refer to *Fig. 4.6*). However, the shape of the softening branch in a stress-(transversal) strain diagram is quite challenging to predict due to the large scatter in the experimental results. In addition to this, the proposed procedure does not account for all potential interactions between the concrete and the reinforcement (as it will be later presented).

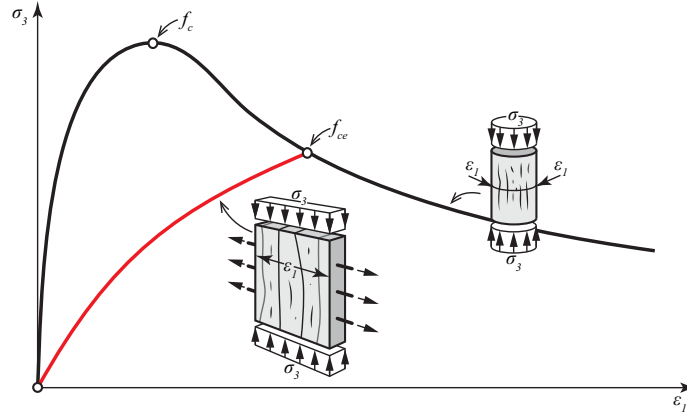


Figure 4.6: Descending branch of a standard cylinder test used as a failure criterion for reinforced concrete panels (adopted from Muttoni et al. [89])

There are three basic failure modes which have been observed in the experimental campaigns involving reinforced concrete panels (observed by Vecchio and Collins [120]):

1. Crushing of the concrete struts (presented in Fig.4.7a);
2. Spalling of the concrete cover (presented in Fig.4.7b);
3. Sliding along an initial crack (presented in Fig.4.7c).

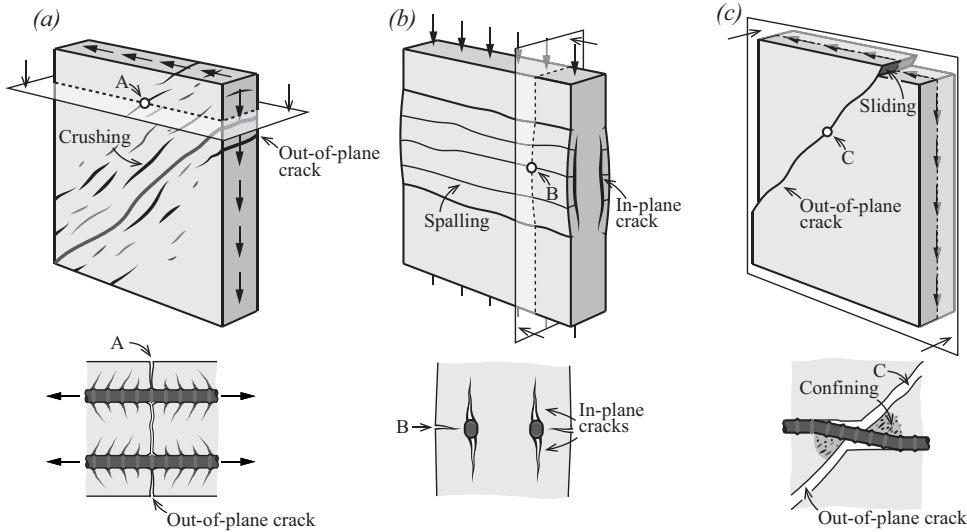


Figure 4.7: Failure mechanisms of reinforced concrete panels: (a) concrete crushing; (b) concrete cover spalling; (c) concrete sliding

First two failure modes are a result of the physical interaction between the rebars and the surrounding matrix. In case of concrete crushing, the resistance of the element is reached when the out-of-plane cracks, imposed through bond by the elongation of the rebars (see Fig.4.7a) soften the surrounding concrete matrix up to its failure. Looking at the horizontal cut, made at the level of the rebars (refer to the bottom of Fig.4.7a) one can observe the formation of the out-of-plane cracks according to the model of Tepfers [115] based on the experimental observations of Goto [38] (point A marks the location of an out-of-plane crack). The described

behaviour is mechanically consistent with the softening of concrete cylinders (presented in *Fig. 4.6*), meaning that the approach of Muttoni [82,89] gives satisfying results when structural elements are failing due to crushing of the concrete.

Concrete cover spalling is governed by the in-plane cracks forming above and below the rebars. Principal concrete compressive stresses are deviated towards the rebar due to the change in stiffness (a similar phenomenon occurs when post-tensioning ducts are present in the concrete webs as will be shown later on). Consequently, tensile stresses are imposed in the cross section, which ultimately leads to cracking. As the in-plane cracks separate the concrete cover from the core, the difference between the average strains of the cover and the core becomes greater. Gradually, the concrete cover begins to bend and form the longitudinal cracks (as presented in *Fig. 4.7b*). Vertical cross-section of the panel, showing the disposition of cracks leading to concrete cover spalling at *point B* is presented in *Fig. 4.7b*.

Finally, sliding failures occur when maximal contact stress that can be transferred through an initial crack (by means of the aggregate interlock combined with the dowel action of the reinforcement) is surpassed, resulting in a relative slip between the two segments of the panel (as presented in *Fig. 4.7c*). The slip can also occur along the plane which contains the points of the rebars weakened by the doweling (this mechanism will be analysed later on in detail). Even though the two hypothesis for the origin of the slip are different, they lead to the same physical results at ULS (sliding of the panel along with the yielding of the reinforcement). A section made through the mid-plane of the panel shows doweling of a horizontal rebar located at the *point C*, as well as its interaction with the surrounding concrete matrix (refer to confining concrete regions in *Fig. 4.7c*).

Failure of panels reported in the experimental campaigns usually combines two or even all three presented mechanisms (crushing, spalling and sliding), which limit the concrete compressive strength simultaneously. Depending on material and geometrical properties of analysed members, one of them is governing at ULS.

One of the first models to account for steel-to-concrete interaction was introduced by Collins [22] in 1978, as a part of the Compression Field Theory:

$$\eta_\varepsilon = \frac{3.6}{1 + \frac{2 \cdot (\varepsilon_1 - \varepsilon_3)}{\varepsilon_0}} \leq 1.0 \quad (4.13)$$

where ε_1 represents the principal tensile stain (introduced as a positive value);

ε_3 represents the principal compressive strain (introduced as a negative value);

ε_0 represents the strains corresponding to cylinder compressive strength (assumed equal to 2‰).

The reduction factor is presented in form of a surface diagram in *Fig. 4.8a*, according to which effective concrete compressive strength depends both on tensile and compression strains.

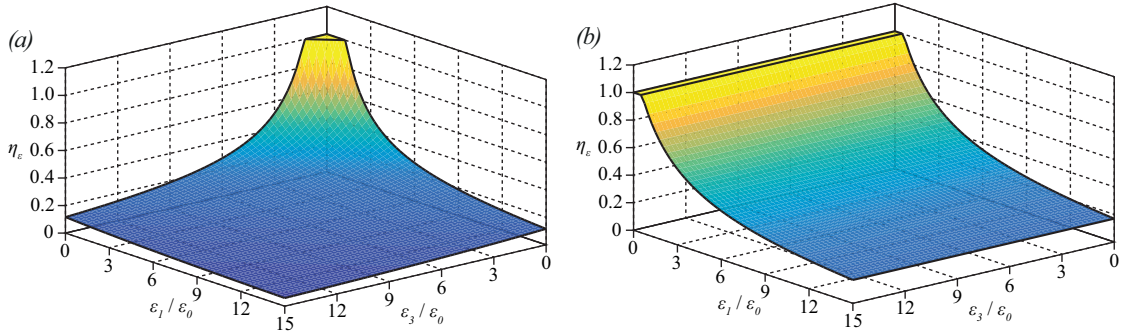


Figure 4.8: Concrete compressive strength softening law taking into account the concrete interaction with reinforcement: (a) according to Collins 1978 [22]; (b) according to Vecchio and Collins 1986 [120]

The proposed empirical expression has two important issues:

1. Reduction of the concrete compressive strength as a function of principal compressive strains is not physically consistent;
2. The fact that the tensile and compressive strains are biased means that the concrete compressive strength depends on the total amount of strains in a system, rather than the amount of imposed tensile strains.

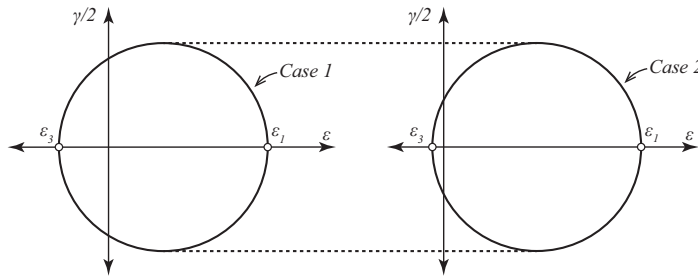


Figure 4.9: Two different strain states of a structural concrete member governing the same concrete compressive strength according to Collins [22]

In other words, the same effective concrete compressive strength is obtained when imposing higher transversal strains into a system, in case this increase is compensated with lower compressive strains. For example, effective concrete compressive strength for *Case A* is identical to the one from *Case B* in Fig. 4.9.

The two inconsistencies were later corrected in 1986, when Vecchio and Collins [120] introduced the Modified Compression Field Theory (MCFT), which is one of the most commonly used expressions for the reduction of concrete compressive strength accounting for the interaction with the reinforcement:

$$\eta_\epsilon = \frac{1}{0.8 + 170 \cdot \epsilon_1} \leq 1.0 \quad (4.14)$$

Eq. 4.14 is presented in a form of a surface graph in Fig. 4.8b. When comparing the failure surface from Fig. 4.8a to that from Fig. 4.8b, it can be seen the reduction of the concrete compressive strength is much smaller for the same amount of transversal tensile strain. In

addition to this, *Eq. 4.14* is completely independent from the principal concrete compressive strains. Compared to experimental results, MCFT proved to be quite accurate and easy to implement (as shown in [120]). Nonetheless, the model of Vecchio and Collins is semi-empirical, and as such it does not distinguish between the various failure modes presented in *Fig. 4.7*. Without a proper prediction of the governing failure mechanism (concrete crushing, spalling or sliding), it is difficult to enhance the strength of an analysed element in the most effective manner.

After the introduction of MCFT, multiple authors have been working on improving the compression softening equation, by conducting additional experimental campaigns in order to invoke all three failure modes presented in *Fig. 4.7*. The range of mechanical properties of tested RC panels was widened, as well as type of loading, the number of reinforcement layers, size of the elements etc. Some of the most significant works in this field includes the approach of Belarbi and Hsu [10]:

$$\eta_\varepsilon = \frac{0.9}{\sqrt{1 + 250 \cdot \varepsilon_1}} \quad (4.15)$$

The proposed expression governs greater strength reduction for elements subjected to lower transversal tensile strains, compared to *Eq. 4.14*. This can be explained by the fact the RC panels that fail in concrete cover spalling or concrete sliding, usually reach smaller principal tensile strains at failure. The expression of Belarbi and Hsu tried to account of such behaviour. Nevertheless, the softening of concrete is still estimated in a semi-empirical manner, depending only on the amount of transversal tensile strains in a panel.

Another semi-empirical softening expression was introduced by Kaufmann [52], who analysed elements which have been subjected to significant transversal strains ($\varepsilon_1/\varepsilon_0$ up to 15, assuming ε_0 equal to equal to 2‰). According to him the effective concrete compressive strength should be accounted for in the following manner:

$$\eta_\varepsilon = \frac{1}{1.08 + 81 \cdot \varepsilon_1} \quad (4.16)$$

It is important to emphasise that according to Kaufmann [52], *Eq. 4.16* should be multiplied with the brittleness concrete compressive strength factor proposed by Muttoni (refer to *Eq. 4.12*, $f_{co} = 20 \text{ MPa}$), in order to obtain the effective concrete strength.

Zwicky [129] also proposed a simplified expression for reducing the concrete compressive strength:

$$\eta_\varepsilon = 0.67 - 14 \cdot \varepsilon_1 \quad (4.17)$$

Previous equation proved to be accurate when compared against a series of structural concrete beams tested by the author, in which case the imposed transversal tensile strains at failure varied between 5‰ and 25‰.

In order to improve the results of MCFT by taking into account the sliding which occurs along the initial cracks of RC panels, Vecchio [117] introduced another expression for concrete compressive strength reduction factor:

$$\eta_\varepsilon = \frac{1}{0.95 + 0.15 \cdot \frac{\varepsilon_1}{\varepsilon_0}} \quad (4.18)$$

Eq. 4.18 was implemented in the Disturbed Stress Field Method [117], which was able to capture the behaviour of panels with small rotation of the principal stress field direction at failure more accurately than MCFT (refer to [120]).

A direct comparison between the different approaches for estimating the softening of concrete compressive strength due to imposed transversal strains (refer to Eq. 4.14 - Eq. 4.18), is presented in Fig. 4.10a. It can be seen that the reduction proposed by Belarbi and Hsu [10], Kaufmann [52] and Zwicky [129] govern similar results, which is slightly different compared to that of Vecchio and Collins [120] and Vecchio [117].

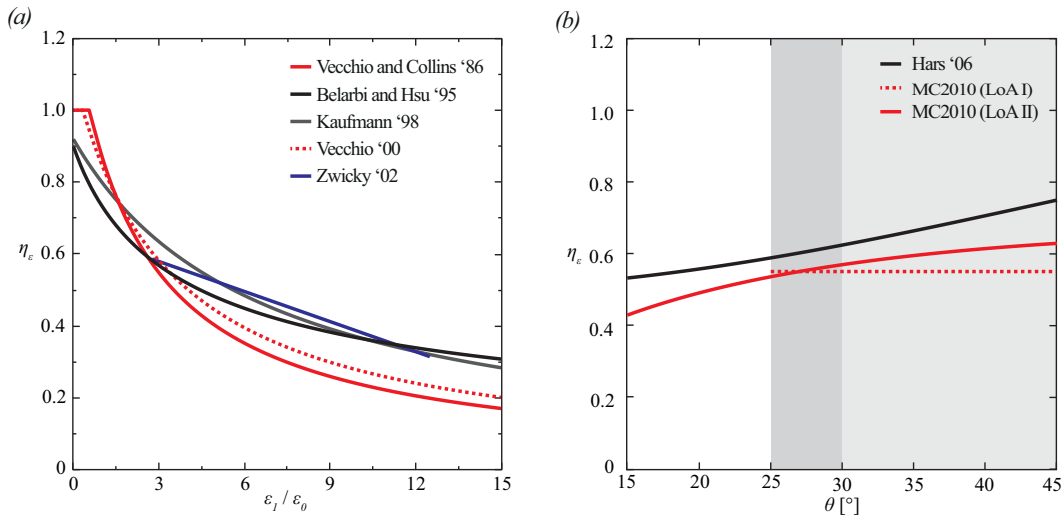


Figure 4.10: Concrete compressive strength softening laws taking into account the presence of transversal strains: (a) according to various authors; (b) simplified approach of Hars [41] and recommendations provided by MC2010 [34]

In general, the first three approaches, indicate more significant concrete compressive strength reduction for elements with less transversal strain, whereas the former two do the same in case of members subjected to higher transversal tensile strains. All proposed expressions showed satisfying behaviour when compared to corresponding databases (refer to the original publications). However, each approach lacks a clear physical background, which would allow it to predict one of the three failure mechanisms presented in Fig. 4.7 as governing (concrete crushing, spalling and sliding). Therefore, the development of a mechanically based model is necessary in order to truly understand the actual behaviour of structural elements. This is important when designing new members, since a variation in the rebar diameter and spacing may significantly influence the concrete compressive strength (see Fig. 4.7). The same can happen when changing the thickness of the concrete cover (refer to Fig. 4.7b). Using current

semi-empirical expressions (refer to *Eq.4.14 – Eq.4.18*) can only suggest if the weakest part of a structure is the concrete or the reinforcement.

Aside from estimating the effective concrete compressive strength in the most accurate manner, it is also important to provide simplified expressions for the design purposes (presented in *Fig.4.10b*). According to Hars [41], the effective concrete compressive strength can be determined based on the direction of the principal concrete compressive stress. Such approach is very straightforward to use, especially in case of reinforced and prestressed concrete beams which is very important in practice:

$$\eta_\varepsilon = 0.5 \cdot (1 + \sin^2 \theta) \quad (4.19)$$

where θ represents the direction of the principal compression stresses.

MC2010 [34] on the other hand introduces the same reduction following the LoA approach in a slightly different manner. In case of the 1st LoA, recommended concrete compressive strength efficiency factor for reinforced and prestressed concrete beams is 0.55. At the same time, the minimal inclination of the principal concrete compressive stresses direction is equal to 30° in case of RC elements, and 25° in case of prestressed concrete elements (refer to *Fig.4.10b*). The 2nd LoA introduces an expression, which estimates the effective concrete compressive strength as a function of the principal tensile strains in the following manner:

$$\eta_\varepsilon = \frac{1}{1.2 + 55 \cdot \varepsilon_1} \leq 0.65 \quad (4.20)$$

$$\varepsilon_1 = \varepsilon_x + (\varepsilon_x + 0.002) \cdot \cot^2 \theta \quad (4.21)$$

where ε_x represents the longitudinal strain at the mid-depth of the effective shear depth.

The minimal principal concrete compressive stress direction for reinforced and prestressed concrete elements is limited to:

$$\theta_{\min} = 20^\circ + 10000 \cdot \varepsilon_x \quad (4.22)$$

Fig.4.10b compares all three simplified approaches for estimating the concrete compressive strength efficiency factor. Even though the approach of Hars [41] governs slightly higher values compared to 2nd LoA of MC2010 [34], the two curves are almost parallel. This indicates that the behaviour of an element does not change significantly when applying the two different methods. It should be noted that even though the approach of Hars [41] is very straightforward to use, it implies that the inclination of the principal compressive field in a reinforced concrete beam can be lower than 20°, which is not necessarily consistent with *Eq.4.22*. The longitudinal strain at the mid-depth (ε_x) is usually positive, meaning that θ_{\min} should not be smaller than 20° (refer to *Eq.4.22*). Finally, according to the MC2010 [34], the effective concrete compressive strength determined using the 1st LoA represents a safe estimate compared to the 2nd LoA in case of RC elements. In case of prestressed concrete however, $\eta_\varepsilon=0.55$ slightly exceeds the limit imposed by the 2nd LoA for angles between 25° and 27°.

From a practical point of view this is not a problem as long as the strength of an analysed element is not governed by the crushing of the concrete. This is due to the fact that the 2nd LoA, allows lowering the direction of the principal concrete compressive stress (thus activating more stirrups), meaning that even though the concrete compressive strength is lower, the ultimate strength of an element is higher. However, if according to the 1st LoA element fails due to crushing of the concrete while the direction of the principal concrete compressive stress is smaller than 27°, switching to the 2nd LoA will slightly decrease its resistance.

4.1.3 Concrete softening caused by the presence of post-tensioning ducts

Placing steel or plastic post-tensioning duct in webs of structural concrete elements influences the flow of the principal compressive stresses throughout the thickness of analysed members. After conducting compressive tests on structural concrete panels (such are the ones presented in Fig.4.11a and b), it has been observed that the presence of post-tensioning ducts invokes out-of-plane strains into the section, which leads to failure of investigated specimens ([37,65,21,18,100,36]). The right-hand side of Fig.4.11a shows the principal compressive stress flow (refer to dashed lines) inside a panel with an empty post-tensioning duct.

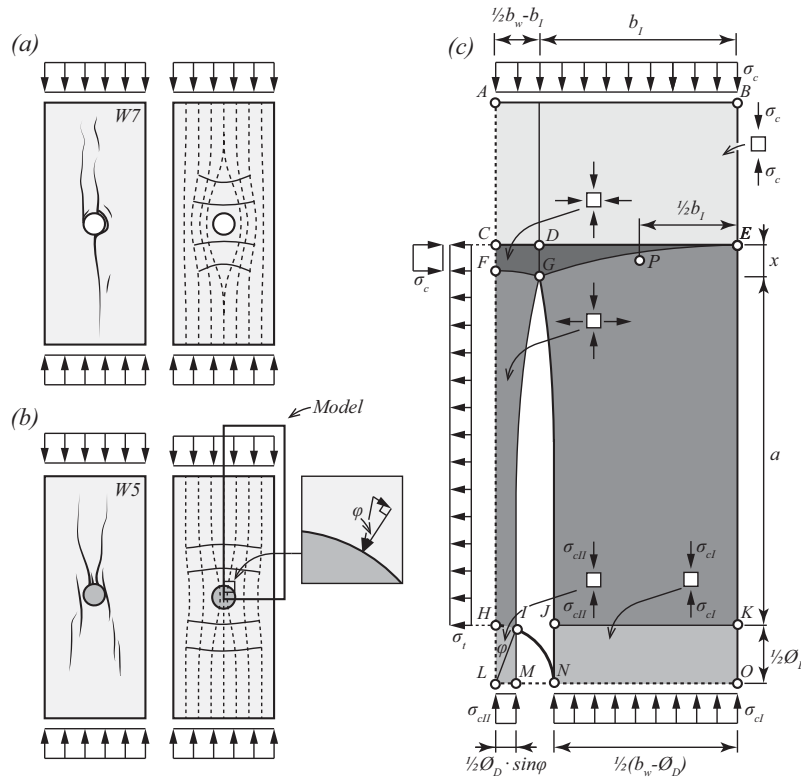


Figure 4.11: Interaction of structural concrete with prestress ducts: (a) crack pattern and stress flow in a panel with an ungrouted duct; (b) crack pattern and stress flow in a panel with a grouted duct; (c) mechanical model proposed by Hars [41]

Given a fact that an empty duct represents a void in the concrete matrix, means that the principal concrete compressive stresses need to deviate around this discontinuity region. Consequently, the tensile strength of concrete is utilized in order to facilitate the necessary

deviation (see full lines in *Fig.4.11a*). At one point, the tensile strength of concrete is surpassed, which leads to formation of in-plane cracks and failure of the panel. Such behaviour can be seen on one of the panels tested by Hars [41] (refer to the left-hand side of *Fig.4.11a*).

Grouted post-tensioning ducts on the other hand present the stiffest zones in the concrete matrix, causing the compressive stresses to deviate towards it (see *Fig.4.11b*). Similar to previous situation, this deviation is accommodated by the tensile strength of concrete (full lines in *Fig.4.11b*). As the applied load increases so does the amount of tensile stress necessary to deviate the stress field in the proximity of the duct, which ultimately leads to cracking and failure (as presented in *Fig.4.11b*).

On average elements containing grouted plastic post-tensioning ducts have reached lower ultimate strength compared to the ones that used grouted steel ducts. This can be explained by the surface roughness of the two materials (plastic and steel, as indicated in *Fig.4.11b*). When the internal compressive force reaches the duct, its tangential projection on the circular surface needs to be equilibrated by the friction occurring between the duct and the concrete in order for the compressive force to pass through. Since plastic is a smoother and less stiff than steel, the amount of compressive force which can be transferred through the duct is smaller. Consequently, more force flows around the duct inducing higher transversal tensile stress in the section, which lowers the element's strength.

Hars [41] developed a mechanically based model, predicting out-of-plane failures of structural panels containing ungrouted or grouted (plastic and steel) post-tensioning ducts. The equilibrium-based model is given in a form of a stress field and presented in *Fig.4.11c*. It shows the internal stress distribution for one quarter of the entire cross section (as indicated in *Fig.4.11b*). A segment of the post-tensioning ducts is located in the bottom left part of *Fig.4.11c*. The panel is subjected to uniaxial compression from the top (resulting in σ_c compressive stress), leaving its side surfaces completely stress-free.

Area *ABCDE* of the stress field (shaded using light-grey in *Fig.4.11c*) is subjected to uniaxial compression (equal to σ_c). Zone *FGEHIJK*, presented in dark grey separates the stress field in two branches – one passing through the duct (branch *FGHI*) and the other going around it (branch *GEJK*). Both branches are subjected to simultaneous tension and compression, and their widths are governed by the surface roughness of the duct, in the following manner:

$$\mu = \tan \varphi \quad (4.23)$$

where μ is the friction coefficient

φ is the angle defined in *Fig.4.11c*.

The top and the middle part of the stress field are separated with a quasi-hydrostatic node that spans over the entire width of the panel (area *CDEFG*). The reason why the node is referred to as quasi-hydrostatic is due to the fact that the *Fig.4.11c* describes a plane stress state, meaning that stress in perpendicular direction is equal to zero. The line *GJ* is defined as a 2nd order parabola, and is not completely perpendicular to the line *GE*. It is assumed that the failure of the element occurs at point *J* once the maximal tensile stress (σ_t) reaches the effective tensile

strength of concrete (f_{cte}). The bottom part of the stress field (zones *HILM* and *JKNO*) is once more subjected to uniform stress state (σ_{cl} and σ_{cl} , respectively), which is higher compared to σ_c .

Equilibrium of the free-body *DGJKE* gives (refer to Hars [41]):

$$\Sigma H: \quad x = a \cdot \frac{\sigma_t}{\sigma_c - \sigma_t} \quad (4.24)$$

$$\Sigma V: \quad \sigma_{cl} = \sigma_c \cdot \frac{2 \cdot b_1}{b_w - \Phi_D} \quad (4.25)$$

$$\Sigma M_P: \quad \sigma_{cl} \cdot (b_w - \Phi_D) \cdot \left(\frac{b_1}{2} - \frac{b_w - \Phi_D}{4} \right) = \sigma_t \cdot a \cdot (a + x) \quad (4.26)$$

After combining previous equations, one can link the maximal compressive stress (σ_c) with maximal tensile stress (σ_t) in the following manner:

$$\sigma_c = \sigma_t \cdot \left\{ \frac{2 \cdot a^2}{b_1 \cdot [2 \cdot b_1 - (b_w - \Phi_D)]} + 1 \right\} \quad (4.27)$$

Vertical equilibrium of free-body *CFHIGD* gives:

$$\Sigma V: \quad \sigma_{cl} = \sigma_c \cdot \frac{b_w - 2 \cdot b_1}{\Phi_D \cdot \sin \varphi} \quad (4.28)$$

Horizontal position of *points D* and *G* can be obtained by assuming that σ_{cl} (Eq. 4.25) is equal to σ_{cl} (Eq. 4.28):

$$b_1 = \frac{b_w}{2} \cdot \frac{1 - \delta}{1 - \delta \cdot (1 - \sin \varphi)} \quad (4.29)$$

$$\delta = \frac{\Sigma \Phi_D}{b_w} \quad (4.30)$$

According to Hars [41], effective concrete tensile strength (f_{cte}) can be estimated in the following manner:

$$\frac{f_{cte}}{f_{ct}} = \frac{750}{f_c^{5/3}} \cdot \left(1 + \frac{\sigma_{3c}}{f_c} \right) \quad (4.31)$$

where σ_{3c} represents the applied compressive stress;

f_{ct} represents the maximal concrete tensile strength equal to:

$$f_{ct} = 0.3 \cdot f_c^{2/3} \quad (4.32)$$

As it can be seen $f_{cte} < f_{ct}$, due to the fact that the concrete is not only subjected to pure tension, but tension combined with compression (σ_{3c}). This effect was observed and investigated by Kupfer [63] and Curbach et al. [24], and Eq. 4.31 was used as a failure criterion

for the model of Hars [41]. Ultimate strength of a panel is reached at *point J*, once the effective tensile strength of concrete is surpassed. Maximal compressive stress is obtained after combining Eq.4.25 and Eq.4.29:

$$\sigma_{3c} = \sigma_{cl} = \sigma_c \cdot \frac{1}{1 - \delta \cdot (1 - \sin \varphi)} \quad (4.33)$$

Equations 4.32 and 4.33 can then be introduced to Eq.4.31, and finally, after assuming that $f_{cte} = \sigma_t$ (from Eq.4.27) as well as normalizing the entire expression with f_c , concrete compressive strength softening coefficient taking into account presence of post-tensioning ducts can be obtained:

$$\eta_D = \left\{ \frac{f_c^2}{225} \cdot \left[1 + \frac{4 \cdot (a/b_w)^2}{\delta \cdot (1 - \sin \varphi)} \cdot \left(\frac{1 - \delta \cdot (1 - \sin \varphi)}{1 - \delta} \right)^2 \right]^{-1} + \frac{1}{1 - \delta \cdot (1 - \sin \varphi)} \right\}^{-1} \quad (4.34)$$

Previous expression is valid for ungrouted as well as grouted (steel or plastic) post-tensioning ducts. The only difference between them is in the amount of compressive stresses which can be transferred through the duct. In other words, the width of *FGHI* branch changes (see Fig.4.11c) as a function of the friction coefficient, which translates into angle φ (refer to Eq.4.23 and Fig.4.11c). In case of ungrouted ducts, the proposed friction coefficient is equal to zero. Grouted plastic ducts on the other hand assume $\mu=0.2$ ($\varphi=0.2$ rad), and finally the friction coefficient of grouted steel ducts is equal to $\mu=0.6$ ($\varphi=0.54$ rad). According to Hars [41] the local stress field disturbance ratio a/b_w (see Eq.4.34) should be equal to two.

Model for estimating the effective concrete compressive strength of structural concrete members containing a post-tensioning duct proposed by Hars [41] has been presented in form of a graph in Fig.4.12a to c. Equation 4.34 assuming $\mu=0$ and varying f_c between 20 MPa and 100 MPa can be seen in Fig.4.12a as a function of δ . Similar curves are given in Fig.4.12b and c, assuming $\mu=0.2$ and $\mu=0.6$, which corresponds to grouted plastic and steel ducts. According to Hars [41] concrete compressive strength reduction caused by the presence of post-tensioning ducts is quite significant, especially in case when empty ducts are combined with high strength concrete. However, in practice grouted steel ducts are used most of the time. Fortunately Hars's model predicts that the effective concrete compressive strength remains relatively high in such cases (see Fig.4.12c).

MC2010 [34] proposes a simplified expression for estimating the effective concrete compressive strength of prestress concrete, which is especially suitable for design purposes. The reduction can be applied on material or geometrical level, by reducing the concrete compressive strength or thickness of the web in the following manner:

$$\eta_D = 1 - k_D \cdot \delta \quad (4.35)$$

$$b_{w,eff} = b_w - k_D \cdot \Sigma \emptyset_D \quad (4.36)$$

where $b_{w,eff}$ represented the effective (reduced) web thickness;

b_w represents the actual web thickness;

k_D represents the post-tensioning duct coefficient, which is equal to 0.5 in case of grouted steel ducts, 0.8 in case of grouted plastic ducts and 1.2 in case of ungrouted duct.

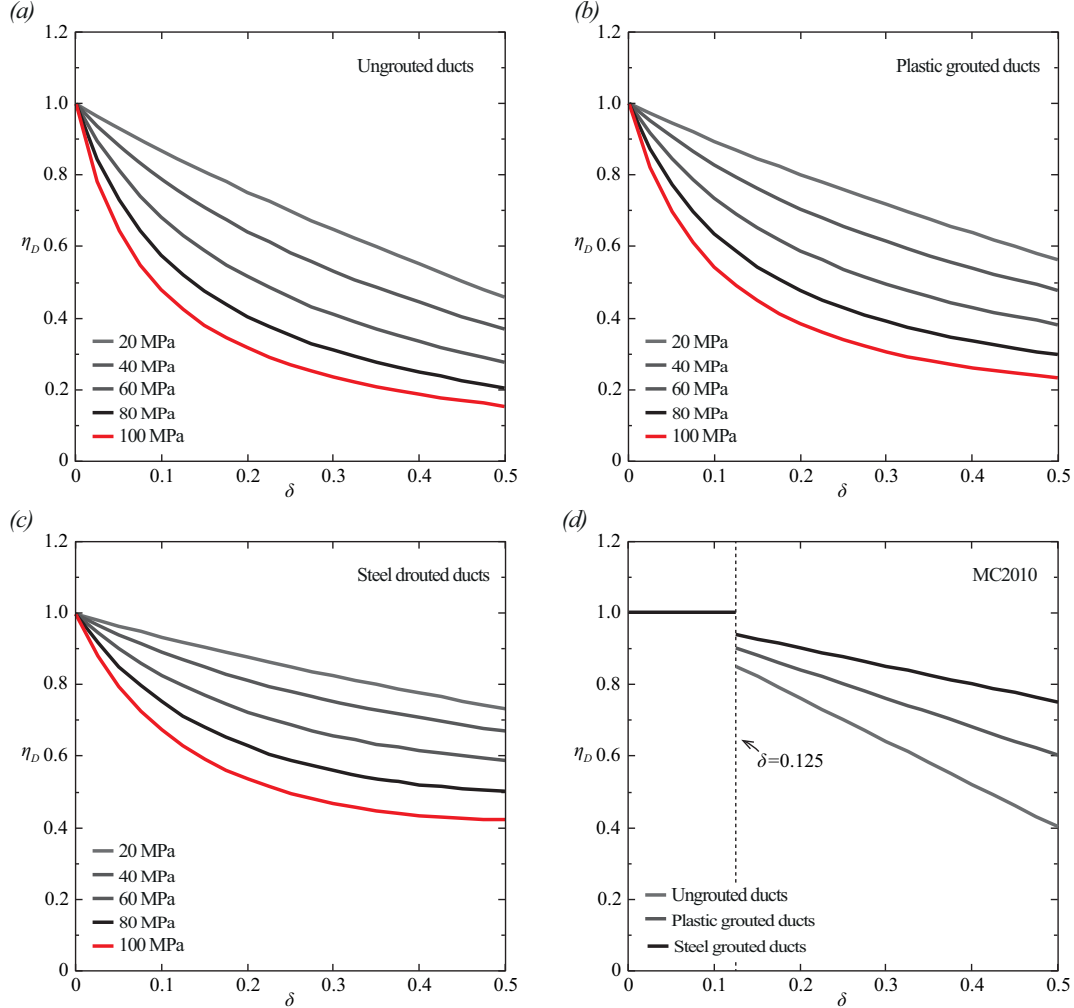


Figure 4.12: Concrete compressive strength reduction factor taking into account the presence of prestress ducts (assuming $a/b_w=2$): (a) model of Hars [41] applied to ungrouted ducts; (b) model of Hars [41] applied to grouted plastic ducts; (c) (a) model of Hars [41] applied to grouted steel ducts; (d) recommendations of MC2010 [34]

Equation 4.35 can be seen in Fig.4.12d, where η_D factor is presented in function of δ (refer to Eq.4.30). Compared to curves proposed by Hars [41], MC2010 [34] does not directly depend on the concrete compressive strength, nor does it take into account the influence of imposed tensile stress on strength of a member. In addition to this, it governs less conservative values of concrete compressive strength (especially in case of high-strength concrete). This is why the multiplicative approach of MC2010 [34] for estimating the effective concrete compressive strength has been investigated and criticized by Hars [41].

4.1.4 Critique of the multiplicative approach for estimating effective concrete compressive strength

When looking at a prestressed concrete panel at ULS (presented in *Fig.4.13a*), it can be seen that there are two distinctive families of cracks:

1. Out-of-plane cracks, accounted for through η_ϵ effectiveness factor;
2. In-plane cracks, accounted for through η_D effectiveness factor

The multiplicative approach of MC2010 [34] (presented in *Eq.4.3*) implies that the two reduction factors (η_ϵ and η_D) should be combined in order to obtain the effective compressive strength. However, when looking at the physical origins of η -coefficients it can be seen that even though they act simultaneously, concrete compressive strength is reduced in two perpendicular planes (as presented in *Fig.4.13a*). Hence, the multiplicative approach of MC2010 [34] does not entirely capture the mechanical behaviour of prestressed concrete panels.

In addition to this, Hars [41] showed that despite the fact that multiplicative approach seems to be on the safe side, this is not the case when ungrouted or grouted plastic post-tensioning ducts are applied, due to the fact that the presence of deviating tensile stress is completely neglected in the cross-section. In order to be more mechanically consistent, Hars [41] proposed following expression for obtaining the effective concrete compressive strength:

$$f_{ce} = f_c \cdot \eta_{fc} \cdot \min \left\{ \begin{array}{l} \eta_D \\ \eta_\epsilon \cdot (1 - k_D \cdot \delta) \end{array} \right. \quad (4.37)$$

where η_D represent the concrete compressive strength factor taking into account the presence of the duct, which should be obtained according to *Eq.4.34* ;

η_ϵ represents the concrete compressive strength effectiveness factor taking into account the presence of transversal strains in the concrete, which should be assumed according to MC2010 [34];

k_D and δ are respectively the duct type coefficient and relative post-tensioning ducts thickness, and should be assumed according to MC2010 [34].

Expression 4.37, clearly distinguishes between the in-plane and out-of-plane failure of panels, while at the same time acknowledges that the presence of the post-tensioning ducts causes additional in-place stress concentration by multiplying the η_ϵ coefficient with $(1 - k_D \cdot \delta)$. *Fig.4.13b to d* gives the results of concrete compressive strength criterion from *Eq.4.37* applied on different types of post-tensioning ducts and various concrete compressive strengths. The effect of η_D was neglected for all the cases when $\delta \leq 0.125$ (as recommended by MC2010 [34]). Each of the graphs clearly indicates whether the minimal concrete compressive strength was governed by η_D or enhanced η_ϵ reduction factor. *Fig.4.13b and c* shows that when high-strength concrete (f_c above 80 MPa) is combined with ungrouted and grouted plastic ducts, it is η_D not enhanced η_ϵ that governs the strength of a member. This means that the MC2010 [34] code provisions are unconservative in such situations. However, in case of grouted steel post-

tensioning ducts current code provisions are on the safe side (as can be seen in *Fig.4.13d*). It is important to mention that the three curves from *Fig.4.13d* (corresponding to concrete compressive strength of 60 MPa, 80 MPa and 100 MPa) are overlapped, which explains why only the red line remains visible.

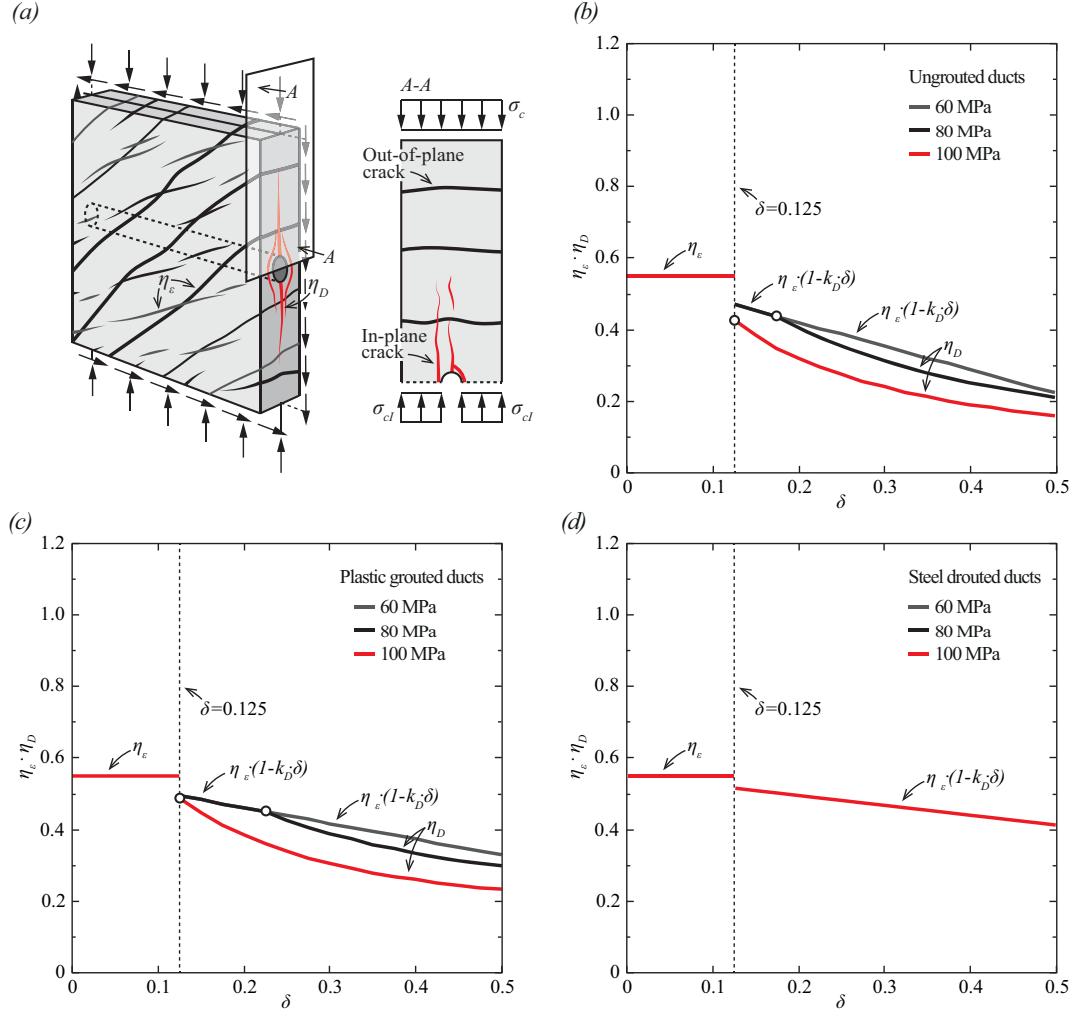


Figure 4.13: Critique of the multiplicative approach for estimating effective concrete compressive strength: (a) crack distribution in an prestressed concrete panel; (b) to (c) parallel approach of Hars [41] compared to multiplicative approach of MC2010 [34] applied on members with ungrouted and grouted plastic/steel ducts

After presenting, comparing and analysing current models used to estimate the concrete compressive strength effectiveness factor (refer to *Eq.4.3 - Eq.4.37*), it becomes clear that the mechanisms limiting in-plane and out-of-plane resistance of structural members need to be clearly distinguished and accounted for separately from each other. Going forward even further, it is necessary to derive a mechanically based model which is able to differentiate between the three failure modes presented in *Fig.4.7*:

1. Crushing of the concrete strut;

2. Sliding of the concrete;
3. Spalling of the concrete cover.

This will allow designers not only to suitably understand the mechanisms governing the structural failures, but to comprehend their interaction as well as.

This chapter presents a mechanical approach for assessing the concrete compressive strength efficiency factor that takes into account actual behaviour of structural panels as well as interactions between steel and concrete. The consistency of the approach was validated by means of extensive comparison to available test data. Finally, the model was used to better understand the relationship between various strength-governing mechanisms.

4.2 Mechanical model for compression softening of reinforced concrete panels

The response of a reinforced concrete panel subjected to shear and/or to bi-axial tension/compression can be described by analysing three physical stages presented in *Fig. 4.14*:

1. The first stage corresponds to a load transfer action valid up to first cracking of the panel (refer to *Fig. 4.14a*);
2. The second stage (refer to *Fig. 4.14b*) describes behaviour which is applicable between first cracking of the panel and yielding of the reinforcement in one direction (this phase is also valid in case a panel fails prior to yielding of any steel);
3. The third and final stage (refer to *Fig. 4.14c*) covers the loading history between yielding of the reinforcement in one direction and failure of the panel (due to the crushing of the concrete or yielding of the reinforcement in both directions).

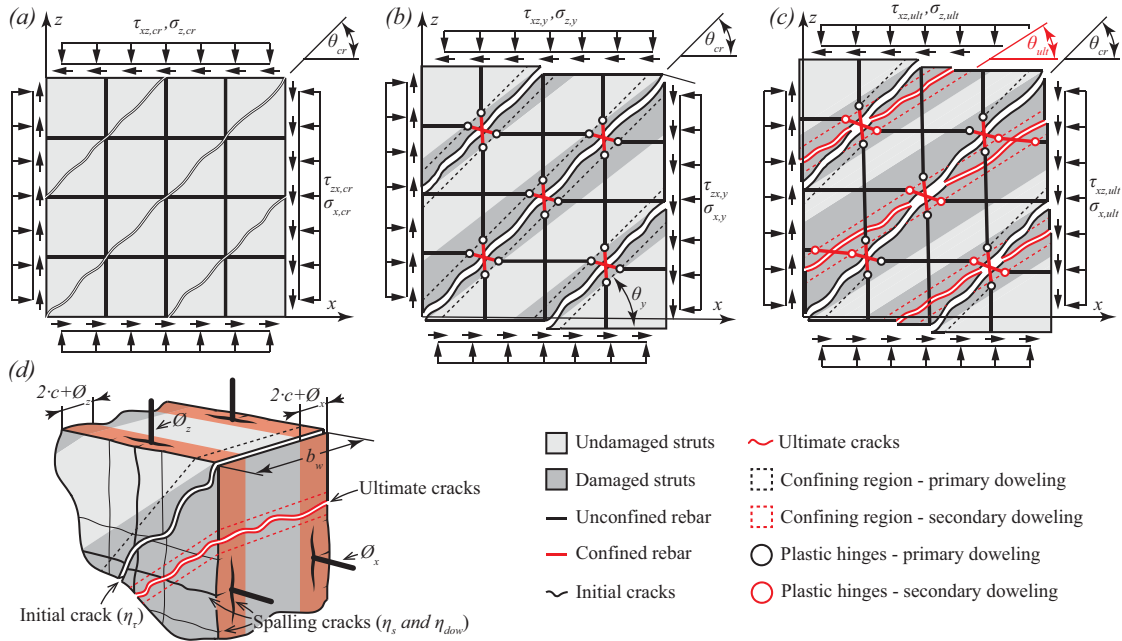


Figure 4.14: Modelling the physical behaviour of a reinforced concrete panel subjected to shear and axial loads: (a) cracking point; (b) onset of yielding; (c) failure of the panel and (d) in-plane and out-of-plane reduction mechanism of concrete compressive strength

4.2.1 Stages of mechanical behaviour

The behaviour of a panel will be characterized for an element as shown in *Fig. 4.15a*. Also the notations indicated in *Fig. 4.15b* and *Fig. 4.15c* will be used to refer to the stress and strain state respectively.

4.2.1.1 First stage : Linear elastic response

During the early phases of loading, a reinforced concrete panel can be analysed assuming a linear elastic behaviour. Once the tensile strength of concrete is reached, cracks start to develop (refer to *Fig. 4.14a*). As the direction of the principal tensile strains can be assumed

parallel to principal tensile stresses for the elastic response, this means that the stress state, strain state and initial cracking angle (θ_{cr}) are unambiguously defined (refer to Fig.4.14a).

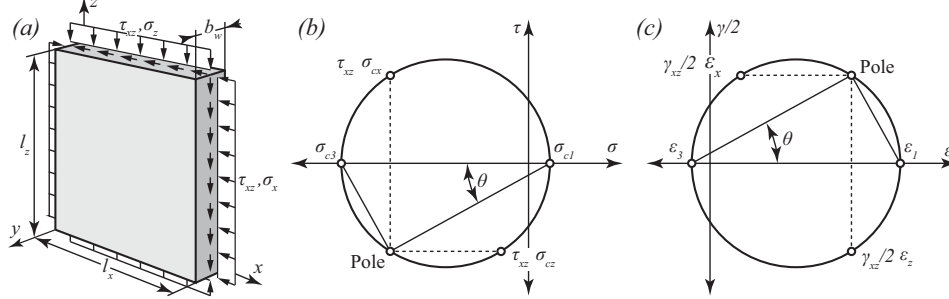


Figure 4.15: (a) Geometry and loading properties of an analysed panel; (b) stress state of a concrete strut and (c) average strain state of the panel

The amount of stress acting along the edge of a panel at any given point in load-history, can be defined using the applied force as follows (refer to Fig.4.14a):

$$\sigma_x = \frac{F_x}{h \cdot b_w} \quad (4.38)$$

$$\sigma_z = \frac{F_z}{l \cdot b_w} \quad (4.39)$$

$$\tau_{xz} = \frac{V_{xz}}{l \cdot h} \quad (4.40)$$

where F_x represents the applied force in x -direction;

F_z represents the applied force in z -direction;

V_{xz} represents the applied shear force;

l represents the size of the panel in the x -direction;

h represents the size of the panel in the z -direction;

b_w represents the thickness of the panel.

Assuming that the panel behaves as a uniform elastic continuum up to the cracking, one can calculate the principle tensile stress of the panel as:

$$\sigma_{cl} = \frac{\sigma_x + \sigma_z}{2} + \sqrt{\left(\frac{\sigma_x - \sigma_z}{2}\right)^2 + \tau_{xz}^2} \quad (4.41)$$

The limit case of the elastic phase is reached when the principle tensile stress becomes equal to the mean tensile strength of concrete ($\sigma_{cl} = f_{ctm}$). According to MC2010 [34], this value can be estimated as:

$$f_{ctm} = \begin{cases} 0.3 \cdot (f_c)^{2/3}, & \text{for } f_c \leq 50 \text{ MPa} \\ 2.12 \cdot \ln(1 + 0.1 \cdot f_c), & \text{for } f_c > 50 \text{ MPa} \end{cases} \quad (4.42)$$

where f_c represents the uniaxial concrete compressive strength measured in cylinder.

The initial cracking angle can now be determined using Mohr's transformations (presented in *Fig.4.15b*) as following:

$$\tan \theta_{cr} = \frac{\sigma_{cx} - \sigma_{c3}}{\tau_{xz}} \quad (4.43)$$

4.2.1.2 Second stage: Cracked behaviour

The initial cracking angle remains unchanged throughout the second stage (as presented in *Fig.4.14b*). However, the direction of the principal compressive stresses starts to rotate in order to remain parallel to the principal compressive strains (θ_y in *Fig.4.14a*). This means that a portion of the concrete compressive struts, named hereafter the damaged struts, crosses the initial cracks (refer to *Fig.4.14b*). The strength of such struts is governed by aggregate interlocking occurring along the initial cracks. The remaining portion of the struts are considered as undamaged struts. Even though they are characterized by the absence of in-plane cracks, their strength is not equal to the concrete compressive strength determined from the standard cylinder test. This is justified as the presence of the reinforcement induces the formation of spalling cracks, leading to out of plane failures (refer to *Fig.4.14d*). These spalling cracks limit the compressive strength of the concrete over a given portion of the panel's thickness (shown in red in *Fig.4.14d*). This effect has been taken into account based on the work of Hars [41]. The spalling reduction applies not only to the undamaged, but to the damaged struts as well. In this manner, the strength of each strut is governed by the presence of in-plane and/or out-of-plane cracks.

With respect to the yield strength of the reinforcement, it is limited by the doweling of the bars in the region near the cracks. As plastic hinges start to develop (indicated using white circles in *Fig.4.14b*), the concrete located between the surfaces of the cracks and the plastic hinges are locally equilibrating the doweling forces (see the red zones along the reinforcement in *Fig.4.14b*). This region, shown using dashed lines in *Fig.4.14b*, which is partly developing in the undamaged and damaged struts, introduces a reduction of the concrete strength due to the out-of-plane tensile stresses, potentially leading to spalling failures (presented in *Fig.4.7b*).

4.2.1.3 Third Stage: Behaviour after yielding

The third and final stage is presented in *Fig.4.14c*. At this point, a second family of cracks develops. Their inclination is assumed to be parallel to the direction of the principal concrete compressive stress (and strain) at failure (θ_{ult}). The presence of a second family of cracks causes additional doweling of the reinforcement (plastic hinges activated at this phase are presented in *Fig.4.14c* using red circles). Given the fact that the direction of principal compressive stress continues to rotate compared to the previous stage means that the percentage of surface corresponding to damaged struts increases, and that of the undamaged struts decreases. The strength reduction mechanisms governing the strength of each type of the concrete struts are methodologically the same compared to previous stage. The stress field continues to rotate until the reinforcement in the other direction reaches eventually yielding or

until the principal compressive stresses become equal to the effective concrete compressive strength.

4.2.2 Plastic strength of rebars subjected to doweling and elongation

As the initial and the ultimate cracks start to open, the horizontal and vertical reinforcement of the panel is subjected to local bending. Consequently, plastic hinges start to develop in the vicinity of the crack faces (refer to *Fig.4.14b* and *Fig.4.14c*), originating doweling action. As the bar is dowelled, this reduces its capacity to carry tensile forces and determines the location at which plastic hinges will originate. Physical evidence of the doweling action in the reinforced concrete panels has been reported for instance by Vecchio et al. [121] in their experimental campaign. In addition to this, panels which have experienced sliding failures at ultimate limit state (refer to *Fig.4.7c*) also show significant doweling of the reinforcement.

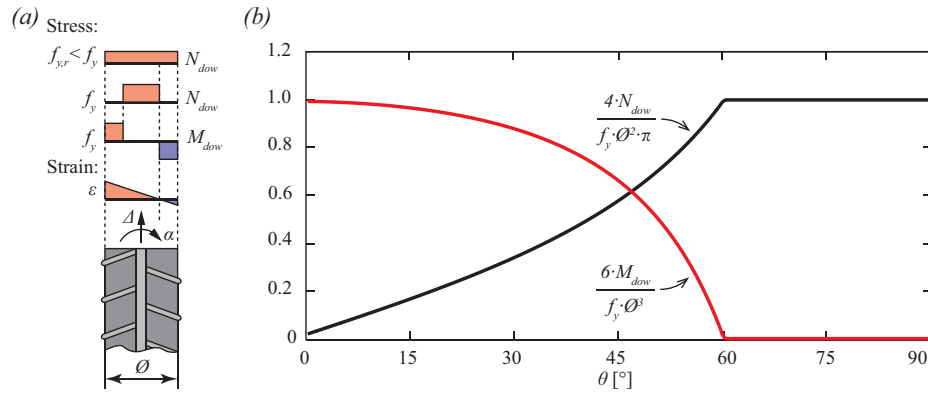


Figure 4.16: (a) Distribution of strains, stresses and internal forces inside a plastic hinge of a rebar; (b) axial strength reduction of a horizontal rebar as a function of the crack opening angle

The plastic stress distribution within a hinge at the ultimate limit state is presented in *Fig.4.16a*. The central part of the cross-section carries tension, while the rest carries the bending moment. In order to account for such interaction, the apparent yield strength of the steel in tension needs to be reduced ($f_{y,r}$). It must be noted, however, that this detrimental effects of the doweling in one direction ($f_{y,r}$), brings some beneficial effects to the opposite direction (V_{dow}), as presented in *Fig.4.17d* and *Fig.4.17e*. This is justified as the bent rebar can resist some shear forces, reducing the amount of the force that has to be carried by the bars in the perpendicular direction. Depending on the inclination of the crack, the number of rebars which are actively contributing in carrying applied loads through the doweling action can vary. In case this angle is higher than 45° (refer to *Fig.4.17d*) the number of rebars is governed by their spacing (s_x and s_z) and the height of a panel (h), whereas in case the angle is lower than 45° (see *Fig.4.17e*) the number is determined based on the length of a panel (l) and the spacing between the rebars (s_x and s_z).

The development of tensile and dowel forces in a plastic hinge for a given crack direction and kinematics is investigated in *Fig.4.17*. The inclination of the initial crack is defined by θ_{cr} , and the direction of its opening by θ . These two angles are considered to account

that the crack is not necessarily (at all cases) parallel to the principal compressive stress and strain direction, and is therefore subjected to simultaneous opening and sliding.

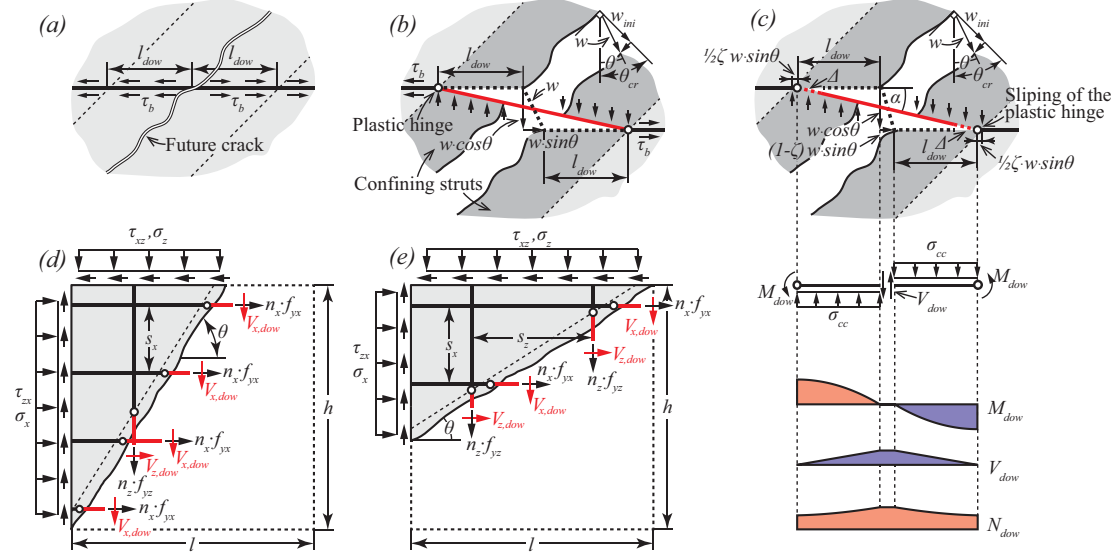


Figure 4.17: Doweling mechanism of the reinforcement: (a) location of the future plastic hinges and the initial crack; (b) local bending of a horizontal rebar in the proximity of an initial crack – no slip along the rebar; (c) local bending of a horizontal rebar in the proximity of an initial crack – accounting for the slip along the rebar; (d) contributing rebars for crack angles bigger than 45° and (e) contributing rebars for crack angles smaller than 45°

The plastic hinges are located at a distance to the crack named the doweling length (l_{dow} , see Fig.4.17a). When the crack opens, the plastic hinges are horizontally and vertically moved from each other (refer to Fig.4.17b). Since the rebar is not perfectly bonded to concrete, it slips for a value which can be expressed as function of the corresponding crack width. This is defined by coefficient ζ in Fig.4.17c. Consequently, the rebar tilts (at a specific angle α) and elongates for $2 \cdot \Delta$. Along the doweling length, the rebar pushes against the surrounding concrete transferring the doweling forces to the concrete (σ_{cc}). According to Rasmussen [99] the doweling length for the case of doweling with no eccentricity and no normal load can be estimated as:

$$l_{dow} = \phi \cdot \sqrt{\frac{f_y}{3 \cdot f_{cc}}} \quad (4.44)$$

where l_{dow} represents the doweling length;

ϕ represents the diameter of the rebar;

f_y represents the initial yield strength of the rebar;

f_{cc} represents the concrete strength in confining state.

Sørensen [111] states that in case of an increased eccentricity and additional normal load, the doweling length actually decreases, which reduces the moment contribution as well

as the percentage of confining (i.e. damaged) struts within a panel (refer to Fig.4.14b and Fig.4.14c). Therefore, the presented approach is slightly conservative.

The enhanced concrete strength equilibrating the doweling forces can be estimated accounting for the influence of the concrete cover. Based on the work of Vintzeleou and Tassios [123], the confined concrete strength can be estimated as:

$$f_{cc} = f_c \cdot \left(1 + \frac{c_{conf,1}}{\phi} \cdot \left(0.02 \cdot \frac{c_{conf,2}}{\phi} + 0.15 \right) \right)^2 \leq 5 \cdot f_c \quad (4.45)$$

where $c_{conf,1}$ represents the concrete cover perpendicular to the confining concrete stress (cannot be larger than 4ϕ) and $c_{conf,2}$ represents the concrete cover parallel to the confining concrete stress (cannot be larger than 8ϕ).

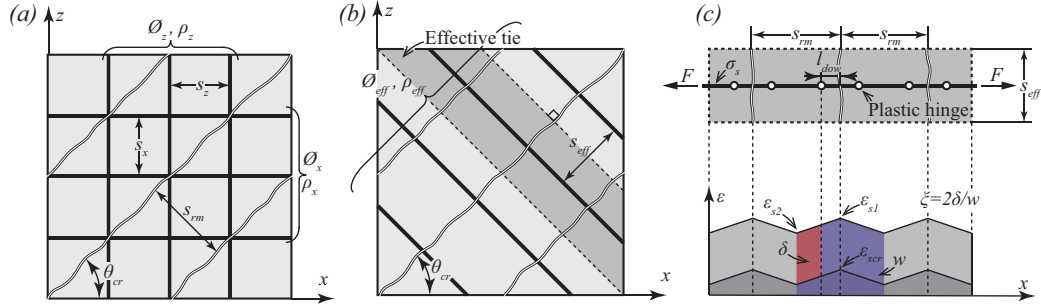


Figure 4.18: (a) Geometry properties of the reinforcement in horizontal and vertical direction; (b) geometry properties of the effective reinforcement and effective tie and (c) strain state along the effective tie

On average, the corresponding values for the confined concrete strength are approximately equal to $3.7 \cdot f_c$. The actual concrete strength (σ_{cc}), is however determined at a later stage accounting for the actual doweling moment in the rebar (M_{dow}), and is always lower than f_{cc} .

Relative rebar slip is estimated using an effective tie presented in Fig.4.18b and Fig.4.18c. Starting from the geometry properties of an analysed panel (given in Fig.4.18a), crack spacing is estimated using the expression resulting for a constant bond strength according to [120]:

$$s_{rm} = \frac{1}{\frac{\sin \theta_{cr}}{s_{rmx}} + \frac{\cos \theta_{cr}}{s_{rmz}}} \quad (4.46)$$

$$s_{rmx} = \frac{3}{2} \cdot \frac{1 - \rho_x}{\rho_x} \cdot \frac{\phi_x}{8} \quad (4.47)$$

$$s_{rmz} = \frac{3}{2} \cdot \frac{1 - \rho_z}{\rho_z} \cdot \frac{\phi_z}{8} \quad (4.48)$$

where ρ_x represents the reinforcement ratio in x -direction;

\varnothing_x represents the diameter of the rebar in x -direction;

ρ_z represents the reinforcement ratio in z -direction;

\varnothing_z represents the diameter of the rebar in z -direction.

and where the effective reinforcement ratio in the direction perpendicular to the direction of cracks (refer to *Fig.4.18b*) is calculated in the following manner:

$$\rho_{eff} = \rho_x \sin^2 \theta_{cr} + \rho_z \cos^2 \theta_{cr} \quad (4.49)$$

The effective rebar spacing is assumed equal to the average spacing of the horizontal and vertical reinforcement projected to the direction of the cracks:

$$s_{eff} = \frac{1}{2} \cdot \left(\frac{s_x}{\sin \theta_{cr}} + \frac{s_z}{\cos \theta_{cr}} \right) \quad (4.50)$$

where s_x represent the spacing between the rebars in x -direction;

s_z represent the spacing between the rebars in z -direction.

Fig.4.18c represents the reinforcement strain distribution inside the effective tie at its cracking point, and for a higher stress level. As it can be seen, both strains are linearly varying between the two consecutive cracks (constant bond strength). Maximal steel strains – ε_{s1} are expected at the location of the crack, while the minimal steel strains – ε_{s2} are expected in the middle of the two consecutive cracks (concrete strains are neglected):

$$\varepsilon_{s1} = \frac{\sigma_s}{E_s} \quad (4.51)$$

$$\varepsilon_{s2} = \frac{\sigma_s}{E_s} - \frac{2 \cdot \tau_b \cdot s_{rm}}{E_s \cdot \varnothing_{eff}} \quad (4.52)$$

where σ_s represents the stress in the reinforcement;

E_s represented the Young's modulus of elasticity;

\varnothing_{eff} represents the effective rebar diameter (presented in *Fig.4.18b*);

τ_b represents the average bond stress, which can be estimated according to Marti et al. [74] (for deformed rebars):

$$\tau_b = 2 \cdot f_{ctm} \quad (4.53)$$

where f_{ctm} represents the mean tensile concrete strength given in *Eq.4.42*

In case of smooth rebars the bond law is calculated according to MC2010 [34]:

$$\tau_b = 0.15 \cdot \sqrt{f_c} \quad (4.54)$$

Plastic hinges are assumed to form at the cracking point of the panel in the vicinity of the initial cracks (as presented in *Fig.4.18c*). As the stress level increases in the rebar, the plastic hinges move towards the crack. The slip (δ) can be estimated by integrating the area marked in

red in *Fig.4.18c*. As presented in *Fig.4.18c*, this value depends on the amount of steel stress (σ_s). A mean value between the steel stress at the point of cracking ($\sigma_{s,cr}$) and the yield strength of the steel (f_y) shall be assumed, in other words:

$$\sigma_s = \frac{\sigma_{s,cr} + f_y}{2} \quad (4.55)$$

$$\sigma_{s,cr} = \frac{f_{ctm}}{\rho_{eff}} \quad (4.56)$$

The amount of slip itself can be estimated as:

$$\delta = \frac{\sigma_s - \sigma_{s,cr}}{E_s} \cdot \left(\frac{s_{rm}}{2} - l_{dow} \right) \quad (4.57)$$

In order to do express the slip of a hinge in a more general manner (in function of the corresponding crack width), the ξ parameter is defined as:

$$\xi = \frac{2\delta}{w} \quad (4.58)$$

$$w = s_{rm} \cdot \frac{\varepsilon_{s1} + \varepsilon_{s2}}{2} \quad (4.59)$$

Based on the mechanism given in *Fig.4.17a*, the rebar tilting angle can be expressed as:

$$\alpha = \arctan \left(\frac{w \cdot \cos \theta}{2 \cdot l_{dow} + (1 - \xi) \cdot w \cdot \sin \theta} \right) \quad (4.60)$$

Going back on the same mechanism, the rebar elongation can be determined in the following manner (refer to *Fig.4.17c*):

$$(2l_{dow} + 2\Delta)^2 = (2l_{dow} + (1 - \xi) \cdot w \cdot \sin \theta)^2 + (w \cdot \cos \theta)^2 \quad (4.61)$$

$$\Delta = \frac{1}{2} \cdot \sqrt{4l_{dow}^2 + 4l_{dow} \cdot w \cdot \sin \theta \cdot (1 - \xi) + w^2 \cdot (1 - 2\xi \cdot (\sin \theta)^2 + (\xi \cdot \sin \theta)^2)} - l_{dow} \quad (4.62)$$

where w represents the total displacement, which can be estimated according to mechanism presented in *Fig.4.17b* as:

$$w = \frac{w_{ini}}{\cos(\theta_{cr} - \theta)} \quad (4.63)$$

where w_{ini} represents the initial crack width.

In order to estimate the amount of rebar doweling based on the crack kinematics, it is necessary to define the incremental difference of the rebar tilting angle and its elongation in function of the crack opening. In other words, one needs to find the first derivatives of *Eq.4.60* and *Eq.4.62*:

$$\dot{\alpha} = \frac{\partial \alpha}{\partial w} = \frac{2l_{dow} \cdot \cos \theta}{4l_{dow}^2 + 4l_{dow} \cdot w \cdot \sin \theta \cdot (1 - \xi) + w^2 \cdot (1 - 2\xi \cdot (\sin \theta)^2 + (\xi \cdot \sin \theta)^2)} \quad (4.64)$$

$$\dot{\Delta} = \frac{\partial \Delta}{\partial w} = \frac{2l_{dow} \cdot \sin \theta \cdot (1 - \xi) + w \cdot (1 - 2\xi \cdot (\sin \theta)^2 + (\xi \cdot \sin \theta)^2)}{2\sqrt{4l_{dow}^2 + 4l_{dow} \cdot w \cdot \sin \theta \cdot (1 - \xi) + w^2 \cdot (1 - 2\xi \cdot (\sin \theta)^2 + (\xi \cdot \sin \theta)^2)}} \quad (4.65)$$

The yield condition of the circular cross section subjected to simultaneous tension and bending is similar to the one derived for a rectangular cross section but is far more complex [111], which is why the doweling of the rebar will be derived using the simpler expression [92]:

$$f(N, M) = m + n^2 - 1 = 0 \quad (4.66)$$

$$m = \frac{M}{M_p} = \frac{6 \cdot M}{\Phi^3 \cdot f_y} \quad (4.67)$$

$$n = \frac{N}{N_p} = \frac{4 \cdot N}{\Phi^2 \cdot \pi \cdot f_y} \quad (4.68)$$

where M represents the bending moment acting on a rectangular cross-section;

N represents the axial force acting on the rectangular cross-section.

Application of the normality condition on *Eq. 4.66* gives:

$$\dot{\alpha} = \lambda \cdot \frac{\partial f(M, N)}{\partial M} = \lambda \cdot \frac{\partial f(M, N)}{\partial m} \cdot \frac{\partial m}{\partial M} = \lambda \cdot \frac{1}{M_p} \quad (4.69)$$

$$\dot{\Delta} = \lambda \cdot \frac{\partial f(M, N)}{\partial N} = \lambda \cdot \frac{\partial f(M, N)}{\partial n} \cdot \frac{\partial n}{\partial N} = \lambda \cdot 2 \cdot n \cdot \frac{1}{N_p} \quad (4.70)$$

where λ represents an integration factor.

After combining *Eq. 4.64*, *Eq. 4.65*, *Eq. 4.69* and *Eq. 4.70*, it is possible to estimate the relative amount of axial tensile force in a rebar for a given crack kinematics:

$$n_{dow} = \left[\frac{3 \cdot \pi}{4 \cdot \Phi} \cdot \frac{2l_{dow} \cdot \sin \theta \cdot (1 - \xi) + w \cdot (1 - 2\xi \cdot (\sin \theta)^2 + (\xi \cdot \sin \theta)^2)}{4 \cdot l_{dow} \cdot \cos \theta} \right] \cdot \sqrt{4l_{dow}^2 + 4l_{dow} \cdot w \cdot \sin \theta \cdot (1 - \xi) + w^2 \cdot (1 - 2\xi \cdot (\sin \theta)^2 + (\xi \cdot \sin \theta)^2)} \quad (4.71)$$

Once the amount of the axial tensile force in a rebar is determined, the amount of moment can be expressed as:

$$m_{dow} = 1 - n_{dow}^2 \quad (4.72)$$

The distribution of these two parameters (n_{dow} and m_{dow}) can be seen in *Fig. 4.16b* as a function of the crack opening angle. As it can be seen, the maximal amount of moment is obtained for $\theta=0^\circ$. At this angle the crack opens perpendicularly to the rebar. For a general case (refer to *point A* in *Fig. 4.19a* and *Fig. 4.19b*), the neutral axis is inside the analysed rebar, which

means that a part of the cross section is subjected to uniform compression while the rest is subjected to uniform tension. When the bar is subjected to pure normal force, the stress state of the *point B* can be achieved through various strain profiles (refer to Fig.4.19b), since the neutral axis is always outside of the rebar's cross section. According to the rigid plastic approach, in *point B* it is therefore possible to have no moment but some level of curvature.

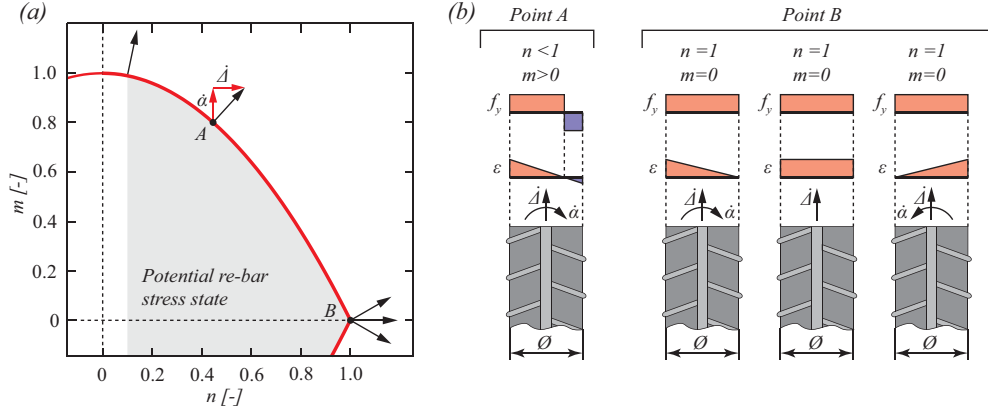


Figure 4.19: (a) Moment - normal force interaction diagram; (b) distribution of strains and stresses in a rebar

The maximal shear carried by doweling can be calculated accounting for the pressure developed in the concrete (Fig.4.17c):

$$V_{dow} = \emptyset \cdot l_{dow} \cdot \sigma_{cc} \quad (4.73)$$

where σ_{cc} represents the effective concrete pressure acting along the dowel length, which may be estimated from a simple free-body equilibrium (Fig.4.17c):

$$\sigma_{cc} = \frac{2 \cdot M_{dow}}{\emptyset \cdot l_{dow}^2} = \frac{m_{dow} \cdot \emptyset^2 \cdot f_y}{3 \cdot l_{dow}^2} \quad (4.74)$$

The total force carried by the doweling can thus be calculated on the basis of Fig.4.17d and Fig.4.17e, by adding the contribution of each bar (V_{dow}) for the total number of bars intersected by the cracks.

4.2.3 Concrete strength accounting for the presence of initial cracks and rebars

The effective concrete compressive strength of the analysed panel can be expressed by combining the resistances of the two types of struts (damaged and undamaged) presented in Fig.4.20a in the following manner:

$$f_{ce} = f_c \cdot \eta_{fc} \cdot [\eta_{DS} \cdot q_{DS} + \eta_{UDS} \cdot (1 - q_{DS})] \quad (4.75)$$

where f_c represents the uniaxial concrete compressive strength measured on a cylinder;

η_{fc} represents the effectiveness factor that accounts for the brittle behaviour of concrete in compression according to Muttoni [82] (refer to Eq.4.12 assuming $f_{c0}=30 \text{ MPa}$);

q_{DS} represents the relative amount of the damaged struts in the panel;

η_{DS} represents the effectiveness factor for the compressive strength of the damaged struts;

η_{UDS} represents the effectiveness factor for the compressive strength of the undamaged struts.

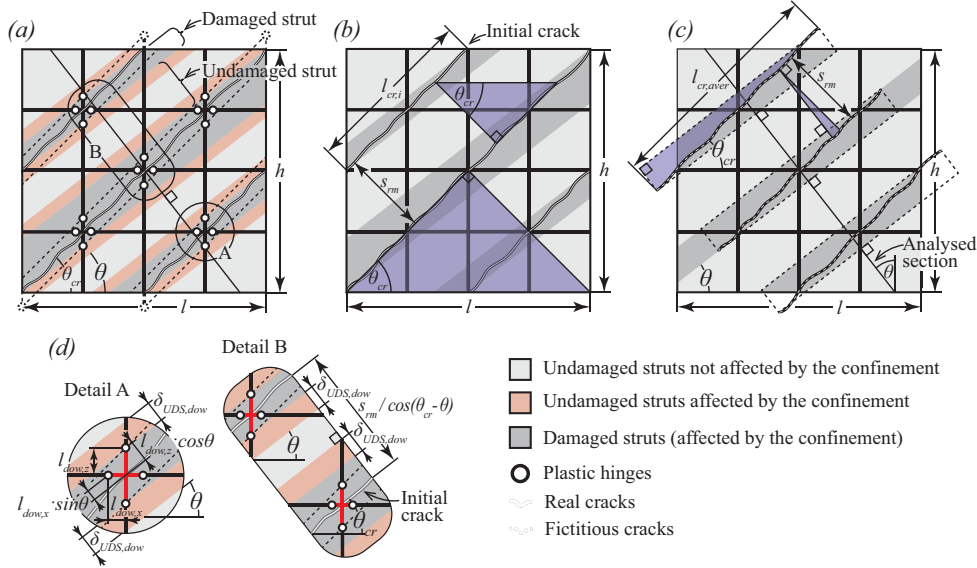


Figure 4.20: (a) Surface quantity and distribution of damaged and undamaged struts in a panel; (b) number of initial cracks in a panel; (c) effective damaged strut length and width; (d) details determining the confining concrete strut width

The relative amount of damaged (and consequently undamaged) struts in the analysed panel depends on the length of the initial cracks (which can be seen in Fig.4.20a and Fig.4.20b). In order to account for their uneven length, an effective (average) crack length is calculated based on geometrical considerations from Fig.4.20b:

$$l_{cr,aver} = \frac{l - 0 \cdot s_{rmx}}{\cos(\theta_{cr})} + 2 \cdot \frac{l - 1 \cdot s_{rmx}}{\cos(\theta_{cr})} + 2 \cdot \frac{l - 2 \cdot s_{rmx}}{\cos(\theta_{cr})} + \dots + 2 \cdot \frac{l - n \cdot s_{rmx}}{\cos(\theta_{cr})} \quad (4.76)$$

$$l_{cr,aver} = \frac{l}{\cos(\theta_{cr})} - \frac{s_{rm}}{\sin(\theta_{cr}) \cdot \cos(\theta_{cr})} \cdot \frac{n \cdot (n+1)}{2 \cdot n+1}$$

where n can be calculated as:

$$n = \frac{l \cdot \sin(\theta_{cr})}{s_{rm}} \quad (4.77)$$

After combining Eq.4.76 and Eq.4.77, it becomes:

$$l_{cr,aver} = \frac{l}{\cos(\theta_{cr})} \cdot \left(\frac{n}{2 \cdot n+1} \right) \quad (4.78)$$

Finally, the relative amount of damaged struts can be estimated on the analysed section (indicated in Fig.4.20c) in the following manner:

$$q_{DS} = \frac{n' \cdot l_{cr,aver} \cdot \sin(\theta_{cr} - \theta) \cdot \cos \theta}{h} \quad (4.79)$$

$$n' = \frac{h \cdot \cos(\theta_{cr} - \theta)}{\cos \theta \cdot s_{rm}} + 1 \quad (4.80)$$

where n' represents the effective number of damaged struts;

s_{rm} represent the average initial crack spacing;

l represents the size of an analysed panel in x -direction;

h represents the size of an analysed panel in z -direction.

4.2.3.1 Strength of the damaged struts

The compressive strength of the damaged struts is limited by the parameter η_{DS} , which takes into account:

1. Presence of the rebars in the concrete struts, governing the out-of-plane failures (η_s , in analogy to Hars [41]);
2. Presence of the initial cracks crossing the damaged struts, governing the in-plane element failures (η_τ , which will be defined further in this paper);
3. Interaction between the in-plane and out-of-plane element failures (adopted from Hars [41]);
4. Presence of doweled rebars (η_{dow} , which will be defined further in this paper).

The value of the effectiveness factor for the compressive strength of the damaged struts can thus be calculated as:

$$\eta_{DS} = \min \left\{ \eta_s, \frac{\eta_\tau \cdot \max \left\{ \frac{0}{b_w - (4c + 2\phi_{ext})} \right\}}{\frac{b_w}{b_w}} + \frac{\eta_\tau \cdot \min \left\{ \frac{b_w}{4c + 2\phi_{ext}} \right\}}{\frac{b_w}{b_w}} \cdot (1 - \eta_{dow} \cdot \delta') \right\} \quad (4.81)$$

where η_s represents the effectiveness factor that accounts for the presence of the reinforcement in concrete (out-of-plane failure);

η_τ represents the effectiveness factor that accounts for the presence of the initial cracks in concrete (in-plane-failure);

η_{dow} represents the factor which takes into account the presence of rebars pressing against the concrete due to the doweling (see Fig.4.17c);

δ' represents the ratio between the external rebar diameter and the sum of two times the concrete cover thickness and the external rebar diameter;

b_w represents the thickness of the panel;

c represents the concrete cover thickness.

With respect to *Eq.4.81* it can be seen that the resistance of a damaged strut is limited either by the presence of the out-of-plane cracks (considered by means of the η_s coefficient), or by the presence of the in-plane cracks (considered by means of the η_τ coefficient) combined with the doweling of the reinforcement (η_{dow}).

The effectiveness factor that accounts for the presence of reinforcement in concrete (η_s) is developed on the basis of the work of Hars [41]. Reinforcement bars introduce local defects into the concrete cover region which may cause it to spall off (see the red strips in *Fig.4.14d*), while the rest of the section remains undisturbed. This effect is physically governed by the out-of-plane cracks (named spalling cracks in *Fig.4.14d*), and can be quite pronounced in case of heavily reinforced concrete panels. On the basis of [41] the effectiveness factor that accounts for the presence of the reinforcement in concrete (η_s) is evaluated as:

$$\eta_s = \frac{\max \left\{ \frac{0}{b_w - (4c + 2\phi_{ext})} \right\}}{b_w} + \frac{\min \left\{ \frac{b_w}{4c + 2\phi_{ext}} \right\}}{b_w}. \quad (4.82)$$

$$\left[\frac{f_c^2}{225} \cdot \left[1 + \frac{4\omega_s^2}{\delta' \cdot (1 - \sin \varphi_s)} \cdot \left(\frac{1 - \delta' \cdot (1 - \sin \varphi_s)}{1 - \delta'} \right)^2 \right]^{-1} + \frac{1}{1 - \delta' \cdot (1 - \sin \varphi_s)} \right]^{-1}$$

$$\omega_s = \min \left\{ \frac{1.5}{2 \cos \theta} \cdot \frac{s_{ext} - \phi_{ext}}{2c + \phi_{ext}} \right\} \quad (4.83)$$

$$\delta' = \frac{\phi_{ext}}{2c + \phi_{ext}} \quad (4.84)$$

$$\varphi_s = \begin{cases} \arctan(0.6) & \text{for plain reinforcement bars} \\ \arctan(1.0) & \text{for ribbed reinforcement bars} \end{cases} \quad (4.85)$$

where c represents the concrete cover;

s_{ext} represents the distance between the external reinforcement bars;

ϕ_{ext} represents the external rebar diameter;

ω_s represents the local stress field disturbance ratio.

It should be noted that the *Eq.4.83* gives the expression for the ω_s coefficient assuming that the external reinforcement is in the vertical direction. In case a horizontal rebar is closer to the panel's surface, $\cos(\theta)$ should be replaced by $\sin(\theta)$ in *Eq.4.83*. As already mentioned, the effectiveness factor that accounts for the presence of the initial cracks in concrete (η_τ) limits the strength of the damaged concrete struts. This coefficient is estimated based on the amount of shear stress that can be transferred through the initial crack.

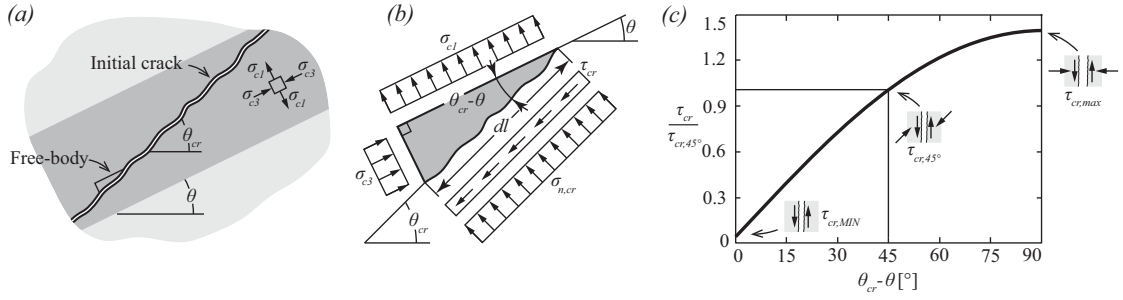


Figure 4.21: (a) Stress state of a damaged strut and the inclination of an initial crack; (b) stresses acting along the sides of the analysed free-body and (c) shear stresses acting along the crack surface in function of the stress field rotation angle

By investigating a free-body indicated in Fig.4.21a and Fig.4.21b, one can find equilibrium of the forces acting along each side of the free-body in the direction of the initial crack (θ_{cr}) as follows:

$$\sigma_{c3} \cdot \sin(\theta_{cr} - \theta) \cdot \cos(\theta_{cr} - \theta) + \sigma_{c1} \cdot \cos(\theta_{cr} - \theta) \cdot \sin(\theta_{cr} - \theta) = \tau_{cr} \quad (4.86)$$

Expressing the principal concrete compressive strength from the previous equation gives:

$$\sigma_{c3} = \frac{2 \cdot \tau_{cr}}{\sin(2 \cdot (\theta_{cr} - \theta))} - \sigma_{c1} \quad (4.87)$$

Since the concrete strength in this free-body is limited by the amount of shear stress that can be transferred through a crack and the brittleness of the concrete, this means that:

$$\sigma_{c3} = f_c \cdot \eta_{fc} \cdot \eta_\tau \quad (4.88)$$

The effectiveness factor that accounts for the presence of the initial cracks in concrete (in-plane-failure) is estimated as:

$$\eta_\tau = \frac{2 \cdot \tau_{cr}}{f_c \cdot \eta_{fc} \cdot \sin(2 \cdot (\theta_{cr} - \theta))} - \frac{\sigma_{c1}}{f_c \cdot \eta_{fc}} \leq 1 \quad (4.89)$$

where τ_{cr} represents the necessary amount of shear stress that can be transferred through a crack;

σ_{c1} represent the average tensile stress in a concrete strut.

Average tensile stress of a strut can be estimated based on the crack spacing, which is assumed equal to 1.5 times the bond length [74]:

$$\sigma_{c1} = \frac{6}{16} \cdot f_{ctm} \approx 0.38 \cdot f_{ctm} \quad (4.90)$$

When the contact forces develop at 45° from the crack surface, this value can be evaluated on the basis of the proposal by Vecchio and Collins [120] (refer to Fig.4.21c):

$$\tau_{cr,45^\circ} = \frac{\sqrt{f_c}}{0.31 + \frac{24 \cdot w_{ini}}{D_{max} + 16}} \quad (4.91)$$

where w_{ini} represents the initial crack width;

D_{max} represents the maximal aggregate diameter [mm] ($D_{max} = 0$ for $f_c > 60$ MPa).

The minimal shear stress which can be transferred through a crack corresponds to a case at which the direction of the principal compressive stress is parallel to the face of a crack (see *Fig.4.21c*). Based on the work of Randl [98] this value can be estimated as:

$$\tau_{cr,min} = 0.2 \cdot \sqrt[3]{f_c} + \begin{cases} 0.8 & \text{if } f_c \leq 35 \text{ MPa} \\ 1.0 & \text{if } f_c > 35 \text{ MPa} \end{cases} \cdot \left[(f_{y,dow,x} - \sigma_{sx}) \cdot \rho_x \cdot \sin(\theta_{cr}) + (f_{y,dow,z} - \sigma_{sz}) \cdot \rho_z \cdot \cos(\theta_{cr}) \right] \quad (4.92)$$

where ρ_x represents the horizontal reinforcement ratio;

ρ_z represents the vertical reinforcement ratio;

σ_{sx} represents the steel stresses in x -direction;

$f_{y,dow,x}$ represents the doweled steel strength x -direction;

σ_{sz} represents the steel stresses in z -direction;

$f_{y,dow,z}$ represents the doweled steel strength z -direction.

For other values of the angle ($\theta_{cr} - \theta$) the value can be calculated as (refer to *Fig.4.21c*):

$$\tau_{cr} = \tau_{cr,min} + \sqrt{2} \sin(\theta_{cr} - \theta) \cdot (\tau_{cr,45^\circ} - \tau_{cr,min}) \quad (4.93)$$

This assumption is based on the fact that the amount of shear that can be transferred through a crack increases quite fast as the stress field starts to rotate [120], and then stabilizes as the θ_{cr} and θ become close to perpendicular. After analysis of 77 reinforced concrete panels, the proposed law showed a good agreement with the test results, although the authors acknowledge that future work is required to verify its general consistency.

The last remaining effectiveness factor from *Eq.4.81* is the η_{dow} , which takes into account the presence of the confining concrete struts. As it was previously mentioned, the enhanced concrete compressive strength along the region influenced by the doweling is already used to equilibrate the shear force of the rebar (see *Fig.4.17c*). This means that this region of the concrete cannot be included in carrying any compressive stresses in the principal direction. This effect can be taken into account in the following manner:

$$\eta_{dow} = \frac{f_{cc}}{f_c} \geq 1.0 \quad (4.94)$$

It is important to emphasize that even in case where the yield strength of the reinforcement is not reduced due to the doweling (*point B* from *Fig.4.19*), the rebars still move

towards the concrete inducing the formation of the cracks and activating the confinement effects of the concrete, meaning that *Eq.4.94* needs to be applied in these cases as well.

4.2.3.2 Strength of the undamaged struts

The compressive strength of the undamaged struts is limited by the parameter η_{UDS} , which takes into account:

1. The presence of the rebars in the concrete struts, governing the spalling failures (as defined in *Eq.4.82*) and limiting the in-plane strength of the concrete (adopted from Hars [41]);
2. The presence of the doweled reinforcement (as defined in *Eq.4.94*).

The parameter itself is proposed to be calculated as:

$$\eta_{UDS} = q_{UDS,dow} \cdot \min \left\{ \frac{\eta_s \cdot \max \left\{ \frac{0}{b_w - (4c + 2\phi_{ext})} \right\}}{\frac{b_w}{b_w}} + \frac{\min \left\{ \frac{b_w}{4c + 2\phi_{ext}} \right\}}{\frac{b_w}{b_w}} \cdot (1 - \eta_{dow} \cdot \delta') \right. \\ \left. + (1 - q_{UDS,dow}) \cdot \min \left\{ \frac{\eta_s \cdot \max \left\{ \frac{0}{b_w - (4c + 2\phi_{ext})} \right\}}{\frac{b_w}{b_w}} + \frac{\min \left\{ \frac{b_w}{4c + 2\phi_{ext}} \right\}}{\frac{b_w}{b_w}} \cdot (1 - (1 - \sin \varphi_s) \cdot \delta') \right\} \right\} \quad (4.95)$$

φ_s represents the angle of the friction between the rebar surface and the surrounding concrete;

$q_{UDS,dow}$ represents the relative amount of the undamaged struts affected by the doweling.

As it can be seen the only difference between the *Eq.4.95* and the *Eq.4.81* is the fact that the factor η_t is now equal to one (since there are no cracks crossing the undamaged struts), and that unlike the damaged struts, the undamaged struts are only partly affected by the doweling. This can be seen in *Fig.4.20a*, where the confining concrete region (marked in dashed lines) crosses the undamaged struts only in their top-right and the bottom-left. The relative width of concrete affected by the doweling (s_{dow}) can be expressed in function of the total width of the undamaged struts.

Based on the geometrical consideration presented in *Fig.4.20d*, this factor can be estimated in the following manner:

$$\delta_{UDS,dow} = \frac{\cos(\theta_{cr} - \theta)}{s_{rm}} \cdot \max \left\{ \begin{matrix} l_{dow,x} \cdot \sin \theta \\ l_{dow,z} \cdot \cos \theta \end{matrix} \right\} \quad (4.96)$$

$$q_{UDS,dow} = \frac{2\delta_{UDS,dow}}{1 - q_{DS}} \quad (4.97)$$

4.2.4 Parameters governing the compressive strength of concrete

As it can be seen, the mechanical model for the effective concrete compressive strength is quite complex and depends on a significant number of parameters. However, the two parameters with the largest significance in the results are the width of the crack at the point of first yielding (w_{ini}), and the ultimate angle of the principal concrete compressive stresses. *Fig.4.22* gives a clear view on how these two parameters influence the concrete compressive strength effectiveness factor.

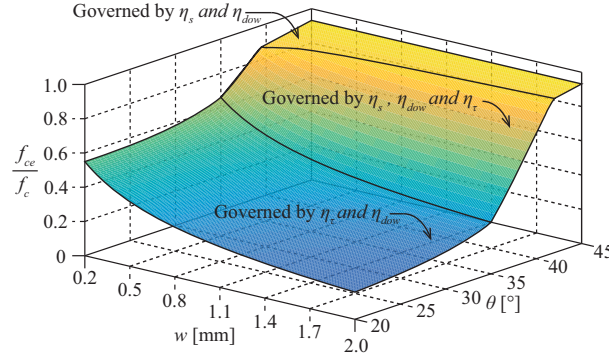


Figure 4.22: Representation of the failure criterion for the concrete compressive strength as a function of the stress-field rotation and the crack opening at first yielding

As it can be seen, there are three different regions in the failure surface. The first corresponds to the situation in which the rotation of the stress field is limited (see *Fig.4.23a*). For these cases, the strength of the damaged and the undamaged struts is governed by the presence of the spalling cracks (η_s) and the doweling action (η_{dow}). It can be seen that the width of the initial cracks does not influence the failure criterion. The stress field rotations, on the other hand, reduce the concrete compressive strength, since the amount of the undamaged struts which are affected by the dowel action of the reinforcement increases.

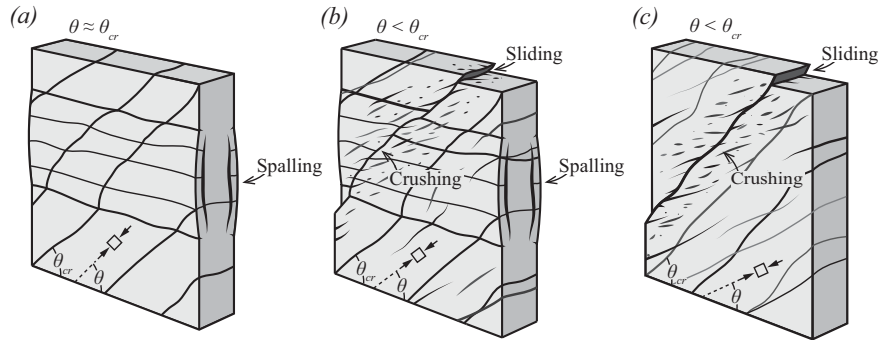


Figure 4.23: Potential failure mechanism of structural panels: (a) spalling of the concrete cover in case of small stress field rotation; (b) spalling and combined crushing with sliding failure in case of moderate stress field rotation and (c) crushing and sliding of the concrete struts in case of significant stress field rotations

As the stress field continues to rotate, the strength of the damaged struts becomes governed by the presence of in-plane cracks (η_τ), while the strength of the undamaged struts remains dependent on the out-of-plane cracks (η_s), as presented in *Fig.4.23b*. This corresponds

to the second region of the failure criterion, which is depended on the initial crack width (the wider the cracks, the larger the reduction of the concrete compressive strength). The physical failure of the concrete struts in this region can occur due to the spalling or the crushing of the material.

As the stress field increases still its rotation, the amount of the undamaged struts in the panel reduces, and eventually becomes zero. This leads to the third stage of the failure criterion, when the strength of the entire panel is dependent only on the characteristics of the in-plane cracks (η_τ) (see *Fig.4.23c*). Once more, the influence of the initial crack width is quite pronounced, and the failure mechanism of the concrete struts corresponds to crushing. Doweling of the reinforcement affects the concrete strength of the second as well as the third region of the failure surface. It has to be noted that when failure occurs by yielding of the reinforcement in both directions, the principal concrete compressive stresses does not reach f_{ce} .

4.3 Numerical solving procedure for the proposed compression softening model

In order to estimate the stress and the strain state of a panel, it is first necessary to define the points that correspond to the limit cases of the three stages of behaviour (the elastic uncracked phase, the onset of yielding and the failure). Once these points are known, full stress-strain curves can be produced by assuming that the stress field rotates linearly in between.

4.3.1 Cracking of the panel

First cracking can be directly calculated on the basis of *Eq.4.38* to *Eq.4.43*.

4.3.2 Onset of yielding or early concrete crushing

Finding the second characterising point in the panels load history requires the use of an iterative procedure (as presented in *Fig.4.24a*). There are three potential cases which can determine the behaviour of a panel:

1. Case 1 (C_1): which results in yielding of the reinforcement in x-direction;
2. Case 2 (C_2): which results in yielding of the reinforcement in z-direction;
3. Case 3 (C_3): which results in concrete crushing prior to yielding of the reinforcement.

After assuming the direction of the principal concrete compressive stresses (θ_σ) and the final width of the initial cracks (w_{ass}), it is possible to estimate the dowel strength of the reinforcement.

The average cracks spacing is assumed equal to be 1.5 times the bond length [74], which means that the average concrete tensile stress within the cracks is equal to:

$$\sigma_{c1} = \frac{3}{16} \cdot \tau_b \quad (4.98)$$

The principal concrete compressive stresses inclination may be calculated by using a Mohr's circle (shown in *Fig.4.15b*):

$$\tan \theta_\sigma = \frac{\tau_{xz}}{\sigma_{c1} - \sigma_{cx}} \quad (4.99)$$

Assuming that the x reinforcement yields the first ($\sigma_{sx} = f_{y,dow,x}$), equilibrium conditions give:

$$\sigma_{cx} + \rho_x \cdot f_{y,dow,x} = v_x \quad (4.100)$$

$$\sigma_{cz} + \rho_z \cdot \sigma_{sz} = v_z \quad (4.101)$$

$$\tau_{xz} = v_{xz} \quad (4.102)$$

Eq.4.98 to *Eq.4.102* present a system of 5 equation with 5 unknowns, which can be solved for τ_{xz} , which can then be used to determine all required stresses in concrete and steel.

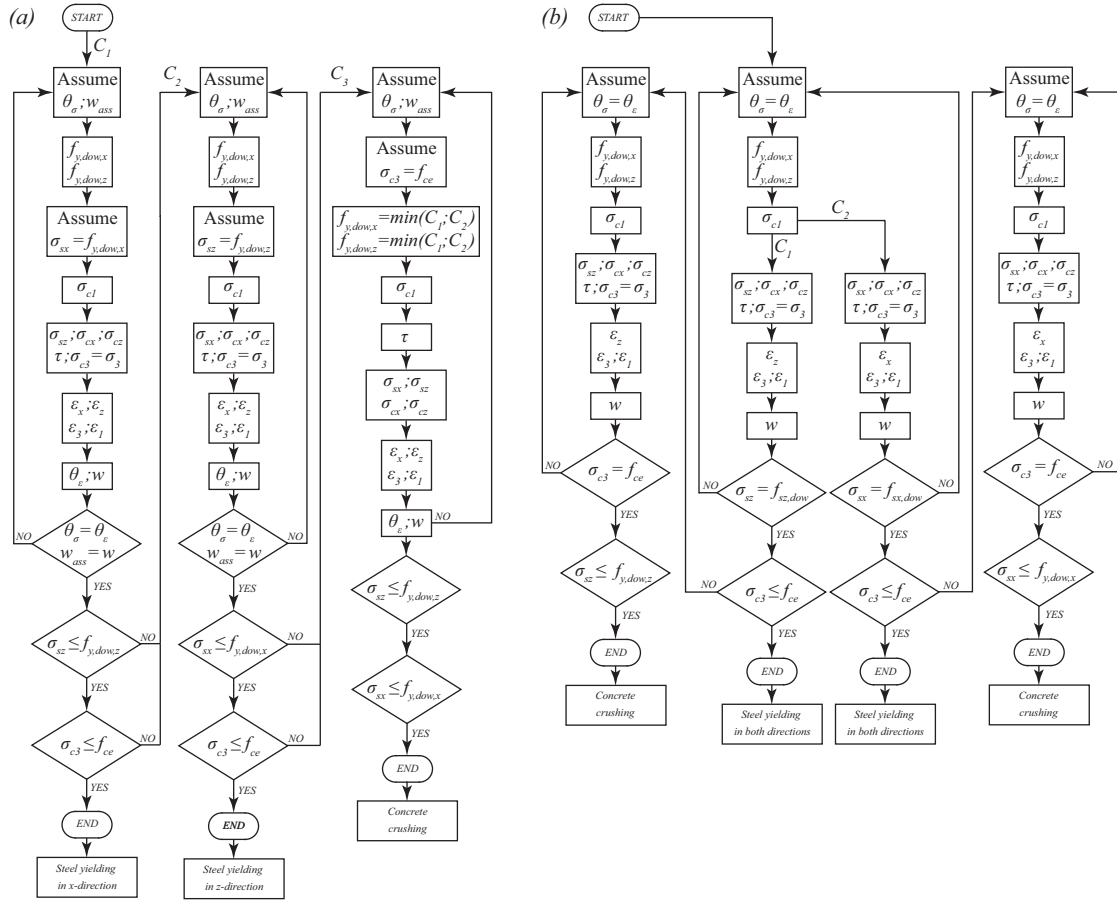


Figure 4.24: (a) Solving procedure at the onset of yielding; (b) solving procedure at failure

Applied stress rate in each direction is usually known, meaning that v_x and v_z can be expressed using v_{xz} . The results are checked determining the strain state of the panel and making sure that the assumed principal stress angle (θ_σ) is equal to the principal the stain angle (θ_ϵ) and by confirming that the assumed initial crack width (w_{ass}) is equal to the calculated one (w).

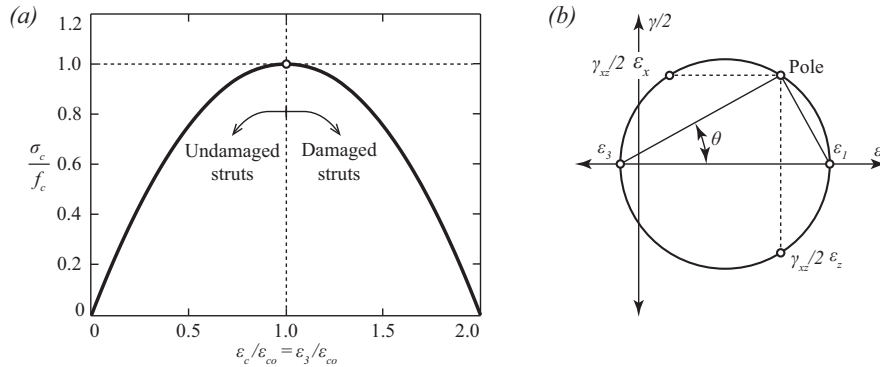


Figure 4.25: (a) Stress-strain parabola for concrete compressive strength; (b) average strain state of the panel

The average strains of the panel in the x -direction and z -direction are equal to:

$$\varepsilon_x = \frac{f_{yx,dow}}{E_s} - \frac{\tau_b \cdot s_{rmx}}{\phi_x \cdot E_s} \quad (4.103)$$

$$\varepsilon_z = \frac{\sigma_{sz}}{E_s} - \frac{\tau_b \cdot s_{rmz}}{\phi_z \cdot E_s} \quad (4.104)$$

s_{rmx} represents the average crack spacing in x -direction;

s_{rmz} represents the average crack spacing in z -direction.

The principal concrete compressive strains can be determined by using the uniaxial stress-strain parabola (refer to *Fig.4.25*), assuming that the undamaged struts follow its ascending branch and that the damaged struts follow its descending branch:

$$\varepsilon_3 = \varepsilon_{3c,DS} \cdot q_{DS} + \varepsilon_{3c,UDS} \cdot (1 - q_{DS}) \quad (4.105)$$

$$\varepsilon_{3c,DS} = \varepsilon_0 \cdot \left(1 + \sqrt{1 - \sigma_{c3}/f_c}\right) \quad (4.106)$$

$$\varepsilon_{3c,UDS} = \varepsilon_0 \cdot \left(1 - \sqrt{1 - \sigma_{c3}/f_c}\right) \quad (4.107)$$

$$\varepsilon_0 = 2 \cdot f_c / E_c \approx -0.002 \quad (4.108)$$

Eq.4.103, *Eq.4.104* and *Eq.4.105* define 3 points in a Mohr's circle, which means that the *Fig.4.25b* can be established, and the principal compressive strain direction can be calculated:

$$\tan \theta_\varepsilon = \frac{\varepsilon_x - \varepsilon_3}{\varepsilon_1 - \varepsilon_x} \quad (4.109)$$

Finally, it is possible to determine the initial crack opening:

$$w_{ini} = s_{rm} \cdot (\varepsilon_1 - \sigma_{c1} / E_c) \quad (4.110)$$

As indicated in *Fig.4.24a*, it is now necessary to verify that the assumed stress state is respected, or try another case if the answer is not complying with this condition.

Case C_2 is almost identical to C_1 , whereas C_3 is a bit simpler. The only difference between the solving procedure C_1 and C_2 is in the fact that the vertical instead of the horizontal reinforcement is assumed to have reached yielding by the end of the second phase of the panel's load-history. Apart from this, all the necessary validations remain identical (refer to *Fig.4.24a*).

The doweled steel strength of x -reinforcement according to case C_1 is lower than that of case C_3 , since the angle θ is higher for case C_1 than for C_3 . In the same way, the doweled steel strength of z -reinforcement according to case C_2 is lower than that of case C_3 . These two values for both doweled steel strengths (of C_1 and C_2) are adopted for case C_3 , which is a slightly conservative simplification.

4.3.3 Failure of the panel

In order to determine the third (and final) characteristic point of the panel's load history, another iterative procedure needs to be applied. Looking at the scheme from *Fig.4.24b*, it can be seen that depending on the determining case from *Fig.4.24a*, it is now possible to estimate the average strain in one direction (ε_x in case of C_2 or ε_z in case of C_1).

The direction of the principal compressive stresses is assumed to be parallel to the direction of the principal compressive strains. The secondary doweling should only be applied on the reinforcement which did not yield during the previous phase (x -direction in case of C_2 and z -direction in case C_1). The additional doweling should only be applied on the remaining steel stresses in the reinforcement that yields second, from the onset of the yielding of the direction yielded first reinforcement.

The stress field rotates until the failure of the concrete or steel is reached. The stress and strain transformation which were applied at the onset of yielding should be applied during this phase as well. In the end of the solving procedure it is verified that the ultimate stress direction is lower than the one at the onset of yielding.

4.4 Experimental validation and comparison to available methods

In order to validate the assumptions of the proposed model, a database comprising 77 structural panels has been collected and presented in *Tab. 4.1*. It contains results of 12 separate experimental campaigns performed by various authors (the corresponding references as well as the basic geometrical and mechanical properties are provided in *Tab. 4.1*).

Table 4.1: Database of the reinforced concrete panels failing in shear

N°	Ref.	Name	b_w [mm]	ϕ_x [mm]	ϕ_z [mm]	ρ_x [%]	ρ_z [%]	f_c [MPa]	f_{yx} [MPa]	f_{yz} [MPa]
1	[119]	PV4	70	3.43	3.43	1.06	1.06	27	242	242
2		PV6	70	6.31	6.31	1.79	1.79	30	266	266
3		PV10	70	6.31	4.72	1.79	1.00	15	276	276
4		PV11	70	6.31	5.39	1.79	1.31	16	235	235
5		PV12	70	6.31	3.15	1.79	0.45	16	469	269
6		PV16	70	4.06	4.06	0.74	0.74	22	255	255
7		PV19	70	6.31	3.99	1.79	0.71	19	458	299
8		PV20	70	6.31	4.44	1.79	0.89	20	460	297
9		PV21	70	6.31	5.37	1.79	1.30	20	458	302
10		PV22	70	6.31	5.83	1.79	1.52	20	458	420
11		PV23	70	6.31	6.31	1.79	1.79	21	518	518
12		PV25	70	6.31	6.31	1.79	1.79	19	466	466
13		PV27	70	6.31	6.31	1.79	1.79	21	442	442
14		PV28	70	6.31	6.31	1.79	1.79	19	483	483
15	[121]	PHS2	70	8.05	5.72	3.23	0.41	66	606	521
16		PHS3	70	8.05	5.72	3.23	0.82	58	606	521
17		PHS5	70	8.05	5.72	3.23	0.41	52	606	521
18		PHS6	70	8.05	5.72	3.23	0.41	50	606	521
19		PHS8	70	8.05	5.72	3.23	1.22	56	606	521
20		PHS9	70	8.05	5.72	3.23	0.41	56	606	521
21		PHS10	70	8.05	5.72	3.23	1.22	51	606	521
22	[75]	PP1	287	19.54	11.28	1.94	0.65	27	479	480
23	[118]	PC1A	70	5.72	5.72	1.65	0.82	28	500	500
24		PC4	70	5.72	5.72	1.65	0.82	25	260	260
25	[94]	A2	178	16.00	16.00	1.20	1.20	41	462	462
26		A3	178	19.50	19.50	1.78	1.78	42	446	446
27		A4	178	25.20	25.20	2.97	2.97	42	469	469
28		B1	178	16.00	11.30	1.20	0.60	45	462	444
29		B2	178	19.50	16.00	1.78	1.20	44	446	462
30		B3	178	19.50	11.30	1.78	0.60	45	446	444
31		B4	178	25.20	11.30	2.97	0.60	45	469	444
32		B5	178	25.20	16.00	2.97	1.20	43	469	462
33		B6	178	25.20	19.50	2.97	1.78	43	469	446
34	[127]	VA1	178	11.30	11.30	1.20	1.20	95	445	445
35		VA2	178	16.00	16.00	2.40	2.40	98	409	409
36		VA3	178	19.50	19.50	3.57	3.57	95	455	455
37		VA4	203	25.20	25.20	5.23	5.23	103	470	470
38		VB1	178	16.00	11.30	2.40	1.20	98	409	445
39		VB2	178	19.50	11.30	3.57	1.20	98	455	445

40		VB3	178	25.20	11.30	5.96	1.20	102	470	445
41		VB4	178	19.50	11.30	1.78	0.60	97	455	445
42	[47]	HB1	178	16.00	11.30	1.20	0.60	67	409	445
43		HB3	178	19.50	11.30	1.78	0.60	67	447	445
44		HB4	178	25.20	11.30	2.98	0.60	63	470	445
45	[56]	SE1	285	19.50	11.30	2.91	0.98	43	492	479
46		SE6	285	19.50	11.30	2.91	0.33	40	492	479
47	[124]	00R	60	6.00	6.00	0.86	0.86	28	310	310
48		15R	60	6.00	6.00	0.86	0.86	28	310	310
49		30R	60	6.00	6.00	0.86	0.86	28	310	310
50		45R	60	6.00	6.00	0.86	0.86	28	310	310
51		00D	60	7.60	7.60	0.87	0.87	28	318	318
52		30D	60	7.60	7.60	0.86	0.87	28	318	318
53		45D	60	7.60	7.60	0.87	0.87	28	318	318
54		00DI	60	7.00	7.00	1.39	1.39	31	294	294
55		22.5DI	60	7.00	7.00	1.39	1.39	31	294	294
56		45DI	60	7.60	7.60	1.30	1.30	31	318	318
57		45DII	60	7.60	7.60	2.61	2.61	31	318	318
58		45PCI	60	5.44	5.44	0.77	0.77	30	1187	1187
59		45PCII	60	5.44	5.44	1.55	1.55	30	1187	1187
60		45PCIII	60	5.44	5.44	1.55	0.77	30	1187	1187
61		45PCIV	60	5.44	5.44	1.55	0.77	45	1187	1187
62	[57]	PK02	70	6.50	6.50	1.07	1.07	19	660	660
63		PK04	70	6.50	6.50	1.07	1.07	20	660	660
64		PK07	70	6.50	6.50	1.07	1.07	21	660	660
65		EGE6F1	100	6.50	6.50	0.66	0.66	16	465	465
66		EGE6F2	100	6.50	6.50	0.66	0.66	16	465	465
67		EGE6F3	100	6.50	6.50	0.66	0.66	15	465	465
68		EGE6F4	100	6.50	6.50	0.66	0.66	17	465	465
69		EGE6F7	100	6.50	6.50	0.66	0.66	19	465	465
70		EGE6F8	100	6.50	6.50	0.66	0.66	13	465	465
71		EGE7F1	100	6.50	6.50	0.66	0.66	16	660	660
72		EGE7F2	100	6.50	6.50	0.66	0.66	15	660	660
73		EGE7F3	100	6.50	6.50	0.66	0.66	17	660	660
74	[106]	#2	100	10.00	10.00	3.14	3.14	26	582	582
75		#6	100	10.00	10.00	1.57	1.57	26	582	582
76	[5]	KP1	140	12.70	12.70	2.03	1.02	25	430	430
77		TP4A	70	6.35	6.35	2.03	2.03	25	450	450

The selected elements vary significantly in concrete compressive strength (from 13 MPa to 103 MPa), reinforcement ratios (from 0.33 % to 5.96 %), steel yield strength (from 235 MPa to 1187 MPa) as well as concerning the ratio of the reinforcement placed in two perpendicular directions (from 0.11 to 1.00). The size of the specimens varied from 500 mm to 2510 mm, while the thickness varied from 60 mm to 287 mm. With respect to the loading conditions, most of the panels have been subjected to pure shear (55 out of 77 specimens), some of them combined shear with compression (19 out of 77 specimens), and a few were loaded to shear and bi-axial traction (3 out of 77 panels). The panels experienced different failure modes (concrete spalling, crushing or sliding) and while some failed due to weakening of the concrete, others yielded reinforcement in both directions.

In order to assess the accuracy of the presented approach and to compare it to some of the existing strain-based approaches, the database from *Tab. 4.1* has been assessed using the Elastic-Plastic Stress Field Method (EPSF) [32] implementing the Vecchio and Collins softening equation [120]. *Tab.4.2* summarizes the results of both analyses, and gives the ultimate strength assessment for each approach. It can be seen that both approaches provide satisfactory accuracy. However, the proposed mechanical procedure shows some higher level of accuracy (1.01 instead of 1.11) and lower scatter of the results (0.12 instead of 0.15) compared to EPSF approach. Additionally, it provides with information on the governing failure mode, which matched for the 77 specimens to the observed one.

Table 4.2: Results of the EPSF analysis and the mechanical model proposed in this paper

N°	Ref.	Name	τ_{TEST} [MPa]	τ_{EPSF} [kN]	τ_{MODEL} [kN]	τ_{TEST}/τ_{EPSF}	τ_{TEST}/τ_{MODEL}
1	[119]	PV4	2.84	2.56	2.62	1.11	1.08
2		PV6	4.47	4.76	4.81	0.94	0.93
3		PV10	3.97	3.69	3.73	1.08	1.06
4		PV11	3.56	3.59	3.63	0.99	0.98
5		PV12	3.13	2.55	3.05	1.23	1.03
6		PV16	2.14	1.89	1.95	1.13	1.10
7		PV19	3.96	3.73	4.01	1.06	0.99
8		PV20	4.26	4.22	4.46	1.01	0.96
9		PV21	5.03	5.18	5.46	0.97	0.92
10		PV22	6.07	6.39	7.11	0.95	0.85
11		PV23	8.88	7.69	8.09	1.15	1.10
12		PV25	9.13	8.39	7.58	1.09	1.20
13		PV27	6.35	6.74	7.94	0.94	0.80
14		PV28	5.61	5.89	6.56	0.95	0.86
15	[121]	PHS2	6.66	5.18	5.21	1.29	1.28
16		PHS3	8.10	7.67	7.92	1.06	1.02
17		PHS5	4.81	3.54	3.96	1.36	1.21
18		PHS6	7.62	7.30	7.80	1.04	0.98
19		PHS8	10.84	9.53	9.91	1.14	1.09
20		PHS9	9.16	7.52	7.87	1.22	1.16
21		PHS10	8.25	7.57	7.82	1.09	1.05
22	[75]	PP1	4.95	5.11	4.79	0.97	1.03
23	[118]	PC1A	5.61	5.84	6.05	0.96	0.93
24		PC4	4.84	5.10	5.75	0.95	0.84
25	[94]	A2	5.37	5.54	6.13	0.97	0.88
26		A3	7.65	7.94	8.49	0.96	0.90
27		A4	11.31	11.91	14.08	0.95	0.80
28		B1	3.96	3.82	4.54	1.04	0.87
29		B2	6.13	6.63	7.25	0.92	0.85
30		B3	4.35	4.59	4.89	0.95	0.89
31		B4	5.06	5.50	5.60	0.92	0.90
32		B5	7.15	8.27	8.03	0.86	0.89
33		B6	9.14	9.96	10.11	0.92	0.90
34	[127]	VA1	6.16	5.34	6.19	1.15	0.99
35		VA2	9.73	9.84	10.62	0.99	0.92
36		VA3	15.08	16.25	16.91	0.93	0.89
37		VA4	21.42	21.05	21.36	1.02	1.00

38		VB1	7.50	7.25	7.82	1.03	0.96
39		VB2	9.14	9.32	8.94	0.98	1.02
40		VB3	9.71	10.55	10.2	0.92	0.95
41		VB4	4.86	4.66	6.28	1.04	0.77
42	[47]	HB1	4.32	3.63	4.41	1.19	0.98
43		HB3	4.89	4.62	5.06	1.06	0.97
44		HB4	5.33	5.84	5.85	0.91	0.91
45	[56]	SE1	6.77	7.52	7.32	0.90	0.92
46		SE6	3.76	3.92	3.96	0.96	0.95
47	[124]	00R	3.14	2.66	2.72	1.18	1.15
48		15R	3.15	2.66	2.72	1.18	1.16
49		30R	3.13	2.66	2.72	1.18	1.15
50		45R	3.42	2.66	2.72	1.29	1.26
51		00D	2.97	2.70	2.83	1.10	1.05
52		30D	2.56	2.70	2.82	0.95	0.91
53		45D	2.84	2.70	2.83	1.05	1.00
54		00DI	4.96	4.10	4.17	1.21	1.19
55		22.5DI	5.06	4.10	4.17	1.23	1.21
56		45DI	3.97	4.15	4.21	0.96	0.94
57		45DII	7.61	8.29	8.35	0.92	0.91
58		45PCI	7.78	6.55	9.26	1.19	0.84
59		45PCII	11.72	8.39	11.46	1.40	1.02
60		45PCIII	9.44	7.35	9.51	1.29	0.99
61		45PCIV	10.63	8.65	11.12	1.23	0.96
62	[57]	PK02	9.12	7.4	8.39	1.23	1.09
63		PK04	8.91	6.64	8.75	1.34	1.02
64		PK07	9.04	6.79	9.06	1.33	1.00
65		EGE6F1	8.00	6.01	7.28	1.33	1.10
66		EGE6F2	8.1	5.68	7.37	1.43	1.10
67		EGE6F3	6.90	5.17	6.72	1.34	1.03
68		EGE6F4	7.20	5.71	7.69	1.26	0.94
69		EGE6F7	8.50	7.32	8.67	1.16	0.98
70		EGE6F8	7.35	5.23	6.03	1.40	1.22
71		EGE7F1	8.20	5.89	7.28	1.39	1.13
72		EGE7F2	7.70	5.32	7.00	1.45	1.10
73		EGE7F3	8.70	6.47	7.93	1.35	1.10
74	[106]	#2	11.78	10.94	9.94	1.08	1.18
75		#6	14.07	9.3	10.93	1.51	1.29
76	[5]	KP1	5.62	6.08	5.79	0.93	0.97
77		TP4A	8.72	8.00	9.2	1.09	0.95
					Aver :	1.11	1.01
					COV :	0.15	0.12

The ratio between the measured and the estimated strength is also presented in *Fig. 4.26* as a function of four basic parameters (concrete compressive strength f_c , steel strength in z -direction (which was the weaker direction) (f_{yz}), reinforcement ratio in x -direction (ρ_x) and reinforcement ratio in z -direction (ρ_z). Each of the plots contains a red line which gives an average value of the 5 nearest τ_{TEST}/τ_{MODEL} points (with respect to a given parameter), along the entire database. As it can be seen, the proposed mechanical approach gives consistent results

over the investigated domain, and shows no clear trends with respect to the four parameters, which is satisfactory.

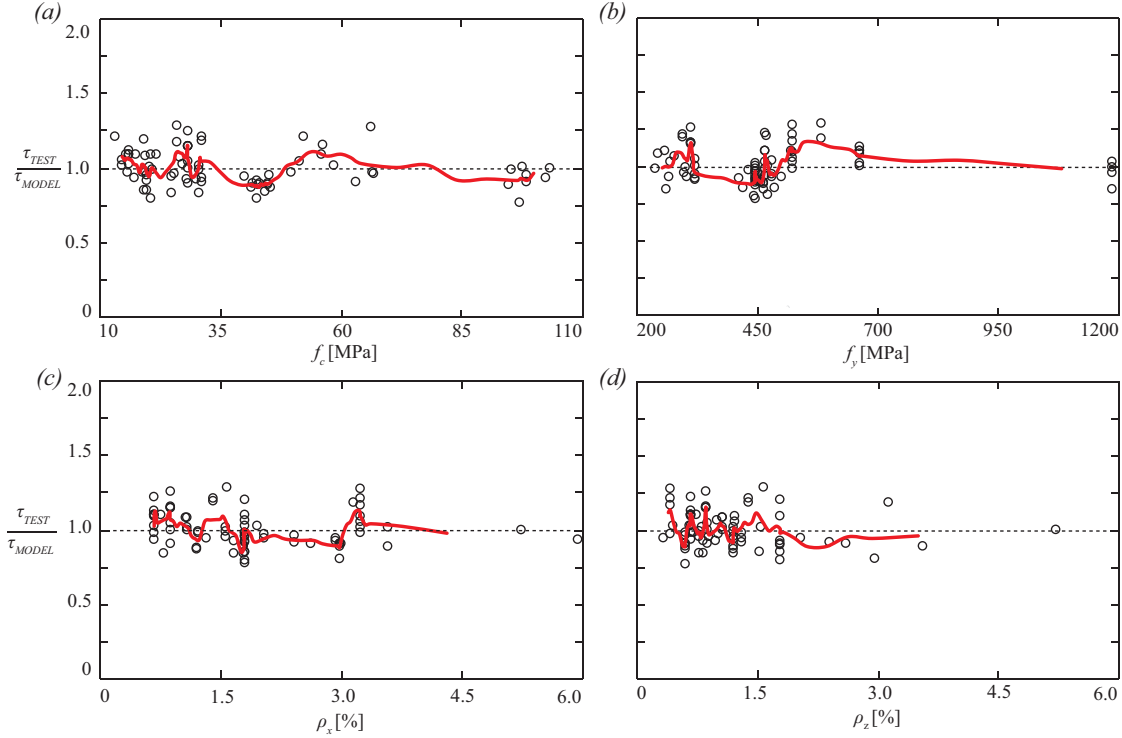


Figure 4.26: Shear strength prediction of the database as a function of: (a) concrete compressive strength; (b) steel yield strength; (c) horizontal reinforcement ratio; (d) vertical reinforcement ratio

Fig.4.27 compares the accuracy of the presented approach to EPSF [32] with respect to the stress field rotation.

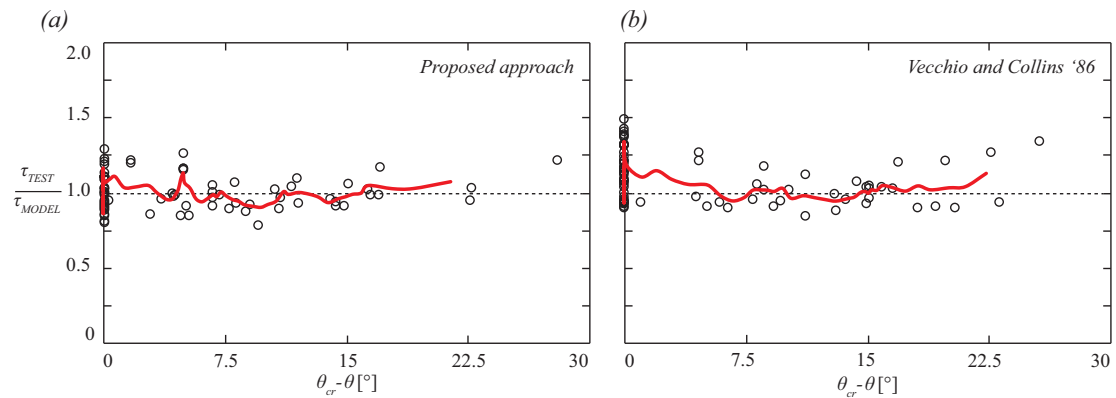


Figure 4.27: (a) Shear strength prediction of the database using the mechanical model presented in this paper; (b) using the softening equation of Vecchio and Collins [120] as a function of stress field rotation angle

As it can be seen the mechanically based model shows better accuracy for panel with small rotations when compared to the Vecchio and Collins softening equation [120] approach,

but most importantly it shows greater precision for panels with large rotations, which is relevant for analysis of prestressed concrete beams. However, it should be noted that the number of panels which experienced significant stress field rotations is not sufficiently large, and more specimens are required in order to consolidate these results.

In order to compare the proposed mechanical procedure to existing strain-based approaches for estimating the effective concrete compressive strength, the ratio between the effective and cylinder concrete compressive strength (f_{ce}/f_c) of each panel has been presented in function of its average principal tensile strain (ϵ_l) in *Fig.4.28*. The red line in the graph corresponds to the concrete compressive strength reduction factor according to Vecchio and Collins [120].

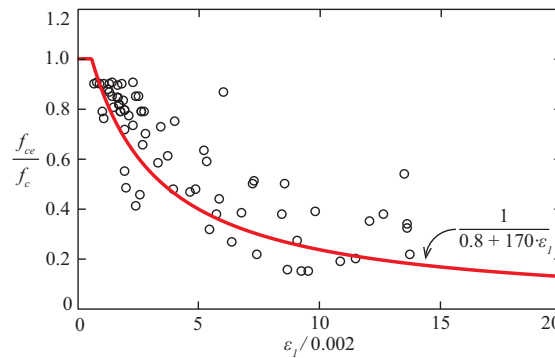


Figure 4.28: Calculated effective concrete compressive strength in function of normalized principal tensile strains

It can be seen that the results of the mechanical approach are consistent with the semi-empirical equation established within the Modified Compression Field Theory [120]. Panels with smaller average tensile strains experience a smaller reduction in strength, while vice-versa. However, unlike the MCFT equations, the mechanical efficiency factor can never be equal to one. Even in panels with relatively low strength concrete ($f_c < 30$ MPa), the presence of the reinforcement will always induce in-plane cracks, and therefore reduce its effective compressive strength. This theoretical result is in agreement to other semi-empirical formulas of Hsu [47] or Kaufmann [52].

Chapter 5: Conclusions and future research

Chapter 2 focused on the differences between the strut-and-tie models and stress fields suitable for the design and assessment of structural concrete members. Elastic-plastic stress fields were used for this purpose, and the obtained results were compared to those acquired using rigid-plastic stress fields. Accuracy and generality of the approach was finally validated, by comparing the estimated failure loads to experimentally measured values from an online database (which can be found at: <http://i-concrete.epfl.ch/epsf/epsf.html>).

In addition to this, advanced modelling techniques for EPSF, which can be applied when analysing structural concrete members with complex loading and geometry was presented in Chapter 3. Special focus was directed towards numerical stability of the approach by performing detailed finite element sensitivity analysis. Cases where structural concrete elements had insufficient anchorage length were investigated, as well as members composed of crossed structural concrete beams (which is particularly interesting when analysing bridge diaphragms for example). In order to profit from increased accuracy of the EPSF method (compared to current code provisions), a procedure for tailoring the partial safety factors was presented.

In order to justify the accuracy and generality of the concrete compression strength softening equation implemented in EPSF method (originally proposed by Vecchio and Collins in 1986 [120]), a mechanically based model that takes into account different failure modes of concrete (crushing, sliding and spalling) was developed and validated in Chapter 4.

Final conclusions resulting from the work presented in this thesis are summarized in following chapter. In addition to this, some recommendations for future work in the field of limit analysis, structural reliability and concrete compressive strength effectiveness factors are provided.

5.1 Conclusions

The main conclusions resulting from the research presented in this thesis, are summarized in the following section. They are divided into three groups, each of them referring to the work described in previous chapters.

5.1.1 Regarding the application of STM and stress fields as tools for design and assessment

This chapter focused on comparing suitable approaches for the design and assessment of structural concrete members using stress fields and strut-and-tie models. Its denouements are synthesised as following.

1. Design and assessment of structural concrete elements can be based on limit analysis, providing that its main hypotheses are respected (having smeared cracks in the elements and sufficient anchorage of the reinforcement). Nevertheless, the two processes should not necessarily be performed following the same strategy.
2. Simple load-carrying models, which are in equilibrium with the external loads, provide sufficient element strength at ULS and ensure a suitable behaviour at SLS are suitable for design of structural concrete members. Solutions leading to simple reinforcement layouts that can be easily inspected and put in place are preferred.
3. Strength assessment of existing structural concrete members should be performed in steps, beginning with simple solutions which are gradually refined until they provide sufficient element strength compared to imposed requirements. According to the limit analysis this refinement can be performed until an exact solution has been reached, which provides the highest possible strength of all the safe estimates (lower-bound solutions). In case imposed strength requirements are still not met the structure needs to be reinforced. However, the quantity of required interventions is minimized. Serviceability issues of such elements can be directly checked in-situ.
4. Stress fields and strut-and-tie models are complementary approaches based on the lower-bound theorem of limit analysis. While strut-and-tie models are simpler to develop for an entire element and particularly useful to determine the amount of required reinforcement, stress fields are most suited for detailing. They are useful to verify the behaviour of concrete in critical regions (if the struts respect the boundary conditions of the element) and indicate nodes which require additional considerations when it comes to anchorage.
5. Exact solutions according to the theory of plasticity can be developed by hand using an iterative procedure, starting from a failure mechanism. In case a corresponding rigid-plastic stress field can be developed inside such a mechanism (respecting the boundary conditions) the solution can be accepted. Otherwise, the failure mechanism needs to be adapted accordingly.
6. Elastic-plastic stress field method is suitable for design and assessment of structural concrete members. The method respects the equilibrium and yield conditions (lower-bound theorem), which are derived from an imposed deformation field. At ULS, this deformation field becomes a licit failure mechanism, meaning that the upper-bound theorem of the limit analysis is also respected. Consequently, the EPSF can be used to obtain exact solutions according to limit analysis in an automated manner.
7. The EPSF automatically accounts for all potential load-carrying mechanism, particularly the ones resulting from the presence of crack control reinforcement. In addition to this, it allows a refined estimation of the effective concrete compressive strength by imposing a softening equation of Vecchio and Collins [120].
8. The exact solutions (according to limit analysis) obtained using the EPSF method show satisfactory behaviour when compared to a database containing 315 elements

(available online at <http://i-concrete.epfl.ch/epsf/epsf.html>). Wide number of different geometries has been analysed (dapped-end beams, deep beams, prestressed girders, corner frames, wall, crossed beams and walls), failing in various types of mechanisms (shear, bending, local failures). The method provided accurate estimates of their strength and showed low scatter of the results, thus confirming the consistency and generality of the approach.

5.1.2 Regarding the advanced modeling of structural concrete with EPSF method

This chapter focused on modelling aspect of elastic-plastic stress field method by analysing its mesh related problems, simulation of particular structural details and application of suitable safety format. Its denouements are synthesised as following.

1. The EPSF method gives stable results for various size of applied finite elements. A general recommendation when selecting an optimal FE size is to use the stirrup spacing as the main grid for meshing, and place two concrete FE triangles in between.
2. The EPSF method gives stable results for very distorted FE triangles ($a:h$ ration equal to 1:5). A general recommendation is to keep this ratio up to 1:3.
3. Orientation of the FE triangles on the other hand has a significant influence of the results. Hence, using the meshes which favour certain FE orientation should be avoided and FE with random or zig-zag inclination of hypotenuses should be selected.
4. Number of iterations until the convergence of the EPSF model at ULS is 250 steps. However, when estimating the strength of a structural concrete elements, it is advised to use less iterations in the beginning in order to reduce the time required for a single simulation. The results obtained with 100 iterations are already quite close to final solution.
5. Structural concrete members with insufficient anchorage length can be analysed using EPSF method with satisfying accuracy. The diameter of a rebar which does not have sufficient anchorage length should be reduced in order to limit the amount of tensile force which can be taken by a single bar FE along the required anchorage length. For this purpose, plastic bond law introduced by Tension Chord Model [74] proved to give satisfying results.
6. Structural concrete elements which are connected and placed in two perpendicular planes can be accurately analysed using the EPSF method, by linking the nodes of the crossing areas with rigid FE bars in order to impose equal deformations between the crossing elements. Providing that the basic meshing recommendations are respected, this procedure gives satisfying results when compared to test results.
7. The Partial Safety Factors can be tailored in order to combine them with EPSF method. Depending on the applied concrete compressive strength and type of failure (shear or flexural), PSF can assume higher or lower values. The method proved to be sensitive to scatter in material properties, meaning that average material resistance and the coefficient of variation need to be properly estimated for each case.

8. For concrete with high compressive strength (over 50 MPa), the partial safety format becomes the global safety format, since both concrete and steel partial safety factors become equal to 1.16.
9. In case of lower concrete compressive strength (around 20 MPa), the tailored partial safety factors assume standard values (1.48 for concrete and 1.16 for steel).
10. In case accurate estimates of concrete compressive strength are not available, standard partial safety factors for concrete and steel should be used ($\gamma_c=1.50$ and $\gamma_s=1.15$)

5.1.3 Regarding the effectiveness factor for concrete compressive strength

This chapter investigated the behaviour of panels subjected to in-plane forces and proposed a model to describe their behaviour and potential failure modes. Its denouements are synthesised as following.

1. The traditional description of the phenomenon of compression-softening due to the transverse cracking, by means of semi-empirical equations based on transverse strains, is simple to use but does not provide information on the actual failure mode or parameters governing failure.
2. A consistent approach to this issue shall account for different stages of behaviour, namely: uncracked, cracked state before yielding and cracked state after yielding with the potential development of a secondary set of cracks.
3. Each stage of behaviour may be governed by different failure modes. These are out-of-plane (spalling) failures, concrete crushing and crack sliding (after rotation of the principal stress direction). These failure modes can be consistently calculated.
4. Doweling of the bars has an influence on the effective concrete compressive strength. It allows carrying shear through the cracks but may originate spalling of the concrete cover. In general, the various shear-carrying actions are thus not independent.
5. A mechanical approach based on the equilibrium and compatibility conditions can be developed accounting for each stage of behaviour and its associated failure modes. A possible manner to do so is proposed in this chapter.
6. The results of the mechanical approach show nice agreement to test results (better than available semi-empirical formulas) and allows for a complete description of the load-deformation response. This is relevant not only for accuracy, but to provide designers with a clear physical understanding of the failure mechanisms and how to enhance the behaviour of the member.

5.2 Future research

The following section provides some suggestions for future researches, which can be conducted with respect to the scope of research presented in this thesis. Once again, the recommendations are divided into three groups, each of them resulting from the work shown in Chapter 2, Chapter 3 and Chapter 4, respectively.

One of the principal ideas behind the work conducted in Chapter 2 of this thesis, was to assemble an open source database containing experimental results of reinforced and prestressed concrete elements found in literature, model them using EPSF method and place the database online (at <http://i-concrete.epfl.ch/epsf/epsf.html>). This accommodates complete transparency of the research, and provides examples for the correct application of the EPSF method. With this in mind:

1. Structural concrete elements from additional experimental campaigns along with corresponding EPSF models could be introduced into the existing database;
2. Accent could be placed on very old experimental investigations (from the beginning of the XX century) in order to validate the applicability of the EPSF approach for such cases (some work has already been done in this direction at IBETON);
3. Improve the solver of ICONC in order to reduce the required computational time, which would allow to efficiently analyze large-scale members without heavy finite element meshes.

Continuing the work from Chapter 3 of this thesis could involve investigating:

1. Validation of the results of EPSF analyses in cases of imposed displacements as a load case;
2. Analyzing the cases with insufficient anchorage length using plane (smooth) rebars;
3. Further investigation of the effect of reliability index in the process of tailoring the PSF for EPSF method;
4. Comparing the ultimate resistance of structural concrete members, when tailored global and partial safety factors have been combined with EPSF method (some work has already been done in this direction at IBETON).

Following the results presented in Chapter 4 of this thesis, further research is required in order to:

1. Propose a simplified expression for the concrete compressive strength efficiency factor, which could be easily implemented in finite element programs or even used in hand calculations;
2. Investigate the accuracy of full and simplified expressions for effective concrete compressive strength on reinforced and prestressed beams failing in shear (some work has already been done in this direction at IBETON);

References

- 1) ACI 318-08 (2008): 'Building Code Requirements for Structural Concrete', ACI Committee 318, 467 p., USA
- 2) ACI Committee 364.1 R-94 (1994): 'Guide for Evaluation of Concrete Structures Prior to Rehabilitation', ACI, 22 p., USA
- 3) ACI Committee 437R-03 (2003): 'Strength Evaluation of Existing Concrete Buildings', ACI, 28 p., USA
- 4) Ali M.A. and White R.N. (2001): 'Automatic Generation of Truss Model for Optimal Design of Reinforced Concrete Structures', ACI Structural Journal, Vol. 98, N° 4, pp. 431-442, USA
- 5) André H.M.O. (1987): 'Toronto Kajima Study on Scale Effects in Reinforced Concrete Elements', University of Toronto, Department of Civil Engineering, PhD Thesis, 267 p., Toronto, Canada
- 6) Argirova G., Fernández Ruiz M. and Muttoni A. (2014): 'How simple can nonlinear finite element modelling be for structural concrete?', Informes de la Construcción, Vol. 66, 8 p., Spain
- 7) Argirova G. and Muttoni A. (2012): 'Verification of details of existing structures with the elastic-plastic stress field method', 9th fib International PhD Symposium in Civil Engineering, Vol. 1, pp. 153-158, Karlsruhe, Germany
- 8) Bach F., Nielsen M.P. and Braestrup M.W. (1980): 'Shear Tests on Reinforced Concrete T-Beams - Series V, U, X, B and S', Structural Research Laboratory, Technical University of Denmark, Report N° 120, 87 p., Copenhagen, Denmark
- 9) Baumann T. and Rüsch H. (1970): 'Schubversuche mit indirekter Krafteinleitung: Versuche zum Studium der Verdübelungswirkung der Biegezugbewehrung eines Stahlbetonbalkens', Deutscher Ausschuss für Stahlbeton, Heft 210, 83 p., Berlin, Germany
- 10) Belarbi A. and Hsu C.-T.T. (1995): 'Constitutive laws of softened concrete in biaxial tension-compression', ACI Structural Journal, Vol. 92, N° 5, pp. 562-573, USA
- 11) Bentz E.C., Vecchio F.J. and Collins M.P. (2006): 'Simplified Modified Compression Field Theory for Calculating Shear Strength of Reinforced Concrete Elements', ACI Structural Journal, Vol. 103, N° 4, pp. 614-624, USA

References

- 12) Biondini F., Bontempi F. and Malerba P. (1996): 'Ricerca di Modelli Strut-and-Tie Mediante Programazione Lineare', Politecnico di Milano, Studi e Ricerche, Vol. 17, pp. 121-156, Italy
- 13) Brena S.F. and Morrison M.C. (2007): 'Factors Affecting Strength of Elements Designed Using Strut-and-Tie Models', ACI Structural Journal, Vol. 104, N° 3, pp. 267-277, USA
- 14) Brown D.B. and Bayrak O. (2006): 'Minimum transverse reinforcement for bottle-shaped struts', ACI Structural Journal, Vol.103, N° 6, pp. 813-821, USA
- 15) Büeler C. and Thoma K. (2010): 'Indirekt gelagerter Spannbetonträger', Lucerne University of Applied Sciences and Arts, 61 p., Lucerne, Switzerland
- 16) Campana S. (2013): 'Éléments en béton armé soumis à une combinaison de flexion, effort tranchant et forces de déviation', EPFL, IBETON, Thèse, N° 5574, 162 p., Lausanne, Switzerland
- 17) Campana S. and Muttoni A. (2011): 'Essais sur angles de cadre d'une tranchée couverte à section polygonale (rapport de synthèse)', EPFL, IBETON, Test Report , 184 p., Lausanne, Switzerland
- 18) Campbell T.I., Batchelor B. and Chitnuyanondh L. (1979): 'Web crushing in concrete girders with prestressing ducts in the web', PCI Journal, Vol. 24, N° 5, pp. 71-87, USA
- 19) Chan T.C-K (1979): 'A Study of the Behavior of Reinforced Concrete Dapped End Beams ', University of Washington, Master Thesis, 167 p., Washington, USA
- 20) Chen W.F. (1982): 'Plasticity in reinforced concrete ', McGraw-Hill Education, 474 p.
- 21) Clarke J.L. and Taylor H.P.J. (1975): 'Web crushing - a review of research', Cement and concrete association, Technical report, Vol. 42, N° 509, 16 p., London, UK
- 22) Collins M.P. (1978): 'Towards a Rational Theory for RC Members in Shear', ASCE, Journal of the Structural Division, Vol. 104, N° 4, pp. 219-231, USA
- 23) Cook W.D. (1987): 'Studies of Disturbed Region Near Discontinuities in Reinforced Concrete Members', Mc Gill University, Department of Civil Engineering and Applied Mechanics, Master Thesis, pp. 153, Montreal, Canada
- 24) Curbach M., Hampel T., Scheerer S. and Speck K. (2002): 'Hochleistungsbeton unter zwei-und dreiaxialer Beanspruchung', Beton-und Stahlbetonbau, Ernst & Sohn, Vol.97, N° 6, pp. 275-280, Berlin, Germany
- 25) De Wilder K., Lava P., Debruyne D., Wang Y., De Roeck G. and Vandewalle L. (2015): 'Stress Field Based Truss Model for Shear-Critical Prestressed Concrete Beams', The Institution of Structural Engineers, Vol. 3, pp. 28-42, London, UK
- 26) Dorn W.S., Gomory R.E. and Greenberg H.J. (1964): 'Automatic Design of Optimal Structures', Journal de Mécanique, Vol. 3, pp. 25-52

-
- 27) Drucker D.C. (1961): 'On Structural Concrete and the Theorems of Limit Analysis', IABSE International Association for Bridge and Structural Engineering, Report, N°21, Zürich, Switzerland
 - 28) Erntroy H.C. (1960): 'The Variation of Works Test Cubes', Cement and Concrete Association, Report, N°10, London, UK
 - 29) Eurocode 2 (2004): 'Design of concrete structures-Part 1-1: General rules and rules for buildings', European Committee for Standardization (CEN), Brussels
 - 30) Exner H. (1979): 'On the Effectiveness Factor in Plastic Analysis of Concrete', IABSE reports of the working commissions, Vol. 29, pp. 35-42, Zürich, Switzerland
 - 31) Fernández Ruiz M. and Muttoni A. (2008): 'Shear strength of thin-webbed post-tensioned beams', ACI Structural Journal, Vol. 105, N° 3, pp. 308-317, USA
 - 32) Fernández Ruiz M. and Muttoni A. (2007): 'On Development of Suitable Stress Fields for Structural Concrete', ACI Structural Journal, Vol.104, N° 4, pp. 495-502, USA
 - 33) Fernández Ruiz M., Muttoni A. and Gambarova P. (2007): 'Relationship between nonlinear creep and cracking of concrete under uniaxial compression', Journal of Advanced Concrete Technology, Vol. 5, N° 3, pp. 383-393, Japan
 - 34) fib (2011): 'Model Code 2010', Special Activity Group 5, 653 p., Lausanne, Switzerland
 - 35) Frey F. and Jirousek J. (2001): 'Méthode des éléments finis (TGC volume 6) Analyse des structures et milieux continues', Presses Polytechnique et Universitaires Romandes, 298 p., Lausanne, Suisse
 - 36) Ganz H.R., Ahmad A. and Hitz H. (1992): 'Load Transfer through Concrete Sections with Grouted Ducts', VSL, Technical report, N° 242, 32 p., Bern, Switzerland
 - 37) Gaynor R.D. (1965): 'Effect of Horizontal Reinforcing Steel on the Strength of Molded Cylinders', ACI Structural Journal, Vol. 62, N° 7, pp. 837-840, USA
 - 38) Goto Y. (1971): 'Cracks Formed in Concrete around Deformed Tension Bars', ACI Journal, N° 68-26, pp. 244-251, Japan
 - 39) Grob J. and Thürlimann B. (1976): 'Ultimate Strength and Design of Reinforced Concrete Beams Under Bending and Shear', IABSE, N° 36, pp. 105-120
 - 40) Gvozdev A.A. (1960): 'The Determination of the Value of the Collapse Load for Statically Indeterminate Systems undergoing Plastic Deformation', (English translation of the Russian original published in Proceedings of the Conference on Plastic Deformations, Akademiia Nauk SSSR, Vol. 1, pp. 19-38, Moskau-Leningrad, December 1936), International Journal of Mechanical Sciences, pp. 322-335, Amsterdam, Netherlands

References

- 41) Hars E. (2006): 'Zum Querkraftwiderstand von Stahl-und Spannbetonträgern mit dünnen Stegen', EPFL, IBETON, Thèse, N° 3551, 275 p., Lausanne, Switzerland
- 42) Heinzmann D. (2012): 'Stringer-Tafelmodelle Für Stahlbeton', ETHZ, Institut für Baustatik und Konstruktion, Dissertation, N° 20303, 197 p., Zürich, Switzerland
- 43) Herzinger R. and Elbadry M. (2007): 'Alternative Reinforcing Details in Dapped Ends of Precast Concrete Bridge Girders', Journal of the Transportation Research Board, N° 2028, pp. 111-121
- 44) Himsworth F.R. (1954): 'The variability of concrete and its effect on mix design', Proceedings of the Institution of Civil Engineers, Vol. 3, N° 2
- 45) Hong S.G., Kim D.-J., Kim S.-Y. and Hong N.K. (2002): 'Shear Strength of Reinforced Concrete Deep Beams with End Anchorage Failure', ACI, Vol. 99, N° 1, pp. 12-22, USA
- 46) Hoogenboom C.J. (1998): 'Discrete Elements and Nonlinearity in Design of Structural Concrete Walls', Technical University Delft, Civil Engineering and Geosciences, 171 p., Delft, Netherlands
- 47) Hsu C.-T.T. and Zhang L.-X. (1997): 'Nonlinear Analysis of Membrane Elements by Fixed-Angle Softened-Truss Model', ACI Structural Journal, Vol.94, N° 5, pp. 483-491, USA
- 48) Ingerslev A. (1922): 'The Strength of Rectangular Slabs', The Institution of Structural Engineers, pp. 3-19
- 49) Johansen K.W. (1931): 'Beregning af Krydsarmerede Jernbetonpladers Brudmoment', BSM 3-1 Bygningsstatistiske Meddelelser, pp. 1-18
- 50) Kani G.N.J. (1964): 'The riddle of shear failure and its solution', ACI Journal, Vol. 61, N° 4, pp. 441-467, USA
- 51) Kaufman M.K. and Ramirez J.A. (1988): 'Re-evaluation of the Ultimate Shear Behavior of High-Strength Concrete Prestressed I-Beams', ACI Structural Journal, Vol. 85, N° 3, pp. 295-303, USA
- 52) Kaufmann W. (1998): 'Strength and Deformations of Structural Concrete subjected to In-Plane Shear and Normal Forces', IBK report, N° 234, 147 p., Zürich, Switzerland
- 53) Kaufmann W. and Marti P. (1998): 'Structural concrete: cracked membrane model', Journal of Structural Engineering, Vol.124, N° 12, pp. 1467-1475, USA
- 54) Kaufmann W. and Marti P. (1996): 'Versuche an Stahlbetonträgern unter Normal- und Querkraft', ETHZ, Institut für Baustatik und Konstruktion, Dissertation, N° 226, 141 p., Zürich, Switzerland
- 55) Khan M.A. (1981): 'A Study of the Behavior of Reinforced Concrete Dapped End Beams ', University of Washington, Master Thesis, 145 p., Washington, USA

-
- 56) Kirschner U. (1986): 'Investigating the behaviour of reinforced concrete shell elements', University of Toronto, Department of Civil Engineering, PhD Thesis, 83 p., Toronto, Canada
- 57) Kollegger J. and Mehlhorn G. (1990): 'Experimentelle Untersuchungen zur Bestimmung der Druckfestigkeit des gerissenen Stahlbetons bei einer Querkzugbeanspruchung', Deutscher Ausschuss für Stahlbeton, Wilhelm Ernst & Sohn, Vol.413, 132 p., Berlin, Germany
- 58) König G. and Hosser D. (1981): 'The simplified level II method and its application on the derivation of safety elements for level I', Comité Euro-International du Béton (CEB), Bulletin N° 147, pp. 147-224, Lausanne, Switzerland
- 59) Kostic N. (2009): 'Topologie des champs de contraintes pour le dimensionnement des structures en béton armé', EPFL, IBETON, Thèse, N° 4414, 235 p., Lausanne, Switzerland
- 60) Kuchma D., Kim K.S., Nagle T.J., Sun S. and Hawkins N.M. (2008): 'Shear Tests on High-Strength Prestressed Bulb-Tee Girders: Strengths and Key Observations', ACI Structural Journal, Vol. 105, N° 3, pp. 358-367, USA
- 61) Kuchma D. and Tjhin T.N. (2001): 'CAST (Computer Aided Strut-and-Tie) Design Tool', ASCE Journal of Structural Engineering, Vol.109, 7 p., USA
- 62) Kumar P. (1977): 'Optimal Force Transmission in Reinforced Concrete Deep Beams', Computers & Structures, Vol. 8, pp. 223-229, UK
- 63) Kupfer H. (1973): 'Das Verhalten des Betons unter mehrachsiger Kurzzeitbelastung unter besonderer Berücksichtigung der zweiachsigen Beanspruchung', Deutscher Ausschuss für Stahlbeton, Vol.229, 131 p., Berlin, Germany
- 64) Kupfer H. (1964): 'Erweiterung der Mörsch'schen Fachwerkanalogie mit Hilfe des Prinzips vom Minimum der Formänderungsarbeit', Comité Euro-International du Béton (CEB), Bulletin d'Information, N° 40, pp. 44-57, Paris, France
- 65) Leonhardt F. (1969): 'Abminderung der Tragfähigkeit des Betons infolge stabförmiger, rechtwinklig zur Druckrichtung angeordnete Einlagen Festschrift Rüsch', pp. 71-78, Berlin, Germany
- 66) Leonhardt F., Koch R. and Rostasy F.S. (1973): 'Schubversuche an Spannbetonträgern', Deutscher Ausschuss für Stahlbeton, Vol. 227, 179 p., Berlin, Germany
- 67) Leonhardt F. and Walther R. (1962): 'Schubversuche an einfeldrigen Stahlbetonbalken mit und ohne Schubbewehrung zur Ermittlung der Schubtragfähigkeit und der oberen Schubspannungsgrenze', Deutscher Ausschuss für Stahlbeton, Wilhelm Ernst & Sohn, Vol. 151, 83 p., Berlin, Germany

References

- 68) Leonhardt F. and Walther R. (1963): 'Schubversuche an Plattenbalken mit unterschiedlicher Schubbewehrung', Deutscher Ausschuss für Stahlbeton, Wilhelm Ernst & Sohn, Vol. 156, 84 p., Berlin, Germany
- 69) Leonhardt F. and Walther R. (1966): 'Wandartige Träger', Deutscher Ausschuss für Stahlbeton, Wilhelm Ernst & Sohn, Vol. 178, 159 p., Berlin, Germany
- 70) Leonhardt F., Waltner R. and Dilger W. (1968): 'Schubversuche an indirekt gelagerten, einseitigen und durchlaufenden Stahlbetonbalken', Deutscher Ausschuss für Stahlbeton, Wilhelm Ernst & Sohn, Vol. 201, 69 p., Berlin, Germany
- 71) Lourenco M. and Almeida J. (2010): 'Adaptive stress field models for structural concrete', 3rd fib International Congress, N° 262, 19 p., Washington D.C., USA
- 72) Mansur M.A., Lee Y.F., Tan K.-H. and Lee S.L. (1991): 'Tests on RC Continuous Beams with Openings', Journal of Structural Engineering, Vol. 117, N° 6, pp. 1593-1606
- 73) Marti P. (1980): 'Zur plastischen Bemessung von Stahlbetonbauten', ETHZ, Institut für Baustatik und Konstruktion, Dissertation, N° 6602, 176 p., Zürich, Switzerland
- 74) Marti P., Alvarez M., Kaufmann W. and Sigrist V. (1998): 'Tension chord model for structural concrete', Structural Engineering International, IABSE, Vol. 8, N° 4, pp. 287-298, USA
- 75) Marti P. and Meyboom J. (1992): 'Response of Prestressed Concrete Elements to In-Plane Shear Forces', ACI Structural Journal, Vol.89, N° 5, pp. 503-514, USA
- 76) Mata Falcón J (2015): 'Serviceability and Ultimate Behaviour of Dapped-end Beams (In Spanish: Estudio del comportamiento en servicio y rotura de los apoyos a media madera)', Universitat Politècnica de València, Valencia, PhD Thesis, 747 p., Valencia, Spain
- 77) Maxwell B.S. and Breen J.E. (2000): 'Experimental Evaluation of Strut-and-Tie Model Applied to Deep Beam with Opening', ACI Structural Journal, Vol.97, N° 1, pp. 142-149, USA
- 78) Moccia F. (2015): 'Investigation of Shear Strength of Post-Tensioned Girders', EPFL, IBETON, Master Thesis, 225 p., Lausanne, Switzerland
- 79) Moore A.M. (2014): 'Shear Behavior of Spliced Post-Tensioned Girders', Faculty of the Graduate School, The University of Texas at Austin, PhD Thesis, 250 p., Austin, USA
- 80) Mörsch E. (1908): 'Der Eisenbetonbau - Seine Theorie und Anwendung', 3. Auflage, 376 p., Stuttgart, Germany
- 81) Muller J. (1978): 'Enseignement tiré de l'exécution des ouvrages pour une meilleure conception', Journées de l'A.P.C., pp. 99-109, France

-
- 82) Muttoni A. (1990): 'Die Anwendbarkeit der Plastizitätstheorie in der Bemessung von Stahlbeton', Birkhäuser Verlag, Institut für Baustatik und Konstruktion ETH Zürich, N° 176, 164 p., Basel, Switzerland
- 83) Muttoni A., Burdet O. and Hars E. (2006): 'Effect of Duct Type on the Shear Strength of Thin Webs', ACI Structural Journal, Vol.103, N° 5, pp. 729-735, USA
- 84) Muttoni A. and Fernández Ruiz M. (2007): 'Shear strength predictions according to the critical shear crack theory and the Swiss code SIA 262 (2003)', Workshop on assessment methods for determining the shear strength of existing structures, 14 p., Rotterdam, Netherlands
- 85) Muttoni A. and Fernández Ruiz M. (2012): 'The levels-of-approximation approach in MC 2010: application to punching shear provisions', Structural Concrete, Vol. 13, N° 1, pp. 32-41
- 86) Muttoni A. and Fernández Ruiz M. (2012): 'Levels-of-approximation approach in codes of practice', Structural Engineering International, Vol. 2, pp. 190-194, Zurich, Switzerland
- 87) Muttoni A. and Fernández Ruiz M. (2008): 'Shear strength of members without transverse reinforcement as function of critical shear crack width', ACI Structural Journal, Vol. 105, N° 2, pp. 163-172, USA
- 88) Muttoni A., Fernández Ruiz M. Niketic F. (2015): 'Design versus Assessment of Concrete Structures Using Stress Fields and Strut-and-Tie Models', ACI Structural Journal, Vol.112, N° 5, pp. 605-616, USA
- 89) Muttoni A., Schwartz J. and Thürlimann B. (1996): 'Design of Concrete Structures with Stress Fields', Birkhäuser Verlag, 143 p., Basel, Switzerland
- 90) Nagrodzka-Godycka K. and Piotrkowski P (2012): 'Experimental and Analytical Investigation of Classic Concrete Beam Tests', ACI Structural Journal, Vol.109, N° 1, pp. 11-20
- 91) Nielsen M.P. (1969): 'Om forskydningsarmering i jernbetonbjælker (Shear reinforcement in beams)', Proceedings of the Sessions Related to Structural Design, Analysis and Testing, ASCE Structural Congress, Vol. 38, N° 2, pp. 33-58
- 92) Nielsen M.P. and Hoang L.C. (2011): 'Limit Analysis and Concrete Plasticity', CRC Press, 3rd edition, 788 p., Boca Raton, USA
- 93) Okamura H. and Maekawa K. (1991): 'Nonlinear analysis and constitutive methods of reinforced concrete', University of Tokyo, 850 p., Tokyo
- 94) Pang X.-B.D. and Hsu C.-T.T. (1995): 'Behavior of Reinforced Concrete Membrane Elements in Shear', ACI Structural Journal, Vol.92, N° 6, pp. 665-667, USA

References

- 95) Pimentel M., Brühwiler E. and Figueiras J. (2014): 'Safety examination of existing concrete structures using the global resistance safety factor concept', *Engineering Structures*, Vol. 70, pp. 130-143
- 96) Placas A. (1969): 'Shear Strength of Reinforced Concrete Beams', Imperial College of Science and Technology, PhD Thesis, 581 p., London, England
- 97) Popovics S. (1998): 'Strength and Related Properties of Concrete: A Quantitative Approach', John Wiley & Sons Inc., New York, USA
- 98) Randl N. (2013): 'Design recommendations for interface shear transfer in fib Model Code 2010', *Structural Concrete*, N° 3, pp. 230-241, Berlin, Germany
- 99) Rasmussen B.H. (1962): 'Strength of transversely loaded bolts and dowels cast into concrete', *Laboratoriet for Bugningastatik*, Denmark Technical University, Meddelelse, Vol. 34, N°2
- 100) Rezai-Jorabi H. and Regan P.E. (1986): 'Shear resistance of prestressed concrete beams with inclined tendons', *The Structural Engineer*, Vol. 64B, N° 3, pp. 63-75, London, UK
- 101) Ritter W. (1899): 'Die Bauweise Hennebique', *Schweizerische Bauzeitung*, pp. 41-149, Zürich, Switzerland
- 102) Rupf M. (2014): 'Querkraftwiderstand von Stahlbeton- und Spannbetonträgern mittels Spannungsfeldern', EPFL, IBETON, Thèse, N° 6004, 132 p., Lausanne, Switzerland
- 103) Rupf M. and Muttoni A. (2012): 'Schubversuche an vorgespannten Stahlbetonträgern mit ungenügender Schubbewehrung', EPFL, IBETON, Test Report, 159 p., Lausanne, Switzerland
- 104) Sagaseta J. and Vollum R.L. (2011): 'Influence of beam cross-section, loading arrangement and aggregate type on shear strength', *Magazine of Concrete Research*, Vol.53, N° 2, pp. 139-155, London, UK
- 105) Saqan E.I. and Frosch R.J. (2009): 'Influence of flexural reinforcement on shear strength of prestressed concrete beams', *ACI Structural Journal*, Vol. 106, N° 1, pp. 60-68, USA
- 106) Schäfer K., Schelling G. and Kuchler T. (1990): 'Druck und querzug in bewehrten betonelementen', *Deutscher Ausschuss für Stahlbeton*, N° 408, pp. 5-85, Berlin, Germany
- 107) Schlaich J., Schäfer K. and Jennewein M. (1987): 'Toward a Consistent Design of Structural Concrete ', *ACI Journal*, Vol.32, N° 3, pp. 75-150, USA
- 108) SIA 262:2013 (2013): 'Structures en béton', *Société suisse des ingénieurs et des architectes*, 102 p., Zurich, Switzerland

-
- 109) SIA 269:2011 (2011): 'Existing Structures - Basis for examination and interventions', Société suisse des ingénieurs et des architectes, 30 p., Zurich, Switzerland
- 110) Sørensen H.C. (1974): 'Shear Tests on 12 Reinforced Concrete T-Beams', Technical University of Denmark, N° R60, 52 p., Lyngby, Denmark
- 111) Sørensen J.H., Hoang L.H., Olesen J.F. and Fischer G. (2016): 'Catenary action in rebars crossing a casting joint loaded in shear', 11th fib International PhD Symposium in Civil Engineering, pp. 735-742, Tokyo
- 112) Tanner P., Lara C. and Hingorani R. (2007): 'Structural Safety - a struggle with uncertainties', Hormigón y Acero, N° 245, pp. 59-78, Madrid, Spain
- 113) Tanner P., Lara C. and Prieto M. (2011): 'Semi-probabilistic models for the assessment of existing concrete structures', Applications of Statistics and Probability in Civil Engineering, Köhler and Nishijima, Taylor & Francis Group, pp. 1039-1047, London, UK
- 114) Tanner P., Lara C. and Prieto M. (2014): 'Analysis of the present condition and deterioration in the main dome over La Laguna cathedral', Proceedings of the IABSE Conference Engineering for Progress, Nature and People, 10 p., Madrid, Spain
- 115) Tepfers R. (1979): 'Cracking of concrete cover along anchored deformed reinforcing bars', Magazine of Concrete Research, Vol.31, N° 106, pp. 3-12, UK
- 116) Thürlimann B., Marti P., Pralong J., Ritz P. and Zimmerli B. (1983): 'Anwendung der Plastizitätstheorie auf Stahlbeton', Institut für Baustatik und Konstruktion ETH Zürich, 252 p., Zurich, Switzerland
- 117) Vecchio F.J. (2000): 'Disturbed Stress Field Model for Reinforced Concrete: Formulation', ASCE Journal of Structural Engineering, Vol.126, Issue 8, pp. 1070-1077, USA
- 118) Vecchio F.J. and Chan C.C.L. (1990): 'Reinforced concrete membrane elements with perforations', ASCE Journal of Structural Engineering, Vol. 116, Issue 9, pp. 2344-2360
- 119) Vecchio F.J. and Collins M.P. (1982): 'Response of reinforced concrete to in-plane shear and normal stresses', Department of civil engineering, University of Toronto, N° 82-03, 332 p.
- 120) Vecchio F.J. and Collins M.P. (1986): 'The modified compression-field theory for reinforced concrete elements subjected to shear', ACI Structural Journal, Vol.83, N° 2, pp. 219-231, USA
- 121) Vecchio F.J., Collins M.P. and Aspiotis J. (1994): 'High-Strength Concrete Elements Subjected to Shear', ACI Structural Journal, Vol.91, N° 4, pp. 423-433, USA

References

- 122) Vecchio F.J. and Shim W. (2004): 'Experimental and Analytical Investigation of Classic Concrete Beam Tests', ASCE Journal of Structural Engineering, Vol.130, N° 3, pp. 460-469, USA
- 123) Vintzeleou E. and Tassios T.P. (1990): 'Eccentric dowels loaded against core of concrete sections ', ASCE Journal of Structural Engineering, Vol. 116, N° 10, pp. 2621-2633
- 124) Watanabe F. and Muguruma H. (1989): 'Ultimate Strength and Deformations of RC Panel', Proceedings of the Sessions Related to Structural Design, Analysis and Testing, ASCE Structural Congress, pp. 31-38
- 125) Xie Y.M. and Steven G.P. (1994): 'Optimal Design of Multiple Load Case Structures Using an Evolutionary Procedure', Engineering Computation, Vol. 11, pp. 295-302, UK
- 126) Yoon Y.-S., Cook W.D. and Mitchell D. (1996): 'Minimum Shear Reinforcement in Normal, Medium and High-Strength Concrete Beams', ACI Structural Journal, Vol.93, N° 5, pp. 576-584, USA
- 127) Zhang L.-X. and Hsu T.T.C. (1998): 'Behavior and Analysis of 100 MPa Concrete Membrane Elements', Journal of Structural Engineering, Vol. 124 N° 1, pp. 24-34, USA
- 128) Zhu R.R.H., Wanichakorn W, Hsu C.-T.T. and Vogel J (2003): 'Crack Width Prediction Using Compatibility-Aided Strut-and-Tie Model', ACI Structural Journal, Vol.100, N° 4, pp. 413-421, USA
- 129) Zwicky D. (2000): 'Bruchversuche an ausgebauten Brückenträgern', Institut für Baustatik und Konstruktion, N° 258, 167 p., Zürich, Switzerland

Appendix

1) Appendix 1 – Summary of the online database

The following appendix gives the mechanical properties of 315 reinforced and prestressed structural elements, which were used to investigate the accuracy of the EPSF method in Chapter 2 of this thesis. Both measured and estimated strength of each member are indicated along with the references to the tests. Basic statistical analysis of the EPSF results has been conducted and presented (the average prediction of the ultimate load and the coefficient of variation for each series).

All the values correspond to the ones available at: <http://i-concrete.epfl.ch/epsf/epsf.html>.

1.1) Reinforced concrete members

N°	Name	f_c [MPa]	ρ [%]	ρ_w [%]	$\sigma_{p,inf}$ [MPa]	Failure mode	Failure Subtype	Q_{test} [kN]	Q_{EPSF} [kN]	$\frac{Q_{test}}{Q_{EPSF}}$
Vecchio F.J. and Shim W. (2004): 'Experimental and Analytical Investigation of Classic Concrete Beam Tests', ASCE Journal of Structural Engineering, Vol.130, N° 3, pp. 460-469, USA										
1	A1	22.6	1.94	0.10	0	V	CR	459	450	1.02
2	A2	25.9	2.44	0.10	0	V	CR	439	452	0.97
3	A3	43.5	2.94	0.10	0	F	CR	420	426	0.99
4	B1	22.6	2.58	0.15	0	V	CR	434	416	1.04
5	B2	25.9	2.58	0.15	0	V	CR	365	331	1.10
6	B3	43.5	3.25	0.15	0	F	CR	342	344	0.99
7	C1	22.6	2.45	0.20	0	V	CR	282	247	1.14
8	C2	25.9	3.89	0.20	0	V	CR	290	290	1.00
9	C3	43.5	3.89	0.20	0	F	CR	265	260	1.02
Average:										1.03
CoV:										0.05
Yoon Y.-S., Cook W.D. and Mitchell D. (1996): 'Minimum Shear Reinforcement in Normal, Medium and High-Strength Concrete Beams', ACI Structural Journal, Vol.93, N° 5, pp. 576-584, USA										
1	N1 N	36	2.8	0.08	0	V	DT	914	840	1.09
2	N2 S	36	2.8	0.08	0	V	DT	726	800	0.91
3	N2 N	36	2.8	0.12	0	V	CR	966	1030	0.94
4	M1 N	67	2.8	0.08	0	V	DT	810	962	0.84
5	M2 S	67	2.8	0.12	0	V	CR	1104	1120	0.99
6	M2 N	67	2.8	0.16	0	V	CR	1378	1370	1.01
7	H1 N	87	2.8	0.08	0	V	DT	966	1012	0.95
8	H2 S	87	2.8	0.14	0	V	DT	1196	1302	0.92
9	H2 N	87	2.8	0.24	0	V	CR	1442	1656	0.87
Average:										0.95
CoV:										0.07
Sagasetta J. and Vollum R.L. (2011): 'Influence of beam cross-section, loading arrangement and aggregate type on shear strength', Magazine of Concrete Research, Vol.53, N° 2, pp. 139-155, London, UK										

Appendix

1	BG1	31.7	3.32	0.50	0	V	CR	950	990	0.96
2	BG2	31.7	3.32	0.83	0	V	CR	1074	1250	0.86
3	BL1	53.1	3.32	0.50	0	V	SY	1169	1126	1.04
4	BL2	53.1	3.32	0.83	0	V	SP	1594	1476	1.08
5	CB1	49.4	2.80	0.36	0	V	SY	1029	1020	1.01
6	CB2	49.4	2.80	0.53	0	V	SY	1429	1257	1.14
7	DB1	49.4	2.80	0.36	0	V	SY	597	540	1.11
Average:										1.03
CoV:										0.09
Mansur M.A., Lee Y.F., Tan K.-H. and Lee S.L. (1991): 'Tests on RC Continuous Beams with Openings', Journal of Structural Engineering, Vol. 117, N° 6, pp. 1593-1606										
1	B1	38.4	1.54	0.28	0	F	SP	135	127	1.06
2	B2	40.5	1.54	0.28	0	F	SP	155	145	1.07
3	B3	43.8	1.54	0.28	0	F	SP	140	144	0.97
4	C1	43.8	1.54	1.01	0	F	SP	260	261	1.00
5	C2	38.4	1.54	1.01	0	F	SP	230	244	0.94
6	C3	40.5	1.54	1.01	0	F	SP	230	232	0.99
7	C4	28.8	1.54	1.01	0	F	SP	240	253	0.95
8	C5	28.8	1.54	1.01	0	F	SP	180	200	0.90
Average:										0.99
CoV:										0.06
Hong S.G., Kim D.-J., Kim S.-Y. and Hong N.K. (2002): 'Shear Strength of Reinforced Concrete Deep Beams with End Anchorage Failure', ACI, Vol. 99, N° 1, pp. 12-22, USA										
1	SS 1	23.5	1.66	0.42	0	V	DT	662.28	610	1.09
2	SS 2	23.5	1.66	0.42	0	V	DT	610.34	538	1.13
3	SS 3	23.5	1.66	0.42	0	L	A	560.66	507	1.11
4	SS 4	23.5	1.66	0.42	0	L	A	479.22	494	0.97
5	LBS 2	23.5	1.66	0.42	0	L	A	579.96	576	1.01
6	VSR 1	23.5	1.66	0.52	0	L	A	593.29	566	1.05
7	VSR 2	23.5	1.66	0.70	0	V	DT	658.07	608	1.08
Average:										1.06
CoV:										0.05
Sørensen H.C. (1974): 'Shear Tests on 12 Reinforced Concrete T-Beams', Technical University of Denmark, N° R60, 52 p., Lyngby, Denmark										
1	T23	34.2	1.06	0.34	0	V	DT	139	139	1
2	T1a	22.9	1.06	0.59	0	F	CR	133	115	1.16
3	T2a	24.6	1.06	0.41	0	F	CR	137	122	1.12
4	T3a	24.6	1.06	0.49	0	V	AS	126	105	1.20
5	T4a	25.2	1.06	0.34	0	V	AS	131	114	1.15
6	T1b	23.1	1.06	0.44	0	V	CR	118	102	1.16
7	T2b	24.9	1.06	0.30	0	V	DT	129	108	1.19
8	T3b	24.6	1.06	0.29	0	V	DT	116	89	1.30
9	T4b	24.7	1.06	0.20	0	V	DT	106	94	1.13
10	T5	25.5	1.06	0.20	0	V	DT	110	95	1.16
Average:										1.16
CoV:										0.06
Leonhardt F. and Walther R. (1963): 'Schubversuche an Plattenbalken mit unterschiedlicher Schubbewehrung', Deutscher Ausschuss für Stahlbeton, Wilhelm Ernst & Sohn, Vol. 156, 84 p., Berlin, Germany										
1	TA1	15.2	0.84	1.29	0	V	CR	670	582	1.15
2	TA2	15.2	0.84	0.86	0	V	SY	638	530	1.20
3	TA3	15.1	0.84	0.59	0	V	SY	544	476	1.14
4	TA4	15.1	0.84	0.34	0	V	SY	458	382	1.20
5	TA13	17.9	0.84	1.29	0	F	CR	700	635	1.10
6	TA14	17.9	0.84	0.86	0	V	SY	666	597	1.12
7	TA15	17.1	0.84	0.59	0	V	SY	584	514	1.14
8	TA9	24.8	0.84	1.29	0	F	Y	700	700	1.00

9	TA10	24.8	0.84	0.86	0	F	Y	714	690	1.03
10	TA11	24.4	0.84	0.59	0	V	SY	670	586	1.14
11	TA12	24.4	0.84	0.34	0	V	SY	530	468	1.13
12	TA5	15.1	0.84	1.30	0	L	SP	453	450	1.01
13	TA17	20.3	0.84	1.30	0	V	CR	677	614	1.10
14	TA18	26.8	0.84	1.30	0	F	Y	709	628	1.13
15	TA6	15.1	0.84	0.59	0	V	SY	465	480	0.97
16	TA16	17.1	0.84	0.59	0	V	SY	587	506	1.16
Average:										1.11
CoV:										0.06
Kaufmann W. and Marti P. (1996): 'Versuche an Stahlbetonträgern unter Normal- und Querkraft', ETHZ, Institut für Baustatik und Konstruktion, Dissertation, N° 226, 141 p., Zürich, Switzerland										
1	VN1	53.9	4.23	0.34	0	V	SY	542	546	0.99
2	VN2	52.6	4.23	0.34	0	V	SY	548	522	1.05
3	VN3	60.2	4.23	0.34	0	V	SY	540	510	1.06
4	VN4	61.9	4.23	0.34	0	V	SY	564	555	1.02
Average:										1.03
CoV:										0.03
Nagrodzka-Godycka K. and Piotrkowski P (2012): 'Experimental and Analytical Investigation of Classic Concrete Beam Tests', ACI Structural Journal, Vol.109, N° 1, pp. 11-20										
1	WB 1 L	36.4	0.63	0.76	0	L	SY	130	126	1.03
2	WB 1 P	36.4	0.63	0.76	0	L	SY	140	126	1.11
3	WB 2 L	36.4	0.63	0.76	0	L	SP	180	188	0.96
4	WB 2 P	36.4	0.63	0.76	0	L	SP	180	180	1.00
5	WB 3 L	36.4	1.26	1.52	0	L	SY	206	206	1.00
6	WB 3 P	36.4	1.26	1.52	0	L	SY	206	206	1.00
7	WB 4 L	36.4	1.26	1.52	0	L	SP	270	272	0.99
8	WB 4 P	36.4	1.26	1.52	0	L	SP	280	272	1.03
9	WB 5 L	36.4	0.56	0.73	0	L	SY	172	180	0.96
10	WB 5 P	36.4	0.84	0.98	0	L	SP	200	248	0.81
11	WB 6 L	36.4	0.56	0.73	0	L	SP	238	256	0.93
12	WB 6 P	36.4	0.84	0.98	0	L	SP	320	354	0.90
Average:										0.98
CoV:										0.07
Mata Falcón J (2015): 'Serviceability and Ultimate Behaviour of Dapped-end Beams (In Spanish: Estudio del comportamiento en servicio y rotura de los apoyos a media madera)', Universitat Politècnica de València, Valencia, PhD Thesis, 747 p., Valencia, Spain										
1	DEB1.1 T1	41.1	1.1	0.27	0	L	SY+SP	484	471	1.03
2	DEB1.2 T1	39.3	0.99	0.27	0	L	SY+SP	365	339	1.08
3	DEB1.2 T2	39.3	0.99	0.27	0	L	SY+SP	332	339	0.98
4	DEB1.3 T1	39.9	1.10	0.23	0	L	SY	303	338	0.90
5	DEB1.3 T2	39.9	1.10	0.23	0	L	SY	332	338	0.98
6	DEB1.4 T1	40.4	1.10	0.27	0	L	SY+SP	457	442	1.04
7	DEB1.4 T2	40.4	1.10	0.27	0	L	SY	426	442	0.97
8	DEB1.5 T1	40.8	0.99	0.27	0	L	SY	313	303	1.03
9	DEB1.6 T1	31.1	2.38	0.55	0	L	SY+SP	773	634	1.22
10	DEB1.6 T2	31.1	2.38	0.55	0	L	SY+SP	627	634	0.99
11	DEB1.7 T1	30.0	2.15	0.55	0	L	SY	486	506	0.96
12	DEB1.7 T2	30.0	2.15	0.55	0	L	SY	472	506	0.93
13	DEB1.8 T1	32.2	1.69	0.41	0	L	SY	488	575	0.85
14	DEB1.8 T2	32.2	1.69	0.41	0	L	SY	498	575	0.87
15	DEB1.9 T1	31.9	1.54	0.41	0	L	SY	354	421	0.84
16	DEB1.9 T2	31.9	1.54	0.41	0	L	SY	364	421	0.86
17	DEB2.1 T1	40.2	1.07	0.27	0	L	SY+SP	487	471	1.03
18	DEB2.1 T2	40.2	1.07	0.27	0	L	SY	499	471	1.06
19	DEB2.2 T1	33.3	2.29	0.54	0	L	SY+SP	805	792	1.02

Appendix

20	DEB2.2 T2	33.3	2.29	0.54	0	L	SY	824	792	1.04
21	DEB2.3 T1	33.3	1.64	0.42	0	L	SY+SP	601	619	0.97
22	DEB2.4 T1	36.9	2.25	0.54	0	L	SY+SP	780	814	0.96
23	DEB2.4 T2	36.9	2.25	0.54	0	L	SY+SP	774	814	0.95
24	DEB2.5 T1	37.1	2.18	0.53	0	L	SY+SP	663	706	0.94
25	DEB2.5 T2	37.1	2.18	0.53	0	L	SY+SP	737	706	1.04
26	DEB2.6 T1	38.3	2.62	0.53	0	L	SY+SP	820	788	1.04
27	DEB3.1 T1	33.7	2.25	0.54	0	L	SY+SP	795	814	0.98
28	DEB3.1 T2	33.7	2.25	0.54	0	L	SY+SP	851	814	1.04
29	DEB3.2 T1	37.2	2.18	0.53	0	L	SY+SP	780	743	1.05
30	DEB3.2 T2	37.2	2.18	0.53	0	L	SY+SP	796	743	1.07
31	DEB3.3 T1	38.8	2.62	0.53	1.24	L	SY+SP	876	847	1.03
32	DEB3.3 T2	38.8	2.62	0.53	1.06	L	SY+SP	841	842	1.00
33	DEB3.4 T1	34.5	2.38	0.55	0	L	SY+SP	654	669	0.98
34	DEB3.4 T2	34.5	2.38	0.55	0	L	SY+SP	665	669	0.99
35	DEB3.5 T1	33.0	2.29	0.54	0	L	SY	849	838	1.01
36	DEB3.5 T2	33.0	2.29	0.54	0	L	SY	856	838	1.02
37	DEB3.6 T1	36.7	1.69	0.41	0	L	SY	567	591	0.96
38	DEB3.6 T2	36.7	1.69	0.41	0	L	SY+SP	553	591	0.94
39	DEB3.7 T1	45.5	2.38	0.55	0	L	SY	832	796	1.04
40	DEB3.7 T2	45.5	2.38	0.55	0	L	SY	821	796	1.03
41	DEB3.8 T1	48.8	2.38	0.55	0	L	SY	908	882	1.03
42	DEB3.8 T2	48.8	2.38	0.55	0	L	SY	904	882	1.02
43	DEB3.9 T1	48.4	2.38	0.55	0	L	SY	886	929	0.95
44	DEB3.9 T2	48.4	2.38	0.55	0	L	SY	925	929	1.00
45	DEB3.10 T1	41.8	0	0.53	1.75	L	SY+SP	887	888	1.00
46	DEB3.1 T2	41.8	0	0.53	1.39	L	SY+SP	925	886	1.04
47	DEB3.11 T1	45.5	0	0.53	2.23	L	SY+SP	1028	1001	1.03
48	DEB3.11 T2	45.5	0	0.53	2.29	L	SY+SP	988	1001	0.99
49	DEB3.12 T1	48.4	0	0.53	3.41	L	SY+SP	1010	1089	0.93
50	DEB3.12 T2	48.4	0	0.53	3.04	L	SY+SP	1033	1085	0.95
Average:										0.97
CoV:										0.07
Chan T.C-K (1979): 'A Study of the Behavior of Reinforced Concrete Dapped End Beams', University of Washington , Master Thesis, 167 p., Washington, USA										
1	1A	33.6	1.71	0.47	0	L	-	144	136	1.06
2	1B	30.5	2.33	0.47	0	L	-	191	184	1.04
3	2A	33.0	1.88	0.44	0	L	-	178	182	0.98
4	2B	30.9	2.33	0.44	0	L	-	169	184	0.92
5	3A	37.0	1.88	0.47	0	L	-	216	194	1.11
6	3B	30.3	2.33	0.47	0	L	-	176	181	0.98
7	4A	30.3	1.88	0.43	0	L	-	189	187	1.01
8	4B	29.4	2.33	0.43	0	L	-	177	169	1.05
Average:										1.02
CoV:										0.05
Khan M.A. (1981): 'A Study of the Behavior of Reinforced Concrete Dapped End Beams ', University of Washington , Master Thesis, 145 p., Washington, USA										
1	1A	28.8	2.39	0.53	0	L	-	215	198	1.09
2	1B	29.8	2.71	0.50	0	L	-	188	190	0.99
3	2A	29.7	2.71	0.54	0	L	-	208	184	1.13
4	2B	31.0	2.97	0.53	0	L	-	189	168	1.13
5	3A	33.7	2.41	0.61	0	L	-	197	210	0.94
6	3B	37.1	2.67	0.59	0	L	-	189	205	0.92
7	4A	29.0	2.16	0.59	0	L	-	176	165	1.06
8	5B1	33.7	2.43	0.60	0	L	-	164	152	1.07
9	5B2	34.5	2.43	0.60	0	L	-	143	148	0.96

Average:										1.03
CoV:										0.07
Cook W.D. (1987): 'Studies of Disturbed Region Near Discontinuities in Reinforced Concrete Members', McGill University, Department of Civil Engineering and Applied Mechanics, Master Thesis, pp. 153, Montreal, Canada										
1	D-1	29.8	2.61	0.4	0	L	-	307	324	0.95
2	D-3	36.3	2.51	0.47	0	L	-	372	382	0.97
3	D-4	36.3	2.60	0.46	0	L	-	340	324	1.05
Average:										0.99
CoV:										0.04
Zhu R.R.H., Wanichakorn W, Hsu C.-T.T. and Vogel J (2003): 'Crack Width Prediction Using Compatibility-Aided Strut-and-Tie Model', ACI Structural Journal, Vol.100, N° 4, pp. 413-421, USA										
1	T2	41.75	0.52	0.25	0	L	-	563	544	1.03
2	T3	33.55	0.64	0.36	0	L	-	538	513	1.05
3	T4	41.46	0.52	0.25	0	L	-	572	618	0.92
4	T5	38.96	0.52	0.36	0	L	-	921	789	1.17
5	T6	43.33	0.52	0.36	0	L	-	467	445	1.05
6	T7	47.08	0.61	0.44	0	L	-	1196	1062	1.13
Average:										1.06
CoV:										0.07
Herzinger R. and Elbadry M. (2007): 'Alternative Reinforcing Details in Dapped Ends of Precast Concrete Bridge Girders', Journal of the Transportation Research Board, N° 2028, pp. 111-121										
1	DEA1.0 T1	38.1	2.31	0.42	0	L	-	216	204	1.06
2	DEA1.0 T2	48.4	2.31	0.42	0	L	-	255	222	1.15
3	DEA0.5 T1	38	2.31	0.45	0	L	-	231	231	1.00
4	DEB1.0 T1	38.6	2.28	0.42	0	L	-	203	219	0.93
5	DEB1.0 T2	40.4	2.28	0.42	0	L	-	226	219	1.03
6	DEB0.5 T1	36.9	2.28	0.45	0	L	-	205	228	0.9
7	DEB0.5 T2	36.9	2.28	0.45	0	L	-	222	228	0.97
8	DEC1.0 T1	39.1	2.3	0.38	0	L	-	181	203	0.89
9	DEC1.0 T2	41.6	2.3	0.38	0	L	-	212	203	1.05
10	DEC*1.0T1	42.2	2.3	0.49	0	L	-	260	275	0.94
11	DEC*u1.0T1	41.9	2.3	0.54	0	L	-	270	269	1.01
12	DED1.0T1	38.8	2.23	0.40	0	L	-	220	222	0.99
13	DEDu1.0T1	36.8	2.23	0.40	0	L	-	213	224	0.95
14	DEDu1.0T2	37.4	2.23	0.40	0	L	-	222	224	0.99
15	DED*1.0T1	39.9	2.21	0.41	0	L	-	214	222	0.96
16	DED*1.0T2	40.5	2.21	0.41	0	L	-	203	222	0.91
17	DEDu*1.0T1	39.2	2.21	0.41	0	L	-	212	220	0.96
18	DEDu*1.0T2	40.3	2.21	0.41	0	L	-	227	220	1.03
Average:										0.99
CoV:										0.06
Campana S. (2013): 'Éléments en béton armé soumis à une combinaison de flexion, effort tranchant et forces de déviation', EPFL, IBETON, Thèse, N° 5574, 162 p., Lausanne, Switzerland										
1	SC26	41.9	0.71	0	0	L	DT	108	117.5	0.92
2	SC27	41.6	0.71	0	0	L	DT	124	127.5	0.97
3	SC31	41.7	0.71	0	0	L	DT	119	127.5	0.93
4	SC34	41.4	0.72	0	0	L	DT	114	107.5	1.06
5	SC35	42.1	0.72	0	0	L	CR	134	127.5	1.05
6	SC38	31.3	0.70	0.17	0	L	DT	110	112.5	0.98
7	SC39	31.1	0.71	0.19	0	L	DT	109	122.5	0.89
8	SC40	30.9	0.7	0.19	0	L	DT	106	125.0	0.85
9	SC41	30.9	0.7	0.22	0	L	CR	132	127.5	1.03
10	SC42	31.0	0.71	0.22	0	L	CR	127	127.5	1.00
11	SC43	31.1	0.7	0.26	0	L	CR	129	127.5	1.01
12	SC44	30.9	0.7	0.19	0	L	DT	118	122.5	0.97

Appendix

13	SC45	30.8	0.7	0.22	0	L	CR	123	125.0	0.99
									Average:	0.97
									CoV:	0.06
Placas A. (1969): 'Shear Strength of Reinforced Concrete Beams', Imperial College of Science and Technology, PhD Thesis, 581 p., London, England										
1	R10	30	0.97	0.21	0	V	CR	76	73	1.03
2	R11	26	1.95	0.21	0	V	CR	90	83	1.08
3	R12	34	4.17	0.21	0	V	CR	110	98	1.12
4	R14	29	1.46	0.14	0	V	DT	90	67	1.34
5	R17	13	1.46	0.21	0	V	CR	70	54	1.30
6	R20	43	1.46	0.21	0	V	CR	90	92	0.98
7	R22	30	1.46	0.21	0	V	CR	80	82	0.98
8	R24	31	1.46	0.21	0	V	DT	93	84	1.10
9	R25	31	4.17	0.21	0	V	DT	105	95	1.11
10	T1	28	0.31	0.21	0	V	DT	111	95	1.16
11	T3	28	0.36	0.21	0	V	DT	105	97	1.08
12	T4	33	0.48	0.21	0	V	DT	110	114	0.96
13	T7	27	0.75	0.21	0	V	DT	110	118	0.93
14	T8	31	1.04	0.21	0	V	DT	125	130	0.96
15	T10	28	0.36	0.14	0	V	DT	87	90	0.97
16	T13	13	0.36	0.21	0	V	DT	90	64	1.41
17	T15	33	1.04	0.21	0	V	SY	105	115	0.91
18	T16	33	1.04	0.14	0	V	SY	90	117	0.77
19	T19	30	1.04	0.21	0	V	CR	113	112	1.00
20	T25	54	0.36	0.21	0	V	SY	115	125	0.92
21	T31	31	0.36	0.21	0	V	SY	95	103	0.92
22	T34	34	2.08	0.21	0	V	SY	113	117	0.96
23	T35	34	0.59	0.21	0	V	SY	115	119	0.97
									Average:	1.04
									CoV:	0.14
Bach F., Nielsen M.P. and Braestrup M.W. (1980): 'Shear Tests on Reinforced Concrete T-Beams - Series V, U, X, B and S', Structural Research Laboratory, Technical University of Denmark, Report N° 120, 87 p., Copenhagen, Denmark										
1	V6002W	35.7	0.72	0.27	0	V	DT	245	233	1.05
2	V6002E	35.7	0.72	0.27	0	V	DT	253	233	1.09
3	V6004W	36.4	0.72	0.43	0	V	DT	306	292	1.05
4	V6004E	36.4	0.72	0.43	0	V	DT	347	292	1.19
5	U6002W	19.5	0.72	0.13	0	V	DT	194	144	1.35
6	U6002E	19.5	0.72	0.13	0	V	DT	200	144	1.39
7	U6004W	21.1	0.72	0.27	0	V	DT	224	193	1.16
8	U6004E	21.1	0.72	0.27	0	V	DT	237	193	1.23
9	X6009W	7.3	0.32	0.27	0	V	DT	133	145	0.92
10	X6009E	7.3	0.32	0.27	0	V	DT	143	145	0.99
11	B6009W	10.7	0.57	0.23	0	V	DT	286	237	1.21
12	B6009E	10.7	0.57	0.23	0	V	DT	245	230	1.07
									Average:	1.14
									CoV:	0.12
Leonhardt F. and Walther R. (1966): 'Wandartige Träger', Deutscher Ausschuss für Stahlbeton, Wilhelm Ernst & Sohn, Vol. 178, 159 p., Berlin, Germany										
1	WT4	28	0.40	0.16	0	F	SY	1526	1590	0.96
2	WT7	30	0.40	2.51	0	F	SY	1119	1130	0.99
3	IWT1	28	0.98	0.71	0	L	CR	1152	1130	1.02
4	IWT2	28	0.98	0.38	0	V	CR	1177	1114	1.06
									Average:	1.02
									CoV:	0.04

Leonhardt F., Waltner R. and Dilger W. (1968): 'Schubversuche an indirekt gelagerten, einseitbrühen und durchlaufenden Stahlbetonbalken', Deutscher Ausschuss für Stahlbeton, Wilhelm Ernst & Sohn, Vol. 201, 69 p., Berlin, Germany										
1	ETI1	30	1.32	0.16	0	V	SY	273	276	0.99
2	ETI2	26	1.40	0.28	0	F	CR	257	250	1.03
3	ETI3	25	1.40	0.76	0	F	CR	240	222	1.08
4	ETI4	27	1.40	0.86	0	F	CR	245	250	0.98
5	ETI5	28	1.42	0.27	0	V	SY	240	246	0.98
Average:										1.01
CoV:										0.04
Baumann T. and Rüsche H. (1970): 'Schubversuche mit indirekter Krafteinleitung: Versuche zum Studium der Verdübelungswirkung der Biegezugbewehrung eines Stahlbetonbalkens', Deutscher Ausschuss für Stahlbeton, Heft 210, 83 p., Berlin, Germany										
1	64/1	59.3	3.48	0.37	0	F	CR	102	102	1.00
2	65/1A	50.5	3.48	0.37	0	L	SY	140	130	1.08
3	65/1B	50.5	3.48	0.37	0	F	CR	104	104	1.00
4	65/2A	56.3	3.48	0.37	0	F	CR	93	92	1.01
5	65/2B	56.3	3.48	0.80	0	F	CR	103	96	1.07
6	65/3A	48.2	3.48	0.37	0	F	CR	92	80	1.15
7	65/3B	48.2	3.48	0.80	0	F	CR	112	98	1.14
Average:										1.06
CoV:										0.06

Notation:

f_c : concrete compressive strength measured on a cylinder;

ρ : longitudinal reinforcement ration;

ρ_w : transversal reinforcement ration;

Q_{test} : measured ultimate load;

Q_{EPSF} : calculated ultimate load.

Failure modes:

F: Flexural failure;

V: Shear failure;

L: Local failure.

Failure subtype:

CR: Concrete crushing

SP: Concrete spalling

DT: Diagonal tension

SY: Reinforcement yielding

AS: Arch stability

A: Anchorage failure

Appendix

1.2) Prestressed concrete members

N°	Name	f_c [MPa]	ρ [%]	ρ_w [%]	$\sigma_{p,inf}$ [MPa]	Failure mode	Failure Subtype	Q_{test} [kN]	Q_{EPSF} [kN]	$\frac{Q_{test}}{Q_{EPSF}}$
Saqaan E.I. and Frosch R.J. (2009): 'Influence of flexural reinforcement on shear strength of prestressed concrete beams', ACI Structural Journal, Vol. 106, N° 1, pp. 60-68, USA										
1	V-4-0	52.1	0	0	1.9	V	DT	488	408	1.2
2	V-4-0.93	52.7	0	0	1.9	V	DT	668	600	1.11
3	V-4-2.37	53.4	0	0	1.9	V	DT	734	734	1.00
4	V-7-0	54.5	0	0	1.94	V	DT	740	552	1.34
5	V-7-1.84	53.1	0	0	1.94	V	DT	968	708	1.37
6	V-7-2.37	53.1	0	0	1.94	V	DT	856	726	1.18
7	V-10-0	51.7	0	0	1.95	V	DT	812	584	1.39
8	V-10-1.51	51.7	0	0	1.95	V	DT	880	702	1.25
9	V-10-2.37	51.7	0	0	1.95	V	DT	880	738	1.19
Average:										1.23
CoV:										0.10
Kaufman M.K. and Ramirez J.A. (1988): 'Re-evaluation of the Ultimate Shear Behavior of High-Strength Concrete Prestressed I-Beams', ACI Structural Journal, Vol. 85, N° 3, pp. 295-303, USA										
1	I-1	57.5	0	0.29	7.45	F	SY	1094	942	1.16
2	I-2	57.5	0	0.24	7.45	V	CR	1288	1130	1.14
3	I-3	57.7	0	0.33	7.66	V	CR	890	890	1.00
4	I-4	57.7	0	0.24	7.76	V	CR	978	908	1.08
5	II-1	62.7	0	0.33	7.94	V	SY	1246	1328	0.94
6	II-2	62.7	0	0.33	7.79	F	SY	1788	1604	1.11
Average:										1.07
CoV:										0.07
Kuchma D., Kim K.S., Nagle T.J., Sun S. and Hawkins N.M. (2008): 'Shear Tests on High-Strength Prestressed Bulb-Tee Girders: Strengths and Key Observations', ACI Structural Journal, Vol. 105, N° 3, pp. 358-367, USA										
1	G1E	83.4	0	0.55	7.7	V	SY	4438	4228	1.05
2	G1W	83.4	0	0.55	7.7	V	SY	5102	4954	1.03
3	G2E	86.9	0	0.93	8.5	V	SY	5916	5100	1.16
4	G2W	86.9	0	0.93	8.5	V	SY	6856	6014	1.14
5	G3E	109.6	0	0.82	9.6	V	SY	6098	5594	1.09
6	G3W	109.6	0	0.82	9.6	V	SY	6634	5870	1.13
7	G4E	112.4	0	1.70	9.6	V	SY	7780	7554	1.03
8	G4W	112.4	0	1.70	9.6	V	SY	7780	7780	1.00
9	G5E	122.7	0	0.18	6.4	V	SY	3626	3454	1.05
10	G5W	122.7	0	0.18	6.4	V	SY	2980	2638	1.13
11	G6E	87.6	0	0.85	10.4	V	SY	5550	5138	1.08
12	G6W	87.6	0	0.85	9.1	V	SY	4842	4484	1.08
13	G7E	86.2	0	0.82	10.4	V	SY	5786	5076	1.14
14	G7W	86.2	0	0.82	10.4	V	SY	6400	6336	1.01
15	G8E	91.7	0	0.82	9.9	V	SY	5508	5738	0.96
16	G9E	66.2	0	1.57	8.5	V	CR	5998	5504	1.09
17	G9W	66.2	0	1.57	8.5	V	CR	5982	5808	1.03
18	G10E	73.1	0	1.14	8.9	V	SY	6116	4932	1.24
19	G10W	73.1	0	1.14	8.9	V	SY	7302	5618	1.30
Average:										1.09
CoV:										0.07
Rupf M. and Muttoni A. (2012): 'Schubversuche an vorgespannten Stahlbetonträgern mit ungenügender Schubbewehrung', EPFL, IBETON, Test Report , 159 p., Lausanne, Switzerland										
1	SR21	30.8	0	0.09	2.5	V	SY	1197	1110	1.08
2	SR22	33.7	0	0.13	2.5	V	CR	1377	1290	1.07
3	SR23	35.3	0	0.06	2.5	V	SY	1092	1065	1.03
4	SR24	31.3	0	0.25	2.5	V	CR	1737	1680	1.03

Summary of the online database

5	SR25	33.1	0	0.09	5	V	CR	1452	1410	1.03
6	SR26	36.9	0	0.06	5	V	SY	1371	1335	1.03
7	SR27	28.3	0	0.19	5	V	CR	1818	1740	1.04
8	SR28	37.8	0	0.09	0	V	SY	666	660	1.01
9	SR29	29.8	0	0.25	2.5	V	CR	1755	1680	1.04
10	SR30	31.4	0	0.25	2.5	V	CR	1743	1620	1.08
11	SR31	31.3	0	0.09	3	V	DT	927	795	1.17
12	SR31B	31.3	0	0.09	3	V	DT	909	795	1.14
13	SR32	35.2	0	0.09	0	V	DT	519	525	0.99
Average:										1.06
CoV:										0.05
Fernández Ruiz M. and Muttoni A. (2008): 'Shear strength of thin-webbed post-tensioned beams', ACI Structural Journal, Vol. 105, N° 3, pp. 308-317, USA										
1	SH1	53.4	0	0.63	4.2	V	CR	2980	3136	0.95
2	SH2	52.3	0	0.63	4.2	V	CR	2520	2400	1.05
3	SH3	55.8	0	0.63	4.2	V	CR	3060	3188	0.96
4	SH4a	49.5	0	0.63	4.2	V	CR	2240	2434	0.92
5	SH4b	60.0	0	0.63	4.2	V	CR	3340	3478	0.96
6	SH5	47.2	0	0.63	4.2	V	CR	3320	3254	1.02
Average:										0.98
CoV:										0.05
Moore A.M. (2014): 'Shear Behavior of Spliced Post-Tensioned Girders', Faculty of the Graduate School, The University of Texas at Austin, PhD Thesis, 250 p., Austin, USA										
1	Tx62-1S	73.1	1.51	0.93	11.8	V	CR	3056	3217	0.95
2	Tx62-2S	82.7	1.51	0.93	12.3	V	CR	3332	3744	0.89
3	Tx62-2N	82.7	1.51	0.93	12.3	V	CR	3630	3742	0.97
4	Tx62-3	80.7	1.51	0.93	0	V	CR	4386	4024	1.09
5	Tx62-4S	95.8	1.51	1.40	12.5	V	CR	3696	4062	0.91
6	Tx62-4N	93.8	1.51	1.40	12.5	V	CR	3701	3738	0.99
7	Tx62-5S	86.2	1.51	0.31	12.5	V	CR	3127	3191	0.98
8	Tx62-5N	86.2	1.51	0.31	12.5	V	CR	3269	3302	0.99
9	Tx62-6S	85.5	1.52	1.14	13	V	CR	4137	3831	1.08
10	Tx62-6N	91.0	1.52	1.14	13	V	CR	4888	4887	1.00
11	Tx62-7S	84.1	1.52	1.14	13	V	CR	5186	4630	1.12
Average:										1.00
CoV:										0.07
De Wilder K., Lava P., Debruyne D., Wang Y., De Roeck G. and Vandewalle L. (2015): 'Stress Field Based Truss Model for Shear-Critical Prestressed Concrete Beams', The Institution of Structural Engineers, Vol. 3, pp. 28-42, London, UK										
1	B101	77.5	2.08	0.27	19.3	V	DT	378	367	1.03
2	B102	77.5	2.08	0.27	19.3	V	DT	322	309	1.04
3	B104	88.9	2.08	0.27	9.6	V	DT	282	303	0.93
4	B105	88.9	2.08	0.27	9.6	V	DT	251	255	0.98
5	B107	89.3	0.97	0.27	10.7	F	CR	271	284	0.95
6	B108	89.3	0.97	0.27	10.7	F	CR	214	221	0.97
Average:										0.98
CoV:										0.04
Leonhardt F., Koch R. and Rostasy F.S. (1973): 'Schubversuche an Spannbetonträgern', Deutscher Ausschuss für Stahlbeton, Vol. 227, 179 p., Berlin, Germany										
1	ILT1	30.4	0.35	1.01	4.3	V	SY	1809	1690	1.07
2	ILT2	30.4	0.35	0.70	4.3	V	SY	1565	1540	1.02
3	IILT1	33.6	0.35	1.01	4.3	v	SY	1667	1552	1.07
Average:										1.05
CoV:										0.03
Büeler C. and Thoma K. (2010): 'Indirekt gelagerter Spannbetonträger', Lucerne University of Applied Sciences and Arts, 61 p., Lucerne, Switzerland										

Appendix

1	LT1	34	0.17	0.25	2.7	F	CR	635	630	1.01
2	LT2	34	0.4	0.25	2.7	F	CR	863	860	1.00
Average:									1.01	
CoV:									0.01	

Notation:

f_c : concrete compressive strength measured on a cylinder;

ρ : longitudinal reinforcement ration;

ρ_w : transversal reinforcement ration;

$\sigma_{p,inf}$: prestress after the initial losses due to wedge slippage;

Q_{test} : measured ultimate load;

Q_{EPSF} : calculated ultimate load.

Failure modes:

F: Flexural failure;

V: Shear failure;

L: Local failure.

Failure subtype:

CR: Concrete crushing

SP: Concrete spalling

DT: Diagonal tension

SY: Reinforcement yielding

AS: Arch stability

A: Anchorage failure

2) Appendix 2 – Reinforced concrete panels subjected to shear

The following appendix gives geometrical and mechanical properties of 77 reinforced concrete panels that were used to validate the mechanical model for estimating the effective concrete compressive strength in Chapter 4 of this thesis. Both measured and estimated failure loads of the panels are indicated, along with the basic statistical analysis of the results (the average prediction and the coefficient of variation).

N°	Name	f_c [MPa]	f_{yx} [MPa]	f_{yz} [MPa]	ρ_x [%]	ρ_z [%]	Failure mode	τ_{test} [MPa]	τ_{model} [MPa]	$\frac{\tau_{test}}{\tau_{model}}$
Vecchio F.J. and Collins M.P. (1982): 'Response of reinforced concrete to in-plane shear and normal stresses', Department of civil engineering, University of Toronto, N° 82-03, 332 p.										
1	PV4	26.6	242	242	1.06	1.06	Y-xz	2.838	2.62	1.08
2	PV6	29.8	266	266	1.79	1.79	Y-xz	4.472	4.81	0.93
3	PV10	14.5	276	276	1.79	1.00	Y-z+C	3.968	3.731	1.06
4	PV11	15.6	235	235	1.79	1.31	Y-xz	3.561	3.633	0.98
5	PV12	16.0	469	269	1.79	0.45	Y-z+C	3.134	3.049	1.03
6	PV16	21.7	255	255	0.74	0.74	Y-xz	2.144	1.947	1.1
7	PV19	19.0	458	299	1.79	0.71	Y-z+C	3.955	4.012	0.99
8	PV20	19.6	460	297	1.79	0.89	Y-z+C	4.261	4.457	0.96
9	PV21	19.5	458	302	1.79	1.30	Y-z+C	5.029	5.462	0.92
10	PV22	19.6	458	420	1.79	1.52	C	6.07	7.114	0.85
11	PV23	20.5	518	518	1.79	1.79	C	8.876	8.086	1.1
12	PV25	19.2	466	466	1.79	1.79	C	9.125	7.583	1.2
13	PV27	20.5	442	442	1.79	1.79	C	6.35	7.935	0.8
14	PV28	19.0	483	483	1.79	1.79	C	5.611	6.56	0.86
1	PV4	26.6	242	242	1.06	1.06	Y-xz	2.838	2.62	1.08
2	PV6	29.8	266	266	1.79	1.79	Y-xz	4.472	4.81	0.93
3	PV10	14.5	276	276	1.79	1.00	Y-z+C	3.968	3.731	1.06
4	PV11	15.6	235	235	1.79	1.31	Y-xz	3.561	3.633	0.98
5	PV12	16.0	469	269	1.79	0.45	Y-z+C	3.134	3.049	1.03
Average:										0.99
CoV:										0.11
Vecchio F.J., Collins M.P. and Aspiotis J. (1994): 'High-Strength Concrete Elements Subjected to Shear', ACI Structural Journal, Vol.91, N° 4, pp. 423-433, USA										
1	PHS2	66.1	606	521	3.23	0.41	Y-z+C	6.662	5.21	1.28
2	PHS3	58.4	606	521	3.23	0.82	Y-z+C	8.098	7.917	1.02
3	PHS5	52.1	606	521	3.23	0.41	Y-z+C	4.805	3.955	1.21
4	PHS6	49.7	606	521	3.23	0.41	Y-z+C	7.617	7.795	0.98
5	PHS8	55.9	606	521	3.23	1.22	Y-z+C	10.837	9.908	1.09
6	PHS9	56	606	521	3.23	0.41	Y-z+C	9.162	7.868	1.16
7	PHS10	51.4	606	521	3.23	1.22	Y-z+C	8.248	7.822	1.05
Average:										1.12
CoV:										0.09
Marti P. and Meyboom J. (1992): 'Response of Prestressed Concrete Elements to In-Plane Shear Forces', ACI Structural Journal, Vol.89, N° 5, pp. 503-514, USA										
1	PP1	27	479	480	1.94	0.65	Y-z+C	4.95	4.794	1.03
Average:										-
CoV:										-
Vecchio F.J. and Chan C.C.L. (1990): 'Reinforced concrete membrane elements with perforations', ASCE Journal of Structural Engineering, Vol. 116, Issue 9, pp. 2344-2360										
1	PC1A	27.9	500	500	1.65	0.82	Y-z+C	5.61	6.045	0.93
2	PC4	24.9	260	260	1.65	0.82	Y-z+C	4.84	5.752	0.84
Average:										0.88

Appendix

CoV:										0.05
Pang X.-B.D. and Hsu C.-T.T. (1995): 'Behavior of Reinforced Concrete Membrane Elements in Shear', ACI Structural Journal, Vol.92, N° 6, pp. 665-667, USA										
1	A2	41	462	462	1.2	1.20	Y-z+C	5.367	6.13	0.88
2	A3	42	446	446	1.78	1.78	Y-z+C	7.655	8.492	0.90
3	A4	42	469	469	2.97	2.97	C	11.31	14.079	0.80
4	B1	45	462	444	1.20	0.60	Y-xz	3.962	4.544	0.87
5	B2	44	446	462	1.78	1.20	Y-xz	6.125	7.246	0.85
6	B3	45	446	444	1.78	0.60	Y-xz	4.354	4.888	0.89
7	B4	45	469	444	2.97	0.600	Y-z+C	5.064	5.597	0.90
8	B5	43	469	462	2.97	1.2	Y-z+C	7.152	8.027	0.89
9	B6	43	469	446	2.97	1.78	Y-z+C	9.143	10.106	0.90
Average:										0.88
CoV:										0.04
Zhang L.-X. and Hsu T.T.C. (1998): 'Behavior and Analysis of 100 MPa Concrete Membrane Elements', Journal of Structural Engineering, vol. 124 n° 1, pp. 24-34, USA										
1	VA1	95.1	445	445	1.20	1.20	Y-z+C	6.156	6.19	0.99
2	VA2	98.2	409	409	2.40	2.4	Y-z+C	9.73	10.615	0.92
3	VA3	94.6	455	455	3.57	3.57	Y-z+C	15.08	16.914	0.89
4	VA4	103.1	470	470	5.23	5.23	C	21.42	21.357	1.00
5	VB1	98.2	409	445	2.40	1.20	Y-z+C	7.497	7.819	0.96
6	VB2	97.6	455	445	3.57	1.20	Y-z+C	9.137	8.94	1.02
7	VB3	102.3	470	445	5.96	1.20	Y-z+C	9.709	10.199	0.95
8	VB4	96.9	455	445	1.78	0.60	Y-xz	4.858	6.276	0.77
Average:										0.94
CoV:										0.08
Hsu C.-T.T. and Zhang L.-X. (1997): 'Nonlinear Analysis of Membrane Elements by Fixed-Angle Softened-Truss Model', ACI Structural Journal, Vol.94, N° 5, pp. 483-491, USA										
1	HB1	66.5	409	445	1.2	0.6	-	4.322	4.41	0.98
2	HB3	66.8	447	445	1.78	0.6	-	4.889	5.064	0.97
3	HB4	62.9	470	445	2.98	0.6	-	5.334	5.85	0.91
Average:										0.94
CoV:										0.01
Kirschner U. (1986): 'Investigating the behaviour of reinforced concrete shell elements', University of Toronto, Department of Civil Engineering, PhD Thesis, 83 p., Toronto, Canada										
1	SE1	42.5	492	479	2.91	0.98	Y-z+C	6.77	7.323	0.92
2	SE6	40	492	479	2.91	0.33	Y-z+C	3.755	3.963	0.95
Average:										0.94
CoV:										0.01
Watanabe F. and Muguruma H. (1989): 'Ultimate Strength and Deformations of RC Panel', Proceedings of the Sessions Related to Structural Design, Analysis and Testing, ASCE Structural Congress, pp. 31-38										
1	00R	28.15	310	310	0.86	0.86	Y-x+C	3.14	2.724	1.15
2	15R	28.15	310	310	0.86	0.86	Y-xz	3.15	2.724	1.16
3	30R	28.15	310	310	0.86	0.86	Y-xz	3.13	2.724	1.15
4	45R	28.15	310	310	0.86	0.86	Y-xz	3.42	2.724	1.26
5	00D	28.15	318	318	0.87	0.87	Y-x+C	2.97	2.831	1.05
6	30D	28.15	318	318	0.86	0.87	Y-xz	2.56	2.823	0.91
7	45D	28.15	318	318	0.87	0.87	Y-xz	2.84	2.831	1.00
8	00DI	31	294	294	1.39	1.39	Y-x+C	4.96	4.167	1.19
9	22.5DI	31	294	294	1.39	1.39	Y-xz	5.06	4.167	1.21
10	45DI	31	318	318	1.3	1.3	Y-xz	3.97	4.213	0.94
11	45DII	31	318	318	2.61	2.61	Y-xz	7.61	8.347	0.91
12	45PCI	30.4	1187	1187	0.77	0.77	Y-xz	7.78	9.264	0.84
13	45PCII	30.4	1187	1187	1.55	1.55	C	11.72	11.456	1.02
14	45PCIII	30.4	1187	1187	1.55	0.77	Y-z+C	9.44	9.512	0.99
15	45PCIV	45	1187	1187	1.55	0.77	Y-z+C	10.63	11.121	0.96

Reinforced concrete panels subjected to shear

Average:										1.05
CoV:										0.12
Kollegger J. and Mehlhorn G. (1990): 'Experimentelle Untersuchungen zur Bestimmung der Druckfestigkeit des gerissenen Stahlbetons bei einer Querkzugbeanspruchung', Deutscher Ausschuss für Stahlbeton, Wilhelm Ernst & Sohn, Vol.413, 132 p., Berlin, Germany										
1	PK02	19.4	660	660	1.07	1.07	C	9.12	8.393	1.09
2	PK04	20.2	660	660	1.07	1.07	C	8.91	8.747	1.02
3	PK07	20.9	660	660	1.07	1.07	C	9.04	9.058	1.00
4	EGE6F1	15.8	465	465	0.66	0.66	C	8.00	7.279	1.10
5	EGE6F2	16	465	465	0.66	0.66	C	8.10	7.372	1.10
6	EGE6F3	14.6	465	465	0.66	0.66	C	6.90	6.722	1.03
7	EGE6F4	17.1	465	465	0.66	0.66	C	7.20	7.686	0.94
8	EGE6F7	18.8	465	465	0.66	0.66	C	8.50	8.674	0.98
9	EGE6F8	13.1	465	465	0.66	0.66	C	7.35	6.025	1.22
10	EGE7F1	15.9	660	660	0.66	0.66	C	8.20	7.282	1.13
11	EGE7F2	15.3	660	660	0.66	0.66	C	7.70	7.004	1.10
12	EGE7F3	17.3	660	660	0.66	0.66	C	8.70	7.931	1.10
Average:										1.07
CoV:										0.07
Schäfer K., Schelling G. and Kuchler T. (1990): 'Druck und querkzug in bewehrten betonelementen', Deutscher Ausschuss für Stahlbeton, N° 408, pp. 5-85, Berlin, Germany										
1	#2	25.8	582	582	3.14	3.14	C	11.775	9.943	1.18
2	#6	25.8	582	582	1.57	1.57	C	14.065	10.93	1.29
Average:										1.24
CoV:										0.04
André H.M.O. (1987): 'Toronto Kajima Study on Scale Effects in Reinforced Concrete Elements', University of Toronto, Department of Civil Engineering, PhD Thesis, 267 p., Toronto, Canada										
1	KP1	25.2	430	430	2.03	1.02	C	5.62	5.794	0.97
2	TP4A	24.9	450	450	2.03	2.03	C	8.72	9.199	0.95
Average:										0.96
CoV:										0.01

Notation:

f_c : concrete compressive strength measured on a cylinder;

f_{yx} : yield strength of the rebars in x (horizontal) direction;

f_{yz} : yield strength of the rebars in z (vertical) direction;

ρ_x : reinforcement ration in x (horizontal) direction;

ρ_z : reinforcement ration in z (vertical) direction;

τ_{test} : measured ultimate shear stress;

τ_{model} : calculated ultimate shear stress;

Failure modes:

C: Concrete crushing;

Y-xz: Yielding of the rebars in both directions;

Y-x: Yielding of the rebars in x (horizontal) direction;

Y-z: Yielding of the rebars in z (vertical) direction;

Filip NIKETIĆ

Structural Engineer with experience in the advanced design and assessment of reinforced, prestressed and post-tensioned concrete members of complex geometry



INFO: Date of birth: 15.08.1987.
Nationality: Serbian
CONTACT: E-mail: filip.niketic@gmail.com

PROFESSIONAL EXPERIENCE:

- 2012-2017 École Polytechnique Fédérale de Lausanne (EPFL)
Faculté Environnement Naturel, Architectural et Construit (ENAC)
Laboratoire de construction en béton - IBETON
- Assessing the strength of existing structural concrete members by means of rigid-plastic and elastic-plastic stress field analysis, focusing on bridge structures
 - Development of mechanical models for concrete compression softening
 - Teaching assistant of the following courses:
Structures en béton, Structure et architecture, Structures I et II, Dimensionnement et analyse des éléments à l'aide de champs de contraintes
- 2011-2012 University of Novi Sad
Faculty of Technical Sciences
- Teaching assistant of following courses:
Structural analysis II and Theory of plates and shells

PUBLICATIONS:

- 2015 Aurelio Muttoni, Miguel Fernández Ruiz, and Filip Niketić, "Design versus Assessment of Concrete Structures Using Stress Fields and Strut-and-Tie Models", ACI Structural Journal, Vol. 112, N°5
- 2016 Aurelio Muttoni, Miguel Fernández Ruiz, Filip Niketić and Marie-Rose Backes, "Assessment of Existing Structures Based on Elastic-Plastic Stress Fields and Modelling of Critical Details and Investigation of the In-Plane Shear Transverse Bending Interaction", FEDRO report N°680
- 2017 Eckart Hars, Filip Niketić and Miguel Fernández Ruiz, "Response of RC panel accounting for crack development and its interaction with rebars", Magazine of Concrete Research, article number MACR-D-17-00077R1

EDUCATION:

- 2006-2010 HONORS BACHELOR DEGREE IN CIVIL ENGINEERING
University of Novi Sad
Faculty of Technical Sciences
- 2010-2011 HONORS MASTER DEGREE IN STRUCTURE DESIGN
University of Novi Sad
Faculty of Technical Sciences

ACHIEVEMENTS:

- The Best Graduate Student of the Faculty of Technical Sciences in 2011
- The Best Graduate Student of the Civil Engineering Department in 2011
- Dositeja Certificate for the academic 2010/11
- Fund for Progress Encouragement of Gifted Students and Young Scientists and Artists Certificate in the academic 2008/09 and 2009/10
- Reward for Outstanding Accomplishments in the academic 2006/07, 2007/08, 2008/09 and 2009/10
- Civil Engineering Department Plaque for the best student in the academic 2006/07, 2007/08, 2008/09 and 2009/10

LANGUAGES:

Serbian Native speaker
English C2 Level
French B1 Level

